EXCEPIENT PHASE TRANSFORMATION IN FROZEN AND FREEZE-DRIED FORMULATIONS AND THEIR IMPACT ON PROTEIN STABILITY

A DISSERTATION

SUBMITTED TO THE FACULTY OF

THE GRADUATE SCHOOL

OF THE UNIVERSITY OF MINNESOTA

BY

JAYESH VIJAY SONJE

IN PARTIAL FULFILLMENT OF THE REQUIREMENTS

FOR THE DEGREE OF

DOCTOR OF PHILOSOPHY

RAJ SURYANARAYANAN, Ph.D. (ADVISER)

MARCH 2022

Acknowledgements

This thesis would be incomplete without the support, guidance, and encouragement of a number of individuals.

First and foremost, I would like to express my sincere and heartfelt gratitude towards my advisor Dr. Raj Suryanarayanan for the opportunity to be a part of his research group. His guidance and mentorship have been instrumental in shaping me as a scientist. I am grateful to him for the various opportunities to pursue research on challenging and interesting topics. I thank him for his unwavering support through many challenging times and encouragement especially during the initial years of my graduate school. I am always inspired by his passion and approach towards solving scientific questions and it will continue to help me develop personally as well as in my professional endeavors.

I would like to thank Dr. Ronald Siegel, Dr. Calvin Sun and Dr. Susan Krueger for serving on my dissertation committee, their valuable inputs and feedback in reviewing my thesis.

I am thankful to all the faculty members at UMN for helping me lay the foundation in Pharmaceutics. A special thank you to Katie, Amanda and Jody who have always gone out of their way to help me with several logistical issues and roadblocks.

A special thank you to Dr. Seema Thakral for guidance, support, scientific inputs, and friendship throughout my time at the University of Minnesota (UMN). I always enjoyed our engaging scientific discussions and brainstorming sessions. It has been an absolute pleasure to collaborate and work with her.

I would like to sincerely thank Dr. Susan Krueger for the opportunity to collaborate and work with her at the National Institute of Standards and Technology (NIST), Maryland. I

would like to express my gratitude for her invaluable contribution to this thesis, scientific inputs and for teaching me various aspects of small angle neutron scattering (SANS).

I would also like to extend my gratitude to my collaborators and mentors from industry, Dr. Jayasree Srinivasan, Dr. Carly Chisholm and Dr. Santosh Thakkar for the valuable inputs, scientific discussions, and feedback on the manuscripts. In addition, I thank Dr. Bakul Bhatnagar for generously offering his time to help me whenever I had a question scientifically as well as in terms of making a career decision. I highly appreciate his guidance and support.

I would like to acknowledge Dr. Wenqian Xu and Dr. Andrey Yakovenko for their help with my X-ray diffractometry (XRD) experiments at Argonne National Laboratory, 17-BM, Illinois. It has been a wonderful experience working with cutting-edge characterization equipment. Dr. Javier Garcia Barriocanal is acknowledged for his help with XRD experiments at the characterization facility, UMN. Dr. Todd Geders and Jason Hermann at Bio-techne, Minnesota are acknowledged for letting me use their facilities for biophysical characterization.

A big thank you to all the past and present Sury lab members for their friendship along with the good times and experiences I had during the past few years. I would like to thank Dr. Alpana Thorat, Dr. Nagakiran Duggirala, Dr. Krishna Kumar, Dr. Bhushan Munjal, Dr. Michelle Fung, Dr. Sampada Koranne, Dr. Navpreet Kaur, Dr. Kweku Konadu, Rahul Lalge, Jinghan Li and Wenqi Gai for several intriguing conversations and making me feel part of the team. I would also like to thank Dr. Davin Rautiola, Dr. Krutika Jain, Dr. Ahmad Hivechi and Ishaan Duggal for their help and engaging discussions.

The William and Mildred Peters endowment fund, Dane O. Kildsig for Center for Pharmaceutical Processing Research (CPPR) and David J.W. Grant & Marilyn J. Grant Fellowship are acknowledged for funding support.

I am grateful to my parents, Sangita and Vijay Sonje, and my brother, Ninad, for their unconditional love and support. My father's hard work and perseverance have always been a source of inspiration for me. I would also like to thank my in-laws for their support. Thank you to Dr. Manisha Desai for guiding me to pursue the doctoral program.

A very special thanks to my wife, Namita, for always encouraging me to pursue my dreams. I am fortunate to have her by my side through several ups and downs. Her help in my research, absolute support and companionship has been instrumental in this journey.

Thank you to my friend, Bhaumik Vashi, for always being there and to all my friends from New Jersey, Iowa City and Chicago who have directly or indirectly helped me in my pursuit.

Dedication

To my mom, dad, brother and wife for their unconditional love and support.

Abstract

Freeze-thaw and freeze-drying are common unit operations in manufacturing of biotherapeutics. Excipients such as sugars, buffers, and surfactants, each with an intended functionality, aid in preventing protein destabilization against stresses encountered during processing or storage. Sugars, specifically added to stabilize proteins, can only be effective if retained in the amorphous state. Selective crystallization of a buffer component during freezing, drying or storage can result in in a pH shift. The first objective of this thesis was to investigate the impact of stress associated with pH shift on protein (lactate dehydrogenase, LDH) conformation in presence of a crystallizing (sodium phosphate) and non-crystallizing (histidine) buffer, during the freezing and thawing stages. This was accomplished using small angle neutron and dynamic light scattering. The significant findings were: (i) LDH, at high concentration, had self-stabilizing effect and exhibited reversible aggregation after 5 freeze-thaw cycles, irrespective of buffer used. (ii) At low LDH concentrations, only with the selection of an appropriate buffer, irreversible aggregation could be avoided. Crystallization of certain excipients such as mannitol, is desirable, from a processing as well as product quality perspective. Mannitol is widely used in freeze-dried formulations and is known to crystallize as an unstable mannitol hemihydrate (MHH). Although, the conditions of formation of MHH are well established, its dehydration kinetics and the impact of the release of lattice water on the formulation stability is not known. The next set of objectives were (i) to investigate MHH dehydration kinetics at different conditions (relative humidity and temperature) in lyophilized mannitol formulations (with and without sucrose), and (ii) to determine the impact of MHH dehydration followed by sucrose crystallization on protein stability. Finally, in protein drug substances which are stored frozen, the use of mannitol as a crystallizing excipient and its role in generating a homogeneous freeze-concentrate was explored. Overall, the thesis highlights the importance of a multidisciplinary approach, using a variety of complementary characterization tools, to gain insights into protein stability.

Table of contents

Acknowledgements i
Dedication iv
Abstract v
List of Tables ix
List of Figures x
Chapter 1 Introduction 1
1.1 Protein structure 1
1.2 Challenges with protein stability 4
1.3 Fill-finish unit operations 8
1.4 Processing induced stresses and stabilization mechanisms by excipients 9
1.4.1 Freezing and frozen storage 9
1.4.2 Mechanism of stabilization by excipients 12
1.4.3 Drying and Storage 14
1.5 Characterization of excipient phase behavior and importance in protein stability 16
1.6 Objectives 17
1.7 Thesis organization 18
Chapter 2 Reversible Self-association in Lactate Dehydrogenase during Freeze-thaw in Buffered Solutions using Neutron Scattering 23
2.1 Introduction 23
2.2 Materials and Methods 30
2.2.1 Materials 30
2.2.2 SANS Measurements 31
2.2.3 SAXS Measurements 32
2.2.4 LDH Structure Modeling 32
2.2.5 Calculation of isoelectric point and net charge on LDH 33
2.2.6 DSC of NaP Buffer Solutions 34
2.2.7 Low-temperature pH of NaP Buffer Solutions 34
2.2.8 Low-temperature XRD of NaP Buffer Solutions 35
2.2.9 Dynamic Light Scattering (DLS) 35
2.3 Results and Discussion 36
2.3.1 Conformation of LDH at Room Temperature 36
2.3.2 Freeze-Thaw of LDH in Histidine Buffer 41

2.3.3 Characterization of Deuterated NaP Buffer Solutions 46
2.3.4 Freeze-Thaw of LDH in NaP Buffers 48
2.3.5 Concentration Dependence of LDH Aggregation 50
2.3.6 Modelling the Aggregates 54
2.4 Significance 59
2.5 Supplementary information 61
Chapter 3 Anomalous behavior of mannitol hemihydrate: Implications on sucrose crystallization in colyophilized systems. 67
3.1 Introduction 67
3.2 Materials and Methods 70
3.2.1 Materials 70
3.2.2 Lyophilization 71
3.2.3 Storage treatments 72
3.2.4 X-ray diffractometry 72
3.2.5 Synchrotron X-ray diffractometry (SXRD) 72
3.2.6 Headspace Humidity Measurement 73
3.2.7 Karl Fischer Titrimetry 74
3.2.8 Stopper moisture content by gravimetric method 74
3.3 Results and Discussion 75
3.3.1 Dehydration behavior of MHH 75
3.3.2 Anomalous MHH dehydration 78
3.3.3 MHH dehydration in co-lyophilized system 79
3.3.4 Sucrose crystallization in final lyophile 84
3.3.5 Movement of water in a sealed vial 88
3.4 Significance 95
3.5 Conclusion 96
3.6 Supplementary Information 98
Chapter 4 Mannitol hemihydrate dehydration in lyophilized protein formulations: Impact on sucrose crystallization and protein stability during storage 105
4.1 Introduction 105
4.2 Materials and Methods 108
4.2.1 Formulations 108
4.2.2 Lyophilization 109
4.2.3 X-ray diffractometry (XRD) 110

4.2.4 Synchrotron X-ray diffractometry (sXRD) 110
4.2.5 Karl Fischer Titrimetry 111
4.2.6 Size exclusion chromatography (SEC) 111
4.2.7 Water sorption-desorption 112
4.2.8 Differential scanning calorimetry (DSC) 112
4.2.9 Headspace moisture analysis (FMS Lighthouse) 113
4.3 Results and Discussion 113
4.3.1 Effect of formulation variables on MHH (formation and dehydration) 114
4.3.2 Effect of lyophilization cycle parameters 124
4.3.3 MHH Role of controlled relative humidity (55% RH) and elevated temperature (40°C) 130
4.4 Significance 139
4.5 Conclusions 141
4.6 Supplementary information 142
Chapter 5 Long-term frozen storage of proteins: use of mannitol to generate a homogenous freeze-concentrate 145
5.1 Introduction 145
5.2 Materials and Methods 150
5.2.1 Materials 150
5.2.2 Differential scanning calorimetry (DSC) 150
5.2.3 Synchrotron X-ray diffractometry (sXRD) 151
5.2.4 Freeze-thaw 152
5.3 Results and discussions 152
5.3.1 Mannitol-sucrose systems 152
5.3.2 Mannitol-trehalose systems 154
5.3.3 Mannitol-trehalose (3:1) systems – effect of isothermal hold 161
5.3.5 HSA aggregation: Effect of processing (annealed versus unannealed) and composition 168
5.4 Conclusion 171
5.5 Supplementary information 172
Chapter 6 Summary 174
Chapter 7 Future work 179
Bibliography 184

List of Tables

Table 2.1. Basic Characterization of LDH at 20°C Before and After Freezing..... 40

Table 2.2. Particle Size of LDH in Solution Before Freezing and After 5 Freeze-Thaw Cycles. ……53

Table 4.1 Freeze drying cycle parameters 109

Table 5.1 Mannitol-trehalose (3:1) – DSC data for isothermal hold (-20°C) experiments..... 162

Table 5.2 Mannitol-sucrose (3:1) – DSC data for isothermal hold (-20°C) experiments 167

List of Figures

Figure 1.1 Levels of structure in proteins the quaternary structure of the multi-subunit protein, in this case hemoglobin [7]. 3

Figure 1.2. Mechanisms and inter-relationships of protein unfolding, self-association, and aggregation [13]. 5

Figure 1.3 Electrostatic interactions as a function of the distance between two charged protein molecules [8]. 7

Figure 1.4. Typical steps involved in lyophilization of biologics. The y-axis represents temperature (color-coded). The temperature range, during different stages of freeze-drying, broadly follows the color scheme. Rectangles with sharp corners represent intermediate stages while rectangles with rounded edges represent the final product. The alphabets adjacent to the arrows represent the predominant mechanisms of protein stabilization during each stage (more details in the text). All the solutes are assumed to remain amorphous, both in the frozen DS/DP and lyophilized DP. A typical freeze-drying process consists of three stages: freezing, primary drying, and secondary drying. Freezing is an efficient desiccation step where most of the solvent is separated from the solutes to form ice. As freezing progresses, the solute phase becomes highly concentrated and is termed the 'freeze concentrate'. During primary drying, ice is transferred from the product to the condenser by sublimation. The primary drying stage is generally the longest and its optimization has a large impact on process economics. During secondary drying, water is desorbed from the freeze concentrate, usually at elevated temperatures and low pressures. Secondary drying normally takes only a few hours. Typically, drying is conducted below Tg' (glass transition temperature of the freeze-concentrate) during primary drying and below Tg (glass transition temperature of the lyophile) during secondary drying [1]. 10

Figure 1.5. Schematic representation of (A) changes in protein structure (native to aggregate) on arbitrary free-energy y-axis. The energy barrier (ΔG_{unf}) is shown with dotted lines. (B) The increase in ΔG_{unf} after addition of a stabilizer representative of preferential exclusion mechanism [8]. 13

Figure 2.1 LDH tetramer (PDB ID 2V6M) [60] visualized in three different orientations using VMD [64]. B. Overlay of buffer-subtracted SANS curves for 1 mg/mL LDH in 10 mM histidine buffer in 100% D_2O (red data points) and in 8% D_2O (blue data points) at 20 °C and the calculated LDH tetramer curve (black curve) from the structure in A using the SasCalc module in SASSIE-web [66]. The 8% D_2O data has been scaled to the 100% D_2O data for easy comparison of their shapes. Error

bars are the standard error of the mean based on the number of pixels used during data averaging. 39

Figure 2.2. SANS I(q) vs q curves. A. LDH (1 mg/mL) in 10 mM histidine buffer in 8% D_2O during cooling at 20, 5, 0, -10, -25 and -45°C from bottom to top. B. The frozen solution (of panel A) during heating at -45, -25, -10, 0, 5 and 20°C from top to bottom. C and D. SANS profiles for the identical composition obtained during cooling and heating but in 100% D_2O. The incoherent scattering from the buffer has not been subtracted from these data in order to show the difference in the incoherent scattering between the 8% D_2O and 100% D_2O buffers. Error bars are the standard error of the mean based on the number of pixels used during data averaging. *In figure 2.2 C, the SANS pattern at -10°C does not align in the 0.01 Å-1 to 0.03 Å-1 range; this discontinuity can be attributed to beginning of ice crystallization or incomplete ice crystallization at -10°C. 44

Figure 2.3. SANS I(q) vs q curves. A. Buffer-subtracted SANS curves of LDH (1 mg/mL) solution buffered in histidine (10 mM; 8% D_2O) at room temperature(red circle), cooled to -45 °C (blue circle), and thawed back to room temperature (green circle). The black curve is the reference LDH tetramer curve. B. The same composition and processing conditions as in panel A, except for the use of 100% D_2O. Error bars are the standard error of the mean based on the number of pixels used during data averaging. 45

Figure 2.4. Characterization of NaP buffer (100 mM) during freezing and thawing (in 100% D_2O). A. Low-temperature pH measurement, when cooled from 20 °C to -25 °C and then heated back to 20 °C. The heating as well as the cooling rate was 0.5 °C/min and the frozen solution was held at -25 °C for 30 minutes. B. The DSC heating curve of frozen solution, heated from -45 °C to 20 °C. The solution was initially cooled from RT to -45 °C, at 0.5 °C/min and held for 30 minutes. Only the final heating curve is shown. C. XRD patterns obtained while the solution was cooled from 20 °C to -40 °C at 0.5 °C/min. The XRD patterns were obtained at -10, -20, 25 and -40 °C. D. XRD patterns obtained when the frozen solution (from C) was heated from -40 to 10 °C at 0.5 °C/min. The XRD patterns were obtained at -20, -10, -5, 1, 5 and 10 °C. 47

Figure 2.5. SANS I(q) vs q curves. A. 1 mg/mL LDH, 100 mM sodium phosphate (NaP) 8% D_2O buffer during cooling at 20, 5, 0, -10, -25 and -45 °C from bottom to top B. 1 mg/mL LDH, 100mM NaP 8% D_2O buffer during heating at -45, -25, -10, 0, 5 and 20 °C from top to bottom. C and D. SANS profiles for 1 mg/mL LDH, 10 mM NaP 8% D_2O buffer during identical cooling and heating series. The incoherent scattering from the buffer has not been subtracted from these data for

comparison to the data in Figures 2A and 2B. Error bars are the standard error of the mean based on the number of pixels used during data averaging. 49

Figure 2.6. Overlay of buffer-subtracted SANS I(q) vs q curves pre and post freeze thaw for 1 mg/mL LDH in A. 10 mM NaP and B. 100 mM NaP buffers in 8% D_2O. Error bars are the standard error of the mean based on the number of pixels used during data averaging. 50

Figure 2.7. Modeling LDH dimers to determine the type of aggregates observed experimentally in 10 mM histidine buffer (100% D_2O) solutions (A) LDH dimers in three different forms, modeled as per Fujisawa et. al. [65]. (B) Overlay of SANS curves for 1 mg/mL LDH in 10 mM histidine buffer in 100% D_2O (blue data points) at -45°C and the reference LDH dimer 1, 2 and 3 curves (black, red and green curves respectively). Error bars are the standard error of the mean based on the number of pixels used during data averaging. 56

Figure 2.8 Modeling LDH aggregates to determine the type of aggregates observed experimentally in 10 mM histidine buffer (100% D_2O) solutions (A) LDH octamers modeled in three different orientations (B) LDH 16-mers modeled in three different orientations (C) Overlay of SANS curves for 1 mg/mL LDH in 10 mM histidine buffer in 100% D2O (blue data points) at -45°C and the reference LDH octamer curves in x, y and z orientations (black, red and green curves respectively) (D) Overlay of SANS curves for 1 mg/mL LDH in 10 mM histidine buffer in 100% D_2O (blue data points) at -45°C and the reference LDH 16-mer curves in x, y and z orientations (black, red and green curves respectively. Error bars are the standard error of the mean based on the number of pixels used during data averaging. 58

Figure 2.9 Guinier fits to the 1.0 mg/mL LDH in 10 mM histidine 8% D_2O buffer SANS data from Figures 2.3A and 2.3B. A. Before freezing and B. after one freeze-thaw cycles (thawed). The Rg and I(0) values from the Guinier fits are presented in Table 2.1. Error bars are from the standard error of the mean of the I(q) vs q data based on the number of pixels used in the data averaging. 61

Figure 2.10A. Guinier fits to the 1.0 mg/mL LDH in 10 mM and 100 mM NaP 8% D_2O buffer SANS data from Figure 2.5. A and C. Before freezing and B and D. after one freeze-thaw cycles (thawed). The Rg and I(0) values from the Guinier fits are presented in Table 2.1. Error bars are from the standard error of the mean of the I(q) vs q data based on the number of pixels used in the data averaging. 62

Figure 2.11 SAXS data from 0.5 mg/mL LDH in 100 mM NaP 0% D2O buffer at RT before freezing and after five freeze-thaw cycles (5X FT). The 5X FT data have been scaled to the RT

data before freezing. The solid line is the calculated SANS curve from the atomic coordinates of the LDH tetramer (PDB ID 8V6M) as described in the *Methods* section. Error bars are the standard error of the mean based on the number of pixels used during data averaging. 63

Figure 2.12 Guinier fits to the 0.5 mg/mL LDH in 100 mM NaP 0% D2O buffer SAXS data from Figure 2.11. A. Before freezing and B. after 5 freeze-thaw cycles (5XFT). The Rg and I(0) values from the Guinier fits are presented in Table 1. Error bars are from the standard error of the mean of the I(q) vs q data based on the number of pixels used in the data averaging..... 64

Figure 2.13 Snapshot of LDH titration curve (surface charge as a function of pH) obtained from ProtPi Tool (*https://www.protpi.ch/Calculator/PeptideTool). The isoelectric point pI for LDH was 7.2 and the net charge at pH 5 is ~ 15 units. The tool is useful to determine the surface charge on LDH at different pH using the titration curve for protein with known amino acid sequence..... 65

Figure 2.14 Characterization of sodium phosphate buffer (10 mM) during freezing and thawing (in 100% D_2O). A. Low temperature pH measurement, when cooled from 20 to -25 °C and then heated back to 20 °C. The heating as well as the cooling rate was 0.5 °C/min and the frozen solution was held at -25 °C for 30 minutes. B. The DSC heating curve of frozen solution, heated from -45 °C to 20 °C. The sample was cooled from 20 to -45 °C and heated back to 20 °C at 0.5 °C/min. Only the final heating curve is shown. C. XRD patterns obtained while the solution was cooled from 20 to -40 °C at 0.5 °C/min. The XRD patterns were obtained at -10, -20, 25 and -40 °C. D. XRD patterns obtained when the frozen solution (from C) was heated from -40 to 10 °C at 0.5 °C/min. The XRD patterns were obtained at -20, -10, -5, 1, 5 and 10 °C..... 66

Figure 3.1 Schematic representation of vial headspace humidity measurement assembly. An expanded view of the sensor is also provided. The vials were stored at 40 °C and the relative humidity data was continuously recorded and stored on the computer connected through a digital recorder. Parts of the diagram have been adapted from www.sensirion.com [103].("Digital Humidity Sensor SHT7x (RH/T)," n.d.) Reproduced with permission. 74

Figure 3.2 XRD patterns of lyophilized mannitol following storage at 11% RH (RT). The gradual reduction in intensity of a characteristic peak of MHH (#) along with the evolution of δ-(¤) and β-(*) mannitol peaks is highlighted. 76

Figure 3.3 MHH dehydration (represented as the normalized* intensity of 17.9° 2θ peak) following storage at 11, 43, 64 and 97% RH (RT). To retain clarity, the error bars are shown only for the dehydration data obtained at 11% RH. The error bars for all the data are shown in Figure 3.11 in

Supplementary material). *The MHH peak intensity in the fresh lyophile was assumed to be 100%, and the peak intensities obtained as a function of storage time, were expressed with respect to the initial intensity. 77

Figure 3.4 XRD patterns of lyophilized mannitol-sucrose (4:1 w/w) following storage at 11% RH (RT). The gradual reduction in intensity of peak attributed to MHH (#) and evolution of δ-(¤) and β- (*) mannitol peaks is highlighted. 81

Figure 3.5 Plot comparing the dehydration kinetics of MHH in lyophilized mannitol and mannitol-sucrose (4:1 w/w) stored at 11% RH (RT). In the mannitol-sucrose system, for the intensity of the 17.9 °2θ MHH peak measured at 49 h, the error bar was smaller than the size of the symbol..... 82

Figure 3.6 XRD patterns of lyophilized mannitol-sucrose (4:1 w/w) following storage at 97% RH (RT). The reduction in intensity of peak attributed to MHH (#) and evolution of δ-(¤) and β-(*) mannitol peaks is highlighted for reference. Notice difference in XRD pattern of samples stored for 10 h and 24 h (regions 19-20 and 26-27 °2θ). 83

Figure 3.7 Crystallization of sucrose following the storage of lyophilized mannitol-sucrose (4:1 w/w) mixture at 57 and 75% RH (RT). The intensity of 11.7° 2θ peak of sucrose is plotted as a function of storage time. The highest intensity was assigned to be 100%, and the rest of the intensities are expressed with respect to this number. The experiments were performed in triplicate and one representative result is shown here. The rest of the data are presented in supplementary material (Figure 3.15). 86

Figure 3.8 Headspace relative humidity (left y-axis) and temperature (right y-axis) in three vials, containing colyophilized mannitol-sucrose (4:1 w/w), stored at 40 °C. A. Data was recorded for three samples. B. The initial rise in RH within first 24 h for representative vial is presented. Notice small overshoot in temperature upon transferring vials from RT to oven set at 40 °C..... 90

Figure 3.9 Normalized intensity of MHH or sucrose peak* (left y-axis) and water content (right y-axis) in mannitol-sucrose (4:1) lyophiles for different days at 40 °C. A new vial was withdrawn at each time point and the same vial was used for water content and XRD analysis. * MHH content (blue bars; 17.9 °2θ peak) or crystalline sucrose content (purple bars; 11.7 °2θ peak). The highest intensities of MHH (17.9 °2θ) and sucrose (11.7 °2θ) peaks at the start and at the end of the experiment respectively were assigned to be 100%, and the rest are expressed as relative intensities. 91

Figure 3.10 XRD pattern of lyophilized mannitol. The calculated pattern of mannitol phases (MHH blue and δ-mannitol (red) are also included. 98

Figure 3.11 MHH dehydration (represented as the normalized* intensity of 17.9° 2θ peak) following storage at 11, 43, 64 and 97% RH (RT) (n=3). *The MHH peak intensity in the fresh lyophile was assumed to be 100%, and the peak intensities obtained as a function of storage time, were expressed with respect to the initial intensity. 98

Figure 3.12 XRD pattern of lyophilized mannitol-sucrose (4:1 w/w) mixture. The calculated pattern of mannitol phases (MHH blue, δ-mannitol (red) and β-mannitol (green) are also included. 99

Figure 3.13 Overlay of XRD patterns of lyophilized mannitol-sucrose (4:1 w/w) mixture stored at 57% RH (RT). XRD patterns were obtained every 6 hours. A characteristic peak of sucrose is highlighted. 99

Figure 3.14 Overlay of XRD patterns of lyophilized mannitol-sucrose (4:1 w/w) mixture stored at 75% RH (RT). XRD patterns were obtained every 6 hours. A characteristic peak of sucrose is highlighted. 100

Figure 3.15 Crystallization of sucrose following storage of lyophilized mannitol-sucrose (4:1 w/w) mixture at 57 (A and B) and 75% RH (C and D). The intensity of 11.7° 2θ peak of sucrose is plotted as a function of storage time. The highest intensity was assigned to be 100%, and the rest of the intensities are expressed with respect to this number. The experiment was conducted in triplicate and one representative data is plotted in Figure 3.7. 100

Figure 3.16 Water uptake by amorphous sucrose at 85% RH (25 °C) for 10 h. The RH was then reduced to 80%. 101

Figure 3.17 Moisture sorption and desorption by amorphous sucrose at 57 (blue) and 75% (red) RH (25 °C). 101

Figure 3.18 Headspace relative humidity in three mannitol-sucrose lyophiles stored at 40 °C (left y-axis). The lyophile water content (right y-axis) was determined by KFT (mean ± SD; n=3). . 102

Figure 3.19 Overlay of XRD patterns of lyophilized mannitol-sucrose (4:1 w/w) -in sealed vials, measured after storage at 40 °C for different times. A new vial was withdrawn at each time point. One characteristic peak of each phase is pointed out. 102

Figure 3.20 Headspace relative humidity in three vials of mannitol-sucrose (4:1) lyophiles stored at 40 °C (left y-axis). Right y-axis represents MHH content (blue bars; 17.9 °2θ peak) or crystalline

sucrose content (purple bars; 11.7 °2θ peak). The highest intensities of MHH (17.9 °2θ) and sucrose (11.7 °2θ) peaks at the start and at the end of the experiment respectively were assigned to be 100%, and the rest are expressed as relative intensities. 103

Figure 4.1 XRD patterns of lyophiles of (i) Mannitol 5% w/v (ii) BSA (2 mg/mL) + mannitol (5% w/v) (iii) mannitol: sucrose (4:1, 5% w/v) (iv) BSA (1 mg/mL) + mannitol:sucrose (4:1, 5% w/v) (v) BSA (2 mg/mL) + mannitol:sucrose (4:1, 5% w/v) and (vi) BSA (5 mg/mL) + mannitol:sucrose (4:1, 5% w/v). 116

Figure 4.2 XRD patterns of lyophiles of (i) HSA (2 mg/mL) + mannitol: sucrose (4:1, 5% w/v), 2 mL fill in 10 mL vial. For all the other samples, the fill volume was 7 mL in 10 mL vial. (ii) HSA (2 mg/mL) + mannitol: sucrose (4:1, 5% w/v) (iii) HSA (5 mg/mL) + mannitol: sucrose (4:1, 5% w/v) (iv) HSA (10 mg/mL) + mannitol: sucrose (4:1, 5% w/v) (v) HSA (25 mg/mL) + mannitol: sucrose (4:1, 5% w/v) and (vii) HSA (50 mg/mL) + mannitol: sucrose (4:1, 5% w/v). 117

Figure 4.3 XRD overlay of BSA (2 mg/mL) with mannitol (5% w/v). The lyophiles were stored (in sealed vials) in a 40°C oven until the time of measurement. The characteristic peak of MHH (17.9° 2θ) is highlighted with a red dashed line. MHH completely dehydrated within 5 days and MHH → β-mannitol transition was observed following its dehydration. 121

Figure 4.4 XRD overlay of BSA (2 mg/mL) with mannitol:sucrose (4:1, 5% w/v). The lyophiles were stored (in sealed vials) in a 40°C oven until the time of measurement. The characteristic peak of MHH (17.9° 2θ) is highlighted with a red dashed line. MHH was retained in the lyophile until day 90 at 40°C. 122

Figure 4.5 Size exclusion chromatography results lyophiles of (i) BSA (2 mg/mL) (ii) BSA (2 mg/mL) + mannitol (5% w/v) (iii) BSA (2 mg/mL) + mannitol:sucrose (4:1, 5% w/v) and (iv) BSA (2 mg/mL) + sucrose (2% w/v). The lyophiles (sealed vials) were stored at 40°C for 90 days. . 124

Figure 4.6 The XRD patterns obtained during the different stages of drying. The prelyophilization solution contained HSA (2 mg/mL) along with mannitol and sucrose (4:1, 5% w/v). The freezing and annealing details are provided in Table 1 (common for all three cycles). Primary drying was conducted at 10°C for 24 hours followed by secondary drying, first at 40°C for 24 hours and then at 50°C for 6 hours. Vials were removed at different time points using a sample thief, both during primary and secondary drying. 126

Figure 4.7 XRD overlay of lyophiles obtained by freeze-drying solutions containing HSA (2 mg/mL) in mannitol:sucrose (4:1, 5% w/v). Table 1 contains the cycle parameters. The lyophile water content at the end of Cycles 1, 2 and 3 were 3.5, 2.5 and 2.3% w/w respectively..... 129

Figure 4.8 XRD overlay of lyophiles obtained by freeze-drying (cycle 1) solutions containing HSA (2 mg/mL) in mannitol: sucrose (4:1, 5% w/v). The sealed vials were stored at 40°C and XRD patterns were collected at day 7 and 14. MHH completely dehydrated and sucrose crystallization was observed in 7 days. Dotted blue lines are sucrose reference peaks and the characteristic MHH 17.9 °2θ peak is highlighted by a solid (red) line. 129

Figure 4.9 Overlay of synchrotron XRD patterns of HSA lyophile obtained using Cycle 3. The lyophile was held at 40°C/55% RH for 10 hours and XRD patterns were collected at 5 minute intervals. The reference patterns for sucrose are shown as dotted blue lines. The calculated patterns of β-,δ- mannitol and MHH are included for reference. 133

Figure 4.10 Relative intensities of 17.9° 2θ peak of MHH, 14.0° 2θ peak for β-mannitol and 11.6° 2θ peak for sucrose plotted as a function of function of time for lyophilized HSA (2 mg/mL) with mannitol:sucrose (4:1, 5% w/v) heated at 40°C and 55% RH for 10 hours. The data points are connected for visual aid to track the dehydration of MHH, crystallization of β-mannitol and sucrose. 134

Figure 4.11 Moisture sorption-desorption behavior of mannitol-sucrose-HSA lyophile (from cycle 3). The lyophile was exposed to 20°C/0% RH for 120 minutes followed by 40°C/55%RH for 70 hours. The primary y-axis indicates the weight change (%) as a function of time indicated by a black curve. The secondary y-axis indicates the temperature as shown by the blue dotted line. 135

Figure 4.12 XRD, KFT and SEC of lyophilized HSA (2 mg/mL) with mannitol:sucrose (4:1, 5% w/v) exposed to 33% RH/RT. Left y-axis shows average aggregates (%) or water content (wt %) and right y-axis shows relative peak intensity* of MHH (XRD peak at 17.9 °2θ) plotted as a function of time. Individual vials from the same batch were pulled at different time points and stored at -20°C until analyzed. 138

Figure 4.13 XRD, KFT and SEC of lyophilized HSA (2 mg/mL) with mannitol:sucrose (4:1, 5% w/v) exposed to 55% RH/RT. Left y-axis shows average aggregates (%) or water content (wt %) and right y-axis shows relative peak intensity* of MHH (XRD peak at 17.9 °2θ) or sucrose** plotted as a function of time. Individual vials from the same batch were pulled at different time points and stored at -20°C until analyzed. 139

Figure 4.14 XRD overlay of lyophiles obtained by freeze-drying (cycle 2) solutions containing HSA (2 mg/mL) in mannitol: sucrose (4:1, 5% w/v). The sealed vials were stored at 40°C and XRD patterns were collected at day 7 and 15. MHH was retained for 15 days. The stick pattern for sucrose reference pattern is highlighted by the solid (pink) lines whereas the characteristic 17.9 2θ peak is highlighted by a dotted (red) line. 142

Figure 4.15 XRD overlay of lyophiles obtained by freeze-drying (cycle 3) solutions containing HSA (2 mg/mL) in mannitol: sucrose (4:1, 5% w/v). The sealed vials were stored at 40°C and XRD patterns were collected at day 5, 10 and 15. MHH was retained for 15 days. The stick pattern for sucrose reference pattern is highlighted by the solid (pink) lines whereas the characteristic 17.9 2θ peak is highlighted by a dotted (red) line. 142

Figure 4.16 DSC of fresh (day 0) M:S 4:1 + 2 mg/mL HSA (Cycle 2) lyophile. Sample was cooled in a hermetically sealed pan from RT to -30°C and heated to 230°C at 10°C/min. The inset highlights the region with glass transition temperature. 143

Figure 4.17 DSC of M:S 4:1 + 2 mg/mL HSA (Cycle 2) lyophile. The lyophile was exposed to 40°C/55%RH for 30 minutes. Sample was cooled in a hermetically sealed pan from RT to -30°C and heated to 230°C at 10°C/min. The inset highlights the region with glass transition temperature. 143

Figure 4.18 Glass transition as a function of water content for sucrose. These values were calculated from the equation $y = 62.859 – 746.96x + 1684.2x^2 – 1862.1x^3$ derived by Yu et al. [134] 144

Figure 4.19 XRD overlay of lyophiles obtained by freeze-drying (cycle 3) solutions containing HSA (2 mg/mL) in mannitol: sucrose (4:1, 5% w/v). The sealed vials were stored at RT/55%RH°C and XRD patterns were collected at regular intervals for up to a month. MHH completely dehydrated in one day while sucrose crystallization was observed starting from day 6. The stick pattern for sucrose reference pattern is highlighted by the dotted (pink) lines whereas the characteristic 17.9 2θ peak is highlighted by a solid (green) line. 144

Figure 5.1 Overlaid DSC heating curves for four different mannitol-sucrose ratios (1:4, 1:2, 1:1 and 2:1) with a solute concentration of 5% w/v. Panel A. The solutions were initially cooled from room temperature to -40°C at 10°C/minute held for 5 minutes and heated to 15°C at 10°C/minute. Only the heating curves are shown. Panel B. Shows a magnified region with Tg' and crystallization exotherm for mannitol-sucrose 2:1 solution from panel A. Panel C. The solutions were initially cooled from room temperature to -40°C at 5°C/minute held for 5 minutes and heated to 15°C at

5°C/minute. Only the heating curves are shown. Panel D. Shows a magnified region with Tg' and crystallization exotherm for mannitol-sucrose 2:1 solution from panel C. 153

Figure 5.2 DSC heating curves for mannitol-sucrose 2:1 ratio with a solute concentration of 5% w/v. Panel A. DSC cooling curve from room temperature to -40°C. The cooling rate was 0.5°C/minute and sample was held at -40°C for 5 minutes. The cooling curve shows an initial exotherm for ice crystallization followed by an additional exotherm. The exotherm at -23°C was attributed to partial mannitol crystallization (inset A). Panel B. DSC heating curve from -40°C to 25°C. The heating rate was 0.5°C. A glass transition was observed at -35°C followed by a crystallization exotherm at -25.0°C (inset B) 154

Figure 5.3 Overlaid DSC heating curves for four different mannitol-trehalose ratios (1:4, 1:2, 1:1 and 2:1) with a solute concentration of 5% w/v. Panel A. The solutions were initially cooled from room temperature to -40°C at 10°C/minute held for 5 minutes and heated to 15°C at 10°C/minute. Only the heating curves are shown. Panel B. Shows a magnified region with Tg' and crystallization exotherm for mannitol-trehalose 2:1 solution from panel A. Panel C. The solutions were initially cooled from room temperature to -40°C at 5°C/minute held for 5 minutes and heated to 15°C at 5°C/minute. Only the heating curves are shown. Panel D. Shows a magnified region with Tg' and crystallization exotherm for mannitol-trehalose 2:1 solution from panel C. 155

Figure 5.4 Mannitol-trehalose 2:1 composition. DSC heating curve from -40°C to 25°C at 0.5°C/min. The inset shows glass transition and crystallization exotherm from -40 to -20°C. The sample was cooled from room temperature to -40°C at 0.5°C/min (cooling curve not shown). . 156

Figure 5.5 DSC heating curves for mannitol-trehalose 3:1 (A) sample was cooled to -20°C at 0.5°C/min held for 2 minutes and further cooled to -60°C at 5°C/min. The frozen sample was heated to 20°C at 5°C/min. Only the heating curve is shown in the figure. (B) sample was cooled to -20°C at 0.5°C/min held for 2 hours and further cooled to -60°C at 5°C/min. The frozen sample was heated to 20°C at 5°C/min. The heating curve in the figure shows the presence of only glass transition event. 157

Figure 5.6 In situ synchrotron XRD patterns for mannitol-trehalose (3:1, 5% w/v) solution. Panel A shows overlays of XRD patterns during cooling from 5°C to -40°C; the solution was frozen from room temperature to -45°C at 1°C/min and held at -45°C for 10 minutes followed by heating the samples back to room temperature at 1°C/min. Mannitol hemihydrate reference pattern is shown at the bottom of the overlays 160

Figure 5.7 In situ synchrotron XRD patterns for mannitol-trehalose (3:1, 5% w/v) solution. Panel B shows overlays of XRD patterns during heating from -45°C to 2°C at 1°C/min; mannitol hemihydrate and δ-mannitol reference patterns are shown at the bottom of the overlays. 160

Figure 5.8 Graphical representation for mannitol:trehalose 3:1 (A) Change in glass transition temperature as a function of annealing time at -20°C (B) Change in heat capacity associated with glass transition temperature as a function of annealing time at -20°C. 163

Figure 5.9 In situ synchrotron XRD patterns for mannitol-trehalose (3:1, 5% w/v) solution during cooling. Panel A shows overlays of XRD patterns during cooling from 5°C to -40°C; β-mannitol reference pattern is shown at the bottom of the overlays. The solution was frozen from room temperature to -12°C, held for 2 hours further cooled to -45°C at 1°C/min and held at -45°C for 10 minutes. 165

Figure 5.10 Insitu synchrotron XRD patterns for mannitol-trehalose (3:1, 5% w/v) solution during heating. Panel B shows overlays of XRD patterns during heating from -45°C to 2°C. The frozen solution was heated from -45°C back to room temperature at 1°C/min. β-mannitol reference patterns are shown at the bottom of the overlays. 165

Figure 5.11 Size exclusion chromatography results for 1 mg/mL HSA with (i) 5% w/w Mannitol (ii) 5% w/w Sucrose (iii) 5% w/w mannitol-sucrose 1:1 (iv) 5% w/w mannitol-sucrose 3:1 (v) 5% w/w Trehalose (vi) 5% w/w mannitol-trehalose 1:1 and (vii) 5% w/w mannitol-sucrose 3:1. One set of formulations were cooled from room temperature to -45°C and held for 30 minutes at -45°C and reheated back to room temperature at 1°C/min, these formulations were labelled as 'unannealed'. Another set of samples were cooled to -20°C held for 2 hours and further cooled to -45°C and reheated back to room temperature at 1°C/min, these formulations were labelled as 'annealed' 171

Figure 5.12 Mannitol-trehalose 2:1 composition. DSC cooling curve from 25°C to -40°C at 0.1°C/min shows ice crystallization exotherm at -4.5°C followed by mannitol crystallization exotherm at ~ -17°C. The inset highlights the exotherm that was observed during cooling. 172

Figure 5.13 Mannitol-trehalose 3:1 composition. DSC cooling curve from 25°C to -40°C at 0.1°C/min shows ice crystallization exotherm at -4.5°C followed by mannitol crystallization exotherm at ~ -17°C. The inset highlights the exotherm that was observed during cooling. 173

Figure 5.14 Mannitol-trehalose 3:1 composition. Sample was cooled to -60°C at 5°C/min and held for 5 minutes. The frozen solution was then heated to -37°C at 5°C and held for 2 hours. The

annealed sample was cooled back to -60°C at 10°C/min and reheated to 15°C at 5°C/min. Only the final heating curve is shown. 173

Figure 6.1 Schematic representation of LDH aggregation behavior in presence of crystallizing and non-crystallizing buffer salts during freeze-thawing 175

Figure 6.2 Schematic representation of the use of mannitol and an isothermal hold step to generate homogeneous freeze-concentrate represented by a single glass transition (Tg'). 178

Chapter 1 Introduction

Therapeutic proteins have gained significant attention since the development of human insulin, the first recombinant DNA derived protein [2]. Drug products developed using proteins are a primary driver for growth in the biopharmaceutical industry and used for a variety of indications, including but not limited to cancers, autoimmunity and genetic disorders. The protein therapeutics market is expected to be worth $290 billion by 2027 at a compounded annual growth rate of ~ 6.8 %, according to a research report by Market Research Future [3]. Monoclonal antibodies (mAb's) contribute to the majority of the biotherapeutic sales along with recombinant proteins and vaccines with newer modalities such as antibody-drug conjugates, biosimilars, cell and gene therapy, siRNA and others, in the research and development pipeline [4]. A large fraction of marketed biotherapeutics are administered parenterally. From a manufacturing and development as well as economic standpoint, a solution formulation is preferred. However, given the marginal stability of proteins, freeze-drying is commonly used to develop proteins as dry solids [5]. Currently, 50% of marketed therapeutics are freeze-dried thus representing a common formulation strategy [6].

1.1 Protein structure

For a formulation scientist, one of the key goals is to stabilize the protein in its native state to achieve long-term stability. However, prior to discussing the rationale for stabilizing protein drug substances into viable drug products, it is important to understand the protein structure. The structure and orientation of a protein plays a significant role in its function.

The first step in protein synthesis is the formation of a primary structure, which is a series of amino acids forming a linear polypeptide chain. The primary structure is formed from a reservoir of 20 different naturally occurring amino acids and constitutes the backbone of proteins. The individual amino acid side chains in the primary structure will have a combination of hydrophilic and hydrophobic charged functional groups. In an aqueous environment, the hydrophobic functional groups will fold to minimize interactions with water leading to a compact structure, while the hydrophilic groups will interact by hydrogen bonding. The linear primary structure folds via weak noncovalent interactions such as van der Waals, coulombic electrostatic or hydrogen bonds, which are responsible for the secondary structures. The commonly known secondary structures are α-helix or β-pleated sheets. The secondary structures pack together to form a highly folded three-dimensional structure which is stabilized by a combination of hydrophilic and hydrophobic interactions.

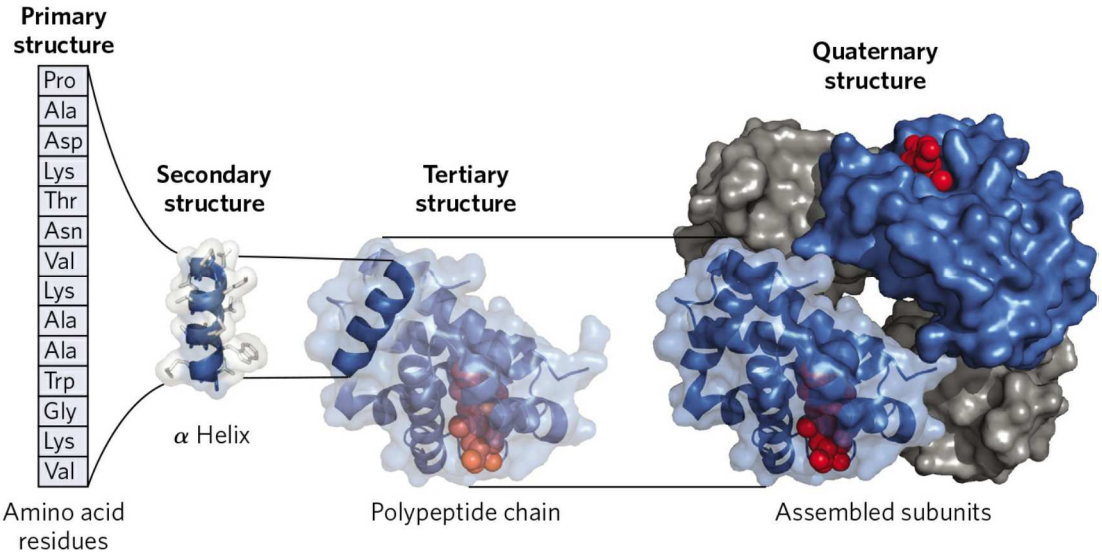

Figure 1.1 Levels of structure in proteins the quaternary structure of the multi-subunit protein, in this case hemoglobin [7].

The driving force for the compact packing of the tertiary structure is to minimize the non-polar interactions between the hydrophobic side chains and water while maximizing the weak interactions between polar groups. The interactions between polar groups and water are critical in stabilizing the tertiary structure. Hence, even in the solid state, proteins are surrounded by water molecules known as bound water. In many cases, proteins are made of more than one tertiary structure known as subunits to form higher order protein complexes called quaternary structures. Figure 1.1 shows an example of the hemoglobin quaternary structure formed from four tertiary subunits. The folded structure with the minimum free energy in a given set of environmental conditions is called the native state. Although a number of interactions at molecular level are required to form the native, the chief forces maintaining the protein structure are weak interactions. Therefore, a small perturbation to the native protein can lead to conformational changes. Conformational changes can result in unfolding and exposure of the hydrophobic groups to the aqueous

environment followed by destabilization. This suggests that proteins have marginal stability under physiological conditions.

The energy barrier for a native protein to unfold can be characterized by its free energy of unfolding (ΔG_{unf}). Under physiological conditions, the free energy difference between the native (biologically active) and unfolded (inactive) protein conformation can be very low (~5 to 20 kcal/mole) [8]. In case of therapeutic proteins, external environments such as pH, temperature, manufacturing unit operations can induce protein instability.

1.2 Challenges with protein stability

Protein instability can broadly be classified into chemical and physical instability [8, 9]. Chemical instability refers to the formation or breakage of covalent bonds leading to deamidation, oxidation, and disulfide bond shuffling. On the other hand, physical instability occurs due to alterations in the native state and cause protein unfolding, resulting in aggregation. Aggregation is a phenomenon that involves the transformation of the folded native state to an unfolded state which can associate and further precipitate [10, 11]. A schematic representation of the pathways and inter-relationships between protein unfolding and aggregation are shown in Figure 1.2. Aggregation of the non-native or partially unfolded molecules is mostly irreversible. These irreversible aggregates (either soluble or insoluble) often occur in the manufacturing process and are a cause for immunogenicity once administered. In addition, the term 'self-association' refers to higher order structures of the native or non-native molecules which are reversible in nature and tend to revert to its native state. The reversibility in certain proteins increases with concentration [12, 13].

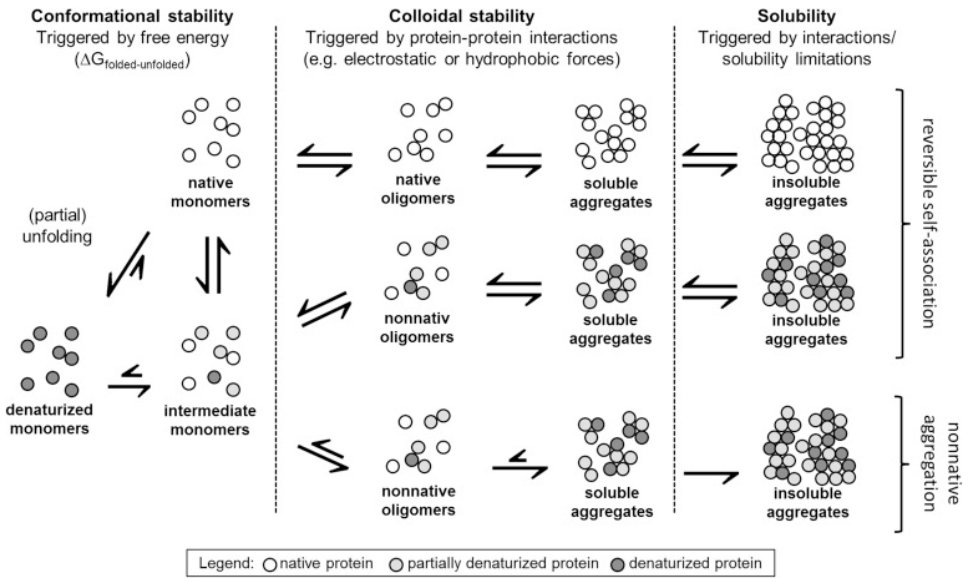

Figure 1.2. Mechanisms and inter-relationships of protein unfolding, self-association, and aggregation [13].

Physical instability can further be divided into conformational and colloidal instability (Figure 1.2). The aggregation that results due to the inherent structure of the native protein is referred to as conformational instability. Denatured protein or intermediate monomers are formed due to the partial unfolding of the native protein. These intermediate monomers associate with each other to form oligomers (higher order structures) and precipitate to form either soluble or insoluble aggregates. However, conformational stability alone cannot prevent aggregation due to changes in pH, salt concentration and ionic strength.

In addition to changes in the native state of individual protein molecules, repulsive and attractive interactions between proteins (native or partially unfolded) themselves can result in the formation of oligomers. Instability is governed by weak interactions such as electrostatic, van der Waals and in some cases hydrogen bond interactions are referred to as colloidal instability. The driving forces for these intermolecular interactions are the

overall charge distribution and hydrophobicity on the protein surface. Electrostatic interactions (F) between two charged protein molecules (x and y) are given by Coulomb's law, stated by the equation $F = k (q_x q_y / r^2)$. Where q_x and q_y, represent the type and quantity of charge on molecules x and y, respectively, while r represents the distance of separation between the two molecules. The symbol k is the coulomb's law constant. When the charged protein molecules x and y are surrounded by water in presence of buffer or salt species, the F is modified because of the net electric field because of the combined effect of the ensemble of positively and negatively charged species. The length scale over which the molecules (x and y) can feel the attractions or repulsions is dictated by the distance between the two surfaces (Figure 1.3). Consider two isocharged molecules (x and y) are separated by distance r, as they start to approach each other from point a (on the x-axis). They need to overcome an energy barrier given by ΔW_1 at point b to physically interact with each other. If the molecules overcome the energy barrier the attractive interactions dominate leading to aggregation. If the molecules cannot overcome the energy barrier, they remain separated as dispersed particles. The magnitude of the energy barrier is modulated by the buffer and salt concentrations. The higher the energy barrier the more dispersed are the molecules.

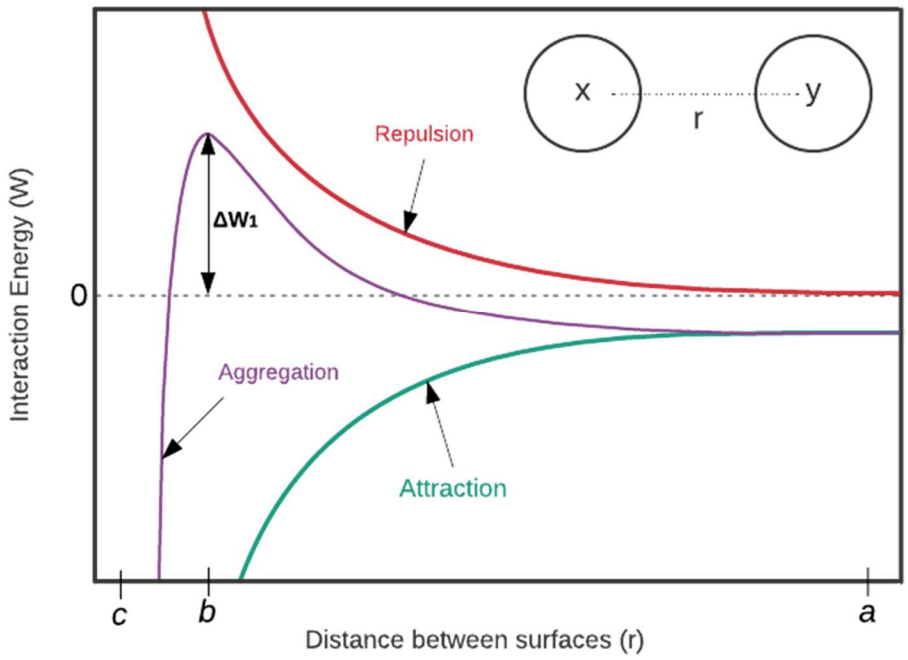

Figure 1.3 Electrostatic interactions as a function of the distance between two charged protein molecules [8].

One of the critical solution parameters that result in physical instability is the solution pH. The pH (buffer type and concentration) of the solution has a strong influence on protein stability. Proteins are retained in the native state over very narrow pH ranges and aggregate as soon as the solution pH is outside these ranges [8]. Every protein has a characteristic isoelectric point (pI). The pH at which the total charge on the protein molecule is zero is called pI. At pH far removed from the pI, the net charge on the protein can either be positive or negative and dictate the aggregation behavior of proteins. The solution pH determines the overall charge distribution on the protein surface, type (positive or negative) as well as magnitude. In case of folded proteins which are highly charged, repulsive interactions dominate. The increase in the magnitude of the charges as a function of acidity or basicity

of the solution will result in increased repulsion and unfolding of the protein. The protein unfolds to achieve a state of lower electrostatic free energy [14]. Optimization of solution pH and selection of appropriate buffer is therefore a critical step in formulation design [8, 15].

Physical instability, conformational as well as colloidal, along with chemical instability can occur simultaneously or can also lead to each other. Along with formulation variables, several manufacturing unit operations are also known to impact protein stability. The factors affecting physical stability are briefly summarized in the next section.

1.3 Fill-finish unit operations

The protein drug substance (DS) undergoes a series of complex fill and finish unit operations as it is formulated into a drug product (DP) for commercial use [16]. The bulk protein DS is manufactured in batches and is often stored in the frozen state for long durations before being formulated into DP. The DP can either be a solution or a freeze-dried formulation. Thus, freezing and freeze-drying are two processes routinely encountered in the use and manufacture of biopharmaceuticals. Freezing reduces the degradation rate of the drug substance by immobilizing the protein in a frozen matrix, protects against microbial contamination or growth and enables efficient transport without the risk of agitation and air-liquid interface-induced denaturation [16, 17]. Although the frozen storage as well as lyophilization are intended to stabilize the protein, stresses encountered during these processes such as cryoconcentration, phase separation, pH shift, changes in ionic strength and exposure of new interfaces are known to result in protein instability (discussed later).

In order to stabilize the protein against these stresses, a common strategy is to add excipients to these formulations [5]. Some of the excipients used in protein formulations include sugars (sucrose, trehalose), sugar-alcohols (mannitol), surfactants (polysorbates) and amino acids among others [18]. An understanding of the physico-chemical fundamentals during freezing, stresses involved and the mechanisms by which excipients enable stable protein is critical to design a successful biotherapeutic formulation.

1.4 Processing induced stresses and stabilization mechanisms by excipients

The stresses to which a protein is exposed during the freezing and drying steps of freeze-drying are generally considered together. Both processes involve removal of water, such as by ice crystallization during freezing and by sublimation/desorption during drying. However, there is a subtle difference with respect to the unfrozen water associated with the solutes during each step. While the unfrozen water is retained in the freeze-concentrate during freezing, the process of drying leads to its removal. As a result, the stresses experienced by a protein during these steps are fundamentally different[19]. Hence in this introduction, the stresses and their prevention by excipients during the freezing step and frozen storage are grouped together while those during drying and storage are discussed separately.

1.4.1 Freezing and frozen storage

The freezing stage conceptually involves two mutually non-exclusive physical events, namely supercooling and ice crystallization, resulting in the formation of a maximally freeze-concentrated solution (Figure 1.4). Accordingly, the stresses experienced by protein

and the possible mechanisms by which the excipients stabilize the native protein state during each event can be distinguished [8].

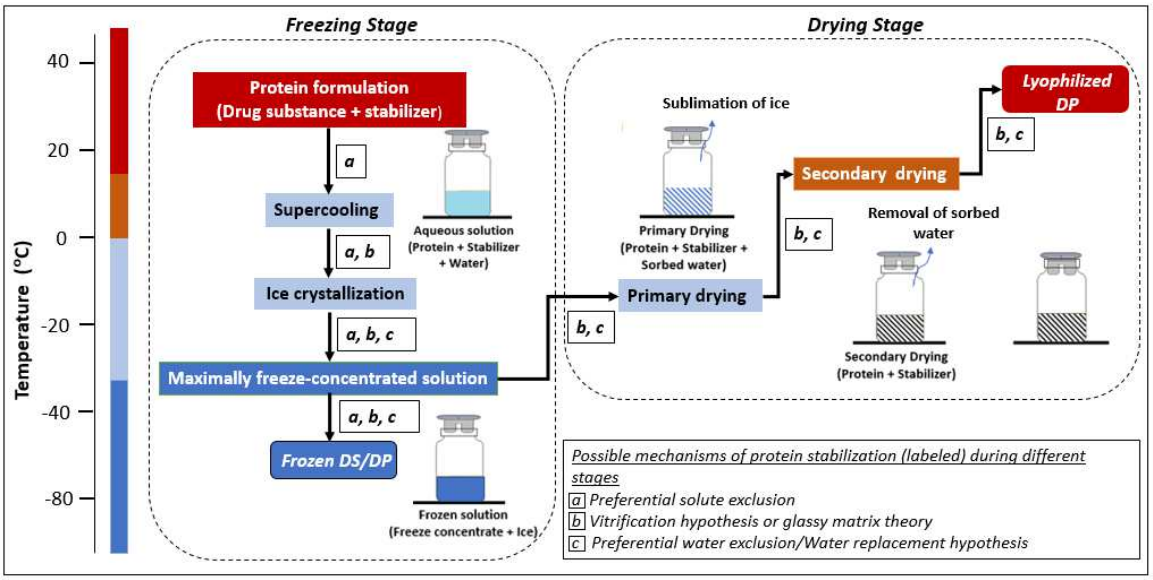

Figure 1.4. Typical steps involved in lyophilization of biologics. The y-axis represents temperature (color-coded). The temperature range, during different stages of freeze-drying, broadly follows the color scheme. Rectangles with sharp corners represent intermediate stages while rectangles with rounded edges represent the final product. The alphabets adjacent to the arrows represent the predominant mechanisms of protein stabilization during each stage (more details in the text). All the solutes are assumed to remain amorphous, both in the frozen DS/DP and lyophilized DP. A typical freeze-drying process consists of three stages: freezing, primary drying, and secondary drying. Freezing is an efficient desiccation step where most of the solvent is separated from the solutes to form ice. As freezing progresses, the solute phase becomes highly concentrated and is termed the 'freeze concentrate'. During primary drying, ice is transferred from the product to the condenser by sublimation. The primary drying stage is generally the longest and its optimization has a large impact on process economics. During secondary drying, water is desorbed from the freeze concentrate, usually at elevated temperatures and low pressures. Secondary drying normally takes only a few hours. Typically, drying is conducted below Tg' (glass transition temperature of the freeze-concentrate) during primary drying and below Tg (glass transition temperature of the lyophile) during secondary drying [1].

Supercooling. When a solution containing the DS and excipients is cooled, spontaneous ice crystallization may not be observed, and the system tends to supercool. This situation generally persists up to -10 to -12 °C in the case of uncontrolled freezing[20]. The factors determining the degree of supercooling include cooling rate and the type and concentration of solutes. Cold denaturation is the process by which protein DS can denature due to unfolding at low temperatures prior to ice crystallization. However, cold denaturation is

not a major concern during freeze drying [21, 22]. Protein unfolding is relatively slow when compared to the timescales of freeze-drying. Interestingly, the presence of additives (such as sucrose and trehalose) and high protein (β-lactoglobulin) concentration, lower the cold denaturation temperature [23].

Ice crystallization and freeze-concentration. Further lowering of temperature eventually induces the formation of ice nuclei followed by crystal growth. Ice crystallization creates ice-water and ice-air interfaces which can induce stress leading to protein destabilization [24, 25]. Water removal (as ice) concentrates the solution (containing the solutes dissolved in the unfrozen water) in the interstitial region, and may alter its ionic strength, viscosity and pH. Additionally, in multicomponent systems, this process may lead to separation of phases differing in their solute composition. The associated changes have the potential to destabilize the proteins [16, 21, 22].

Rate of cooling: The processing parameters that have a direct impact on the freezing stage are the cooling rates as well as formulation composition. The cooling rate should be considered in the context of the time required for a solution to freeze i.e., transition from solution to supercooled to glassy state as described earlier and should not be referred to as the drop in the shelf temperature over time [26]. The rate of cooling, fast or slow, can vary based on the solute concentration, volume, type and orientation of the container as well as the process used to freeze the drug substance (controlled vs uncontrolled freeze-thaw equipment) [23]. These factors can indirectly impact the nature of ice interface created [26]. A faster cooling rate can result in a higher degree of supercooling followed by sudden and abrupt formation of many small ice crystals with a higher surface area. Slow or progressive

cooling leads to ice formation earlier in the process followed by its growth and hence lower surface area [21, 26].

Frozen storage. As mentioned above, biologics are often stored frozen. The product is often stored in large containers and the cooling rate can be uncontrolled. The optimal storage temperature can be determined by characterizing the protein before and after storage at different temperatures [16]. In the context of frozen storage, the stresses due to: (i) freezing and thawing, and (ii) extended storage in the frozen state mandate careful consideration. A wide variety of chemically diverse compounds, known as cryoprotectants, can protect proteins from freezing-induced stresses. Multiple mechanisms have been proposed to explain their stabilizing effects in frozen systems.

1.4.2 Mechanism of stabilization by excipients

Preferential exclusion (also known as solute exclusion or preferential hydration): In aqueous solutions, the water molecules interact with the polar groups on the protein surface making the protein preferentially hydrated. In the initial stages of the freezing process, the cryoprotectant molecules are selectively excluded from the immediate vicinity of the protein surface. This exclusion of solute molecules increases the free energy of unfolding (ΔG_{unf}), thus favoring and stabilizing the native state (Figure 1.5) [19].

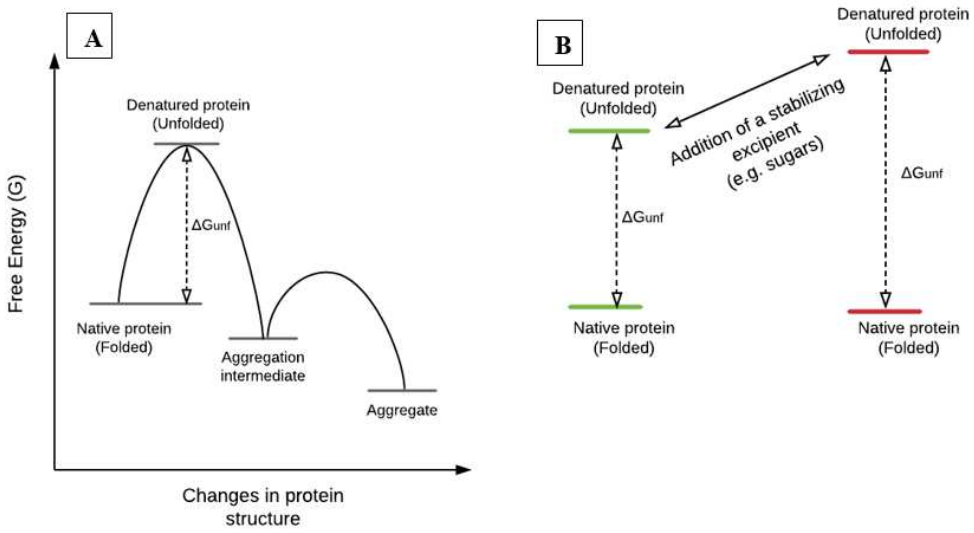

Figure 1.5. Schematic representation of (A) changes in protein structure (native to aggregate) on arbitrary free-energy y-axis. The energy barrier (ΔG_{unf}) is shown with dotted lines. (B) The increase in ΔG_{unf} after addition of a stabilizer representative of preferential exclusion mechanism [8].

Addition of a stabilizer such as sucrose was shown to reduce the aggregation rate of two different proteins INF-γ and GCSF [15]. Sucrose thermodynamically stabilizes the native state by preferential exclusion and increases the ΔG_{unf} thus preventing aggregation. Addition of excipients that favor the native state by preferential exclusion is a commonly used strategy to stabilize the proteins based on the pioneering work from Timasheff et al. [27].

*Vitrification hypothesis (*or glassy matrix theory): Ice crystallization and freeze-concentration eventually drives the system to approach a glassy state having restricted mobility. The presence of cryoprotectants such as sugars and polymers result in an increase in viscosity of the freeze concentrate, which reduces molecular mobility, thereby slowing down all dynamic processes. The protein becomes virtually immobilized. Since mobility is a pre-requisite for denaturation and degradation reactions, the restricted mobility in the

glassy state makes the protein relatively stable in the timescales of practical interest in freeze-drying [22, 28].

Water replacement (substitute) hypothesis (or preferential solute interaction): As a result of freeze concentration, sufficient water molecules may not be available to adequately hydrogen bond with the polar protein surfaces. This allows selective interaction of solutes with the protein, suggesting another plausible mechanism known as the *water replacement (substitute) hypothesis* or 'preferential solute interaction' [29]. An investigation on cryopreservation of cells using *in situ* Raman suggested that the cryoprotective action of sucrose could be attributed to its direct interaction with the cell membrane [30]. It encompasses the concept that the hydroxyl groups (of the sugar) hydrogen bonds with the protein, thereby replacing hydrogen bonds between water and the protein. This replacement of hydrogen bonds enables the protein's native conformation to be maintained.

These mechanisms are proposed to be simultaneously involved for the stabilization of proteins during different steps of the freezing process (Figure 1). In particular, preferential exclusion is expected to be predominant in the initial stages of the freezing process, while vitrification and water replacement may take over as the solution freeze-concentrates [24]. For the stabilizer to be effective, it must be amorphous and a part of the freeze-concentrate.

1.4.3 Drying and Storage

During the drying stage of lyophilization, frozen water is removed by sublimation (primary drying) and non-frozen 'bound' water by desorption (secondary drying). Since hydrogen bonding between water and protein is critical to the thermodynamic stability of protein,

removal of water constitutes the major stress during drying and can cause irreversible loss of biological activity for some labile proteins [5]. Many effective cryoprotectants fail to retain their stabilizing effect during drying. Stabilizers that can protect the protein during drying as well as storage are often referred as lyoprotectants [28]. Furthermore, the physical state of the protein during both drying and storage is similar, with the only difference being the water content of the amorphous phase in these conditions. From this perspective, it is postulated that the fundamental mechanisms governing stability during drying also govern stability during storage of the dried product [28]. The additional stress factors during storage include unintended temperature excursions and excipient phase separation during the product shelf-life. In addition, protein degradation via chemical processes such as deamidation and oxidation is observed during storage [26]. The mechanisms of excipient-induced protein stabilization during drying and storage have some parallel with that of frozen storage. The two main mechanisms of stabilization during drying and storage are 'vitrification' and 'water replacement', which result in the preservation of the protein structure by reducing molecular mobility and preventing changes in protein structure respectively. Although the underlying mechanisms differ, both hypotheses require the protein and the stabilizer to be in the same amorphous phase [31, 32].

In addition, it is generally accepted that for effective stabilization, the protein and sugar must be in the same phase. The sugar can phase separate either by forming a distinct amorphous region or by crystallization. This process causes a loss of necessary interactions, coupled with the induction of stresses on the protein [5]. These mechanisms are not mutually exclusive, and it is often difficult to attribute stabilization to one specific

mechanism. However, an understanding of these mechanisms enables the formulator to try targeted approaches for designing stable drug products.

1.5 Characterization of excipient phase behavior and importance in protein stability

For stabilizers (cryo or lyoprotectants), it is important that they are retained in the same phase as the proteins (amorphous) throughout various stages of processing as well as during storage to ensure protein stability by the mechanisms mentioned above. However, there are several reports of inadvertent solute crystallization resulting in unstable protein [4, 18, 23]. The excipients that have shown crystallization on long-term frozen storage in presence of proteins at temperatures > T_g' include sorbitol and trehalose [33, 34]. In addition, freezing induced selective crystallization of buffer salt components can result in pH shifts in the freeze-concentrate, thus impacting protein stability [35-39]. Based on the buffer concentration, starting pH and presence of additional solutes, a number of buffers such as phosphate, succinate, histidine has been reported to show pH shifts. In addition, certain crystallizing excipients, amino acids (glycine) and sugar-alcohol (mannitol) are used in freeze-dried formulations as bulking agents. The solid form (anhydrous vs. hydrate) and phase behavior (crystalline vs. amorphous) in presence of other solutes and as a function of processing parameters dictate the success of the formulations.

Most of the protein formulations are multicomponent systems. Phase and state diagrams of individual excipients have been used to understand the excipient phase behavior in terms of its crystallization and eutectic temperatures or retention in the amorphous state and its glass transition temperatures. However, the behavior of protein formulations with multiple excipients can be highly complex [18]. Hence, it is critical to characterize and evaluate the

phase behavior of the excipients while simultaneously performing biophysical characterization of the proteins, both as a function of formulation composition as well as processing parameters (cooling rate, freezing, annealing, drying and storage). The use of advanced characterization techniques such as high intensity X-ray (synchrotron) as well as neutron scattering along with orthogonal techniques such as differential scanning calorimetry and biophysical techniques (dynamic light scattering and size exclusion chromatography) will help us develop deeper understanding of excipient-protein interactions. This in turn can be used in the rational selection of excipients and their concentration, as well as the processing parameters to develop robust formulations.

1.6 Objectives

Frozen state stabilization of proteins and other macromolecules is of immense interest to the pharmaceutical community. Currently, more than half of biotherapeutic products are stored in the frozen state and a large of fraction are manufactured in the dried state by freeze-drying [40]. These bulk drug substances are semi-formulated, for instance, with a buffer, surfactant, or sugar to protect the protein from freezing induced stress and ensure successful long-term storage. However, there are several reported cases of process and formulation induced instability [23]. Various factors such as cooling rate, excipient phase separation, and interactions at ice interfaces are known to cause protein aggregation in the long term. Successful bulk storage will result in efficient bioprocess capacity use on the large scale as well as reduce the overall cost of production [40]. While protein aggregation has been predominantly linked to stresses induced due to crystallization of solute, change in microenvironmental pH and ice interface denaturation, there is a lack of direct evidence

of any of these stresses leading to instability in the frozen state. As a result, there is incomplete understanding of the mechanism of stabilization by excipients. Therefore, there is a critical need for research that can help develop a comprehensive understanding in this area.

The aim of our research is to systematically understand the impact of solute crystallization, change in pH and ice interfaces on protein stability. These studies will facilitate the rational selection of excipient combinations and will lead to the development of stable and robust protein formulations. Moreover, the studies with respect to freeze-drying process will lead to an in-depth understanding of the complex interplay between process variables, excipients, primary packaging components, and the effect of storage conditions on drug product stability.

1.7 Thesis organization

This thesis is organized into four research chapters and a brief overview of the individual chapters is stated below:

Chapter 2

Our goal was to develop a fundamental understanding of the effect of buffer salt crystallization during freeze-thawing and its impact on protein conformational stability. Specifically, sodium phosphate buffers and associated 'pH shifts' due to selective crystallization of buffer components are known to impact protein stability. However, direct evidence of buffer crystallization on protein structure (conformational stability) has not been shown.

The overall objective was to elucidate the aggregation behavior of LDH *during* freezing and thawing. Lactate dehydrogenase (LDH, MW 144 kDa) with either crystallizing sodium phosphate (10 or 100 mM) or non-crystallizing histidine buffer (10 mM) was used as a model system. The aims of this work were to evaluate the effect of freezing and thawing stresses on lactate dehydrogenase (LDH) stability under three conditions. (i) In a solution buffered with sodium phosphate (NaP). The selective crystallization of disodium hydrogen phosphate during freezing caused a pronounced pH shift. (ii) In a solution buffered with histidine, where there was no pH shift due to buffer salt crystallization. (iii) At different concentrations of LDH to determine its self-stabilizing ability. The change in LDH tetrameric conformation was measured by small angle neutron scattering (SANS). The pH of the phosphate buffer solutions was monitored as a function of temperature to quantify the pH shift. The conditions of buffer component crystallization from solution were identified using low temperature X-ray diffractometry. Dynamic light scattering (DLS) enabled us to determine the effect of freeze-thawing on the protein aggregation behavior.

Chapter 3

This chapter focused on studying the solid-state of commonly used excipient combinations and the implications of temperature excursions on freeze-dried product stability. Mannitol is widely used as a bulking agent in freeze-dried formulations. When solutions containing mannitol and sucrose are freeze-dried, depending on the processing conditions and the formulation composition, mannitol can crystallize in the anhydrous forms (α-, β- and δ-forms), as mannitol hemihydrate (MHH; $C_6H_{14}O_6 \cdot 0.5H_2O$) or as a mixture of the two.

MHH is known to have a stoichiometric water content of 4.5 wt. %. The retention of MHH in the final lyophile, and its dehydration during product storage and the associated release of water could lead to instability of the final drug product. There was a gap in the literature with respect to the available knowledge of MHH dehydration behavior.

Our aim was to determine the influence of water vapor pressure on the kinetics of MHH dehydration and the implications on the physical stability of sucrose. Therefore, the lyophiles were exposed to a range of controlled relative humidities (RH) and the kinetics of MHH dehydration and sucrose crystallization were monitored by X-ray diffractometry. The second set of vials (rubber stoppers fitted with humidity/temperature sensor) were stored at 40°C, the headspace RH was continually recorded, and water content was determined by Karl Fischer titrimetry. We had two specific objectives. (i) To study the dehydration behavior of MHH in lyophiles prepared with or without sucrose. (ii) To determine the influence of MHH dehydration on sucrose crystallization. In our experiments, the physical forms of mannitol (and sucrose) were monitored following storage of the lyophiles at different water vapor pressures (at RT). The preliminary results led to the third objective. (iii) To study the dynamics of water movement in sealed vials by simultaneously monitoring headspace humidity and determining the physical form and the water content in the lyophile. Our attempts to comprehend the movement of water from the lyophiles necessitated the evaluation of the critical role of rubber stoppers in modulating the water vapor pressure in sealed vials.

Chapter 4

The conditions of formation of MHH due to processing and formulation variables are well established in the literature. The dehydration kinetics of MHH in presence and absence of sucrose were investigated in Chapter 3. However, the dehydration kinetics of MHH, in the presence of both sucrose and protein and its impact on protein stability has not been systematically evaluated. The overall objective of this study was to identify conditions (temperature and humidity) under which MHH can dehydrate on storage and the consequences of the released water on sucrose phase behavior and protein stability. In a mannitol-sucrose-protein lyophile, the purpose of this study was (i) to investigate the dehydration behavior of MHH, (ii) to determine the influence of dehydration on sucrose crystallization and (iii) the effect of moisture released due to MHH dehydration on model protein (bovine serum albumin, BSA or human serum albumin, HSA) aggregation. The phase behavior of MHH in mannitol-sucrose-protein lyophile as a function of relative humidity and temperature was monitored using X-ray diffractometry (synchrotron as well as laboratory source) and differential scanning calorimetry (DSC), water content was monitored using Karl-Fischer titrimetry (KFT) and protein stability was measured using size exclusion chromatography (SEC).

Chapter 5

Bulk proteins, when stored frozen, may be subjected to several freeze-thaw cycles before being formulated into a drug product. The protein solution composition and the freezing protocol may lead to incomplete ice crystallization in the frozen state. This can also result

in freeze-concentrate heterogeneity characterized by multiple glass transition temperatures. Multiple glass transitions theoretically suggest phase separation. While sugars have been extensively used for this purpose, and in general serve as cryoprotectants, their effectiveness is by no means universal. Our goal was to investigate the advantage of using a crystallizing excipient such as mannitol in combination with sugars (sucrose or trehalose).

We hypothesize that in frozen systems, mannitol crystallization during freezing can result in a homogeneous freeze concentrate (characterized by a single T_g'). We also hypothesize that complete mannitol crystallization can be accomplished by isothermally holding the solution during cooling. In other words, the goal of our work was to use a crystallizing excipient to promote ice crystallization and obtain a freeze-concentrate of consistent and constant composition. The addition of mannitol, a readily crystallizing excipient, will facilitate ice crystallization. Inclusion of an isothermal hold during cooling (annealing) maximized the mannitol crystallization resulting in a homogenous freeze-concentrate of a constant composition characterized by a single glass transition temperature. The role of cooling rate and annealing on both mannitol and ice crystallization were discerned using high intensity synchrotron radiation.

Chapter 2 Reversible Self-association in Lactate Dehydrogenase during Freeze-thaw in Buffered Solutions using Neutron Scattering*

*Reprinted with permission from (Sonje, J., Thakral, S., Krueger, S. and Suryanarayanan, R.(2021). Reversible Self-Association in Lactate Dehydrogenase during Freeze-Thaw in Buffered Solutions Using Neutron Scattering. Mol. Pharm., 18 (12), 4459-4474).

2.1 Introduction

Protein biotherapeutics have gained significant attention in recent years. Numerous proteins (drug substances) are stored in the frozen state, sometimes for prolonged time periods, before they are formulated as solutions or freeze-dried drug products [26]. The unique three-dimensional structure, known as the native, is responsible for the biologic activity of proteins. The native structure is a result of the overall non-covalent interactions which include electrostatic and hydrophobic interactions, hydrogen bonding, and van der Waals forces. In addition to the inter and intramolecular interactions, the stability of the native structure in solution is also influenced by the conformational entropy as well as external factors such as temperature, pH, protein concentration and presence of excipients[8]. The stresses encountered during both freezing and freeze-drying can destabilize the protein. Our current discussion will be restricted to protein destabilization in frozen systems. Several excipients can aid in stabilizing the protein and retain it in the native state. These include sugars, buffers, and surfactants, each with an intended role (functionality) in the formulation. Sugars (e.g., trehalose and sucrose) play a major role in stabilizing protein formulations. In order to exert their function, they have to be retained amorphous and resist crystallization [18]. The aggregation on long term frozen storage of a monoclonal antibody formulation was attributed to crystallization of trehalose [34]. Selective crystallization of

buffer components is also known to cause pH shifts. Many studies have indirectly shown that pH change can be detrimental to protein stability [35, 37, 41-43].

During the freezing process, cooling of an aqueous solution result in ice crystallization leading to concentration of excipients and protein. While some of the excipients may also crystallize, most excipients as well as the active ingredient (protein) also do not crystallize. Thus, ice crystallization leads to, among other things, a pronounced increase in ionic strength and viscosity. The ice crystallization and cryo-concentration induce stresses which can lead to protein aggregation[35, 44]. Additionally, there is a large body of evidence suggesting loss in protein activity due to its adsorption at the hydrophobic interfaces generated at the ice-water and ice-air interfaces[45]. In most investigations, the protein stability (specifically aggregation and activity) was evaluated before and after one or multiple (up to five) freeze-thaw cycles. Similar studies have also been conducted after the entire freeze-drying cycle by reconstituting the lyophile. Due to the limitations, both in analytical techniques and in molecular modelling, the stresses experienced by the proteins during cryo-concentration have not been thoroughly studied. However, in certain cases molecular dynamic simulation and design of experiment approaches can aid in estimating the degree of protein saturation in the freeze-concentrate, gain insight into the mechanism of unfolding and aggregation at the ice-air or ice-freeze concentrate interface as well as determine the optimum freezing rates which will result in maximum protein stability during the freeze-thawing processes [44, 46].

Among the numerous potential degradation pathways, aggregation is one of the most well-known and highly studied phenomena which can occur in diverse protein modalities

differing with respect to their conformations and molecular size. Non-native aggregation, conventionally referred to as aggregation, is the formation of oligomeric units as a result of the interactions either due to conformational changes or chemical modifications in the monomeric unit. Non-native irreversible aggregates have been extensively investigated and thoroughly characterized due the risks they pose, such as loss of efficacy and immunogenicity in protein biotherapeutics. However, a well-known but less studied behavior observed in many enzymes and some protein modalities is native and reversible aggregation. These reversible aggregates can be attributed to non-covalent interactions between the 'native' protein structures by a phenomenon referred to as 'reversible self-association'[47].

In order to evaluate destabilization during freezing, the conventional approach is to freeze-thaw the protein solution and characterize the analyte in the thawed solution. Our interest was to characterize the influence of excipients on the native protein conformation during the freezing and thawing processes. Small-angle neutron scattering (SANS) was an ideal technique for this purpose. It can provide information with respect to the size (on a length scale of 1 nm to 100 nm) and conformation of proteins in solution, when frozen and in the dried state [48]. In contrast to X-rays, neutrons are sensitive to light elements such as carbon, hydrogen, nitrogen and oxygen, which are the building blocks of proteins. They can differentiate between isotopes of many elements, especially hydrogen. The advantages offered by neutron scattering makes it a suitable technique to characterize proteins [48-50]. SANS has been used to study protein-protein interactions in two high-concentration monoclonal antibody (mAb) formulations. The higher viscosity of the mAb1 formulation

was attributed to attractive protein-protein interactions whereas charge repulsion dominated in case of mAb2, resulting in a lower viscosity [51]. SANS was also used to study protein (lysozyme) crowding in presence of sorbitol. Sorbitol was effective in reducing protein crowding in solution as well as in the freeze-concentrated states, thus protecting the protein from forming irreversible aggregates [50]. Contrast variation studies performed in lysozyme solutions containing glucose, trehalose and sodium chloride demonstrated the power of this technique to assess the protein structure in the frozen state. Irrespective of the starting excipient as well as protein concentration, a freeze-concentrate of constant composition was obtained wherein the lysozyme existed in the monomeric state. A second population of large, reversible (in the absence of high salt) aggregates at the ice-water (freeze concentrate) and/or ice-air interface was also observed [49].

Lactate dehydrogenase (LDH, Molar mass 144 kDa), a globular enzyme with a tetrameric native state and an isoelectric point (pI) of ~7.2, was chosen as the model protein. It is known to be sensitive to freezing stresses, specifically at low pH (< 5) values [52, 53]. LDH has been used as a model protein in several studies to determine the effect of freeze-thawing (freezing rates, buffer crystallization, effect of surfactants, etc).

When LDH solutions were prepared in phosphate buffer (sodium salt), frozen and thawed, there was pronounced protein aggregation [54]. The instability was attributed to the pH shift during freezing of the solutions. It is well known that sodium phosphate (NaP) buffer solutions, when cooled, can exhibit pH shifts of up to ~ 4 units due to the selective crystallization of disodium phosphate (one of the buffer components) [35]. While a pH shift during freezing appeared to be detrimental to proteins, a direct cause and effect relationship

between pH shift and protein instability has not been established. This can be done by charactering the system in the frozen state and again after thawing.

The LDH aggregation in frozen systems has also been attributed to adsorption on ice [55, 56]. As the surface area of ice increased (ice crystal size decreased), the effect was more pronounced [57]. LDH was shown to partially unfold at the ice-freeze concentrate interface and the unfolding decreased in presence of polysorbate 80 [56]. These observations were made on the cold stage of an infrared spectrometer. Interestingly, when LDH was frozen in presence of sucrose, a well-known and effective cryoprotectant, its activity was retained. The sucrose concentration was selected to prevent ice formation to a low temperature. In the absence of ice, even when cooled to low temperatures, LDH retained its activity and did not undergo cold denaturation [55].

It is important to recognize that in most, if not all of these studies, the LDH concentration was < 100 μg/mL. It is questionable whether these results can be extrapolated to higher protein concentration systems. In light of the recent interest in high-concentration protein formulations, it will be useful to evaluate the effect of these stresses when the protein concentration is increased. For example, LDH solutions at concentrations ≥ 1 mg/mL, can be considered "high concentration", since the aggregation was reversible. In other words, the protein demonstrated self-stabilization. A similar stabilization effect was observed in certain high-concentration mAb systems[47]. Thus, this effect may be observed in different modalities of proteins. In frozen solution, proteins are also known to exhibit a concentration dependent inhibition of excipient crystallization. For example, an albumin fusion protein inhibited the crystallization of mannitol, an excipient with a strong crystallization

propensity[58]. If the buffer salt crystallization is inhibited by the protein, then the potential detrimental effects due to pH shift would be avoided.

The first set of studies were conducted in solutions buffered with histidine. With this non-crystalizing buffer (pKa 6.0), we do not expect pronounced pH shifts during freezing. Therefore, any protein destabilization could be attributed to the stresses associated with freezing and thawing. The second set of studies were conducted with NaP buffer at two concentrations, 10 mmoles and 100 mmoles/L (mM). The buffer pKa of relevance (second pKa of ~6.8 at room temperature (RT)) is close to the isoelectric point of LDH (pI ~ 7.2), rendering it ideal for use in solutions at RT. However, NaP buffer solution, when cooled, is known to exhibit a pH shift due to selective crystallization of one of the buffer components. At 100 mM buffer concentration, a detrimental effect due to pH shift was observed in case of ribonuclease A. When a 100 mM NaP buffer with a starting pH of 6.4 was frozen from 25°C to -20°C in presence of ribonuclease A (1.5 mg/mL), the pH decreased to 4.3 as opposed to a pH drop to 4.6 in buffer alone system [59]. Even a higher protein concentration of 10 mg/mL (BSA or β-galactosidase) did not significantly attenuate the pH when the NaP buffer concentration was 100 mM [42]. Therefore, this buffer concentration was considered the "worst case" (negative control). Although a pH shift is observed when a 10 mM phosphate buffer is frozen, the presence of LDH, in a concentration dependent manner, is expected to inhibit buffer crystallization and attenuate the pH shift.

The overall objective of the study was to elucidate the aggregation behavior of LDH *during* freezing and thawing. The specific aims of the study were to evaluate the effect of freezing

stresses on LDH stability under three conditions: (i) In a solution buffered with NaP. The selective crystallization of disodium hydrogen phosphate during freezing is known to cause a pH shift. The magnitude of pH shift was altered by using two different concentrations of NaP buffer (10 mM and 100 mM). (ii) In a solution buffered with histidine (10 mM). In this system, there will be no pH shift due to buffer salt crystallization. (iii) At different concentrations of LDH to determine its self-stabilizing ability. These systems were subjected to multiple freezing and thawing. The protein behavior was characterized in real time using SANS, during freezing and thawing. Molecular modeling was used to determine the nature of the aggregates and thereby gain mechanistic insight into the aggregate reversibility.

While SANS was the predominant analytical technique, several orthogonal techniques were used. Native size and shape of LDH in NaP buffered solutions was also determined using small-angle X-ray scattering (SAXS). The pH of the NaP buffer solutions was monitored as a function of temperature to quantify the pH shift. The low-temperature powder X-ray diffractometry of these solutions enabled us to identify the conditions of buffer component crystallization from solution. Differential scanning calorimetry (DSC) allowed the measurement of the melting temperature of the NaP buffer solutions. Finally, dynamic light scattering enabled us to determine the effect of freeze-thawing on the protein aggregation behavior for LDH at different concentrations in NaP and histidine buffers.

2.2 Materials and Methods

2.2.1 Materials

Lactate Dehydrogenase (LDH) from rabbit muscle (Mw = 144 kDa) was obtained from Sigma-Aldrich (St. Louis, MO) at 5 mg/mL or 10 mg/mL as a suspension in 3.2 moles/L (M) ammonium sulphate (pH 6.0). Sodium phosphate heptahydrate, sodium phosphate dibasic monohydrate, L-histidine and L-histidine monohydrochloride were purchased from Sigma-Aldrich (St. Louis, MO).

Deuterium oxide, D_2O (99.9%), was purchased from Cambridge Isotope (Tewksbury, MA). Prior to SANS measurements, the LDH was dialyzed at 4 °C into either 10 mM histidine buffer containing 8% D_2O, 10 mM histidine buffer containing 100% D_2O, 10 mM NaP buffer containing 8% D_2O, or 100 mM NaP buffer containing 8% D2O. Before dialysis, LDH was diluted to 2 mg/mL or 3 mg/mL using the dialysis buffers. The dialysis was accomplished using 20KDa MWCO Slide-A-Lyzer mini dialysis devices (ThermoFisher Scientific, Waltham, MA) for 0.5 mL to 2.0 mL volume. Buffer was exchanged after 2 hours, and the samples were then left to dialyze overnight. The LDH as received was a turbid suspension, but the solution was clear following dialysis. LDH concentration was measured after dialysis using a Nanodrop® spectrophotometer (ThermoFisher Scientific, Waltham, MA) using an extinction coefficient at 280 nm of 1.9 mL/mg cm at 280 nm. Samples for SAXS measurements were prepared in 100 mM NaP buffer containing 0% D2O in a similar manner.

2.2.2 SANS Measurements

SANS measurements were performed on the NGB 30 m SANS instrument at the National Institute of Standards and Technology (NIST), Center for Neutron Research (NCNR) in Gaithersburg, MD26. The samples were loaded into demountable 1 mm sample path length titanium (Ti) cells with Ti windows and cooled from 20 °C to −45 °C at a ramping rate of 0.5 °C per minute using a closed-cycle refrigerator with a two-position sample holder. The samples were measured at 20, 5, 0, -10, -25 and -45 °C. Counting times at each temperature were ~1.0 hours per sample at 20 °C and 0.5 hour per sample at all other temperatures, effectively holding the samples at each temperature for 1 hour to make the measurements before proceeding to the next temperature. Samples were then heated back to 20 °C at the same ramping rate and measured at the same temperatures for the same times as during cooling. Empty cells were also measured in both sample positions for ~0.5 hour at 20 °C.

A neutron wavelength of $\lambda = 6$ Å was used with a wavelength spread $\Delta\lambda / \lambda = 0.14$. The scattered neutrons were detected with a 64 cm x 64 cm two-dimensional position-sensitive detector with 128 pixels x 128 pixels at a resolution of 0.5 cm/pixel. Data reduction was performed using IGOR Pro (Wavemetrics Inc., Lake Oswego, OR) with SANS macros developed at the NCNR 27. Raw counts were normalized to a common neutron intensity and corrected for empty cell counts, ambient room background and nonuniform detector response before being placed on an absolute scale by normalizing the intensity to the incident beam flux. Finally, the data were radially averaged to produce the scattered intensity, *I(q) vs q*, where $q = 4\pi\sin(\theta)/\lambda$ and 2θ is the scattering angle. Sample-to-detector

distances of 13 m, 4.5 m and 2 m were used for each measurement to obtain a q range between 0.004 and 0.3 $Å^{-1}$. Scattering from the buffer was subtracted from a subset of the samples to compare the buffer-subtracted data with calculated SANS curves from atomic coordinates. Guinier fits were made to a subset of the buffer-subtracted data to obtain the radius of gyration, R_g, and the forward scattering intensity, $I(0)$.

2.2.3 SAXS Measurements

Aqueous LDH solutions and buffers were filled in 1.5 mm quartz capillaries, which were sealed hermetically. SAXS measurements were performed on a SAXSLab Ganesha 300XL. Cu Kα X-rays (λ = 1.54 Å) generated by a Xenocs Geni3DX source were collimated through 2 sets of 4-bladed slits (JJ X-ray, A/S). Two-dimensional SAXS images were acquired using a Dectris EIGER R 1M detector (7.72 cm x 7.99 cm rectangular area) with 1030 pixles x 1065 pixels (75μm x 75 μm pixel size) at a sample-to-detector distance of 45 cm. Each sample was measured for 2 hours. SAXS images were azimuthally integrated using SAXSGUI, to obtain one-dimensional scattered intensity I(q) versus q plots. The data were placed on an absolute scale by normalizing the intensity to the incident beam flux. Background subtraction and Guinier fits were performed using IGOR Pro as described above.

2.2.4 LDH Structure Modeling

LDH dimers, tetramers, octamers and 16-mers were modeled from the tetramer structure of the apo form of LDH from Thermus thermophilus [60], Protein Data Bank Identifier (PDB ID) 2V6M. Missing H atoms and residues were added to the structure using PSFGEN [61] to

create a tetramer structure suitable for modeling using the CHARMM force field [62]. This structure was energy minimized and then subjected to a 10 ps molecular dynamics (MD) simulation using NAMD [61] to ensure that the structure was stable. To make LDH octamers and 16-mers, the energy-minimized and MD-subjected structure was aligned along its principle axes with its center of mass at the origin using the Build Utilities module in SASSIE-web [63]. Using VMD [64], identical tetramers with different positions along the x, y and z principal axes were created in order to construct three different octamers and 16-mers along these axes using only geometrical considerations. The energy-minimized and MD-subjected tetramer structure was also used to construct three dimer structures [65]. Model SANS curves and *Rg* were calculated from the model structure using the SasCalc module in SASSIE-web [66]. Expected I(0) values were calculated using the Contrast Calculator module in SASSIE-web [67].

2.2.5 Calculation of isoelectric point and net charge on LDH

The isoelectric charge (pI) as well as the net charge (z) on the LDH amino acid sequence as a function of pH was determined using the Prot pi Peptide tool

(https://www.protpi.ch/Calculator/PeptideTool). The determination was performed using the known LDH structure from the protein data bank (PDB ID 2V6M – same as that used for structure modeling). The representative snapshot of the values obtained for the surface charge on LDH at particular pH is included in the supplementary information.

2.2.6 DSC of NaP Buffer Solutions

A differential scanning calorimeter (model Q2000 TA instruments, USA) equipped with a cooling system was used to perform low-temperature thermal analysis. The instrument was periodically calibrated with indium and tin. Dry nitrogen at a flow rate of 50 mg/mL was used as purge gas. Aluminum pans, hermetically sealed with 15 mg to 20 mg of sample, was weighed and cooled to 45 °C, held for 10 minutes to achieve equilibrium, and warmed to 20 °C at 0.5 °C/min. Due to the stochastic nature of cooling curves, the information obtained was only used for qualitative purposes. For any quantitative data interpretation, the heating curves were used.

2.2.7 Low-temperature pH of NaP Buffer Solutions

The NaP buffer solutions were frozen and thawed in a jacketed beaker using a controlled temperature program. 50 mL of sample solution was place in a 250 mL jacketed beaker and the temperature was maintained using a circulating external water bath (Neslab RTE 740, Thermo electron, USA). A low-temperature pH electrode (Inlab®cool, Mettler Toledo, Switzerland) was used for measurement of pH using Friscolyte-B® as a reference solution which enables measurement of electromotive force (EMF) at temperatures up to -30 °C. The probe is placed at center of the solution in the 250 mL beaker taking care to prevent it from touching the base of the beaker and is connected to a pH meter (pH 500 series, Singapore). The measured EMF was then used to calculate the solution pH. A copper-constantan thermocouple (Omega, USA) with Teflon insulation was connected to a bench top digital read out device (± 0.2 °C, OmegaMDSi8 Series, USA). The instrument

calibration procedure and calculation of pH from EMF potential was performed based on previous literature reports [6, 36].

2.2.8 Low-temperature XRD of NaP Buffer Solutions

An X-ray diffractometer (D8 Advance, Bruker AXS, USA) with variable temperature stage (TTK 450, Anton Paar, Austria) and Si strip one-dimensional detector (LynxEye, Bruker AXS, USA) was used. The NaP buffer sample (~ 100 µL) was placed in a copper XRD sample holder with a thermocouple used to record the sample temperature. The solutions were subjected to controlled temperature program and the diffraction curves using Cu Kα radiation (1.54 Å; 40kV x 40 mA) were obtained by scanning over an angular range of 7° to 35° (2θ) with a step size of 0.05°. A dwell time of 0.5 seconds for the 100 mM NaP buffer and 4 seconds for 10 mM NaP buffer was used. The samples were cooled and heated at 0.5 °C/min and scans were collected at selected time points during cooling and heating.

2.2.9 Dynamic Light Scattering (DLS)

Dynamic light scattering experiments were performed to determine the LDH aggregates pre- and post-freeze-thaw in solution at room temperature. The hydrodynamic radius (nm) of the particles and the particle size distribution were measured using UNCLE instrument (Unchained Labs, CA). The sample volume for individual measurements was 9 µL. Each measurement was an average of 5 scans with a run time of ~ 10 seconds. A similar dialysis procedure to that noted above was used to prepare 1000 µg/mL LDH solutions in 10 mM histidine, 10 mM and 100 mM NaP buffers, as mentioned earlier. These stock solutions were diluted to prepare 10 µg/mL and 100 µg/mL LDH solutions in the different buffer

conditions. The solutions were cooled from RT to -45 °C at 0.5 °C/min, held at -45 °C for 30 minutes and heated back to RT at 0.5 °C/min in a benchtop freeze drier (Virtis, SP Scientific, PA). The procedure was repeated five times (5XFT). Samples were stored in dry ice until analyzed.

2.3 Results and Discussion

Our first set of studies in histidine buffer were aimed at determining the native protein conformation of LDH and its conformations in the frozen state. These preliminary measurements enabled identification of LDH in the frozen state using different ratios of H_2O to D_2O in the buffer. After establishing the protein conformation, comparative studies were conducted in NaP buffered solutions (10 mM and 100 mM). The analyses were carried out in the following stages: (i) immediately after preparing a solution at RT, (ii) during freezing to -45 °C, and (iii) during thawing to RT.

2.3.1 Conformation of LDH at Room Temperature

Figure 1A shows three views of the LDH structure from PDB ID 2V6M [60]. Figure 1B contains the buffer-subtracted SANS data from LDH (~ 1 mg/mL) buffered in histidine (10 mM) in 100% D_2O and 8% D_2O at RT before freezing. Due to its higher scattering length density and low incoherent scattering, D_2O was initially used as the solvent medium for the SANS experiments. The vertical dotted line splits the data into the low q scattering region (LQS) for $q < 0.025$ Å^{-1}, and the high q scattering region (HQS) for $q > 0.025$ Å^{-1}. While D_2O was ideally suited for gaining conformational insights in the HQS, especially for $q > 0.1$ Å^{-1}, the hydrophobic effect induced by deuterium promoted aggregation in the

solution immediately after dialysis, which is evident in the LQS. Moreover, the protein signal was compromised on freezing due to the pronounced scattering from the ice-air interface, as was shown in Curtis et al. [49] The contrast match point of 8% D_2O and 92% H_2O, where the ice-air scattering became invisible, was also established in that work. Thus, contrast variation measurements under these conditions enabled us to determine the structure of LDH in the frozen state without interference from the scattering at the ice-air interface.

The model SANS curve calculated as described in the *Methods* section is shown as the solid black line in Figure 2.1B. It predicts the solution scattering of the structure in Figure 2.1A averaged over all possible orientations. There is little difference between the model SANS curves calculated for LDH in 8% D_2O and 100% D_2O buffers. It is important to note that the scattering from the modelled LDH tetramer shows two characteristic features: (i) a flat shape in the LQS region which is expected due to the absence of large structures or aggregates and is also an indication of monodispersed solution and (ii) two features in the HQS region from 0.03 to 0.1 $Å^{-1}$ and one at ~ 0.15 $Å^{-1}$.

The calculated SANS curve matched the data in 8% D_2O buffer very well, confirming the existence of LDH as a tetramer at RT in 10 mM histidine buffer. Although the data in 100% D_2O showed aggregation in the LQS, they matched the calculated SANS curve very well in the HQS, including the subsidiary maximum at q ~ 0.15 $Å^{-1}$, suggesting that that there is still a significant population of tetramers in 100% D_2O buffer. We also confirmed the tetrameric state of LDH by comparing the Guinier-derived R_g and $I(0)$ values from the 8%

D_2O data to those calculated from the LDH tetramer structure. The results are shown in Table 2.1. Virtually identical results were obtained from LDH in 8% D_2O 10 mM and 100 mM NaP buffers, as shown in Table 1. Guinier fits to SAXS data obtained from LDH in 0% D_2O 100 mM NaP buffer further confirmed the existence of the tetramer in solution at RT and these results are also included in Table 2.1. The lower $I(0)$ values after thawing could be due to loss of sample from formation of air bubbles that remain after thawing, resulting in less sample in the beam. The SAXS data, as well as the Guinier plots from the SANS and SAXS data, are presented in the Supplementary Information as Figure 2.9 to Figure 2.12.

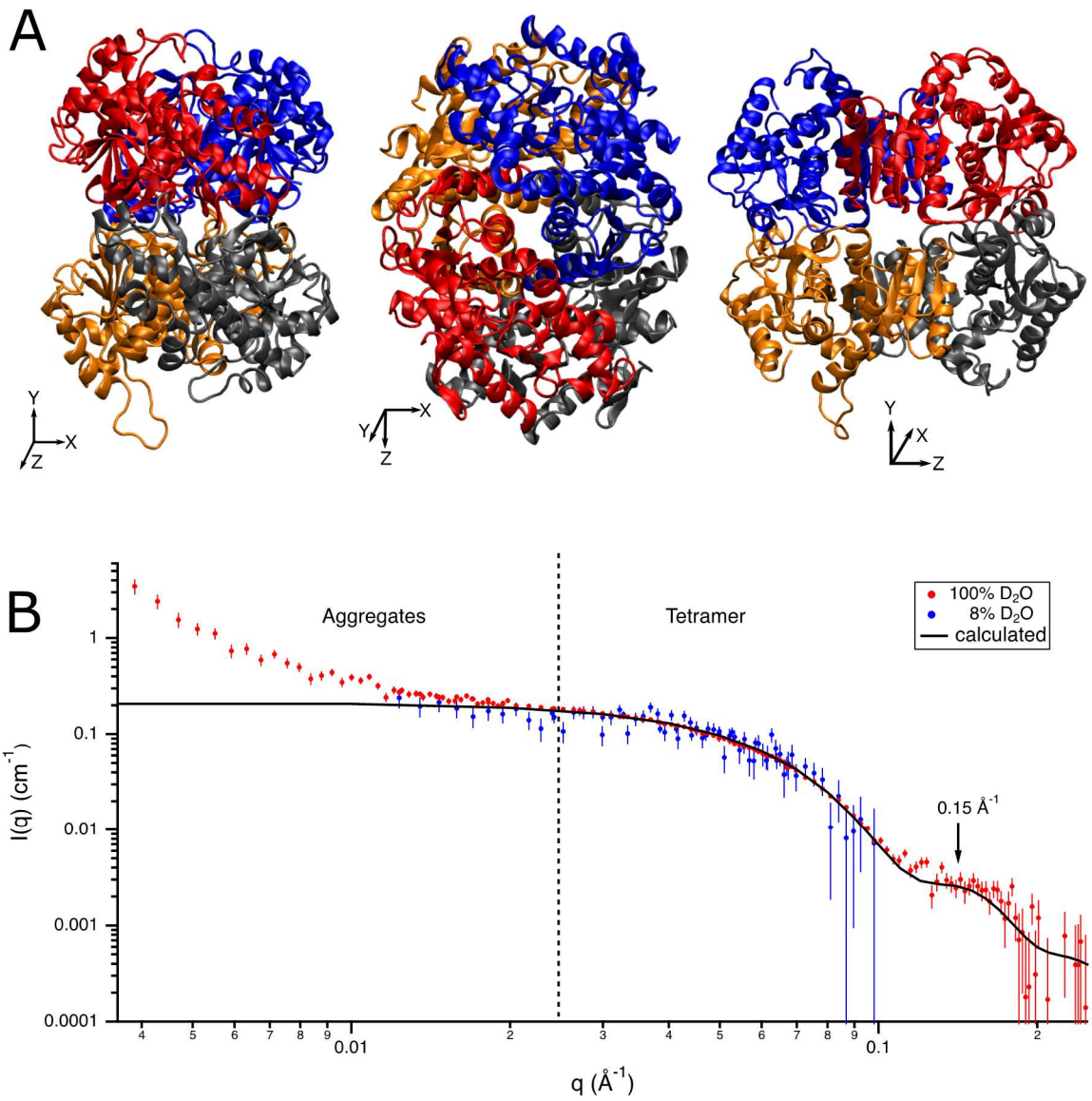

Figure 2.1 LDH tetramer (PDB ID 2V6M) [60] visualized in three different orientations using VMD [64]. B. Overlay of buffer-subtracted SANS curves for 1 mg/mL LDH in 10 mM histidine buffer in 100% D_2O (red data points) and in 8% D_2O (blue data points) at 20 °C and the calculated LDH tetramer curve (black curve) from the structure in A using the SasCalc module in SASSIE-web [66]. The 8% D_2O data has been scaled to the 100% D_2O data for easy comparison of their shapes. Error bars are the standard error of the mean based on the number of pixels used during data averaging.

Table 2.1. Basic Characterization of LDH at 20°C Before and After Freezing.

Sample	LDH concentration (mg/mL)	Guinier R_g (Å)	qR_g range	Guinier I(0) (cm^{-1})	Calculated I(0) (cm^{-1})
SANS (8% D2O)					
10 mM NaP	1.25	27 ± 2	0.62 – 1.29	0.057 ± 0.002	0.055
10 mM NaP, 1X FT	1.25	28 ± 3	0.53 – 1.29	0.040 ± 0.002	0.055
100 mM NaP	1.27	33 ± 3	0.66 – 1.29	0.063 ± 0.004	0.056
100 mM NaP, 1X FT	1.27	32 ± 3	0.62 – 1.29	0.051 ± 0.004	0.056
10 mM histidine	0.89	28 ± 3	0.34 – 1.28	0.041 ± 0.002	0.039
10 mM histidine, 1X FT	0.89	28 ± 3	0.63 – 1.28	0.037 ± 0.003	0.039
SAXS (0% D_2O)					
100 mM NaP	0.6 – 0.7	28 ± 2	0.63 – 1.28	0.080 ± 0.003	0.06 – 0.07
100 mM NaP, 5X FT	0.6 – 0.7	28 ± 2	0.66 – 1.27	0.038 ± 0.003	0.06 – 0.07

Error bars on the measured concentration for the SANS samples are about 5%. Error bars on R_g and I(0) are standard errors on the slope and intercept, respectively, from the linear Guinier fit to ln[I(q)] vs q^2. The calculated R_g from the coordinates (PDB ID 2V6M) [60] is 30 Å using the SasCalc module in SASSIE-web [66] . Calculated I(0) values were obtained using the Contrast Calculator module in SASSIE-web [67].

2.3.2 Freeze-Thaw of LDH in Histidine Buffer

The next objective was to determine the effect of freeze-thawing on LDH conformation. We will first discuss the results from freeze thawing LDH in 10 mM histidine buffer. The samples were cooled to -45 °C at 0.5 °C/min, held for 2 hours and then heated back to 20 °C at the same rate. SANS curves were collected at different temperatures during freezing and thawing. During cooling to 5 °C in 8 % D_2O buffer (Figure 2.1A), there was no change in LQS, suggesting the retention of the protein in the native state. As it was further cooled from 0 to -45 °C, we see a dramatic increase in LQS intensity at -10 °C, indicative of LDH aggregation when the sample froze, followed by a more gradual increase as the temperature is decreased further. Recall that the scattering from the ice-air interface is absent in 8% D_2O buffer and we can thus attribute the measured intensity entirely to LDH aggregates.

Cooling the buffer solution resulted in ice crystallization leading to buffer component (histidine) freeze concentration. At the concentration used (10 mM, pH 6.0), the buffer remains amorphous [68]. The decrease in temperature will influence the pKa of histidine. This dpKa/dT has been calculated to be -0.022 K^{-1} [69]. In 20 mM L-histidine buffer solution, the pH increased from 5.37 to 6.14 when the temperature was decreased from 25 °C to -30 °C [69]. It is instructive to recognize that our buffer concentration was lower (10 mM) and the pH of our buffer solution at RT was 6.0 (close to the pKa_2 of histidine at RT). Thus, while the decrease in temperature and the attendant freeze-concentration would bring about a small change in the pH, we do not know the magnitude of this effect in the presence of LDH.

The LDH aggregation that was observed in the frozen solution could be attributed to charge-charge interactions. When the pH of the solution is 6.0 units, the calculated net positive charge on LDH was 10 units (Figure 2.13). Thus, the aggregation could have been brought about by the high net positive surface charge on LDH [47, 70]. Close packing of these positively charged LDH molecules can result in charge-charge repulsion resulting in expansion or modification of the tetramer conformation to accommodate the charge which in turn can facilitate favorable long range coulombic interactions. These long-range coulombic attractions may lead to the formation of higher order aggregates in the freeze-concentrate [9, 47, 70, 71]. In addition, aggregation brought about by interaction at the ice-water and/or ice-air interfaces cannot be ruled out.

During warming of the frozen solution (Figure 2.2B), from -45 °C to 0 °C, the aggregation persisted, and the ice melting was not complete. Even when the ice melting was complete at 5 °C, the aggregates persisted. By 20 °C, there is still some scattering in the LQS, compared to none before freezing, indicating that some aggregates were retained upon thawing from -45 °C. Thus, aggregation was predominantly reversible and, but a fraction of the sample possibly undergoes irreversible aggregation. Another possible explanation is that, at 1000 μg/mL LDH concentration, the aggregation is reversible, but it was not complete at the time we measured the sample, i.e., immediately after thawing.

Similar SANS curves were obtained in 100% D_2O 10 mM histidine buffer (Figure 2.2C and Figure 2.2D). However, due to the lower incoherent background, more detail can be observed in the HQS. Figure 2.2C shows that freezing occurred at -10 °C, where in fact,

we see a discontinuous SANS intensity (green curve) since the sample froze after the LQS scattering had been measured. Upon freezing, we see that the scattering in the LQS increases and that scattering curve in the HQS between q = 0.025 Å^{-1} and 0.1 Å^{-1} decreases as well as changes in shape, indicating that the population shifts from mostly tetrameric molecules to higher order aggregates as the freezing progresses. The LQS scattering is higher than that observed in 8% D_2O due to the added contribution from the ice-air interface that is absent in the 8% D_2O data. Figure 2.2D shows that the sample thawed between 5 °C and 20 °C and that the aggregation at RT was higher after thawing, as observed in the 8% D_2O sample.

The buffer-subtracted data for LDH in 8% D_2O and 100% D_2O 10 mM histidine buffers at RT, before and after freezing, and at -45 °C are shown in Figure 3 along with the calculated SANS curve. At RT, the calculated scattering curve matched the measured scattering curve well in both the LQS and HQS for the 8% D_2O data and in the HQS for the 100% D_2O data, as already shown in Figure 2.1. Upon cooling to -45 °C a pronounced deviation from the native structure is evident for the LQS scattering in both buffers and a loss of the tetramer signal is seen in the HQS between q = 0.025 Å^{-1} and 0.1 Å^{-1}. However, there is still some evidence of the subsidiary maximum from the tetrameric structure at q = 0.15 Å^{-1} in 100% D_2O buffer (Figure 2.3B, region in box). This shows that the aggregates that form in the frozen state likely assemble from the tetramer. Thus, the native tetrameric structure is not lost upon freezing, but rather becomes the building block for the higher order aggregates.

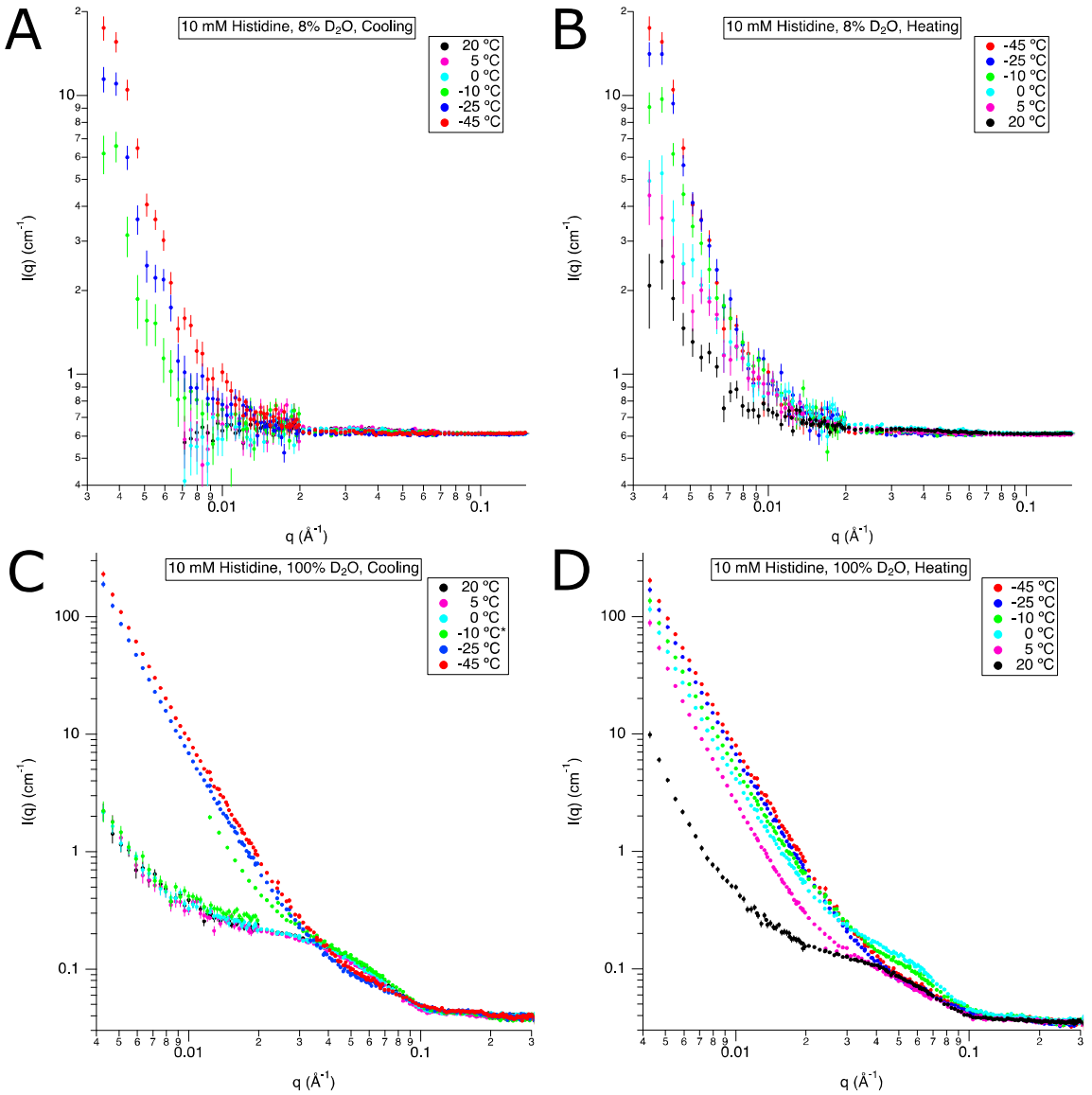

Figure 2.2. SANS I(q) vs q curves. A. LDH (1 mg/mL) in 10 mM histidine buffer in 8% D_2O during cooling at 20, 5, 0, -10, -25 and -45°C from bottom to top. B. The frozen solution (of panel A) during heating at -45, -25, -10, 0, 5 and 20°C from top to bottom. C and D. SANS profiles for the identical composition obtained during cooling and heating but in 100% D_2O. The incoherent scattering from the buffer has not been subtracted from these data to show the difference in the incoherent scattering between the 8% D_2O and 100% D_2O buffers. Error bars are the standard error of the mean based on the number of pixels used during data averaging. *In figure 2.2 C, the SANS pattern at -10°C does not align in the 0.01 Å-1 to 0.03 Å-1 range; this discontinuity can be attributed to beginning of ice crystallization or incomplete ice crystallization at -10°C.

On thawing back to 20°C, the pre- and post-freeze-thaw SANS curves (LQS < 0.01 $Å^{-1}$) at 20 °C did not overlap, revealing the existence of additional higher order structures. The use of 100% D_2O enabled the confirmation of the tetramer as the building block for the aggregates upon freezing since the lower incoherent scattering allowed the subsidiary maximum at q = 0.15 $Å^{-1}$ to be observed and tracked throughout the freeze-thaw process. The SANS curves obtained, both during freezing and post thawing, confirmed the existence of higher order structures upon freezing. Since the 100% D_2O curves also contain a contribution from the air-ice interface, the 8% D_2O curves were needed in order to confirm that the LDH was, in fact forming higher order structures upon freezing. Thus, the two freeze-thaw sets of SANS data in 8% D_2O and 100% D_2O gave complementary information about the structure of LDH during the freeze-thaw process.

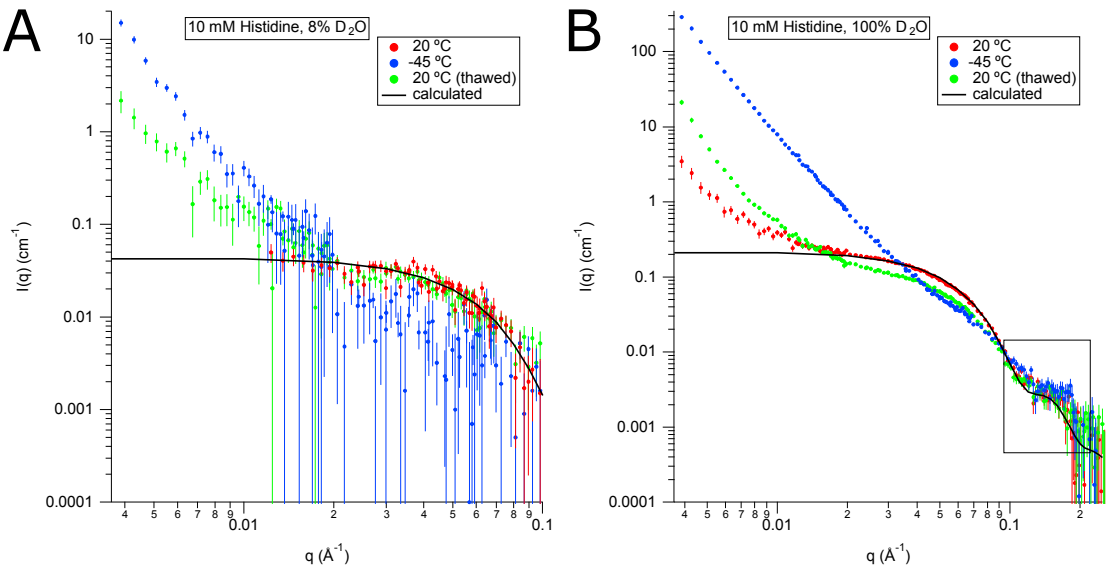

Figure 2.3. SANS I(q) vs q curves. A. Buffer-subtracted SANS curves of LDH (1 mg/mL) solution buffered in histidine (10 mM; 8% D_2O) at room temperature (red circle), cooled to -45 °C (blue circle), and thawed back to room temperature (green circle). The black curve is the reference LDH tetramer curve. B. The same composition and processing conditions as in panel A, except for the use of 100% D_2O. Error bars are the standard error of the mean based on the number of pixels used during data averaging.

2.3.3 Characterization of Deuterated NaP Buffer Solutions

The phase behavior of aqueous phosphate buffer solutions of different concentrations, following freezing and thawing, have been reported in the literature [35, 72]. Therefore, our current work was restricted to characterization of NaP buffer systems (10 mM and 100 mM) in 100% D_2O. When NaP buffer solution (100 mM in D_2O; pH of 7.0 at 25 °C) was cooled to -20 °C, the pH decreased to 4.1. Thus, a pH shift of 3.9 (± 0.7; n=3) units was observed (Figure 4A). The magnitude was similar to that observed in H_2O solutions. The pH shift was attributed to selective crystallization of disodium hydrogen phosphate dodecahydrate ($Na_2HPO_4{\cdot}12H_2O$) [42, 72]. On cooling, peaks characteristic of the dodecahydrate along with ice (Ice I, D_2O) were first observed at -10 °C in the XRD patterns (Figure 2.4C). The buffer salt peak intensities increased as the sample was cooled further to -40°C. During heating, as the temperature of the sample increased from -40 to 10 °C, the dodecahydrate peaks persisted until 1°C, whereas the ice peak intensity gradually decreased starting at -5 °C and vanished at 5 °C (Figure 2.4D). We believe that there is an overlapping of the eutectic (dodecahydrate–ice) and ice melting. The results can be explained by the higher melting temperature (+ 3.4°C) of ice I (D_2O) which was evident from DSC (Figure 2.4B).

On cooling a buffer solution of a lower concentration (10 mM), the pH shift was 3.3 (± 0.1; n=3) (Figure 2.14A). Thus, reducing the buffer concentration resulted in a lower pH shift. As before, from low-temperature XRD studies, selective crystallization of the dodecahydrate was evident during cooling (Figure 2.14C). The behavior of the system was

substantially similar to that observed at the higher buffer concentration (Figure 2.14B and Figure 2.14D).

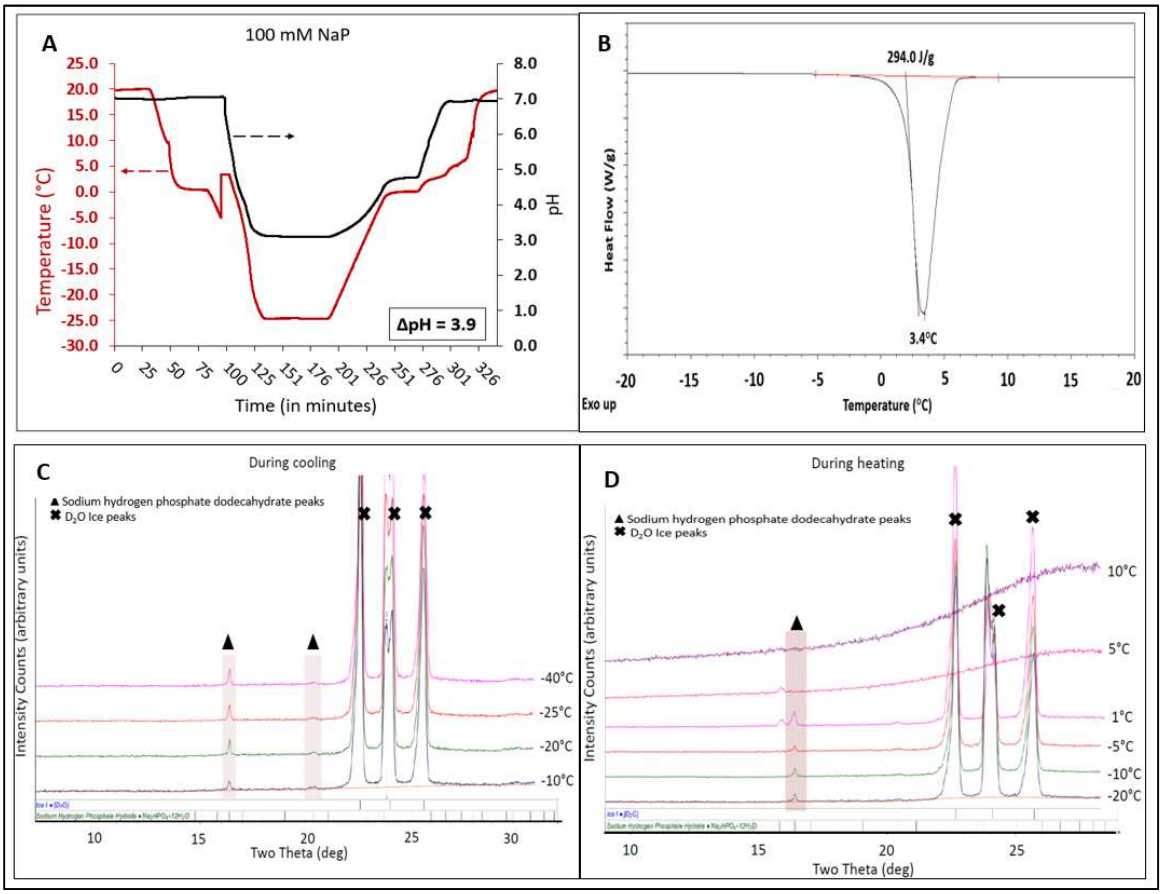

Figure 2.4. Characterization of NaP buffer (100 mM) during freezing and thawing (in 100% D_2O). A. Low-temperature pH measurement, when cooled from 20 °C to -25 °C and then heated back to 20 °C. The heating as well as the cooling rate was 0.5 °C/min and the frozen solution was held at -25 °C for 30 minutes. B. The DSC heating curve of frozen solution, heated from -45 °C to 20 °C. The solution was initially cooled from RT to -45 °C, at 0.5 °C/min and held for 30 minutes. Only the final heating curve is shown. C. XRD patterns obtained while the solution was cooled from 20 °C to -40 °C at 0.5 °C/min. The XRD patterns were obtained at -10, -20, 25 and -40 °C. D. XRD patterns obtained when the frozen solution (from C) was heated from -40 to 10 °C at 0.5 °C/min. The XRD patterns were obtained at -20, -10, -5, 1, 5 and 10 °C.

2.3.4 Freeze-Thaw of LDH in NaP Buffers

LDH buffered in NaP (10 and 100 mM) was subjected to freezing and thawing and the SANS curves were collected at select temperatures. At the higher buffer concentration, during cooling (Figure 2.5A), no changes in the SANS curves were observed at 20, 5, 0 and -10 °C, suggesting the retention of protein in the native state. At -25 and at -45 °C, we see a gradual increase in intensity at LQS indicative of tetramer aggregation. Above, we reported simultaneous ice and buffer salt crystallization at -10 °C based on XRD. The selective buffer salt crystallization led to a pH shift of ~ 3.9 units (low-temperature pH measurement). The tetramer aggregation may be attributed to one or more of the following factors: (i) ice crystallization leading to interfacial stress, (ii) freeze-concentration, also a consequence of ice crystallization, and (ii) pH shift due to selective buffer crystallization. During warming of the frozen solution (Figure 2.5B), from -45 to 0°C, the aggregation was retained. Even at 0 °C, ice melting was not complete, and aggregation persisted (this was explained earlier in the context of Figure 2.2B). At 5 and 20 °C, even though the ice melting was complete, aggregation was evident though it was much less pronounced than at the lower temperatures. At 20°C, some of the aggregates were retained. These post-thawing results were similar to that in histidine buffer, except that there was more residual scattering in the LQS for LDH in histidine buffer.

A similar set of experiments were carried out for LDH solutions in 10 mM NaP buffer (Figure 2.5, panels C and D). We had earlier observed that freezing the buffer solution resulted in a pH shift of 3.3 units (Figure 2.14). This was lower than the shift of 3.9 units observed when a 100 mM phosphate buffer solution was cooled (Figure 2.4). The

aggregation after freeze-thawing was about the same in the two systems (Figure 2.6). These results suggest that the magnitude of pH shift as well as the buffer concentration did not have a discernible effect on the protein aggregation behavior.

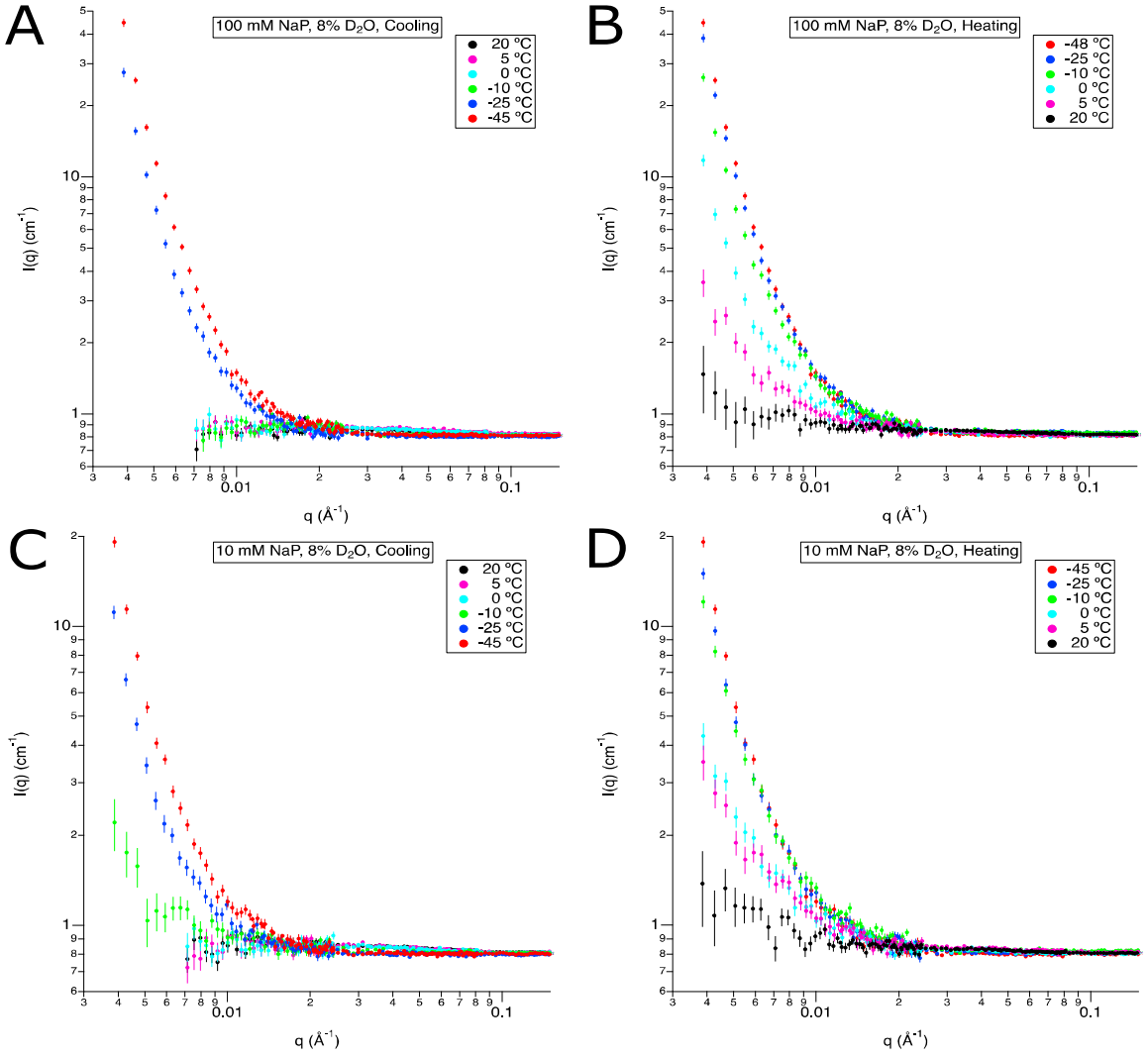

Figure 2.5. SANS I(q) vs q curves. A. 1 mg/mL LDH, 100 mM sodium phosphate (NaP) 8% D_2O buffer during cooling at 20, 5, 0, -10, -25 and -45 °C from bottom to top B. 1 mg/mL LDH, 100mM NaP 8% D_2O buffer during heating at -45, -25, -10, 0, 5 and 20 °C from top to bottom. C and D. SANS profiles for 1 mg/mL LDH, 10 mM NaP 8% D_2O buffer during identical cooling and heating series. The incoherent scattering from the buffer has not been subtracted from these data for comparison to the data in Figures 2A and 2B. Error bars are the standard error of the mean based on the number of pixels used during data averaging.

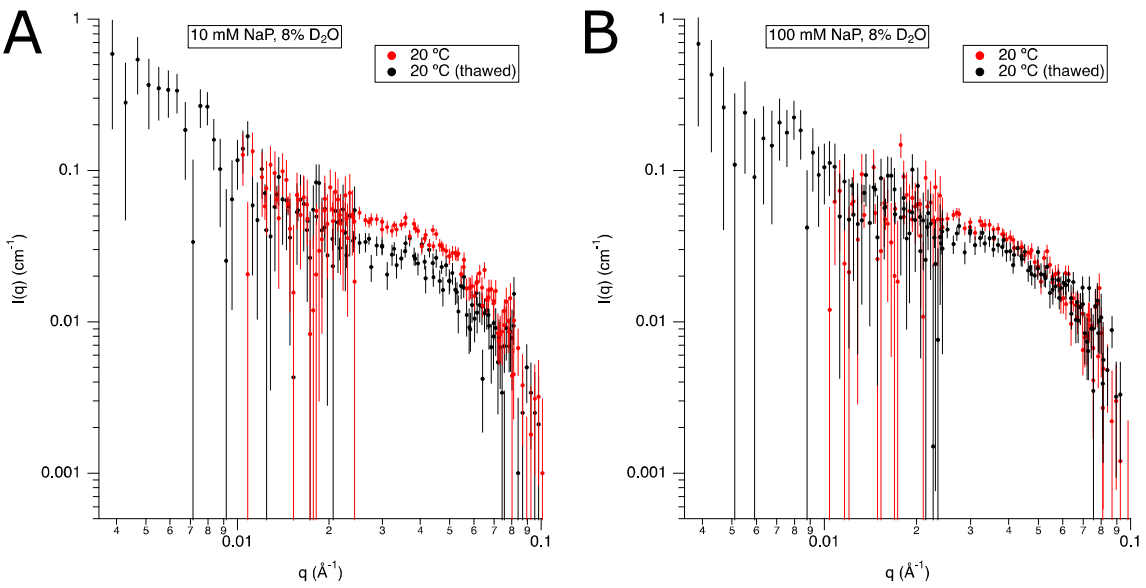

Figure 2.6. Overlay of buffer-subtracted SANS I(q) vs q curves pre and post freeze thaw for 1 mg/mL LDH in A. 10 mM NaP and B. 100 mM NaP buffers in 8% D_2O. Error bars are the standard error of the mean based on the number of pixels used during data averaging.

2.3.5 Concentration Dependence of LDH Aggregation

LDH in solution, irrespective of the buffer used, aggregated on freezing. The aggregation was almost completely reversed on thawing. There appeared to be a small effect depending on the buffer used (perhaps more residual scattering from aggregates in histidine vs. NaP), but there is no discernable effect on the buffer concentration (10 and 100 mM) for the NaP buffers. The SANS studies necessitated a protein concentration of 1000 µg/mL so as to discern the conformation during different stages of freezing and thawing. We had earlier stated that LDH aggregated in freeze-thawed solutions when the LDH concentration was typically ≤ 100 µg/mL [54-57]. This apparent difference in behavior could be attributed to the relatively high protein concentration in the SANS experiments leading to self-stabilization. In addition, the SANS results are based on a single freeze-thaw cycle. While it would be highly desirable to conduct multiple freeze-thaw cycles, this was not possible because of

the limited availability of the beam time. It is noteworthy that each freeze-thaw cycle was 22 hours long and only two samples were measured during that time.

The aggregation behavior in protein solutions of much lower concentrations (~10 μg/mL) can be evaluated by dynamic light scattering. An added advantage of this technique is the extremely short analysis time of ~ 10 seconds. Solutions subjected to multiple freeze-thaw cycling could be immediately analyzed after thawing. This technique was therefore an excellent complement to SANS. Hence, the two limitations of the SANS technique, inability to analyze solutions with low protein concentration and evaluating the effect of multiple freeze-thaw cycles, were overcome using DLS.

The LDH protein solutions subjected to 5 freeze-thaw cycles and analyzed before and after freezing. The results are presented in Table 2.2. The key parameter of interest is the Z-average diameter, which is the intensity weighted mean hydrodynamic size of the ensemble collection of particles. When buffered either with histidine or phosphate, irrespective of the starting LDH concentration, the hydrodynamic diameter is ~ 7 nm. This suggests that LDH exists as a tetramer in a monodisperse state, consistent with the SANS and SAXS results in **Table 2.1**. Dilute monodispersed solutions are a prerequisite for SANS/SAXS data [48]. In histidine buffer, at 10 μg/mL LDH concentration, there is a discernible increase in diameter after 5 freeze-thaw cycles, suggesting aggregation. Interestingly, at higher LDH concentrations (100 and 1000 μg/mL), the increase in diameter is much less pronounced. At a LDH concentration of 1000 μg/mL, even after five freeze-thaw cycles, there appears very little, if any, increase in diameter. Thus, by combining the SANS and

DLS results for LDH at 1000 μg/mL, we see evidence of aggregation in the frozen state with nearly complete reversibility (self-stabilization) after both one and five freeze-thaw cycles.

When the NaP buffer is at a low concentration (10 mM), after five freeze-thaw cycles, the Z-average diameter is substantially increased at a low protein concentration (10 μg/mL). The observed diameter is higher than that observed in the histidine system. One possible explanation is the additional stress induced by buffer salt crystallization and the attendant pH shift. As the protein concentration is increased, first to 100 and then to 1000 μg/mL, it is progressively more effective in inhibiting buffer salt crystallization. The consequence of this inhibition is the lower diameter after the freeze-thaw cycling with the high protein concentration (1000 μg/mL) resulting in almost the same diameter as the control. This is consistent with the SANS results after one freeze-thaw cycle.

Since both the SANS and DLS experiments were conducted at a protein concentration of 1000 μg/mL, it is useful to compare them. At low buffer concentration (10 mM; histidine or NaP), there is no evidence of aggregation at RT after one freeze-thaw (SANS) or five freeze-thaw (DLS) cycles. Thus, solutions with high protein concentration coupled with low buffer concentration exhibited resistance to freezing and thawing stress.

Table 2.2 Particle Size of LDH in Solution Before Freezing and After 5 Freeze-Thaw Cycles.

	Buffer	LDH concentration (µg/mL)	Z-avg diameter (nm) from DLS	
			Control	5X FT
a.	10 mM Histidine	10	6.3	291.3
			9.5	156.0
			5.8	155.0
		100	7.7	21.2
			8.2	7.4
			9.9	22.2
		1000	8.0	9.0
			8.0	11.3
			7.9	8.7
b.	10 mM NaP	10	8.0	771.0
			9.5	> 1000
			6.3	272.0
		100	7.5	116.0
			8.2	> 1000
			9.9	> 1000
		1000	8.0	8.6
			7.9	8.7
			8.0	8.2
c.	100 mM NaP	10	5.0	> 1000
			12.9	> 1000
			16.9	> 1000
		100	7.9	> 1000
			7.3	> 1000
			8.1	> 1000
		1000	8.4	> 772.8
			8.3	> 1000
			8.0	> 1000

The LDH concentrations were (i) 10 µg/mL, (ii) 100 µg/mL and (iii) 1000 µg/mL in three different buffer solutions (a) 10 mM histidine (b) 10 mM NaP and (c) 100 NaP. The freezing and thawing was carried out five times and the runs were carried out for three aliquots, while the individual runs were an average of five scans. The three values were not averaged since the number of particles were not necessarily the same in the three aliquots.

At a low protein concentration of 10 µg/mL, irrespective of the buffer used, the stresses associated with the freeze-thaw cycling were sufficient to cause aggregation. Thus, the protein concentration appears to be a dominant factor when considering the stresses associated with freezing and thawing. In case of proteins that are susceptible to aggregation at low concentration, the use of additional excipients may offer a viable approach for stabilization.

2.3.6 Modelling the Aggregates

The dissociation of LDH tetrameric structure and its stabilization due to factors such as temperature, pH, additives, and processing conditions (freeze-thaw and freeze-drying) has been a topic of several investigations [54, 73-75]. In an earlier gel chromatographic study performed at RT by Lovell et al., LDH (2 mg/mL) was shown to dissociate from tetramer to dimer when the pH of solution was adjusted from pH 7 to 5 using acetate-chloride. In addition, when exposed to pH 5, the conversion to LDH dimers was very rapid and the reaction was complete within a minute. Interestingly, when the solution pH was restored to pH 7, there was ~70% retention of activity. This was attributed to reversibility of the LDH dimers to the native tetrameric form. However, prolonged exposure of the dimers to pH 5 resulted in an increase in irreversible aggregation [73].

LDH is known to self-stabilize at higher concentrations (> 500 µg/mL) during freeze-thawing and freeze-drying [54]. However, at lower LDH concentrations (≤ 500 µg/mL) the reduction in activity recovery was reported in presence of Na_2HPO_4 salt formed as a result of a combination of NaCl with KPO_4. The crystallization of Na_2HPO_4 at low temperature

was shown to cause an acidification effect leading to dissociation of the tetrameric structure into dimers. The pH shift ($\Delta pH_{pH22°C - (-20°C)}$) in 10 mM KPO_4 , 0.1 M NaCl in the absence of LDH was 3 units. Addition of stabilizers such as BSA and PVP prevented LDH dissociation and resulted in maintenance of tetrameric LDH in the frozen state [54]. We believe that LDH exerts a self-stabilization effect which is concentration dependent. The model SANS curves for LDH dimers were calculated (described in the *Methods* section). Figure 2.7A shows LDH dimers modelled as per Fujisawa et al [65]. The predicted SANS scattering of these dimers averaged over all possible orientations are overlaid with the SANS pattern from LDH (1000 µg/mL) in 10 mm histidine buffer (100% D_2O) at -45°C (frozen state, Figure 2.7B). The characteristic features of the modelled LDH dimers do not show any overlap with the experimental SANS pattern in the HQS for $q > 0.1$ $Å^{-1}$. (We would not expect overlap at lower q values due to the difference in size between LDH dimers and the aggregates formed upon freezing.)

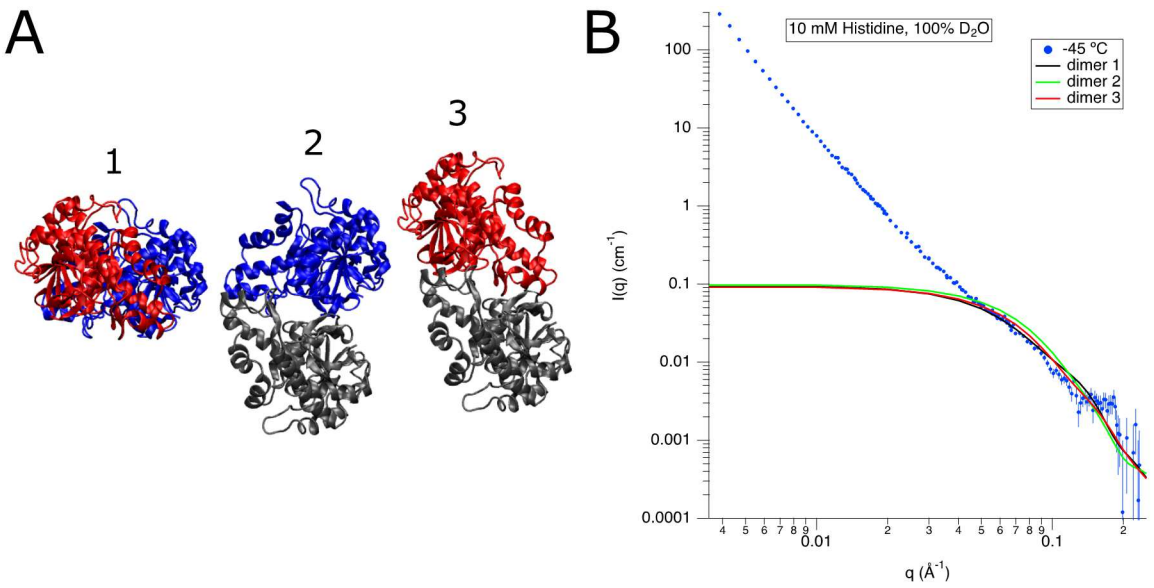

Figure 2.7. Modeling LDH dimers to determine the type of aggregates observed experimentally in 10 mM histidine buffer (100% D_2O) solutions (A) LDH dimers in three different forms, modeled as per Fujisawa et. al. [65]. (B) Overlay of SANS curves for 1 mg/mL LDH in 10 mM histidine buffer in 100% D_2O (blue data points) at -45°C and the reference LDH dimer 1, 2 and 3 curves (black, red and green curves respectively). Error bars are the standard error of the mean based on the number of pixels used during data averaging.

These results were also consistent with SANS patterns obtained in presence of NaP buffer (data not shown). As mentioned earlier, we suggested that aggregates that form in the frozen state likely assemble from the tetramer. Thus, the native tetrameric structure is not lost upon freezing, but rather becomes the building block for the higher order aggregates. To probe this further, higher order aggregates of the native tetramer were modelled including octamers, (Figure 2.8A) and 16-mers (Figure 2.8B), and their respective SANS patterns were calculated (Figure 2.8C and Figure 2.8D). These calculated patterns were overlaid with the SANS pattern from LDH (1000 µg/mL) in 10 mm histidine buffer (100% D_2O) at -45 °C. Comparing the SANS scattering in Figures 8C and 8D, at -45 °C a pronounced deviation from the octamer and 16-mer structure is evident for the LQS

scattering as well as a loss of signal is seen in the HQS between q = 0.025 and 0.1 $Å^{-1}$. However, there is still some evidence of the subsidiary maximum at q = 0.15 $Å^{-1}$ which can be attributed to the native tetramer, the precursor for formation of higher-order structures. Two important conclusions are: (i) we did not observe the dissociation of LDH tetramer into dimers in the presence of histidine or NaP buffer in the frozen state, and (ii) the aggregates that formed in the frozen state were higher order assemblies of the native tetrameric state (>> 16-mer). These higher order LDH aggregates were almost completely reversible after a single freeze-thaw cycle in 10 mM histidine buffer and 10- or 100-mM NaP buffer solutions. The retention of the tetrameric state as the basic unit in the formation of higher order aggregates was responsible for its reversibility post-thawing.

The above results were interesting given the fact that the LDH tetrameric structure did not dissociate into dimers and was reversible post freeze-thawing at ~1000 μg/mL in both histidine as well as NaP buffer solutions, even in the absence of a stabilizing excipient such as a sugar or surfactant. The results are partly consistent with earlier observations from Anchordoquy *et al*. where they proposed a direct correlation between maintenance of LDH quaternary structure in the frozen state by stabilizers such as BSA and PVP and its activity recovery post freeze-thawing and freeze-drying [54, 74]. In comparison with earlier reports, wherein the behavior of LDH in the frozen state was followed by indirect studies and extrapolated from freeze-thaw studies, this is the first report where the conformation of LDH in the *frozen state* has been systematically evaluated using neutron scattering.

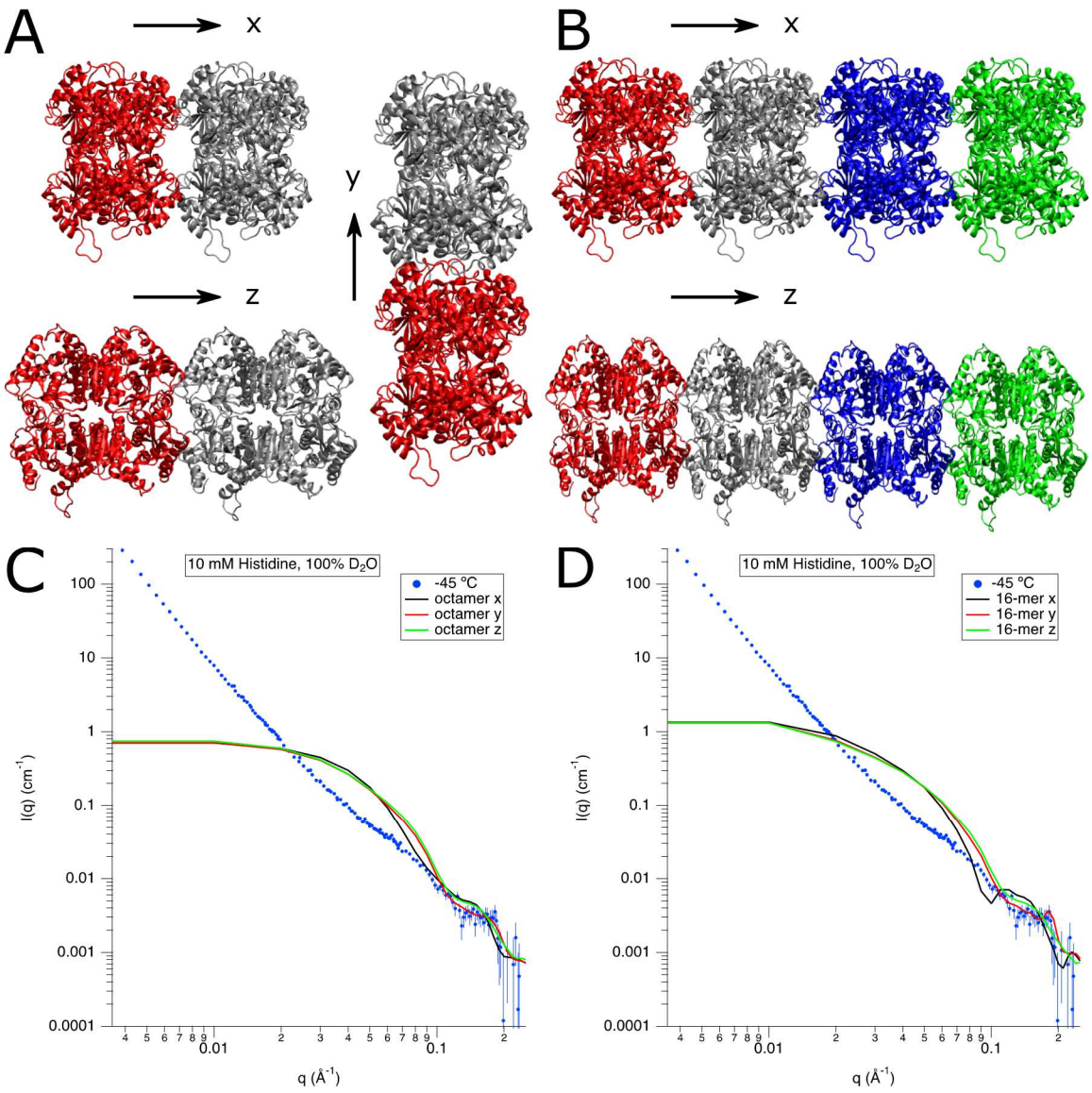

Figure 2.8 Modeling LDH aggregates to determine the type of aggregates observed experimentally in 10 mM histidine buffer (100% D_2O) solutions (A) LDH octamers modeled in three different orientations (B) LDH 16-mers modeled in three different orientations (C) Overlay of SANS curves for 1 mg/mL LDH in 10 mM histidine buffer in 100% D2O (blue data points) at -45°C and the reference LDH octamer curves in x, y and z orientations (black, red and green curves respectively) (D) Overlay of SANS curves for 1 mg/mL LDH in 10 mM histidine buffer in 100% D_2O (blue data points) at -45°C and the reference LDH 16-mer curves in x, y and z orientations (black, red and green curves respectively. Error bars are the standard error of the mean based on the number of pixels used during data averaging.

2.4 Significance

The stresses induced during freezing and thawing of protein solutions and their consequences on its stability are of immense interest to the pharmaceutical community. In most stress studies, the protein characterization is performed at the end of the freeze-thaw cycle and usually at room temperature. However, characterization in the frozen state is important for two reasons: (i) Aggregation during freezing can be an intermediate or precursor to irreversible protein aggregation. Thus, aggregate characterization may aid in the development of mitigation strategies. (ii) If the aggregation is reversible on thawing, the reversibility kinetics is of practical importance.

In LDH solutions (1000 μg/mL), irrespective of the buffer used (histidine or NaP), the aggregation observed in the frozen state was completely reversed when the solutions were thawed. The use of phosphate buffer provided an avenue to simultaneously evaluate the effects of stresses induced by freezing and pH shift. Phosphate buffer solutions are known to undergo pH shifts when frozen and at high buffer concentration (100 mM), the pH shift can be very pronounced. At this buffer concentration, LDH aggregation was evident following multiple freeze-thaw cycling. However, aggregation was reduced when the buffer concentration was lowered to 10 mM (both histidine and phosphate). Interestingly, when the protein concentration was lowered (10 or 100 μg/mL), the impact of the freezing stress was pronounced. These results suggest that the potential problems with the use of phosphate buffer may be overstated in the literature.

However, there was a limitation with the SANS studies. In order to get adequate signal, the protein concentration was 1000 μg/mL. Proteins are known to be self-stabilizing at high concentrations[9]. Protein solutions at much lower concentrations could be investigated by light scattering. Moreover, during long-term storage, a protein solution may undergo multiple freeze-thaw cycles. Therefore, the combined effects of low concentration and multiple freeze-thaw cycling were investigated by light scattering.

By combining SANS and DLS, a comprehensive characterization was possible which could not have been accomplished with the individual techniques. At a protein concentration of 1000 μg/mL (10 mM phosphate), SANS revealed self-association in the frozen state which was reversed on thawing. DLS confirmed the reversibility of the self-association even after five freeze-thaw cycles. However, DLS alone would not have revealed association of the native tetramer in the frozen state. While SANS provided qualitative information with respect to protein aggregation, the insights from DLS were quantitative with respect to the particle size of the aggregates.

Irrespective of the buffer used and the buffer concentration, there was evidence of aggregation when the LDH concentration was low (10 μg/mL). However, when the protein concentration was higher (≥ 100 μg/mL), only the high phosphate buffer concentration (100 mM) appeared to facilitate aggregation. Thus, the combined effects of potential pH shift and the repeated stress of freezing and thawing (five cycles) seem to be detrimental to protein stability.

2.5 Supplementary information

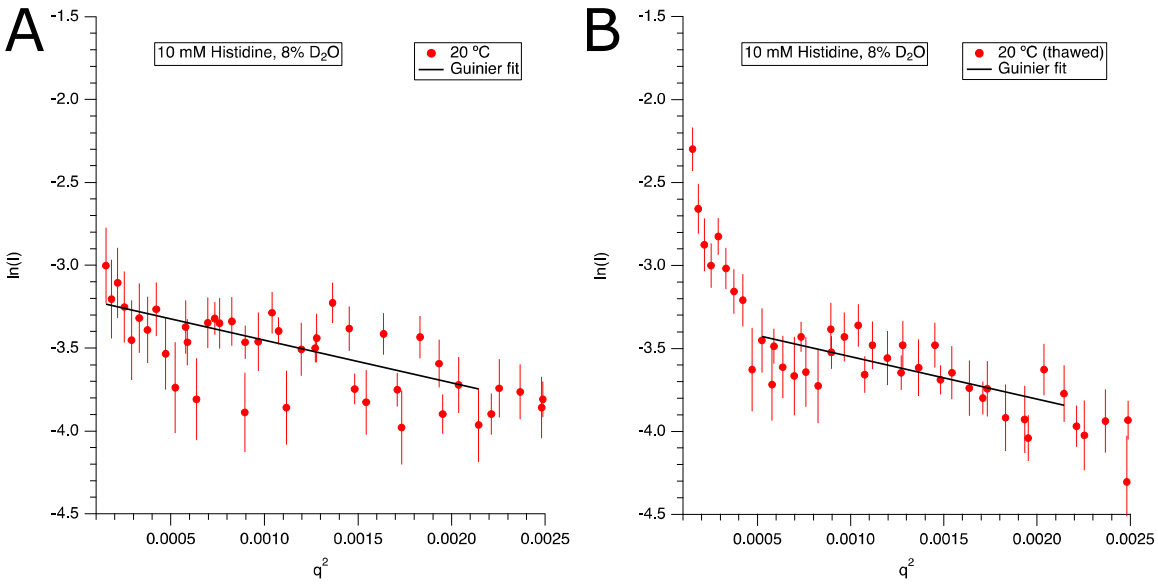

Figure 2.9 Guinier fits to the 1.0 mg/mL LDH in 10 mM histidine 8% D_2O buffer SANS data from Figures 2.3A and 2.3B. A. Before freezing and B. after one freeze-thaw cycles (thawed). The Rg and I(0) values from the Guinier fits are presented in Table 2.1. Error bars are from the standard error of the mean of the I(q) vs q data based on the number of pixels used in the data averaging.

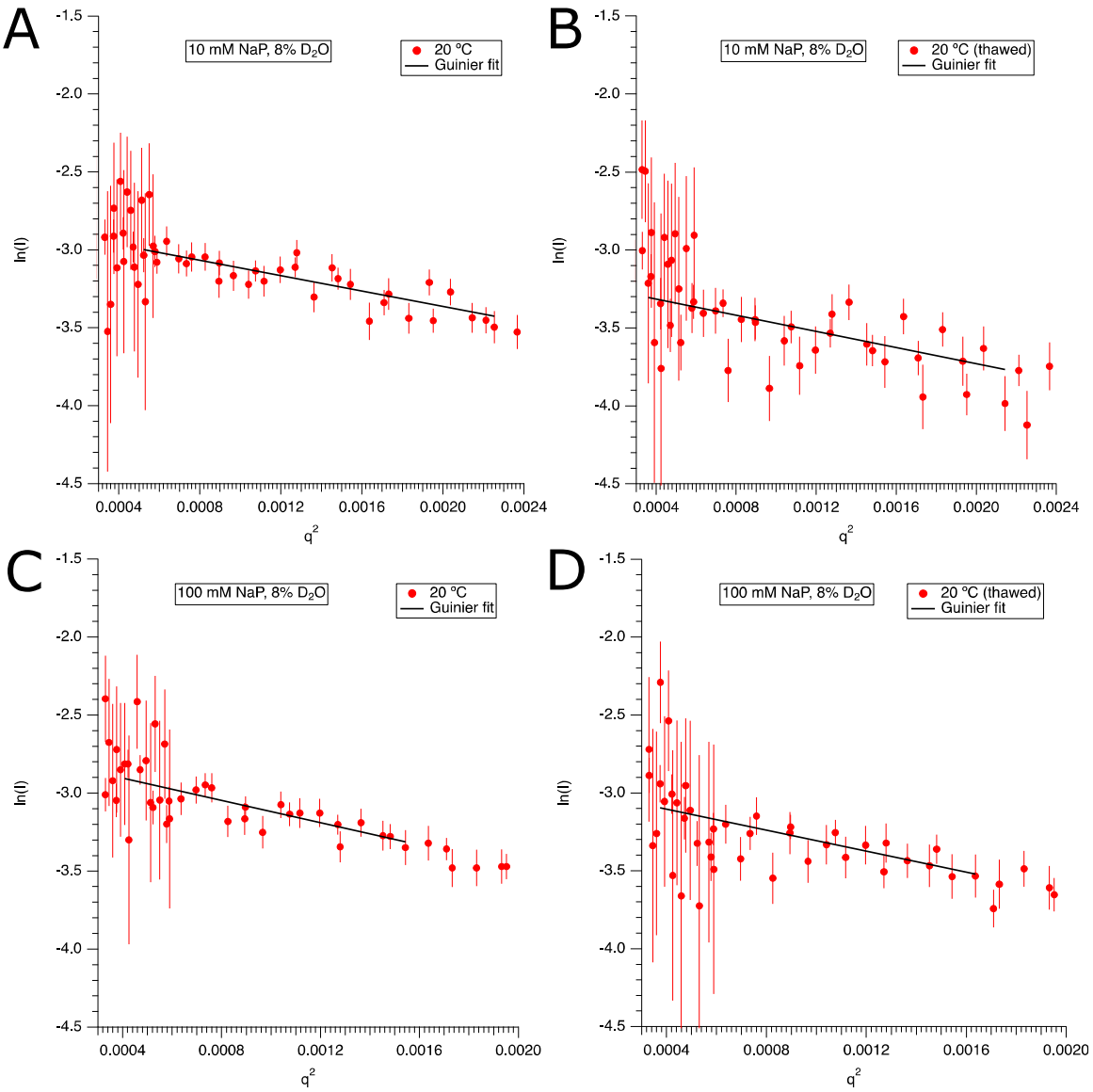

Figure 2.10A. Guinier fits to the 1.0 mg/mL LDH in 10 mM and 100 mM NaP 8% D_2O buffer SANS data from Figure 2.5. A. and C. Before freezing and B and D. after one freeze-thaw cycles (thawed). The Rg and I(0) values from the Guinier fits are presented in Table 2.1. Error bars are from the standard error of the mean of the I(q) vs q data based on the number of pixels used in the data averaging.

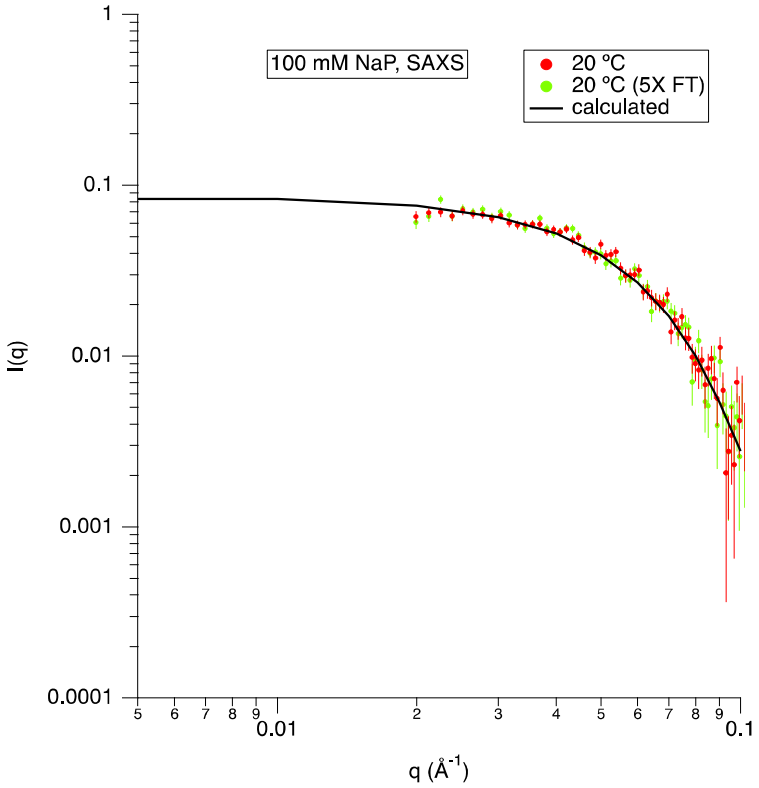

Figure 2.11 SAXS data from 0.5 mg/mL LDH in 100 mM NaP 0% D2O buffer at RT before freezing and after five freeze-thaw cycles (5X FT). The 5X FT data have been scaled to the RT data before freezing. The solid line is the calculated SANS curve from the atomic coordinates of the LDH tetramer (PDB ID 8V6M) as described in the *Methods* section. Error bars are the standard error of the mean based on the number of pixels used during data averaging.

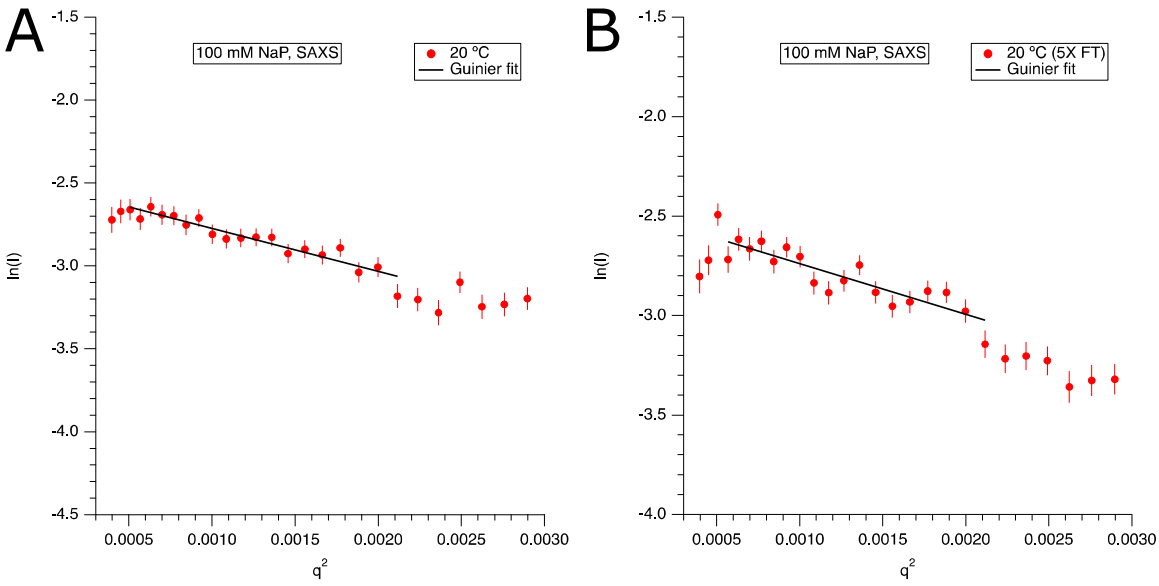

Figure 2.12 Guinier fits to the 0.5 mg/mL LDH in 100 mM NaP 0% D2O buffer SAXS data from Figure 2.11. A. Before freezing and B. after 5 freeze-thaw cycles (5XFT). The Rg and I(0) values from the Guinier fits are presented in Table 1. Error bars are from the standard error of the mean of the I(q) vs q data based on the number of pixels used in the data averaging.

Figure 2.13 Snapshot of LDH titration curve (surface charge as a function of pH) obtained from ProtPi Tool (*https://www.protpi.ch/Calculator/PeptideTool). The isoelectric point pI for LDH was 7.2 and the net charge at pH 5 is ~ 15 units. The tool is useful to determine the surface charge on LDH at different pH using the titration curve for protein with known amino acid sequence.

Note: The plot of net surface charge on LDH as a function of pH does not consider the LDH concentration and change in microenvironmental conditions in the freeze-concentrate. However, this information is helpful in the context of understanding the aggregation behavior of LDH as consequence of pH change.

**Certain commercial equipment, instruments, materials, suppliers, or software are identified in this paper to foster understanding. Such identification does not imply recommendation or endorsement by the National Institute of Standards and Technology, nor does it imply that the materials or equipment identified are necessarily the best available for the purpose.*

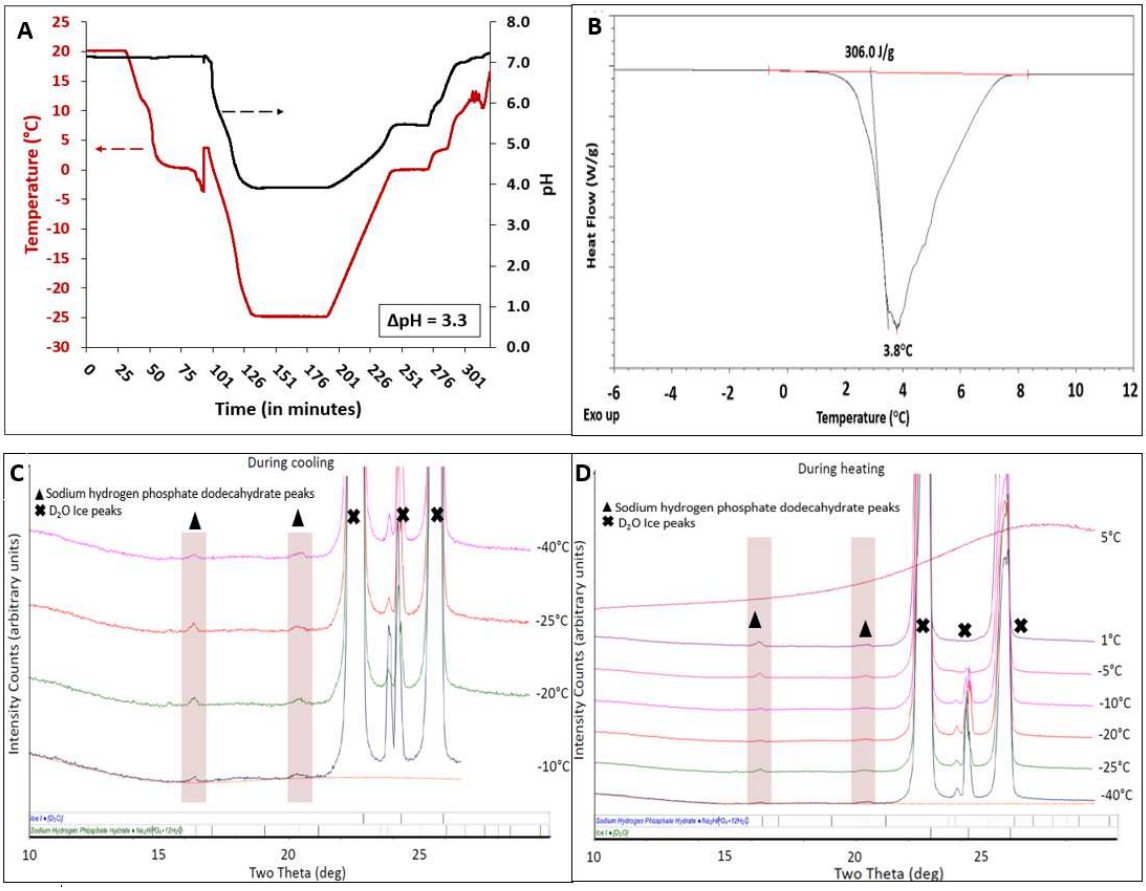

Figure 2.14 Characterization of sodium phosphate buffer (10 mM) during freezing and thawing (in 100% D_2O). A. Low temperature pH measurement, when cooled from 20 to -25 °C and then heated back to 20 °C. The heating as well as the cooling rate was 0.5 °C/min and the frozen solution was held at -25 °C for 30 minutes. B. The DSC heating curve of frozen solution, heated from -45 °C to 20 °C. The sample was cooled from 20 to -45 °C and heated back to 20 °C at 0.5 °C/min. Only the final heating curve is shown. C. XRD patterns obtained while the solution was cooled from 20 to -40 °C at 0.5 °C/min. The XRD patterns were obtained at -10, -20, 25 and -40 °C. D. XRD patterns obtained when the frozen solution (from C) was heated from -40 to 10 °C at 0.5 °C/min. The XRD patterns were obtained at -20, -10, -5, 1, 5 and 10 °C.

Chapter 3 Anomalous behavior of mannitol hemihydrate: Implications on sucrose crystallization in colyophilized systems*

*Reprinted from Anomalous behavior of mannitol hemihydrate: Implications on sucrose crystallization in colyophilized systems. 587/119629, Thakral, S., Sonje, J., and Suryanarayanan, R., 1-11, Copyright (2020), with permission from Elsevier [International Journal of Pharmaceutics].

3.1 Introduction

Mannitol, a sugar alcohol, is a popular bulking agent in freeze-dried pharmaceutical formulations. It has a high propensity to crystallize during lyophilization and the crystalline form provides structural support and elegance to the resulting cake. Its eutectic temperature with ice, ~ -1.5 °C, enables primary drying at a high temperature [76, 77]. The unintended vial breakage associated with mannitol crystallization can be minimized through careful design of the freeze-drying cycle[1]. Recent studies have shown that crystalline mannitol, by favorably affecting the cake attributes, decreased the reconstitution time of high concentration lyophilized protein formulations[78]. When retained amorphous, mannitol can serve as a cryoprotectant [79-81].

Depending upon the formulation components and processing parameters, during lyophilization, mannitol often crystallizes as a mixture of anhydrous polymorphs - α-, β- and δ- forms. The polymorphic form of anhydrous mannitol does not seem to have any measurable impact on the quality attributes of the drug product [82-85]. However, mannitol may also crystallize in a manner that two mannitol molecules associate with one water molecule, forming the lattice with an overall stoichiometry of a hemihydrate [mannitol hemihydrate (MHH); $C_6H_{14}O_6 \cdot 0.5H_2O$] [84, 86-88]. In contrast to anhydrous forms, the

formation of MHH during freezing and its retention in the lyophile might have implications on the final product performance (*vide infra*).

Upon freezing, many solutes incorporate water in the lattice and crystallize as hydrates. Some examples of pharmaceutical interest are sodium chloride dihydrate, sodium phosphate dodecahydrate, tert-butyl alcohol dihydrate, citric acid monohydrate and pentamidine isethionate trihydrate [77, 89]. When aqueous solutions are cooled, ice crystallization leads to solute supersaturation and formation of a freeze-concentrate [20]. When mannitol is a solute, it may partially crystallize during freezing. The extent of crystallization and the phase crystallizing from solution will depend on several factors including total solute content, formulation composition and the cooling rate [90, 83]. Mannitol may form a metastable glass and crystallize when heated above its glass transition temperature. Experiments have shown that the physical form of mannitol crystallizing from frozen solution is dictated by the annealing temperature, with MHH being the least soluble form at temperatures $\leq$ -20 °C, while the anhydrous form crystallizing preferentially at temperatures $\geq$ -10 °C [84, 91, 92].

The presence of cosolutes, for example trehalose, sucrose, sodium chloride, polyvinyl pyrrolidone or buffer salts, in the prelyophilization solution promotes formation of MHH, with the effect being most pronounced in presence of sodium chloride [85, 93, 94]. When lyophilized with protein, the MHH content retained in the final lyophile was dependent on the type and concentration of protein. As an example, lysozyme promoted while bovine serum albumin inhibited the formation of MHH [95]. With a fusion protein, the maximum

MHH content was observed at an intermediate protein concentration, with higher protein content inhibiting mannitol crystallization. Addition of sucrose to the formulation also facilitated MHH formulation [96]. Liao et al have shown that MHH formation was inhibited in the presence of an albumin fusion protein [97], while Cao et al reported that a fusion protein facilitated MHH formation in a concentration dependent manner (upon annealing at -20 °C) [98]. Interestingly, MHH was not observed when mannitol was colyophilized either with sucrose or trehalose. This can be attributed to secondary drying at elevated temperatures of 33 or 40 °C [99, 100].

In formulations, generally, it will be prudent to use the most stable physical form of the drug and excipients. This will decrease the risk of phase transitions during processing and storage. Under ambient conditions, MHH is a metastable hydrate. It will tend to dehydrate and form anhydrous mannitol. Structurally, the instability of the phase can be attributed to the deformation of the second mannitol molecule, incorporated into lattice through strong intermolecular forces with water. Solid-state density functional theory simulations of MHH crystal structure were employed to comprehend the deformation [91, 101]. The existence of MHH in lyophilized formulations is believed to be associated with several implications. (i) Inconsistent formation of MHH during the lyophilization cycle which undermines the reliability of the manufacturing process. (ii) Requirement of an aggressive drying cycle to dehydrate MHH; as a result, there is potential to cause decomposition of drug substance. (iii) Release of lattice water during storage, which can have a significant impact on the physical and chemical stability of the formulation components. The released water can be sorbed by the amorphous formulation components, resulting in a reduction in glass

transition temperature, and increase in their reactivity [84, 85, 88, 93]. While these possibilities have been repeatedly pointed out, there is little experimental evidence of the detrimental effects of released water. The only preliminary evidence is the pioneering study by Johnson et al, where sucrose crystallization was observed when formulations containing mannitol, sucrose and protein were stored at RT for 1 year [87]. In a recent study, MHH had no impact on the stability of the investigated monoclonal antibody following temperature stress studies [102].

In light of the above discussion, the present study was conducted with two initial objectives. (i) To study the dehydration behavior of MHH in lyophiles prepared with or without sucrose. (ii) To determine the influence of MHH dehydration on sucrose crystallization. In our experiments, the physical forms of mannitol (and sucrose) were monitored following storage of the lyophiles at different water vapor pressures (at RT). The preliminary results led to the third objective: (iii) to study the dynamics of water movement in sealed vials by simultaneously monitoring headspace humidity and determining the physical form and the water content in the lyophile. Our attempts to comprehend the movement of water from the lyophiles necessitated evaluation of the critical role of rubber stoppers in modulating the water vapor pressure in sealed vials.

3.2 Materials and Methods

3.2.1 Materials

Mannitol ($C_6H_{14}O_6$) and sucrose ($C_{12}H_{22}O_{11}$), were purchased from Sigma Aldrich (St. Louis, MO, USA) and used as received. Saturated salt solutions, prepared from salts

purchased from Fisher Scientific (Waltham, MA, USA), were used to prepare chambers with different relative humidities (RH): lithium chloride (11% RH), potassium carbonate (43% RH), sodium bromide (57% RH), sodium nitrite (64% RH), sodium chloride (75% RH) and potassium sulfate (97% RH) at ambient temperature.

3.2.2 Lyophilization

Solutions of mannitol alone or with sucrose as the second component in a 4:1 weight ratio, were prepared in de-ionized water (total solute content 5% w/v). The solutions were filled into 10 mL glass vials (DWK Wheaton, either 2- or 7-mL fill volume), partially covered with rubber (chlorobutyl-isoprene blend, uncoated) stoppers (20 mm, 2 Leg Lyo, Gry Butyl Sil, Wheaton) and loaded into the freeze-dryer. Lyophilization was carried out in a bench top unit (VirTis AdVantage, Gardiner, NY). The shelf was cooled to -45 °C at 2 °C/min and held for 6 h. Primary drying was conducted at -25 °C (200 mTorr; 48 h). During secondary drying, the shelf was heated to +10 °C and held for 24 h. At the end of the cycle, the chamber was backfilled with dry N_2 gas and the vials were stoppered within the sealed chamber and stored at -20 °C until further analysis.

Preliminary experiments indicated that the fill volume influenced the MHH content in the lyophile. Therefore, a fill volume of 7 mL was used when a high MHH content were desired. In addition, secondary drying conducted at 10 °C, reduced the possibility of MHH dehydration during the process.

3.2.3 Storage treatments

Lyophiles, containing mannitol alone or mannitol sucrose, were stored in desiccators containing saturated salt solutions (11, 43, 64 and 97% RH at RT) and samples were regularly analyzed by X-ray diffractometry. Separate desiccator was used for replicate measurements. Co-lyophilized mannitol-sucrose samples were additionally stored in chambers containing saturated salt solutions (57% and 75% RH at RT), sampled every 6 hours and sealed hermetically in aluminum pans. Pans were stored at -20 °C and subjected to synchrotron XRD.

3.2.4 X-ray diffractometry

A powder X-ray diffractometer (D8 Advance; Bruker AXS, Madison, WI) equipped with a Si strip one-dimensional detector (LynxEye) was used. Samples were exposed to Cu Kα radiation (40 kV × 40 mA) over an angular range of 5-35° 2θ with a step size of 0.02° and a dwell time of 0.5 s.

3.2.5 Synchrotron X-ray diffractometry (SXRD)

The lyophile samples packed in aluminum pans were mounted vertically in a specially fabricated plate. Experiments were performed in the transmission mode in the 17-BM-B beamline at Argonne National Laboratory (Argonne, IL, USA). A monochromatic X-ray beam [wavelength 0.45452 Å; beam size 300 μm × 300 μm] and a two-dimensional area detector (XRD-1621, PerkinElmer) were used. A triple-bounce channel-cut Si single crystal monochromator with [111] faces polished was used, which limited the line broadening to its theoretical low limit, *i.e.*, the Darwin width. The sample to detector

distance was set at 900 mm. Corundum (Al_2O_3: SRM 674a, NIST) was used as the calibration standard. During data collection, the sample was oscillated (±1 mm from the center along the horizontal axis) using a stepper motor. Each sample was scanned 10 times, with an exposure time of 1 s for each scan.

3.2.6 Headspace Humidity Measurement

In a select set of vials (total number 25), rubber stoppers were fitted with digital humidity/temperature sensors (EK- H4, Sensirion AG, Switzerland). At the end of lyocycle, all the stoppers were lowered into vials in the N_2-backfilled chamber. Immediately after taking the vials out of the lyophilizer, the sensor in rubber stopper was connected through an interface to a computer. The vials were then transferred to a convection oven set at 40 ºC. The temperature and headspace RH were continually recorded, in three representative vials, for 20 days (set-up shown in Figure 3.1). At predetermined times, a vial was removed from the oven. The XRD pattern and water content of lyophile were recorded. Thus, we were able to monitor the headspace RH continuously while the water content and physical state of lyophile components were determined at defined time intervals.

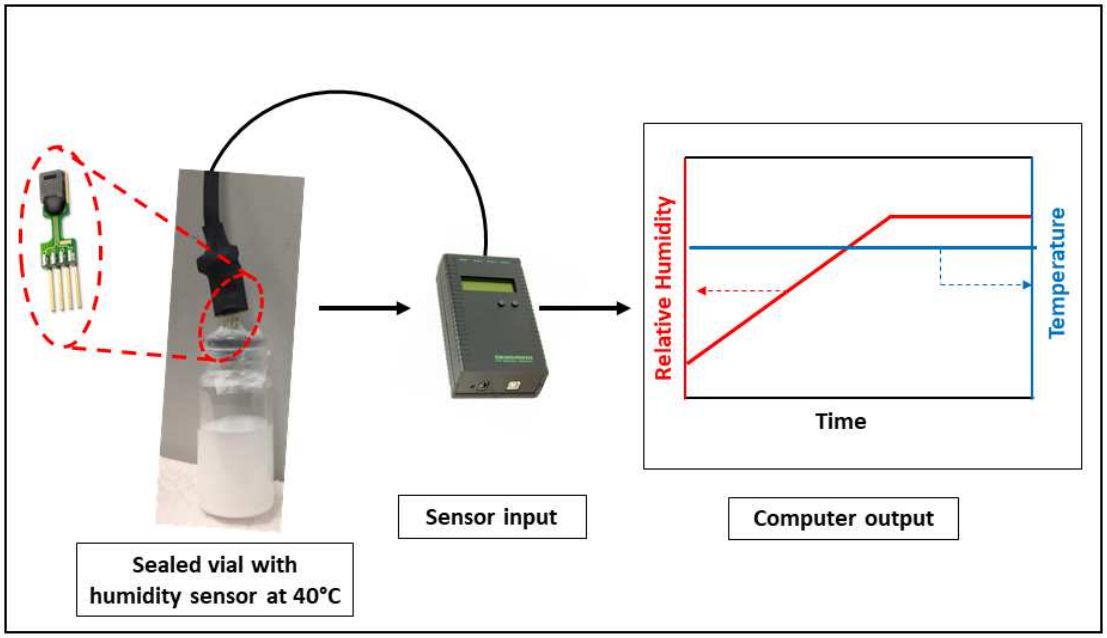

Figure 3.1 Schematic representation of vial headspace humidity measurement assembly. An expanded view of the sensor is also provided. The vials were stored at 40 °C and the relative humidity data was continuously recorded and stored on the computer connected through a digital recorder. Parts of the diagram have been adapted from www.sensirion.com [103].("Digital Humidity Sensor SHT7x (RH/T)," n.d.) Reproduced with permission.

3.2.7 Karl Fischer Titrimetry

The sample was added to the titration cell, and the water content was determined coulometrically using a Karl Fischer titrimeter (DL36, Mettler Toledo, Columbus, OH).

3.2.8 Stopper moisture content by gravimetric method

After completion of the headspace RH measurements, the three rubber stoppers were dried in a convection oven at 105 °C. The weight of the stoppers before and after drying were recorded [104].

3.3 Results and Discussion

3.3.1 Dehydration behavior of MHH

The XRD pattern obtained after lyophilizing mannitol (5% w/v solution) contained intense peaks at 16.5 and 17.9 °*2θ* peak, which are characteristic of MHH. The characteristic peaks of α- and β-mannitol, observed at 13.6 and 14.6 °*2θ* respectively, were absent. The low intensity peak at 20.4 °*2θ* indicated that a small fraction of mannitol occurred as the anhydrous δ- polymorph (Supplementary Information Figure 3.10). Thus, the lyophile consisted predominantly of MHH. MHH presence was attributed to the high fill volume coupled with conduction of secondary drying at 10 °C.

The dehydration behavior of MHH was strongly influenced by the storage RH. When stored at 11% RH, over the course of 6 days, there was a gradual reduction in the intensity of the 17.9 °*2θ* peak (Figure 3.2). After about two days (46 h), a peak split was observed, wherein the MHH peak at 9.6 °*2θ* was followed by the appearance of a peak at 9.7 °*2θ* attributed to δ-mannitol. The gradual increase in intensity of peaks at 9.7 and 20.4 °*2θ*, as a function of storage time, provided additional evidence of MHH → δ-mannitol transformation. In addition, appearance of a low intensity peak at 14.6 °*2θ* in samples stored beyond 46 h also suggested partial MHH → β-mannitol transformation. MHH dehydration was substantially complete in 148 h (Figure 3.2). The presence of seeds of δ-mannitol might have enabled the preferential transformation to this polymorph. Burger et al established that though the δ-form of anhydrous mannitol is thermodynamically unstable under ambient conditions, it shows significant kinetic stability[82].

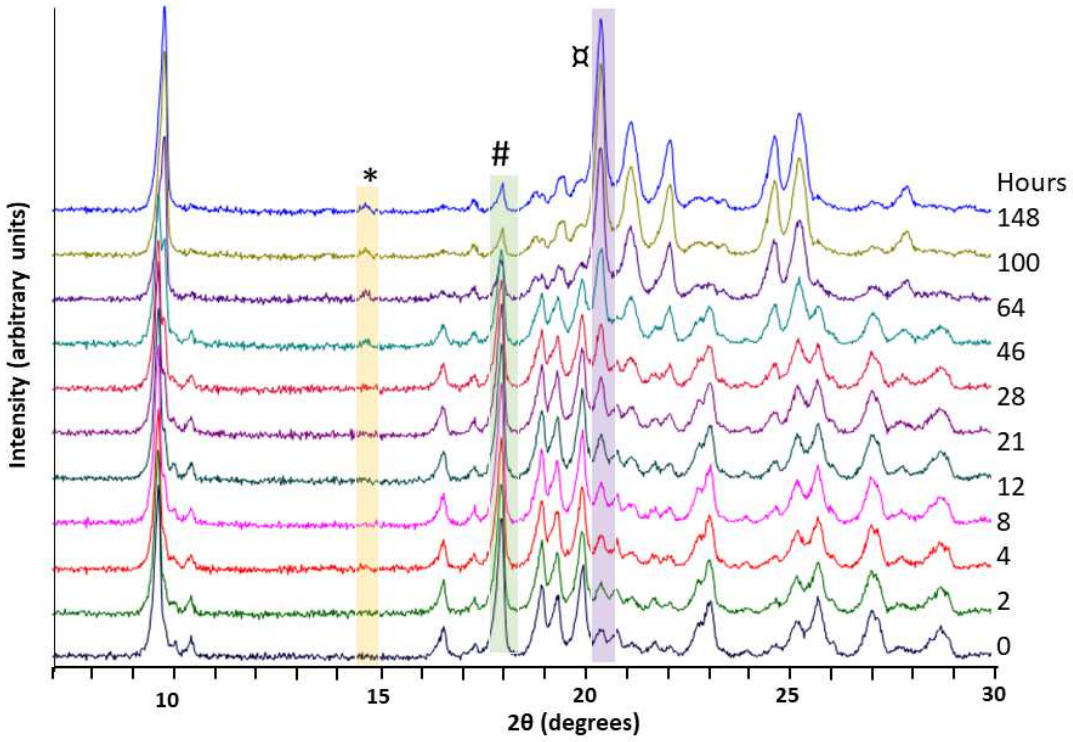

Figure 3.2 XRD patterns of lyophilized mannitol following storage at 11% RH (RT). The gradual reduction in intensity of a characteristic peak of MHH (#) along with the evolution of δ-(¤) and β- (*) mannitol peaks is highlighted.

The MHH peak intensity in the fresh lyophile was assumed to be 100%, and the peak intensities obtained as a function of storage time, were expressed with respect to the initial intensity (Figure 3.3). Such an approach enabled us to compare the results obtained following the storage of the samples at different RH values. When stored at 11% RH, a sharp reduction in MHH peak intensity at 2 h was followed by an increase at 8 h which was quite pronounced. Continued exposure led to a gradual reduction in MHH content. Cao et al have also observed a similar trend in the MHH dehydration [86]. This seemingly anomalous behavior, though reproducible, was not investigated further in the present study.

After storage for 21 h, the MHH content was reduced to 80% [± 12%; n=3)] and even after 148 h, 11% [± 3%] of MHH was retained in the lyophile.

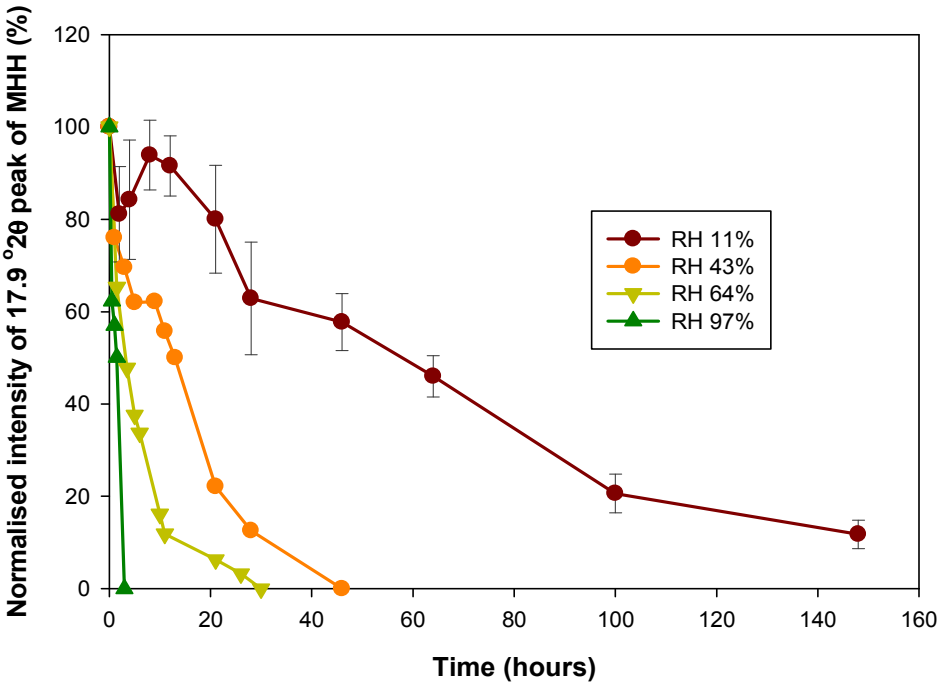

Figure 3.3 MHH dehydration (represented as the normalized* intensity of 17.9° 2θ peak) following storage at 11, 43, 64 and 97% RH (RT). To retain clarity, the error bars are shown only for the dehydration data obtained at 11% RH. The error bars for all the data are shown in Figure 3.11 in Supplementary material). *The MHH peak intensity in the fresh lyophile was assumed to be 100%, and the peak intensities obtained as a function of storage time, were expressed with respect to the initial intensity.

When stored at 43% RH, the reduction in 17.9° *2θ* peak intensity was faster than at 11% RH. After 21 h, MHH content reduced to 22% [± 7%] and the peak was absent at *46* h. The sample had dehydrated to δ- mannitol, though the low intensity peak at 14.6° *2θ* suggested a trace of β-mannitol (data not shown). For samples stored at 64% RH, MHH dehydration was even faster than at 11 and 43% RH. MHH content decreased to ~10% just after 11 h. MHH completely dehydrated in 21 h, again predominantly to the δ- form. The dehydration

was fastest at 97% RH, and was complete in < 3h, with the anhydrous form again being the δ-mannitol. Lyophilized mannitol is not expected to be exposed to 97% RH. This storage condition was used with the goal of developing a comprehensive understanding of MHH dehydration.

In general, hydrates demonstrate a decrease in dehydration rate with an increase in water vapor pressure [105]. However, MHH dehydration was the slowest at 11% RH and fastest at 97% RH. Such an anomalous behavior of MHH has been reported for the first time.

3.3.2 Anomalous MHH dehydration

An increase in the dehydration rate of crystalline hydrates with an increase of water vapor pressure, over a limited range of vapor pressures, was first observed by Topley and Smith and is known as the Smith-Topley effect[106]. Such behavior has been exhibited by several inorganic hydrates, including hydrated sulfate salts of copper, iron, magnesium, nickel, lithium, calcium, zinc and manganese, nickel nitrate heptahydrate, and cobalt chloride hexahydrate. In addition, organic salts of some cations, such as oxalates of manganese (dihydrate) and calcium (monohydrate) also exhibit maximum dehydration at an intermediate water vapor pressure[107]. Among materials of pharmaceutical relevance, dehydration of dicalcium phosphate dihydrate, when exposed to RH values ranging from 0% to 80% at 60 °C, occurred most rapidly at RH values ≥ 40% [108]. Caffeine hydrate also exhibited a constant dehydration rate between 0 and 13% RH and a slight increase at 24% RH [109]. The fact that mannitol hydrate exhibits such an unexpected behavior is interesting in view of the extreme popularity of mannitol as a pharmaceutical excipient.

Among different mechanisms suggested for the Smith-Topley effect, product recrystallization in presence of H_2O is the most popular [107]. The recrystallization process is believed to result in the formation of additional channels, cracks and pores between product grains, which facilitate water vapor removal from the reaction zone and, as a result, the rate of dehydration increases. A further increase in RH can promote rehydration and hence for most of the examples listed above, the fastest dehydration is observed at an intermediate RH [110].

The above argument can be used to explain the anomalous behavior of mannitol. At low RH, MHH dehydration is expected to lead to the formation of a poorly crystalline anhydrous phase, which forms a layer on the particle surface and impedes further dehydration. At higher water vapor pressures, crystallization, through the formation of cracks and opening up of channels, causes a change in the nature of the product layer and facilitates further water removal. Formation of MHH is a low-temperature phenomena and occurs by recrystallization from frozen solution. MHH cannot be prepared by exposing mannitol to high RH. At ambient temperature, rehydration at elevated RH conditions is thus not possible and under the range of humidity conditions studied, maximum dehydration was observed at the highest RH.

3.3.3 MHH dehydration in co-lyophilized system

The successful lyophilization of proteins requires addition of a lyoprotectant such as sucrose or trehalose, which 'protects' the protein from the stresses induced during freezing and drying. These stabilizers are required to remain in the amorphous state, not only during

freeze-drying but also the entire shelf-life of the product. A popular approach to achieve an elegant and stable lyophilized product is to add a crystalline bulking agent along with an amorphous lyoprotectant, with the former at a higher concentration [111]. Mannitol - sucrose mixture, in a 4:1 weight ratio, has been used to successfully stabilize numerous proteins in lyophilized formulations[87]. At this composition, MHH formation is widely reported [92, 93, 95]. In light of its practical significance, MHH dehydration in this combination was investigated.

The solutions containing mannitol and sucrose were lyophilized, with the higher fill volume (7 mL in 10 mL vials) and secondary drying was conducted at the lower temperature (+10 °C), so as to retain MHH [92]. XRD pattern of the final lyophile showed the presence of MHH and δ-mannitol (peaks at 17.9 and 20.4 °*2θ* respectively) along with a small amount of β-mannitol (peak at 14.6 °*2θ;* Figure 3.12).

Storing the lyophile at 11% RH led to gradual dehydration of MHH, as evident from the reduction in intensity of the 17.9 °*2θ* peak (Figure 3.4). Interestingly, the anhydrous product formed was a mixture of β- and δ-mannitol, as evident from the gradually increasing intensities of the 14.6 and 20.4 °*2θ* peak respectively. The MHH peak could not be detected after ~16 days. A comparison of MHH dehydration kinetics in mannitol alone and in presence of sucrose is presented in Figure 5. The presence of amorphous sucrose appears to delay MHH dehydration. Ostensibly, MHH perceived a lower water vapor pressure (or 'drier' environment) in presence of sucrose and hence the decrease in dehydration rate. As expected, sucrose crystallization was not observed at such low RH.

Amorphous sucrose has been shown to resist crystallization for 3 years at RH <12% (25 °C) [112].

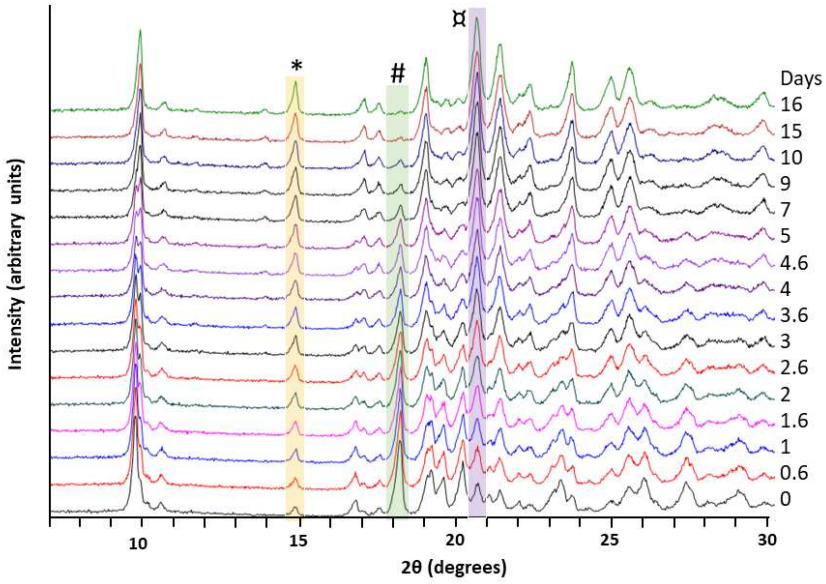

Figure 3.4 XRD patterns of lyophilized mannitol-sucrose (4:1 w/w) following storage at 11% RH (RT). The gradual reduction in intensity of peak attributed to MHH (#) and evolution of δ-(¤) and β- (*) mannitol peaks is highlighted.

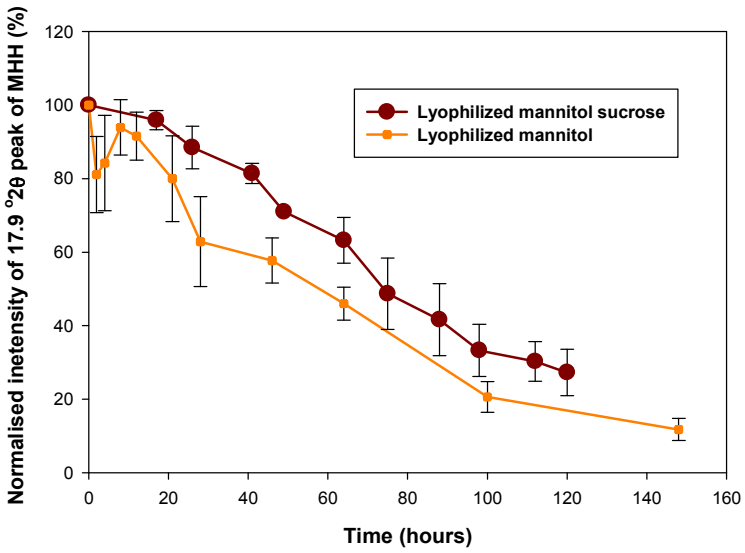

Figure 3.5 Plot comparing the dehydration kinetics of MHH in lyophilized mannitol and mannitol-sucrose (4:1 w/w) stored at 11% RH (RT). In the mannitol-sucrose system, for the intensity of the 17.9 °2θ MHH peak measured at 49 h, the error bar was smaller than the size of the symbol.

Storing lyophilized mannitol-sucrose at 97% RH led to rapid MHH dehydration and peaks attributed to MHH vanished after exposure for 2 h (Figure 3.6). The dehydration kinetics were comparable to that of lyophilized mannitol at the same water vapor pressure. An interestingly phase transformation, MHH → δ-mannitol → β-mannitol, was noticed in this case. MHH dehydration was followed by an increase in intensity of peaks attributed to δ-mannitol, which continued for ~10 h. However, the XRD pattern of the sample after 24 h storage show increase in intensity of β-mannitol peaks. This continued on further storage and all the peaks in the XRD pattern of sample stored for 4 days could be attributed to β-mannitol.

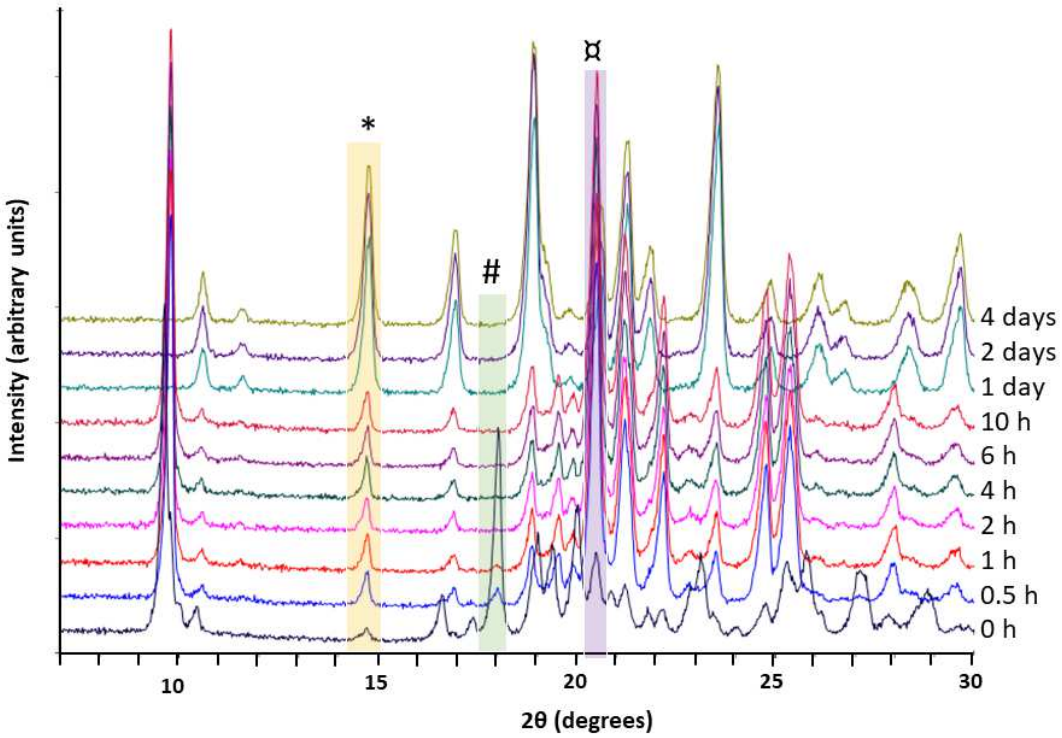

Figure 3.6 XRD patterns of lyophilized mannitol-sucrose (4:1 w/w) following storage at 97% RH (RT). The reduction in intensity of peak attributed to MHH (#) and evolution of δ-(¤) and β-(*) mannitol peaks is highlighted for reference. Notice difference in XRD pattern of samples stored for 10 h and 24 h (regions 19-20 and 26-27 °2θ).

In the XRD patterns of the samples stored at 97% RH for 4 days, there was no evidence of crystalline sucrose. Physical examination revealed collapse of the lyophile. This is understandable given that the RH was higher than the critical RH of sucrose, leading to its deliquescence (RH_0 of sucrose = 85% at 25 ºC [113]). While retained amorphous after lyophilization, on exposure to high RH, sucrose must have rapidly crystallized and immediately deliquesced [114]. This process must have occurred very rapidly since characteristic peaks of sucrose (for example at 8.4 and 11.7 °*2θ*) were not observed. The solution of sucrose could have served as the medium for the solution-mediated phase

transformation for anhydrous mannitol forms. The anhydrous δ-form, present initially as well formed by dehydration of MHH, dissolved in the sucrose solution. The β-form, seeds of which were present and which is the most stable form, crystallized out of the solution. The process continued until conversion of the δ- to β-mannitol was complete.

3.3.4 Sucrose crystallization in final lyophile

Unintended crystallization of an amorphous component, such as sucrose [115], can lead to loss of lyoprotectant activity. Moreover, the release of the unfrozen water associated with sucrose can compromise product stability. The non-isothermal and isothermal (under varying environmental conditions) crystallization of sucrose is well characterized [116]. In general, an increase in RH decreases the crystallization onset time. As RH increases, more water is available to facilitate sucrose mobility (that is, as the water content increases, the Tg decreases and sucrose mobility increases) and thus speeds crystallization [114]. Even at low RH, crystallization of amorphous sucrose is believed to occur through the formation of a viscous solution [117]. Sucrose crystallization was delayed when its physical mixture with various saccharides was stored in a controlled water vapor pressure environment [118].

We were next interested in monitoring the crystallization kinetics of sucrose, at lower RH values (in the range of 50 to 75%), over a short period of time (< 1 week). The laboratory XRD was inadequate to detect low levels of crystalline components (< 3%) formed at early stages of phase transformation. The use of high intensity synchrotron radiation coupled with an area detector, substantially enhanced the sensitivity of the technique. Colyophilized mannitol-sucrose were stored at 57 and 75% RH and XRD patterns were collected at the

synchrotron beamline every 6 h (Figure 3.13 and Figure 3.14). Upon storage at both RH conditions, MHH dehydration occurred rapidly. The dehydration was faster at 75% RH than at 57%. The characteristic peak of MHH peak was not detectable after 24 and 12 h in samples stored at 57 and 75% RH respectively. Sucrose crystallization was evident in both the samples and the intensity of 11.7 °2θ peak, enabled quantification of its crystallization (Figure 3.7). The onset of sucrose crystallization was observed after 18 h and ~ 70 h in samples stored at 57% and 75% RH respectively. Interestingly, the crystallization kinetics was very different at the two RH conditions. At 57% RH, crystallization commenced early but was gradual while it was delayed at 75% RH but was rapid once initiated. Surprisingly, the earlier crystallization onset at 57% RH, in comparison to 75% RH, is not in agreement with the reported behavior of amorphous sucrose [119]. Therefore, this issue was investigated in detail (*vide infra*).

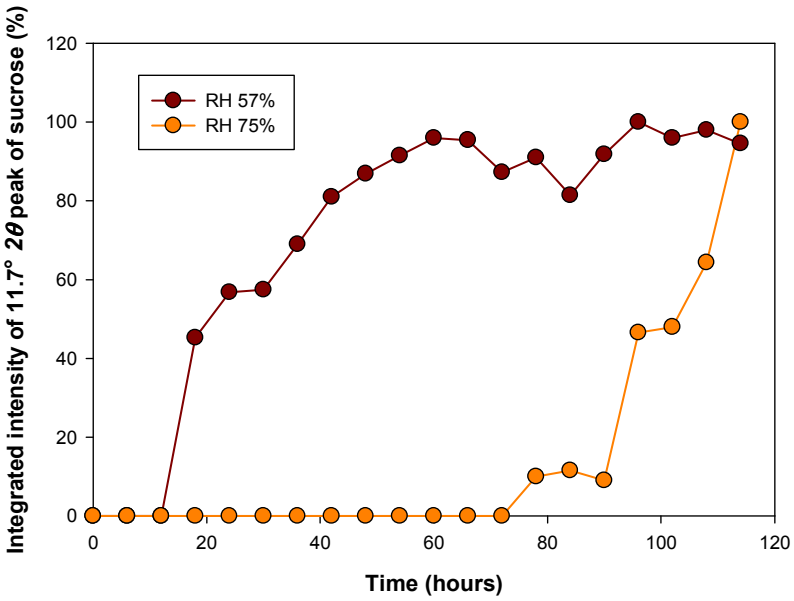

Figure 3.7 Crystallization of sucrose following the storage of lyophilized mannitol-sucrose (4:1 w/w) mixture at 57 and 75% RH (RT). The intensity of 11.7° 2θ peak of sucrose is plotted as a function of storage time. The highest intensity was assigned to be 100%, and the rest of the intensities are expressed with respect to this number. The experiments were performed in triplicate and one representative result is shown here. The rest of the data are presented in supplementary material (Figure 3.15).

When exposed to high water vapor pressure, amorphous sucrose sorbs enough water to crystallize (called moisture-induced crystallization), with the attendant release of the sorbed water. Numerous studies have established a correlation between the water content and percent crystallinity of sucrose samples [117]. A rapid decrease in water content in (partially) amorphous sucrose results in a sharp increase in percent crystallinity since crystalline sucrose is anhydrous. In an effort to understand the unexpected sucrose crystallization (delayed at 75% RH and earlier at 57% RH) behavior in colyohilized mannitol-sucrose, we studied the moisture sorption profile of amorphous sucrose under the relevant RH conditions. It was realized that the moisture sorption profiles of colyophilized

systems would be quite complicated due to multiple simultaneous events (MHH dehydration, sucrose water sorption and desorption, crystallization).

It is relevant to thoroughly understand movement of water in the mannitol-sucrose lyophile, when stored at 57 and 75% RH. Results from synchrotron studies show that at 57% RH, MHH dehydrated slowly (Figure 3.13 and Figure 3.14). It is reasonable to assume that the water is released sufficiently slowly so that equilibrium is maintained. In other words, the lyophile continuously experiences a fixed RH of 57%. On the other hand, at 75% RH, MHH dehydrated very rapidly. As a result of the rapid water loss, we postulate that the headspace experienced a transient increase in RH to > 75%. If the headspace RH is ≥ 80%, sucrose dissolution in the sorbed water will occur. The resulting 'dilution' would not be favorable for sucrose crystallization. However, the system will tend towards the equilibrium RH of 75%. The delay in sucrose crystallization could be explained by the transient disturbance to the system equilibrium. However, since there is a pronounced T_g lowering (due to the sorption of water), once initiated, the crystallization would progress rapidly.

It is recognized that the kinetics of water sorption in a constant humidity chamber (a 'static' environment), would be different from that in an automated water sorption apparatus [120]. The dynamic environment in the latter, brought about by the nitrogen flow, would facilitate rapid attainment of equilibrium. In an effort to understand the water sorption and crystallization behavior of sucrose, amorphous sucrose was exposed to 85% RH followed by 80% RH. Sucrose sorbed ~30% w/w water at 85% RH. When the RH was reduced to

80%, there was immediate weight loss, suggesting simultaneous desorption and sucrose crystallization (Figure 3.16). Studies on moisture uptake by amorphous sucrose were also conducted at 57 and 75% RH (Figure 3.17). Sucrose sorbed ~7 and 17% w/w water (degree of supersaturation 6.1 and 2.9 respectively) at 57 and 75% RH respectively. The moisture sorption profile at 75% RH showed rapid weight increase followed by weight loss, reflecting that water sorption and the consequent sucrose crystallization occurred very quickly. The entire process was complete in ~3 h. On the other hand, at 57% RH, sucrose crystallization (the weight loss) was quite slow and was incomplete even after 20 h. The difference in weight loss kinetics at the two RH conditions provides a fitting explanation for the difference observed with the kinetics of sucrose crystallization in the synchrotron studies (Figure 3.13 and Figure 3.14).

3.3.5 Movement of water in a sealed vial

The controlled RH studies confirmed the role of water vapor pressure (measured as RH) in modulating MHH dehydration as well as sucrose crystallization. Contrary to the behavior of conventional hydrates, MHH dehydration is constrained at low RH conditions. This observation has significant potential implications on the detrimental effects of MHH in final lyophile. If the headspace RH in a vial is maintained low (as is the popular industrial practice), both MHH dehydration and sucrose crystallization is expected to be quite slow. As a result, mannitol, even if retained as metastable MHH, *might not* exhibit any change in the physical form in timescales of practical importance. In order to follow the movement of water, the next set of studies were conducted in sealed vials. This unique arrangement enabled us to continuously monitor the headspace RH and temperature in three vials.

Simultaneously, at selected time-points, the physical form of mannitol and the water content were determined. For each time-point, a fresh vial was opened.

First, we present the data collected with the three RH sensors (Figure 3.8). As the vials were backfilled with nitrogen gas in the lyophilizer, the initial headspace RH in the three vials was ~3%. The vials were transferred to an oven at 40 °C where headspace RH and temperature were continuously monitored for 20 days (Figure 3.8). There was a distinct, two step increase in headspace RH. The very act of transferring vials from RT to 40 °C led to an initial increase in RH to 24, 20 and 22% in vials 1, 2 and 3 respectively. In general, an increase in temperature is expected to cause a reduction in RH. The observed RH increase in this case suggests release of water from lyophile, presumably from MHH dehydration. The RH remained almost stable for some time, the duration being variable among the three vials. This was followed by a steep rise in RH to 78, 71 and 78% respectively in the three vials. Interestingly, though the trend was similar in all the three vials, the time scale of the second step rise was quite variable (8, 18 and 6 days respectively). This variability can be attributed to the inter-vial variation within a batch, a phenomenon widely known in the freeze-drying community.

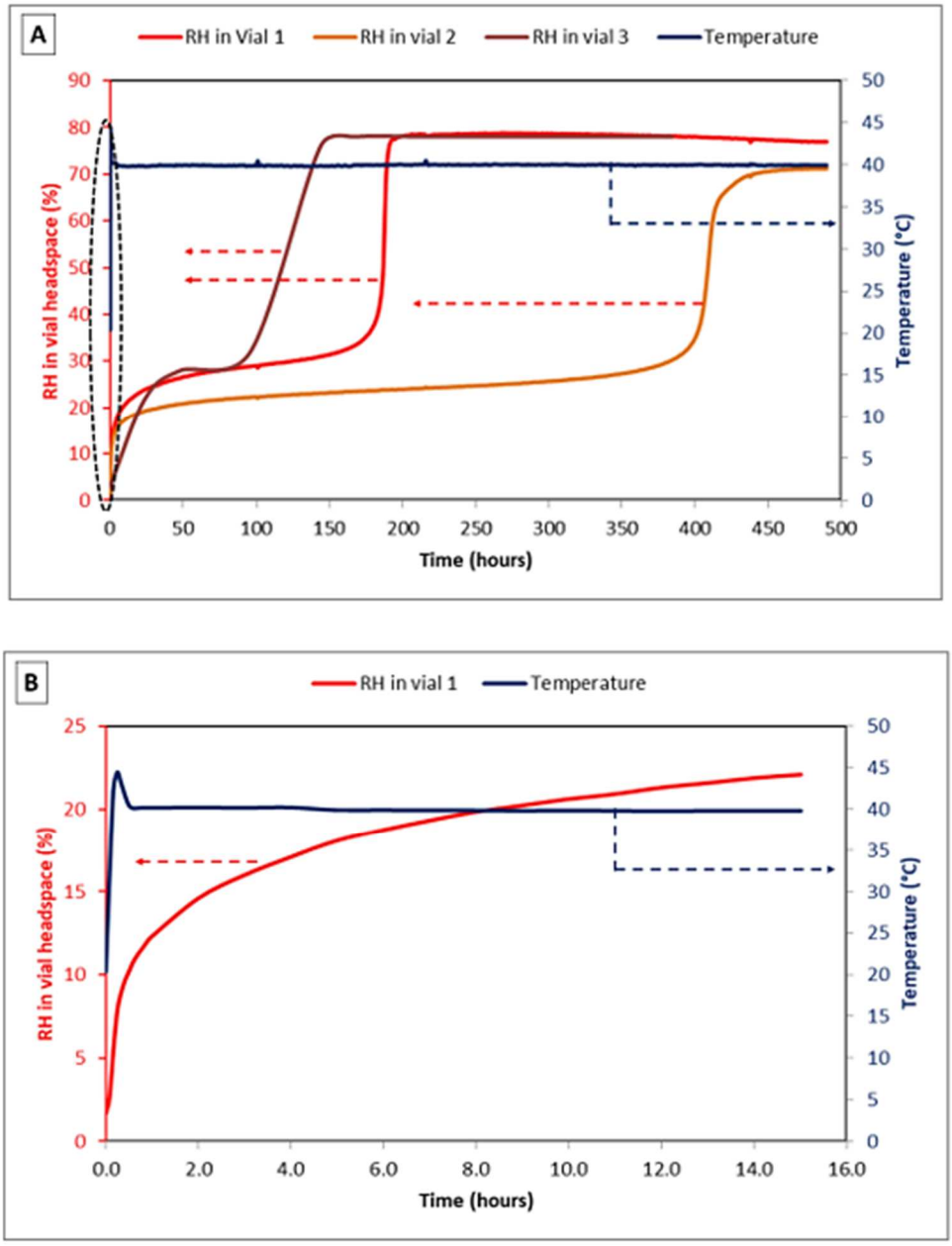

Figure 3.8 Headspace relative humidity (left y-axis) and temperature (right y-axis) in three vials, containing colyophilized mannitol-sucrose (4:1 w/w), stored at 40 °C. A. Data was recorded for three samples. B. The initial rise in RH within first 24 h for representative vial is presented. Notice small overshoot in temperature upon transferring vials from RT to oven set at 40 °C.

While the three vials, fitted with the RH and temperature sensor were monitored continuously, a new vial, from the same lyophilized batch, was removed and analyzed at predetermined intervals. The water content was determined by KFT while XRD enabled the physical characterization of the lyophile. The initial water content was ~6.3% w/w, reflective of high MHH content (Figure 3.9). Interestingly, just after 1 day, the water content had reduced to ~4.1%. There was a gradual reduction in the water content upon continued storage, with a content of ~1% after 400 hours. The concomitant reduction in lyophile water content and increase in headspace RH is indicative of movement of water from the lyophile to the headspace (Figure 3.18).

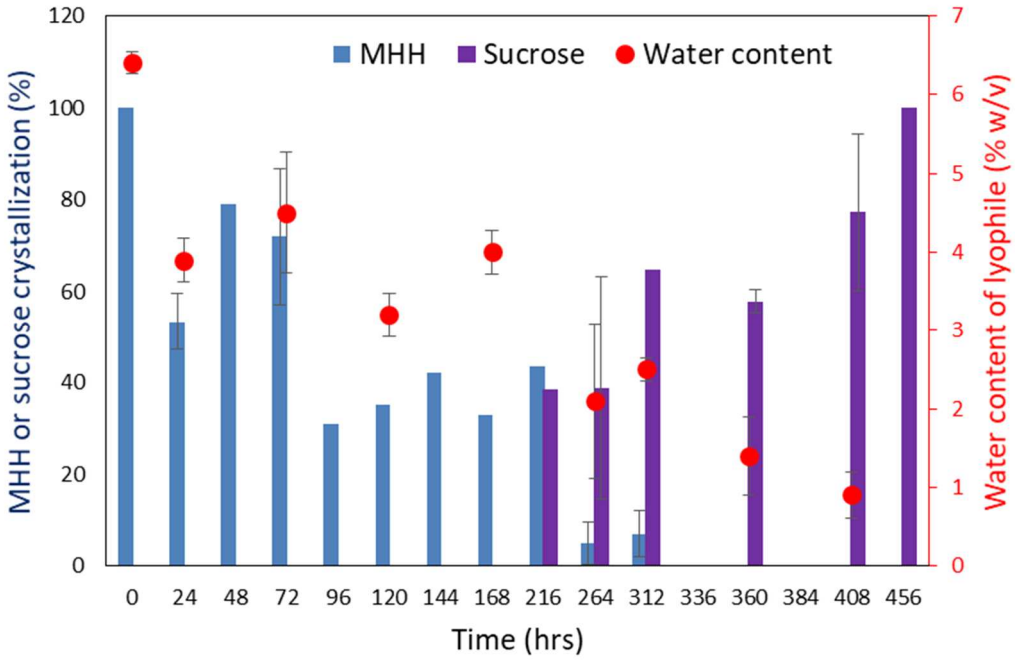

Figure 3.9 Normalized intensity of MHH or sucrose peak* (left y-axis) and water content (right y-axis) in mannitol-sucrose (4:1) lyophiles for different days at 40 °C. A new vial was withdrawn at each time point and the same vial was used for water content and XRD analysis. * MHH content (blue bars; 17.9 °2θ peak) or crystalline sucrose content (purple bars; 11.7 °2θ peak). The highest intensities of MHH (17.9 °2θ) and sucrose (11.7 °2θ) peaks at the start and at the end of the experiment respectively were assigned to be 100%, and the rest are expressed as relative intensities.

Determination of the physical form of lyophile by XRD confirmed that the water loss in the lyophile was due to dehydration of MHH (Figure 3.19). The XRD of fresh lyophile revealed the presence of only MHH, and none of the peaks attributable to the three anhydrous forms of mannitol were detectable. After storage at 40 °C for 1 day, there was a pronounced reduction in the intensity of MHH peaks suggesting dehydration. This was accompanied by appearance of some new peaks, which could be attributed to δ- and β-mannitol. The storage had caused a reduction in lyophile water content to ~4% w/w. During this short period of time, there was increase in headspace RH to ~24% (Figure 3.8 and Figure 3.9). All these observations suggest that on transferring vials from RT to 40 °C, there was partial dehydration of MHH. Srinivasan et al have shown burst release of water, attributed to MHH dehydration, in mannitol-trehalose-sodium chloride formulation, when the secondary drying temperature was increased to 40 °C [85].

The XRD of lyophiles in the vials withdrawn during the following days (from day 2-9) showed a reduction in intensity of MHH peaks. There was some vial to vial variation in the anhydrous form of mannitol crystallizing as a result of MHH dehydration. Peaks attributed to δ-mannitol were observed in all the vials, while there was variation in the formation of β-mannitol. In Figure 9, the MHH and crystalline sucrose concentrations as a function of storage time are plotted along with the water content. No MHH peak was detectable after 9 days. The second stepwise increase in headspace RH to ~75% was observed after 6-18 days (Figure 3.8B), which could be attributed to MHH dehydration. An overview of data from these studies suggest an initial dehydration of MHH attributed to an increase in temperature, which led to the first stepwise rise in headspace RH. This

was followed by a transient equilibrium and a second stepwise rise attributed to further MHH dehydration (Figure 3.20). There was an excellent correlation between the water content and MHH content in the lyophiles (Figure 3.9). Interestingly, sucrose crystallization was observed only during the later stages of MHH dehydration. There was a gradual increase in the intensity of peaks attributed to sucrose, suggesting slow sucrose crystallization. Surprisingly, we did not observe any noticeable cake collapse in vials even after 20 days. Thus, contrary to general belief, sucrose crystallization did not lead to cake collapse [121]. Since the ratio of mannitol to sucrose was high (4:1), it is possible that mannitol provides supports even upon sucrose crystallization.

The sensors from the three vials were disconnected after 20 days and the lyophiles were characterized. The XRD of all three lyophiles revealed anhydrous mannitol (β- and δ-forms), and substantially but not completely crystalline sucrose. The lyophile water content was ~1% w/w. It is instructive to compare the systems – immediately after lyophilization and after storage at 40 °C after 20 days. Following lyophilization, the lyophile water content was ~ 6% w/w and it was composed predominantly of MHH and amorphous sucrose and the headspace RH was 3% w/w (25 °C). After storage at 40 °C for 20 days, the lyophile water content was ~ 1% w/w and it was composed predominantly of anhydrous mannitol and partially crystalline sucrose and the headspace RH was 75% (40 °C). Assuming that all the mannitol was crystalline (this assumption is reasonable since sucrose, at the low concentration (20% w/w), may not inhibit mannitol crystallization), the water is expected to be associated with the amorphous sucrose. To summarize, the lyophile released ~5% w/w water.

To comprehensively follow the movement of water within the vial, we will consider the volumes of the lyophile and air in each vial. The volume of air in the sealed vials is ~ 9.75 cm^3. This accounts for the calculated volume of lyophile (~0.25 cm^3), based on the true density of MHH and sucrose. Following storage at 40 °C, the headspace RH, which was initially ~ 3%, increased gradually to 75% and was approximately constant thereafter. This increase in RH is attributed to the water released by the dehydration of MHH (XRD studies reveal that sucrose crystallization occurred after RH stabilized to this value). Complete dehydration of MHH (stoichiometric water content of 4.7% w/w; neglecting presence of anhydrous or amorphous mannitol), would result in the release of ~13 mg of water. However, the amount of water required to raise the RH of the headspace to ~75% (40°C) is only ~ 0.4 mg (detailed calculations provided in Supplementary Information). Thus, in this closed system, the quantity of water released was far in excess of the amount accounted for by: (i) increase in headspace RH and, (ii) final water content in the lyophile. The "excess" water was ~ 12 mg per vial.

These results were quite surprising and compelled us to monitor closely all the components in this closed system, which had the potential to interact with water, including the packaging. In an effort to account for the "excess" water released by MHH dehydration, the water content in the three rubber stoppers (these were the stoppers which had sensors fitted in them) were determined gravimetrically. Interestingly, the amount of water in vial stopper #s 1, 2 and 3 were 9.08, 8.53 and 7.52 mg respectively. The initial water content in the rubber stopper was ~5.0 mg. Thus, during the 20 day storage period, all the vials had sorbed water and the amount taken up (by each stopper) ranged between ~ 2.5 and 4.0 mg.

The results suggest the dynamic influence of rubber stopper in establishing equilibrium between headspace RH and lyophile content. Though we were not able to achieve mass balance with respect to water content in the sealed vial, we were able to document the movement of water from *lyophile to headspace to rubber stopper*. The vial stopper acted as a 'water sink' and helped maintain the vial headspace at an approximately constant water vapor pressure (75% RH at 40 °C). Thus there appears to be a dynamic equilibrium between the water contents of the rubber stopper and lyophile [104].

We were not able to achieve mass balance with respect to water content in the sealed vials, possibly due to diffusion of water through the stopper. Use of the non-destructive analytical tools such as spectroscopic headspace analysis of water vapor pressure might provide more comprehensive information [122].

3.4 Significance

MHH dehydration appears to be a good example of a system where the reaction product accelerates the reaction rate. The initial dehydration of MHH can lead to an increase in headspace RH, which can then accelerate further dehydration. In the present study, the high fill volume was selected to achieve maximum MHH formation. Secondary drying was conducted at 10 °C to retain the MHH formed. Thus, the processing conditions were selected to drive the system towards preferred MHH crystallization. However, we believe that the results can be extrapolated to lyophiles where only a small fraction of the mannitol is present as a hemihydrate. For a mannitol-sucrose formulation (weight ratio 4:1, 5% w/w, 2 mL fill volume in 10 mL vial), even if only 10% of mannitol is retained as MHH, the

lyophile would contain 0.376 mg water. However, the release of 0.202 mg of water, in a 10 mL sealed vial at 25 °C, can lead to increase in RH to 90% (assuming an initial RH of 0%), which can promote further and faster MHH dehydration.

The effect of temperature can be quite complex. MHH dehydration rate appears to be strongly dependent on temperature. A decrease in temperature, for example to 4°C, should result in a much slower dehydration rate than at 40°C. On the other hand, at a given water vapor pressure, a decrease in temperature will lead to an increase in RH. This change in RH can be pronounced even over a small temperature range of 15 to 20 °C. The increased RH should accelerate the dehydration rate of MHH. Thus, in a 'closed environment' (as in a vial), the overall effect will be a complex interplay of the multiple factors influencing the dehydration kinetics. Therefore, accelerated stability studies, wherein the system is investigated at an elevated temperature and attempts are made to extrapolate the results to a lower temperature, may not be meaningful. As sealed vials are 'closed' systems, results from this study should be applicable when samples are stored at higher RH. However, our results establish the importance of temperature excursions in modulating headspace RH in a sealed vial. Our next set of studies to understand the influence of MHH dehydration on protein aggregation are currently under progress.

3.5 Conclusion

Mannitol hemihydrate, a metastable form of mannitol, is commonly encountered in lyophilized formulations. Due to its unpredictable formation and dehydration behavior, coupled with the possibility of product degradation and instability due to the released

water, MHH is generally regarded as an undesired physical form in a final lyophile. The results from the present study show the strong influence of headspace relative humidity and temperature on MHH stability. Contrary to the conventional hydrate behavior, MHH dehydration rate is decreased as the RH is lowered. In light of the propensity of MHH to dehydrate over a wide range of RH (3 to 97%; RT), we propose complete dehydration of MHH during secondary drying. This will eliminate the risk of physical or chemical changes to the formulation components which can be brought about by the released water during storage. If MHH is retained in the final lyophile, storage under refrigeration conditions (2 to 8 °C), might be an effective strategy to sufficiently delay MHH dehydration so as to minimize its implications.

3.6 Supplementary Information

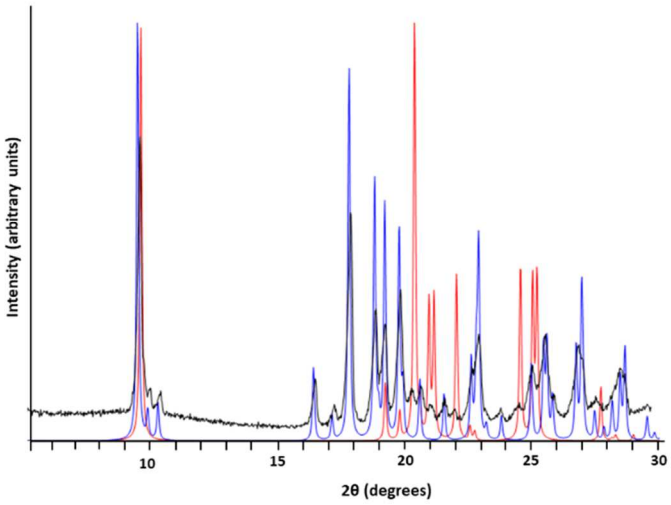

Figure 3.10 XRD pattern of lyophilized mannitol. The calculated pattern of mannitol phases (MHH blue and δ-mannitol (red) are also included.

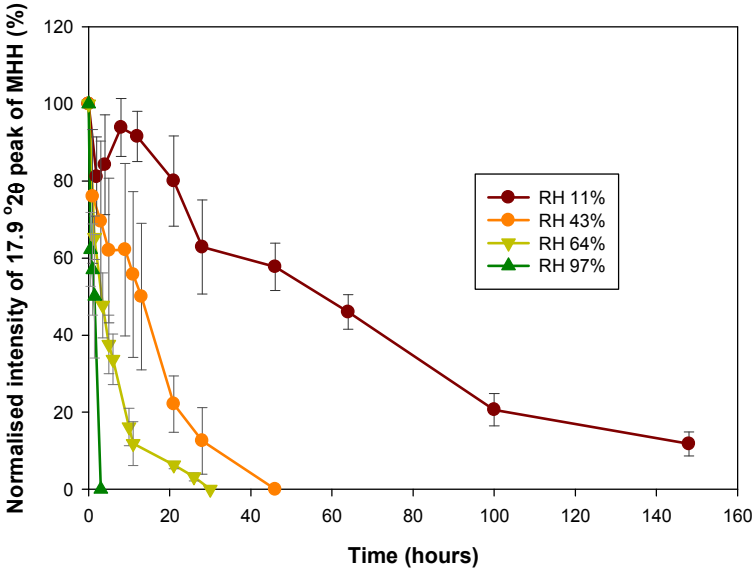

Figure 3.11 MHH dehydration (represented as the normalized* intensity of 17.9° 2θ peak) following storage at 11, 43, 64 and 97% RH (RT) (n=3). *The MHH peak intensity in the fresh lyophile was assumed to be 100%, and the peak intensities obtained as a function of storage time, were expressed with respect to the initial intensity.

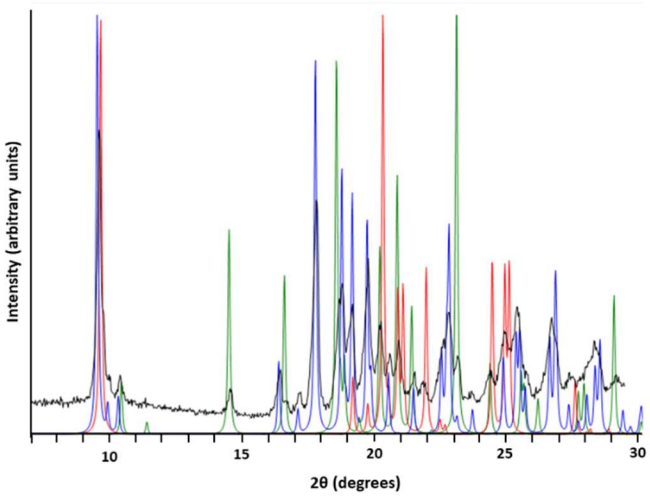

Figure 3.12 XRD pattern of lyophilized mannitol-sucrose (4:1 w/w) mixture. The calculated pattern of mannitol phases (MHH blue, δ-mannitol (red) and β-mannitol (green) are also included.

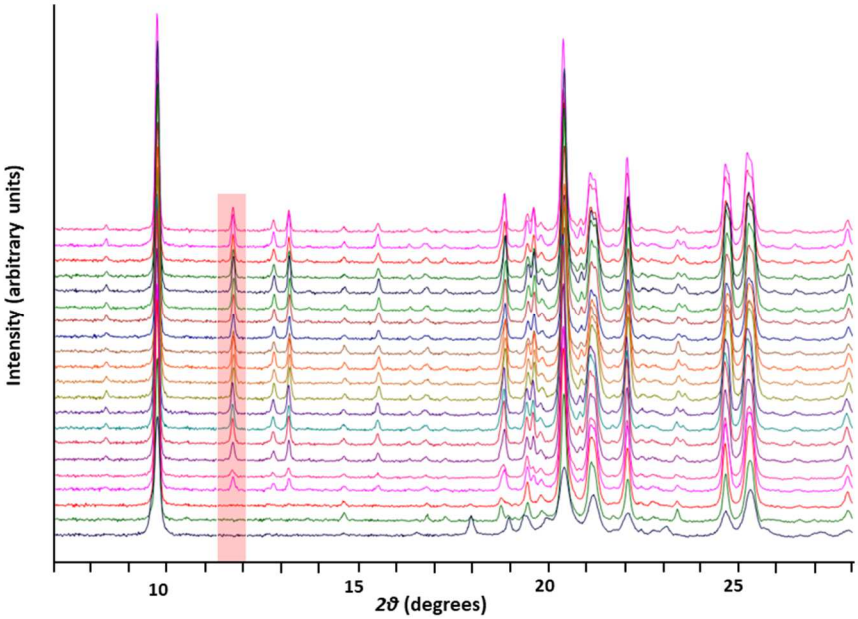

Figure 3.13 Overlay of XRD patterns of lyophilized mannitol-sucrose (4:1 w/w) mixture stored at 57% RH (RT). XRD patterns were obtained every 6 hours. A characteristic peak of sucrose is highlighted.

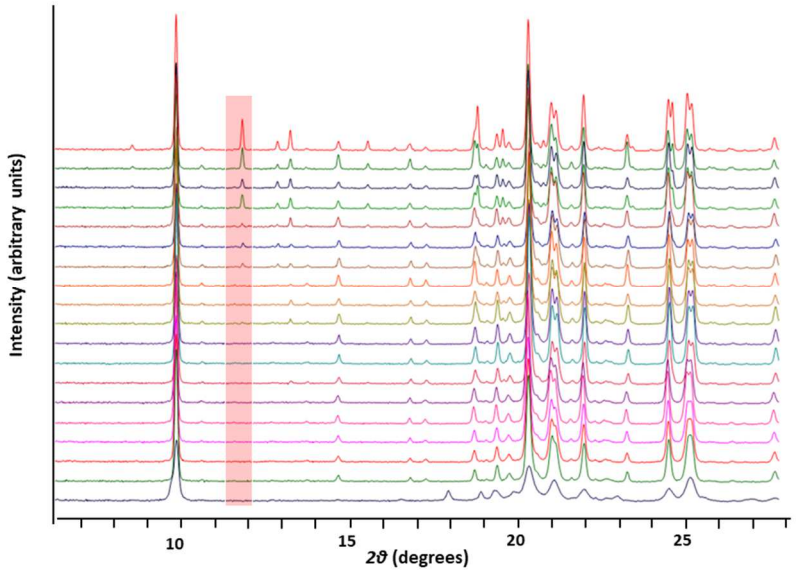

Figure 3.14 Overlay of XRD patterns of lyophilized mannitol-sucrose (4:1 w/w) mixture stored at 75% RH (RT). XRD patterns were obtained every 6 hours. A characteristic peak of sucrose is highlighted.

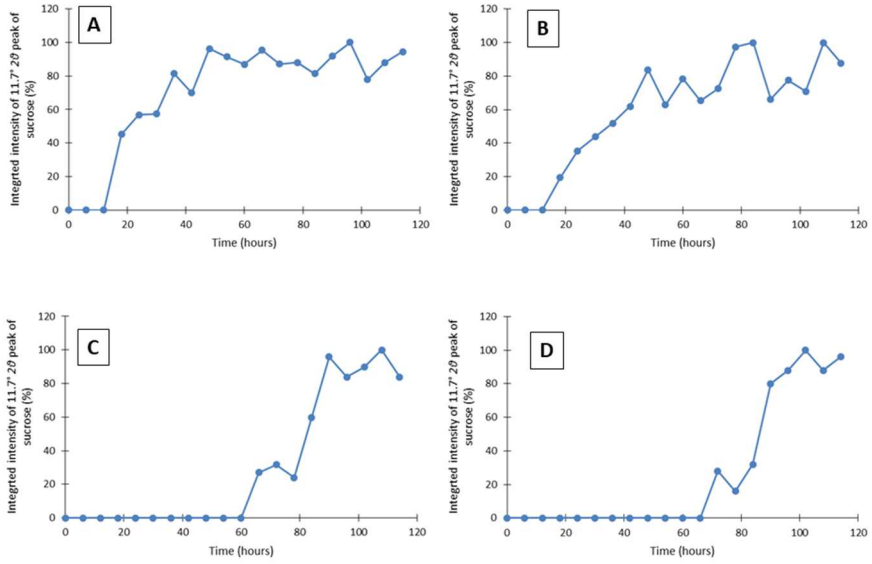

Figure 3.15 Crystallization of sucrose following storage of lyophilized mannitol-sucrose (4:1 w/w) mixture at 57 (A and B) and 75% RH (C and D). The intensity of 11.7° 2θ peak of sucrose is plotted as a function of storage time. The highest intensity was assigned to be 100%, and the rest of the intensities are expressed with respect to this number. The experiment was conducted in triplicate and one representative data is plotted in Figure 3.7.

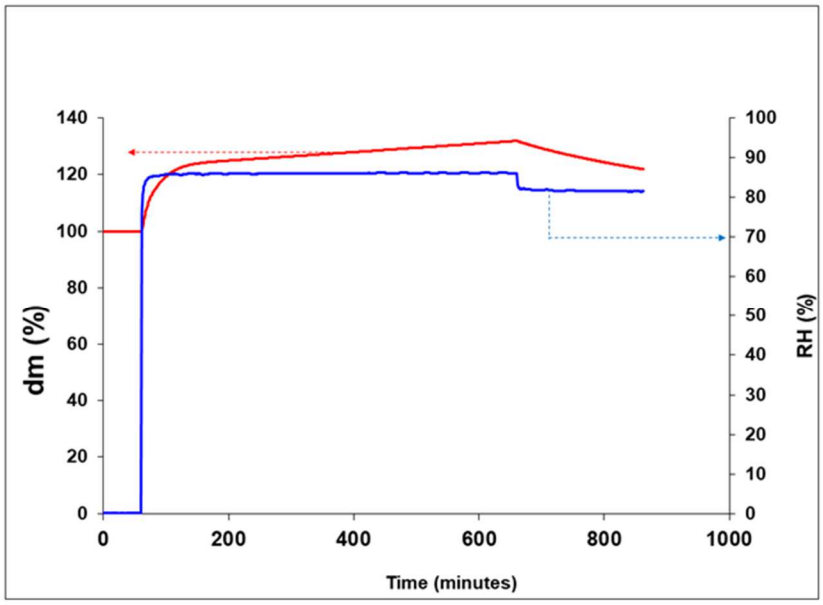

Figure 3.16 Water uptake by amorphous sucrose at 85% RH (25 °C) for 10 h. The RH was then reduced to 80%.

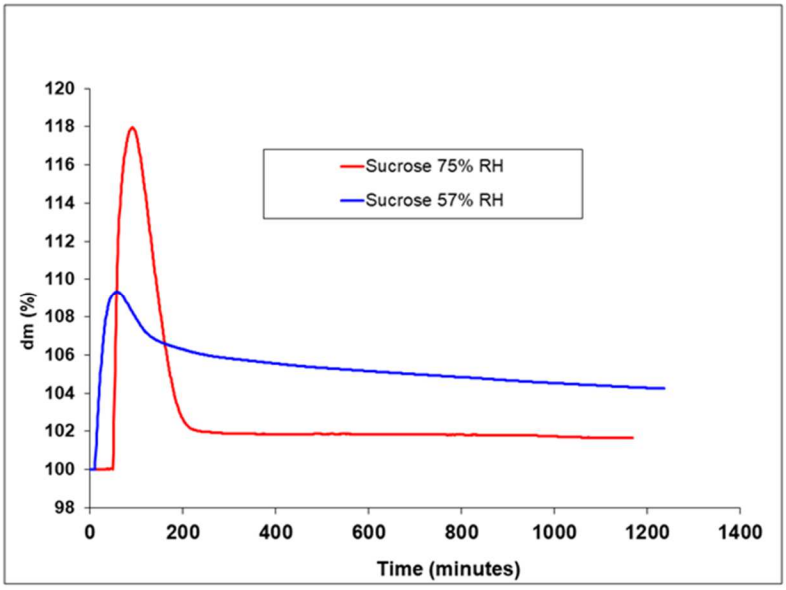

Figure 3.17 Moisture sorption and desorption by amorphous sucrose at 57 (blue) and 75% (red) RH (25 °C).

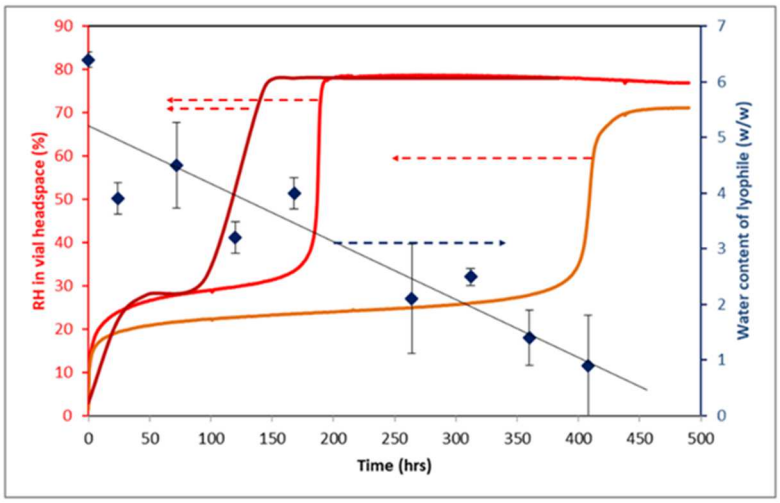

Figure 3.18 Headspace relative humidity in three mannitol-sucrose lyophiles stored at 40 °C (left y-axis). The lyophile water content (right y-axis) was determined by KFT (mean ± SD; n=3).

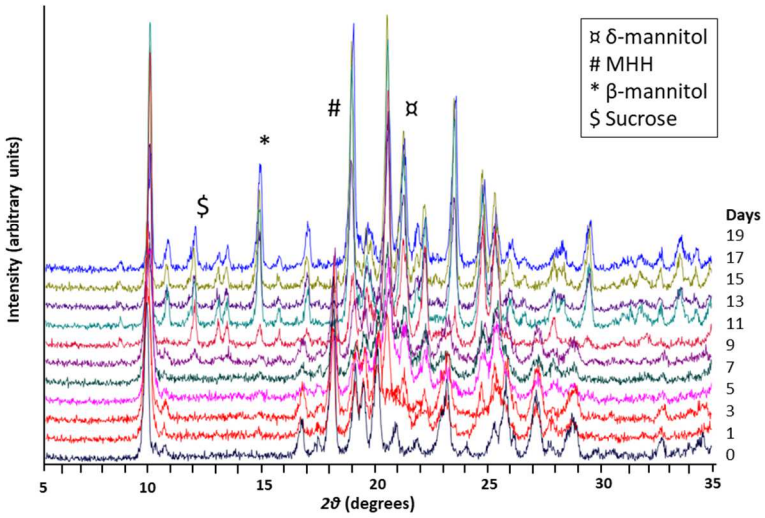

Figure 3.19 Overlay of XRD patterns of lyophilized mannitol-sucrose (4:1 w/w) -in sealed vials, measured after storage at 40 °C for different times. A new vial was withdrawn at each time point. One characteristic peak of each phase is pointed out.

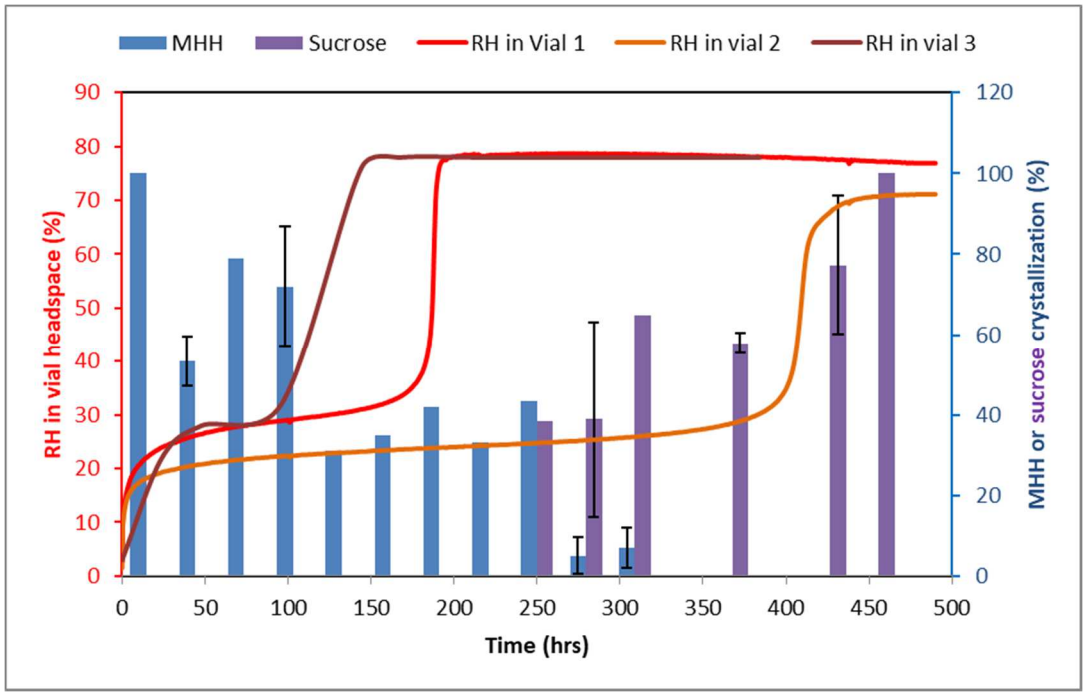

Figure 3.20 Headspace relative humidity in three vials of mannitol-sucrose (4:1) lyophiles stored at 40 °C (left y-axis). Right y-axis represents MHH content (blue bars; 17.9 °2θ peak) or crystalline sucrose content (purple bars; 11.7 °2θ peak). The highest intensities of MHH (17.9 °2θ) and sucrose (11.7 °2θ) peaks at the start and at the end of the experiment respectively were assigned to be 100%, and the rest are expressed as relative intensities.

Calculations of water movement in a sealed vial

Volume occupied by lyophile

True density MHH* = 1.451 g/cm^3

True density sucrose* = 1.587 g/cm^3

(*Reference Cambridge Structure Database)

Lyophile contains 280 mg of mannitol + 70 mg of sucrose.

Total volume occupied by lyophile = 0.237 cm^3

Amount of water required to raise the vial head space RH value to ~ 75% (at 40 °C)

Relative humidity = (water vapor pressure in the atmosphere * 100) / saturated water vapor pressure

At 40 °C, saturated vapor pressure = 7.4 kPa.

When the RH is 75%, the water vapor pressure = 0.75 x 7.4 kPa = 5.55 kPa

According to the ideal gas law,

PV = nRT

where, P is the pressure of the gas (pascals), V is the volume of the gas (m^3), n is number of moles), T is the temperature of the gas and R is the universal gas constant (8.314 $J \cdot K^{-1} \cdot mol^{-1}$).

The number of moles (n) is equal to the mass (m) (in grams) divided by the molar mass (M) (in grams per mole):

$$n = \frac{m}{M}$$

Replacing 'n' in the above Equation with m/M and substituting the values of P, V, R, T and M, the amount of water needed to increase the equilibrium relative humidity to 80% at 40 °C is calculated follows:

Mass of water (m) = $\frac{18 \text{ x } 5.55 \text{ x } 0.00000976}{8.314 \text{ x } 314}$ = 3.74 x 10^{-4} g = 0.374 mg

Chapter 4 Mannitol hemihydrate dehydration in lyophilized protein formulations: Impact on sucrose crystallization and protein stability during storage

4.1 Introduction

Lyophilization (or freeze-drying) is commonly used as a method of choice for formulating thermolabile proteins in the dry state. There are numerous formulation as well as processing related factors that can directly or indirectly impact protein stability. The overall goal during product development is to retain the native conformation of the protein when exposed to these stresses. Minor perturbations to the native state can result in protein unfolding, aggregation and loss in its activity [8]. From a formulation standpoint, for successful lyophilization of proteins broadly, two competing criteria must be fulfilled: (i) the presence of stabilizers that can exist in the amorphous state throughout different stages of processing, during storage as well as distribution and, (ii) an elegant cake which can provide mechanical strength to the cake without collapsing during primary drying [5, 87].

A combination of mannitol along with an amorphous sugar in a particular ratio fulfils both the criteria for successful development of lyophilized protein formulations [87]. Sugars such as sucrose and trehalose are widely used as lyoprotectants due to their ability to remain amorphous during processing as well as storage. Sugars can protect the proteins by a combination of mechanisms in the solution, frozen, and the dried state [18, 21]. In the dried state, the amorphous sugar retains the protein in its native conformation by hydrogen bonding (water replacement mechanism). In parallel, the amorphous sugar also immobilizes the protein by forming a glassy matrix at temperatures ($T < T_g$) hence preventing protein aggregation [28, 123]. Mannitol, a sugar-alcohol, given its strong

propensity to crystallize along with its high eutectic melting temperatures (-2.2 °C) is widely used as a bulking agent (in low concentration protein formulations) and aids in reducing primary drying cycle times [124]. However, the crystallization of mannitol and the consequent phase separation prevents it from "interacting" with proteins. The crystalline nature of mannitol prevents cake collapse and results in an elegant cake thus, serving as an ideal excipient for lyophilized formulations.

Mannitol can crystallize either as a hemihydrate (MHH) or in an anhydrous form or as a combination of both [88, 125]. The three widely occurring anhydrous polymorphic forms are α-, β- and δ. The formation of MHH is dependent on several factors including the annealing temperature and the presence and concentration of other solutes and proteins [85, 90, 93, 125]. MHH is known to form at subambient temperatures ($\leq$ -15°C) [84]. Although unstable in nature, once formed, MHH has high kinetic stability and can be retained in the final lyophile and also during subsequent storage. In addition, it is well known that high secondary drying temperatures can result in complete dehydration of MHH [85, 87, 97]. The conditions of formation and dehydration of MHH during processing have been well established. The major factor limiting the use of mannitol-sucrose combination in lyophilized protein formulations is the formation of MHH. Its presence in the final lyophile is presumed to impact drug product critical quality attributes [84, 88, 126]. However, there are very few reports that focus on the implications of MHH dehydration on excipient as well as protein stability.

Mannitol-disaccharide ratios have been investigated by various research groups. In the case of a monoclonal antibody (rhumAb HER2) freeze-dried using either sucrose or trehalose

with mannitol, a specific molar of ratio of 360:1 (sugar-to-protein) provided sufficient lyoprotection. No aggregation was observed in the samples which were stored at 40°C for 3 months. Sucrose and trehalose individually prevented protein aggregation to a similar extent, while mannitol, which was partially amorphous, was shown to be less effective. In addition, the combination of mannitol and disaccharide showed similar protective functionality when compared with sugar alone samples [37]. When four different proteins (0.5 to 1.0 mg/mL) were lyophilized using mannitol and sucrose (4:1), based on the annealing as well as the drying temperatures, mannitol either crystallized as the hydrate or an anhydrate (α, β or δ) or a combination of both while sucrose remained amorphous. The protein stability was retained in these samples for up to 12 months when stored in sealed vials, both at 5°C and ~ 25°C. However, when exposed to ambient conditions in open vials (40 °C for 6 months), sucrose crystallization and cake collapse were observed. However, the factors governing the crystallization and collapse were not investigated further [87]. To our knowledge, this was the first report of sucrose crystallization likely brought about by the water released by MHH dehydration. Recently, a mAb (10, 30 or 60 mg/mL) was freeze dried using varying mannitol to sucrose ratios. The presence of MHH in the final lyophile had no negative effect on the mAb stability following storage for 3 months at 40°C. The molar ratio of amorphous sucrose-to-protein was shown to be the factor governing protein stability irrespective of the presence or absence of MHH [102].

We had previously documented the anomalous dehydration behavior of MHH. In MHH prepared by lyophilization (of a 5% w/v mannitol solution), the dehydration rate increased as a function of water vapor pressure (measured as relative humidity). A similar trend was

observed in lyophilized mannitol:sucrose (4:1, 5% w/v) systems. The counterintuitive dehydration behavior was attributed to the Smith-Topley effect. The water released following the dehydration of MHH was sorbed by sucrose leading to its crystallization [125]. The stoichiometric water content of MHH is ~ 4.5 % w/w. The release of such a high amount of water can result in protein aggregation either due to compromised lyoprotectant function (sucrose crystallization) or an increased molecular mobility. Based on the above results, we hypothesize that during storage of mannitol-sucrose-protein lyophilized formulations, MHH dehydration in the lyophile and the release of associated lattice water will result in: (i) plasticization of amorphous sucrose leading to its crystallization and (ii) consequent loss in its lyoprotectant function leading to protein aggregation.

4.2 Materials and Methods

4.2.1 Formulations

Mannitol ($C_6H_{14}O_6$), sucrose ($C_{12}H_{22}O_{11}$), lyophilized serum albumin (bovine as well as human source, BSA and HSA) were purchased from Sigma Aldrich (St. Louis, MO, USA). No further processing was performed prior to use of the proteins for sample preparation. Magnesium chloride ($MgCl_2$) and sodium bromide (NaBr) salts were purchased from Fischer Scientific (Waltham, MA, USA). These were used to prepare saturated salt solutions in desiccators equilibrated to achieve relative humidity (%RH) of 33% ($MgCl_2$) and 53% (NaBr) at ambient temperature. Formulations of either BSA or HSA (1 to 5 mg/mL) with mannitol:sucrose (4:1, weight ratio) or mannitol alone or sucrose alone were prepared. The total solute (excipient) content was maintained constant at 5% w/v for all the formulations.

4.2.2 Lyophilization

The formulations were filled into 10 mL glass vials (DWK Wheaton) partially stoppered with 20 mm rubber stopper (Gry Butyl Sil, Wheaton) and freeze-dried either in a benchtop drier (VirTis AdVantage, Gardiner, NY) or a LyoStar III (SP Scientific, Stone Ridge, NY). 7 mL of the pre lyophilization solutions were filled into 10 mL vials. The fill volume was optimized from our previous work with a goal to consistently get maximum mannitol hemihydrate in the dried formulation [125]. Three different lyophilization cycles were used as shown in Table 4.1. At the end of the freeze-drying cycle, the vials were stoppered under vacuum and stored at -20°C until further analysis.

Table 4.1 Freeze drying cycle parameters

	Process parameters	Freezing	Annealing	Primary drying	Secondary drying
Cycle 1	Temperature (°/C)	-45	-25	-25	NA
	Rate (°/C)	1	1	0.5	
	Time (in hours)	4	6	170	
	Pressure (mTorr)	NA	NA	200	
Cycle 2	Temperature (°/C)	-45	-25	-25	10
	Rate (°/C)	1	1	0.5	0.5
	Time (in hours)	4	6	48	24
	Pressure (mTorr)	NA	NA	200	200
Cycle 3	Temperature (°/C)	-45	-25	-25	40
	Rate (°/C)	1	1	0.5	0.5
	Time (in hours)	4	6	48	6
	Pressure (mTorr)	NA	NA	200	200

4.2.3 X-ray diffractometry (XRD)

Powder X-ray diffraction measurements were performed using the SMART LAB SE X-ray diffractometer (Rigaku, Japan). The diffraction patterns were collected in the 7 to 30°, 2θ range with a step size of 0.001° at ambient temperature using the Cu-Kα source.

4.2.4 Synchrotron X-ray diffractometry (sXRD)

An aluminum sample block with an airtight lid on the top held in place with six screws and a heat-insulating tape to allow for a tight seal when closed was used to investigate *in situ* changes in lyophile at desired temperature and humidity. The sample chamber was previously designed and used by Koranne et al and more details with respect to the engineering design can be found in the published article [127]. The temperature of the chamber is controlled by a Newport/Omega PT32-305 PID process controller. The temperature and relative humidity of the chamber was monitored with a handheld hygrometer with the probe placed close to the sample holder. A plastic cuvette with minimum background was used to fill the lyophile which was freshly opened prior to the experiment. Two circular windows, sealed with Kapton tape, permitted the entrance and exit of the X-ray beam.

Experiments were performed in the transmission mode in the 17-BM-B beamline at Argonne National Laboratory (Argonne, IL, USA). A monochromatic X-ray beam [wavelength 0.45452 Å; beam size 300 μm × 300 μm] and a two-dimensional area detector (XRD-1621, PerkinElmer) were used. A triple-bounce channel-cut Si single crystal monochromator with [111] faces polished was used, which limited the line broadening to its theoretical low limit. The sample to detector distance was set at 900 mm. Corundum

(Al_2O_3: SRM 674a, NIST) was used as the calibration standard. During data collection, the sample was oscillated (±1 mm from the center along the horizontal axis) using a stepper motor. The sample chamber was set at 40°C and the humidity inside the chamber was maintained at 53 to 55% RH using NaBr saturated salt solution. XRD scans were collected every 5 minutes for 10 hours to monitor phase changes in HSA (2 mg/mL) with mannitol:sucrose (4:1) formulation. At each time point, the sample was scanned 10 times, with an exposure time of 1 s for each scan and the results were averaged. The synchrotron radiation (λ = 0.4545 Å) data were converted and plotted for Cu Kα radiation (λ = 1.54 Å), so as to enable direct comparison with the reference patterns.

4.2.5 Karl Fischer Titrimetry

The sample (~ 10 to 20 mg) was added to the titration cell, and the water content was determined coulometrically using a Karl Fischer titrimeter (C20, Mettler Toledo, Columbus, OH).

4.2.6 Size exclusion chromatography (SEC)

SEC was used to assess changes in mass during storage due to aggregation or fragmentation. In SEC, separation was performed using an Agilent 1110 or 1200 series HPLC on a TOSOH Bioscience TSKgel G3000SWxl, 7.8mm x 30 cm, 5 µm. The mobile phase was 0.1 M phosphate buffer, 0.15 M sodium chloride at pH 6.8 with a flow rate of 0.8 mL/min. Standards and samples were reconstituted with purified water as needed and diluted 1:1 with mobile phase prior to analysis. Samples were controlled at 5 °C and the column was maintained under ambient conditions throughout the sequence. An injection

volume at 50 µL for both standards and samples with a detection at 280 nm was utilized. System suitability was checked using a comparative standard and a molecular weight standard prior to sample analysis. The reported value of % high molecular weight species (%HMW) or % low molecular weight species (%LMW) was calculated using the following equation:

$$\%\text{HMW}/\%\text{LMW} = \frac{\text{Area under the curve of HMW/LMW peak}}{\text{Total area under the curve of all peaks}} \times 100\%$$

4.2.7 Water sorption-desorption

Water sorption and desorption studies were performed using Q5000 automated water sorption analyzer (TA Instruments, New Castle, DE). About 5 to 7 mg of the lyophile (powder) was placed in a quartz sample pan and equilibrated at 0.0% RH for 120 minutes at 20 °C and a nitrogen flow rate of 200 mL/min. The RH was raised, at increments of 10%, up to 90%. Following which the RH and the temperature were raised to 55% and 40°C respectively. The data was analyzed using commercial software (Universal Analysis 2000, TA Instruments, New Castle, DE).

4.2.8 Differential scanning calorimetry (DSC)

A differential scanning calorimeter (Q2000, TA Instruments, New Castle, DE) equipped with a refrigerated cooling accessory was used. Dry nitrogen gas was purged at 50 mL/min. The DSC was calibrated, at 2 and 5°C/min heating rates, using indium, mercury and distilled water as standards. Approximately 7 to 10 mg of lyophile (powder) were weighed in an aluminum pan, sealed hermetically, cooled from RT to -30°C and heated to 230°C at

10°C/min. The cooling and heating rate (10°C/min) was based on the objective of determining the change in glass transition of the lyophile.

4.2.9 Headspace moisture analysis (FMS Lighthouse)

A frequency modulated spectroscopy-based moisture analyzer (FMS 1400, Lighthouse instruments, Charlottesville, VA) was used to determine the vapor pressure in sealed vials. The headspace water vapor pressure (torr) was measured in vials sealed under vacuum containing fresh HSA-mannitol-sucrose lyophiles from (Cycle 3). As the FMS is a non-destructive method, the same vials which were analyzed at day 0 were stored at 40 and 50°C and were analyzed for up to 10 days. The instrument was calibrated using two standards: 5.1 Torr (water vapor *partial* pressure, 10051) and 200 Torr (*absolute* pressure, 22002). Dry N_2 was used to flush moist laboratory air off the sample during each measurement. A 3D printed insert was used to hold the 10 mL vial in the beam path. The vials stored at elevated temperatures were allowed to cool to room temperature before taking individual measurements. The water vapor pressure at 25°C is ~ 23.8 mm of Hg and at 40 °C is 55.3 mm of Hg. These values were used to convert the pressure values generated from the instrument in Torr to relative humidity.

4.3 Results and Discussion

We had earlier optimized the formulation and processing conditions to maximize retention of MHH in the final lyophile. The mannitol to sucrose ratio was 4:1, the total solute concentration in the prelyophilization solution was 5% w/v and the fill volume was 7 mL (in a 10 mL vial) [125]. We used the same freeze-drying parameters for the current study

which are described in the Experimental section (Cycle 2). The goal of the previous work was to understand the conditions of dehydration of MHH in the final lyophile in a sealed vial. MHH dehydration was complete in 20 days and was accompanied by sucrose crystallization. The current work is aimed at answering the questions: (i) Are these events observed in the presence of protein? (ii) Is there a consequent detrimental effect on protein stability?

Bovine and human serum albumin were the model proteins. The feasibility studies, to gauge of extent of MHH formation, were conducted with both the proteins. However, the influence of MHH dehydration on protein stability were initiated with BSA since it is known to undergo moisture induced aggregation [128].

The results are organized into the following sections: (i) Effect of formulation variables on MHH (formation and dehydration). (ii) Effect of process variables on MHH (formation and dehydration). (iii) Role of vial headspace RH on MHH stability.

4.3.1 Effect of formulation variables on MHH (formation and dehydration)

When a solution of BSA (5 mg/mL) with mannitol (5% w/v) was freeze-dried, the XRD patterns showed characteristic peaks of MHH at 16.5 and 17.9 °2θ, β-mannitol at 14.6 °2θ and δ-mannitol at 20.4 °2θ (Figure 4.1). Similar results were obtained in the absence of protein [125]. Therefore, BSA did not seem to influence the MHH formation. The XRD pattern of freeze-dried mannitol:sucrose (4:1) formulation was similar to that of mannitol with or without BSA, reflecting the presence of a mixture of MHH and β-mannitol. Interestingly, when the BSA concentration was progressively increased, overall mannitol crystallinity including MHH peak intensities decreased (Figure 4.1). Similar results have

been reported earlier. For example, an albumin fusion protein, in a concentration dependent manner, inhibited mannitol crystallization [58].

The mannitol peak intensities provided a measure of its crystallinity. MHH peak intensities were most pronounced in the absence of any non-crystallizing solute. The presence of sucrose or BSA, caused a small but discernible decrease in peak intensities and increase in peak widths. The presence of two amorphous solutes, BSA and sucrose, caused a more evident inhibition of MHH crystallization. As the BSA concentration increased, there was further reduction in MHH peak intensities. Thus, the higher the total non-crystalline solute content, the lower was the MHH crystallinity.

Similar results were obtained with HSA as the model protein (Figure 4.2). The concentration dependent inhibition of mannitol crystallization continued as the protein concentration was increased up to 50 mg/mL. Starting at 10 mg/mL protein, the low intensity peaks of mannitol could no longer be readily discerned. The pronounced amorphous halo also posed a challenge with respect to the quantification of peak intensities. Our objective was to investigate quantitatively the effect of MHH dehydration on sucrose crystallization. Therefore, a formulation composition, with a low protein concentration of 2 mg/mL was selected. The MHH peak intensities were pronounced enabling us to monitor the dehydration kinetics based on the intensity of a characteristic peak of MHH (17.9° 2θ), as a function of storage time.

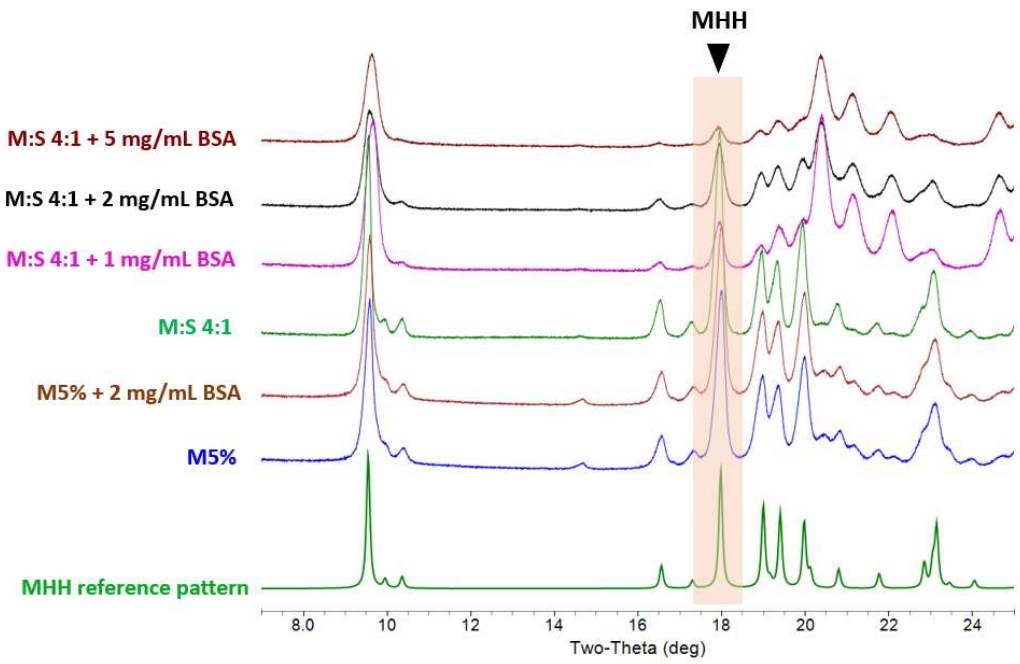

Figure 4.1 XRD patterns of lyophiles of (i) Mannitol 5% w/v (ii) BSA (2 mg/mL) + mannitol (5% w/v) (iii) mannitol: sucrose (4:1, 5% w/v) (iv) BSA (1 mg/mL) + mannitol:sucrose (4:1, 5% w/v) (v) BSA (2 mg/mL) + mannitol:sucrose (4:1, 5% w/v) and (vi) BSA (5 mg/mL) + mannitol:sucrose (4:1, 5% w/v).

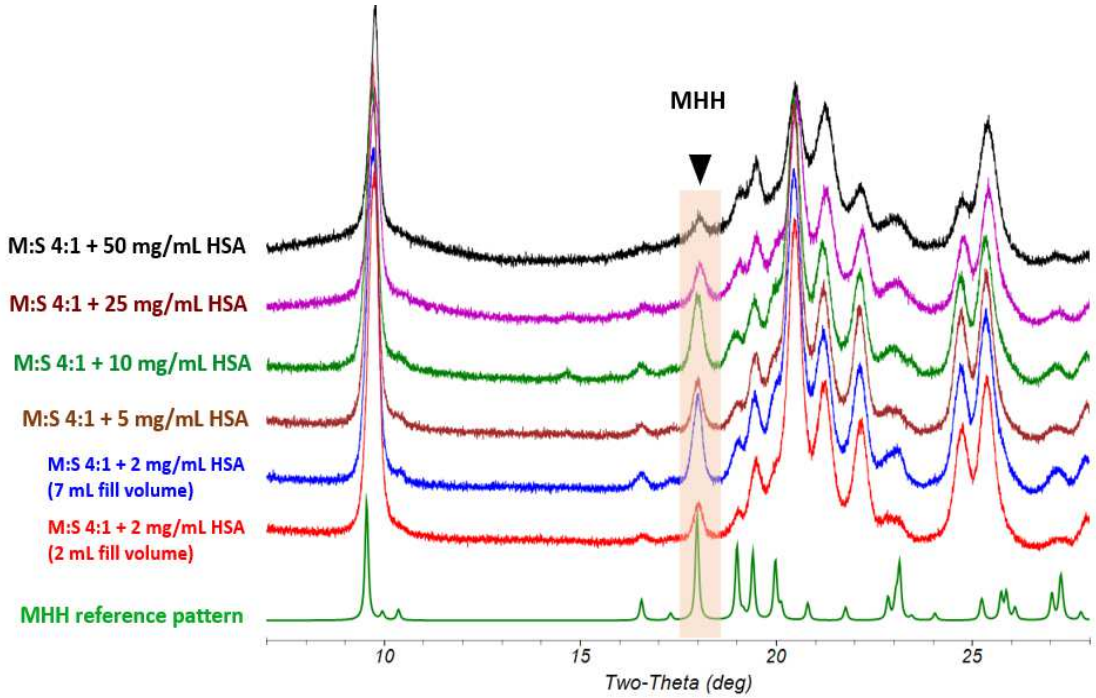

Figure 4.2 XRD patterns of lyophiles of (i) HSA (2 mg/mL) + mannitol: sucrose (4:1, 5% w/v), 2 mL fill in 10 mL vial. For all the other samples, the fill volume was 7 mL in 10 mL vial. (ii) HSA (2 mg/mL) + mannitol: sucrose (4:1, 5% w/v) (iii) HSA (5 mg/mL) + mannitol: sucrose (4:1, 5% w/v) (iv) HSA (10 mg/mL) + mannitol: sucrose (4:1, 5% w/v) (v) HSA (25 mg/mL) + mannitol: sucrose (4:1, 5% w/v) and (vii) HSA (50 mg/mL) + mannitol: sucrose (4:1, 5% w/v).

Initially four compositions with (i) BSA (2 mg/mL) only, and BSA with (ii) mannitol (5% w/v), (iii) sucrose (2% w/v) and (iv) mannitol:sucrose (4:1, 5% w/v) were freeze-dried using cycle 2. The final lyophiles, sealed under vacuum, were stored at 40°C and the XRD patterns and water content (KFT) were obtained at different time points.

In mannitol lyophile (no other excipient), MHH dehydration was complete in five days, as evident from the complete disappearance of its characteristic peak at 17.9 °2θ (Figure 4.3). This was accompanied by the formation of the anhydrous form, *i.e.,* MHH → β-mannitol, based on the pronounced increase in the intensity of the 14.6 °2θ peak (Figure 4.4). A similar dehydration kinetics was observed in lyophilized mannitol, without protein [125]. The presence of protein (protein weight fraction in the final lyophile is ~ 0.03) at a low

concentration did not appear to influence the MHH dehydration kinetics. Storage for up to 60 days, did not cause any further changes in the XRD pattern. The lyophile water content decreased from 4.5% (day 0) to 0.4% (day 5) suggesting that the water released by dehydration was not retained in the lyophile.

When a solution of BSA (2 mg/mL) with mannitol and sucrose (4:1, 5% w/v) was freeze-dried using cycle 2, the XRD patterns revealed the presence of MHH (peaks at 16.5 and 17.9 °2θ) and δ – mannitol (peak at 20.4 °2θ) (Figure 4.4). While a small initial decrease in the MHH peak intensity was observed after 10 days (the peak at 17.9° 2θ is identified in Figure 4.4) no further changes were evident up to 90 days. The initial decrease in MHH content can be attributed to change in temperature from 10°C (final secondary drying temperature) to 40°C. The initial water content in these lyophiles was 2.3% (day 0). During storage, the water content fluctuated between 1.5 and 2.0% until day 90.

The presence of amorphous sucrose at a modest concentration (weight fraction of ~ 0.2), along with protein, inhibited MHH dehydration. The initial MHH dehydration (first 10 days) was accompanied by a water release of 0.3 to 0.8%. We believe that the water released is rapidly taken up predominantly by the sucrose. The rapid water removal from the vicinity of the MHH particles, results in a "dry" environment which is known to be not conducive to further MHH dehydration. This anomalous dehydration behavior of MHH and the increased resistance to dehydration as the water vapor pressure is lowered, was described earlier [125].

These results are surprising in the context of MHH dehydration in mannitol-sucrose (4:1) lyophiles in the absence of protein [125]. Addition of protein along with sucrose significantly

delayed the dehydration process of MHH. In BSA with sucrose formulations, only KFT measurements were performed, and the water content remained constant at about 1.8% for up to 90 days.

The water content in the final lyophile can be rank ordered as: mannitol + sucrose (~ 6.0%) > mannitol + protein (~4.5%) > mannitol + sucrose + protein (~2.3%). In the mannitol-protein lyophile, the weight fraction of mannitol was ~0.96 (based on the total solids content). If all the mannitol existed as the hemihydrate, the calculated water content would be ~ 4.3%. While the XRD pattern revealed the formation of highly crystalline MHH, there was also a trace amount of β-mannitol (Figure 4.3). Therefore, we believe that the major fraction of the water is associated with the mannitol lattice (as MHH). However, the existence of some sorbed water cannot be ruled out.

In our previous study, the highest residual water content was observed in the mannitol-sucrose lyophile [125]. Again, the XRD pattern revealed that MHH was the predominant component with some evidence of β-form. The presence of sucrose is expected to inhibit the crystallization of a fraction of the mannitol (discussed later; mannitol recrystallization). The amorphous components (sucrose and mannitol) are expected to sorb water. Therefore, the total water can be attributed to both lattice (MHH) and sorbed water.

Similarly, in the presence of the two amorphous components, protein and sucrose, a fraction of the mannitol is expected to be retained amorphous. This is evident from the decrease in the intensities of the MHH peaks (Figure 4.4). Considering that the mannitol weight fraction is 0.77 if all the mannitol had crystallized as a hemihydrate, the calculated water content due to mannitol alone would be 3.4%. The inhibition of mannitol

crystallization as well as the decrease in MHH XRD peak intensities, support the experimentally determined water content of 2.3% in the lyophile. In addition, since there would be sorbed water associated with the amorphous components, we cannot attribute all the water to be a part of the lattice (MHH).

Following storage at 40°C in sealed vials, the MHH dehydration propensity in the lyophile can be rank ordered as (complete dehydration time in parenthesis): mannitol + protein (~5 days) > mannitol + sucrose (~ 11 days) [125] > mannitol + sucrose + protein (dehydration was not complete for 90 days). In the mannitol-protein lyophile, crystalline MHH forms the major component. When the vials were transferred from the freeze-dryer (after secondary drying at 10°C) to the stability chamber (40°C), the temperature increase is expected to initiate MHH dehydration. The release of a small amount of water due to initial MHH dehydration, will result in its rapid movement to the headspace. The attendant increase in headspace RH, will accelerate further and faster MHH dehydration.

In the mannitol-sucrose lyophile, a similar dehydration is expected to be initiated when the vials are transferred from 10 °C to 40°C. However, the released water will be sorbed by the amorphous sucrose. As a result, the headspace RH will continue to remain low. We had earlier documented the role of headspace RH on MHH dehydration behavior [125]. In mannitol-sucrose lyophiles stored at 40°C in vials, the headspace RH was very low (< 25 %) for up to 16 days [125]. Eventually, sufficient dehydration resulted in a rapid and abrupt increase in headspace RH. This was immediately followed by complete MHH dehydration. Thus, the presence of amorphous sucrose delayed MHH dehydration. However, once the MHH dehydration was complete, the sucrose crystallization was initiated.

Interestingly the addition of protein at a very low concentration to the mannitol-sucrose system, exerted two effects: (i) inhibition of MHH formation, leading to a lower residual water content in the lyophile and (ii) stabilization of MHH leading to its retention for prolonged time periods (> 90 days). Though the precise mechanism is not known, we postulate a combined effect of sucrose and protein in sorbing the water released by MHH. Consequently, the headspace RH is maintained low preventing further MHH dehydration.

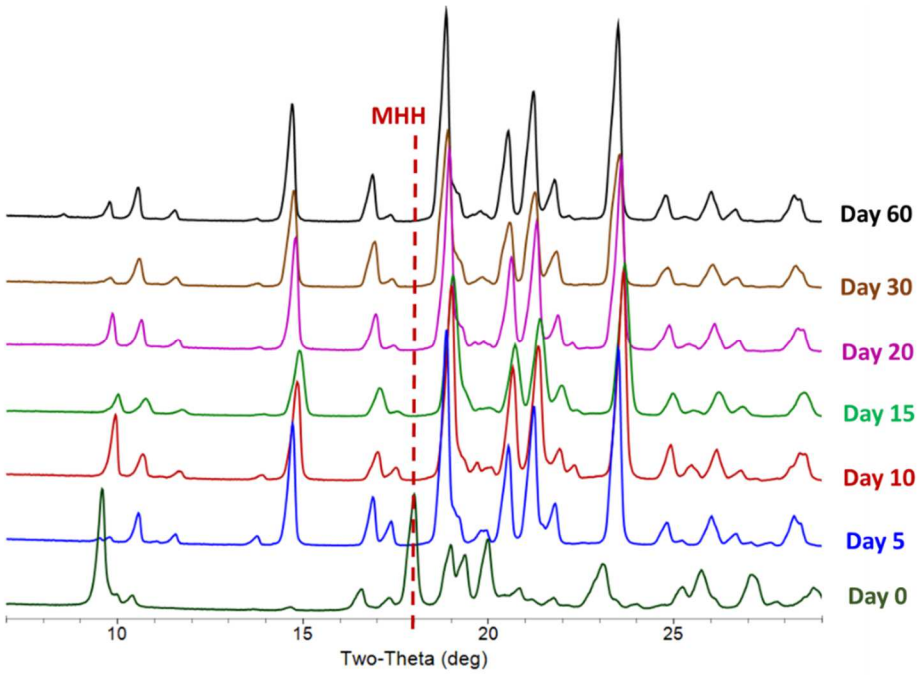

Figure 4.3 XRD overlay of BSA (2 mg/mL) with mannitol (5% w/v). The lyophiles were stored (in sealed vials) in a 40°C oven until the time of measurement. The characteristic peak of MHH (17.9° 2θ) is highlighted with a red dashed line. MHH completely dehydrated within 5 days and MHH → β-mannitol transition was observed following its dehydration.

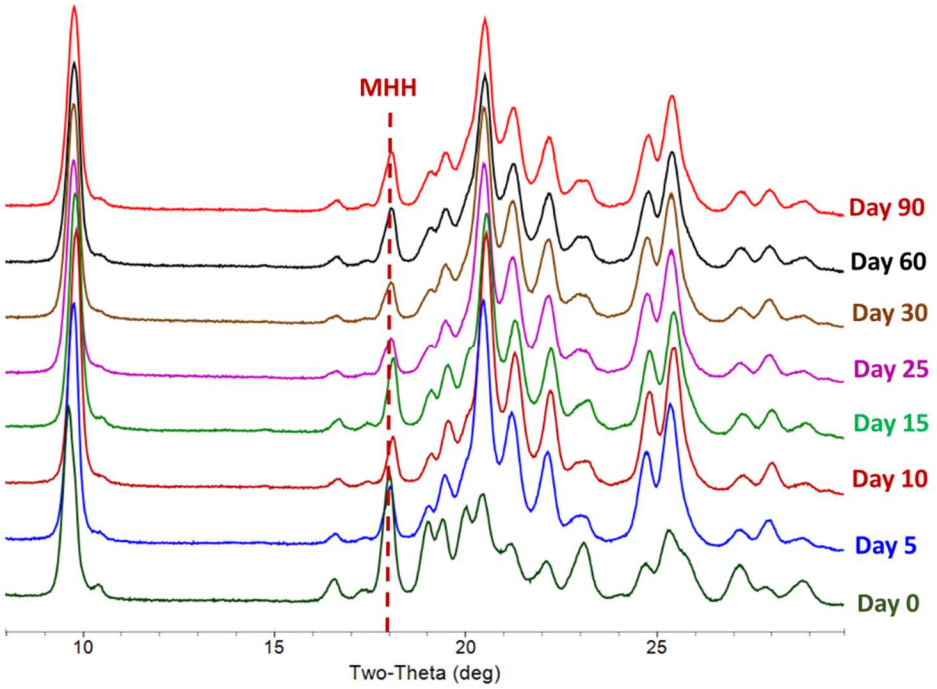

Figure 4.4 XRD overlay of BSA (2 mg/mL) with mannitol:sucrose (4:1, 5% w/v). The lyophiles were stored (in sealed vials) in a 40°C oven until the time of measurement. The characteristic peak of MHH (17.9° 2θ) is highlighted with a red dashed line. MHH was retained in the lyophile until day 90 at 40°C.

Finally, the influence of formulation composition on BSA stability was evaluated. The aggregation behavior was used as a measure of stability. The final lyophiles, stored at 40°C, were sampled periodically and were subjected to size exclusion chromatography (SEC) (Figure 4.5). The percentage high molecular weight species (% HMWS) provides a measure of the protein instability due to aggregation.

The BSA formulation with no excipient and with mannitol alone were used as controls to evaluate the effect of freeze-drying on BSA stability in the absence of a stabilizer (Figure 4.5). The high initial aggregate concentration reveals processing-induced instability. The presence of mannitol seemed to facilitate aggregation during freeze-drying. Furthermore, in both these systems, there appeared to be a gradual increase in % HMWS as a function

of time. This result is consistent with the XRD data (Figure 4.3). The dehydration of MHH and the water released therefore may be responsible for the observed increase in aggregates. A similar trend was observed in the absence of mannitol (only BSA). In this formulation, the residual water content (1.8%) could have facilitated the aggregation during storage.

BSA formulations with sucrose or with mannitol-sucrose exhibited no increase in aggregates over the entire storage period. This result strongly suggests the benefit of adding a stabilizer to the formulation. The addition of mannitol to a sucrose formulation had no destabilizing effect. In these formulations, mannitol crystallized as MHH. During storage, there is no evidence of mannitol dehydration (Figure 4.4). This was in sharp contrast to lyophiles containing only mannitol, where rapid MHH dehydration was observed during storage. Thus, the presence of sucrose stabilized MHH (as explained earlier).

Our next set of studies were conducted with HSA, which is similar to BSA in size. The reason for this investigation was two-fold: (a) no aggregation of BSA was observed in the mannitol-sucrose formulation even after 3 months of storage at 40 °C and (b) the monomer purity of BSA reference standard is < 90% with a HMWS level of > 10% which made the interpretation of results challenging. HSA exhibited a monomer purity > 90%.

Our next objective was to modulate the water content in the final lyophile, using the optimized formulation composition of 4:1 ratio of mannitol to sucrose with a total solute content of 5% w/v and HSA concentration of 2 mg/mL.

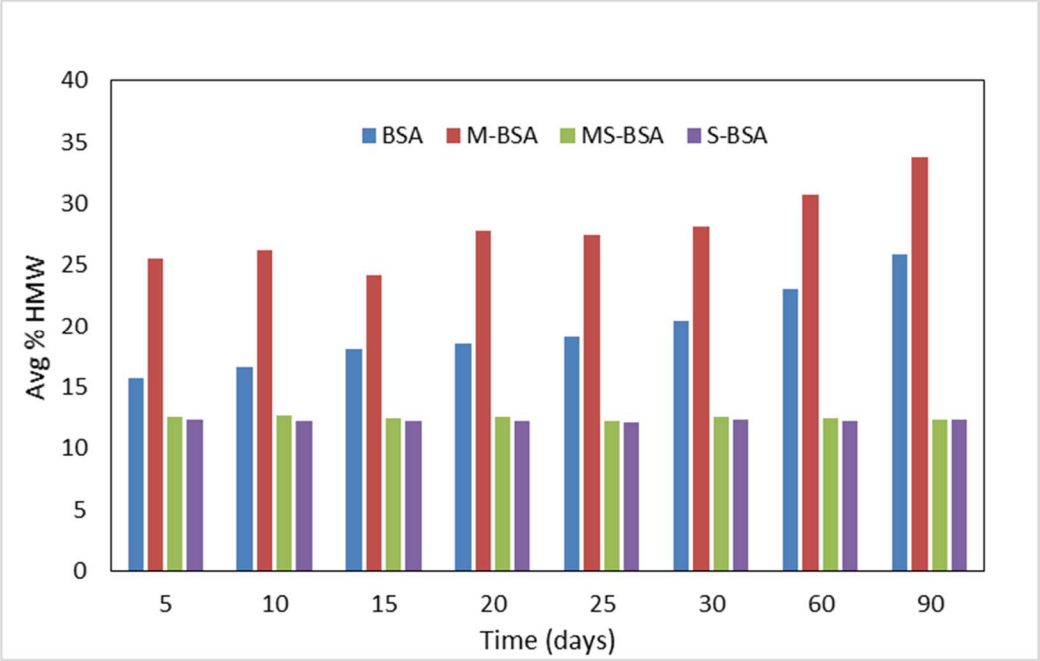

Figure 4.5 Size exclusion chromatography results lyophiles of (i) BSA (2 mg/mL) (ii) BSA (2 mg/mL) + mannitol (5% w/v) (iii) BSA (2 mg/mL) + mannitol:sucrose (4:1, 5% w/v) and (iv) BSA (2 mg/mL) + sucrose (2% w/v). The lyophiles (sealed vials) were stored at 40°C for 90 days.

4.3.2 Effect of lyophilization cycle parameters

Physical form of mannitol and sucrose in the final lyophile. Three separate cycles were conducted wherein the secondary drying conditions differed (Table 1). For reference, no secondary drying was conducted for cycle 1. Secondary drying took place at 10 °C for 24 hours for cycle 2 and at 40 °C for 6 hours for cycle 3. The lyophile water contents for the 3 cycles were 3.5%, 2.5% and 2.3% respectively. The lyophilization cycle parameters also influenced the MHH content in the final lyophile. Even after drying at 40°C for 6 hours (cycle 3), MHH dehydration was incomplete.

There are literature reports of MHH, when present alone or with sucrose, dehydrating at secondary drying temperatures > 30°C. It was surprising that the presence of protein in the

lyophiles, though at a very low concentration (weight fraction of 0.03), appears to inhibit MHH dehydration. It was therefore of interest to map the MHH dehydration behavior, as the freeze-drying cycle progressed through the primary and secondary drying stages. A freeze-dryer (Lyostar 3) equipped with a sample thief enabled us to remove vials *during* primary and secondary drying. These "in process" samples were subjected to XRD (Figure 4.6). The MHH formed during annealing is essentially retained during the entire primary drying cycle. Vial to vial variability is likely responsible for the observed intensity differences in the samples removed at 10°C. At the higher secondary drying temperature of 40°C, there was rapid onset of dehydration. However, the dehydration was not complete even after 24 hours, as is evident from the retention of MHH peak. A higher drying temperature of 50°C was needed to cause complete dehydration. Thus, it is not surprising that after drying for 6 hours at 40°C (Cycle 3; Figure 4.7), MHH was retained.

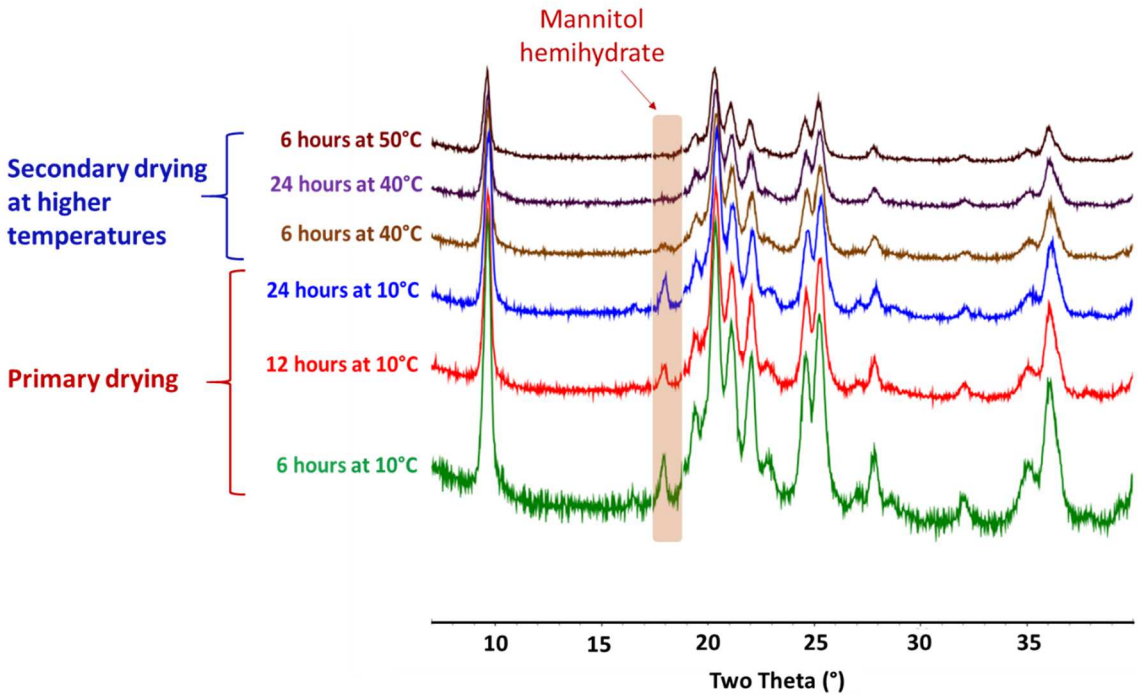

Figure 4.6 The XRD patterns obtained during the different stages of drying. The prelyophilization solution contained HSA (2 mg/mL) along with mannitol and sucrose (4:1, 5% w/v). The freezing and annealing details are provided in Table 1 (common for all three cycles). Primary drying was conducted at 10°C for 24 hours followed by secondary drying, first at 40°C for 24 hours and then at 50°C for 6 hours. Vials were removed at different time points using a sample thief, both during primary and secondary drying.

In the absence of secondary drying (Cycle 1), the characteristic peaks of MHH were readily discerned (Figure 4.7). Therefore, a major fraction of the water is associated with the mannitol lattice (as hemihydrate). However, in the absence of secondary drying, we also expect a small but significant fraction of sorbed water. The introduction of a secondary drying step (Cycle 2), while removing a substantial fraction of the sorbed water, retained mannitol as a hemihydrate (Figure 4.7). Thus, the secondary drying conditions, while causing water desorption, did not result in pronounced MHH dehydration. An increase in drying temperature (40°C) caused only a partial dehydration of MHH. The elevated drying

temperature is expected to reduce the sorbed water content. Thus, when we go from Cycle 1 to Cycle 2, the change in water content is likely due to reduction in sorbed water content. However, the reduced water content following Cycle 3 is likely due to a combination of desorption and partial MHH dehydration (reduction in XRD peak intensity).

The lyophiles with different water contents were stored at 40°C for 15 days (Figure 4.7). The goal was to evaluate the effect of residual water content (a combination of sorbed and lattice water) on MHH dehydration. In the lyophiles subjected to secondary drying (cycles 2 and 3), there was a small decrease in the intensity of the 17.9° 2θ peak of MHH suggesting partial dehydration. However, no other changes in the XRD pattern were observed (Figure 4.14; supplementary information).

In the lyophile from cycle 1, MHH dehydration was complete in 7 days and was followed by sucrose crystallization (Figure 4.8). This rapid dehydration can be explained by a "wet microenvironment" due to the sorbed water in the system. The sorbed water, by raising the headspace RH, can promote MHH dehydration. The dehydration, based on the disappearance of the 17.9° 2θ peak, was complete in 7 days. The complete MHH dehydration was followed by sucrose crystallization, which also became first evident at 7 days. The sucrose peak intensities increased with time and the crystallization became more pronounced at 15 days. The water released by MHH dehydration will be sorbed by sucrose. The plasticization caused by the sorbed water will decrease the glass transition temperature (discussed in detail in the next paragraph). The attendant increase in molecular mobility facilitates crystallization [116, 129] .

At the end of the storage period, the lyophile water content decreased to 2.5%. Since MHH dehydration was complete, all of the water is believed to exist as sorbed water. Since these were sealed vials, the decrease in water content observed during storage, cannot be attributed to water leaving the system. Therefore, we believe that there is moisture transfer from the cake to the rubber stopper. Such moisture transfer to stoppers was documented by us earlier [125]. These studies highlight two factors: (i) the role of sorbed water on the dehydration behavior of MHH and (ii) more importantly, the potential for the water released by MHH dehydration to cause sucrose crystallization.

It is instructive to note that the lyophiles from Cycles 2 and 3 did not exhibit any pronounced changes following storage, both in their XRD patterns and residual water contents. Thus, a small difference in residual water content (3.5% in Cycle 1 vs. $\leq$ 2.5% in Cycles 2 and 3) resulted in a pronounced difference, both in the dehydration behavior of MHH and sucrose crystallization behavior.

Having established the role of residual water, our final interest was to evaluate: (i) the effect of headspace RH on the phase behavior of mannitol and sucrose and (ii) attempt to use headspace RH as a predictor of product stability (using controlled humidity environment). We hypothesized the sequence of events as: MHH dehydration → sucrose crystallization → HSA aggregation. Therefore, in the next set of experiments, the stability was evaluated at two RH values.

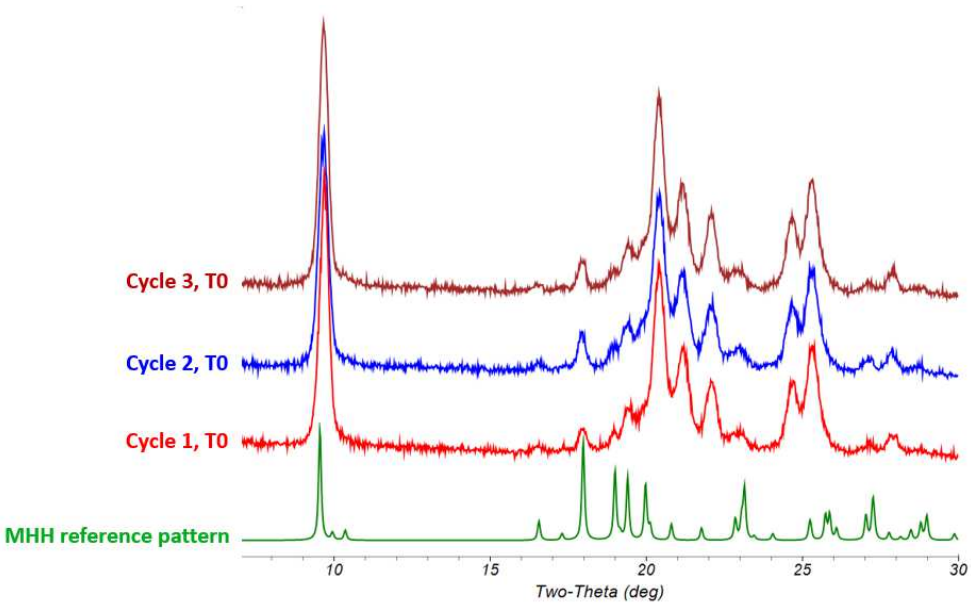

Figure 4.7 XRD overlay of lyophiles obtained by freeze-drying solutions containing HSA (2 mg/mL) in mannitol:sucrose (4:1, 5% w/v). Table 1 contains the cycle parameters. The lyophile water content at the end of Cycles 1, 2 and 3 were 3.5, 2.5 and 2.3% w/w respectively.

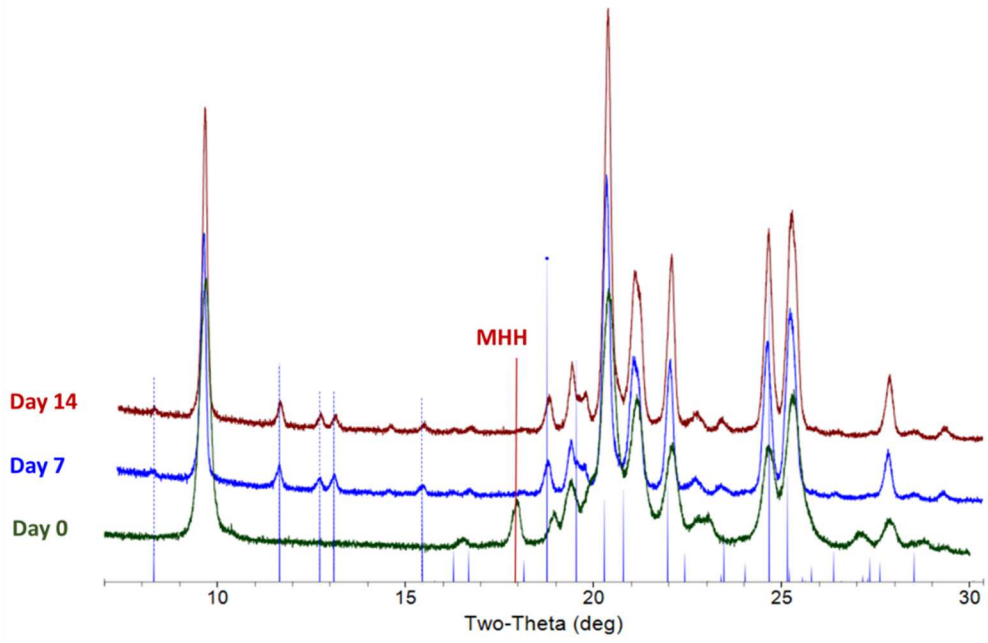

Figure 4.8 XRD overlay of lyophiles obtained by freeze-drying (cycle 1) solutions containing HSA (2 mg/mL) in mannitol: sucrose (4:1, 5% w/v). The sealed vials were stored at 40°C and XRD patterns were collected at day 7 and 14. MHH completely dehydrated and sucrose crystallization was observed in 7 days. Dotted blue lines are sucrose reference peaks and the characteristic MHH 17.9 °2θ peak is highlighted by a solid (red) line.

4.3.3 MHH Role of controlled relative humidity (55% RH) and elevated temperature (40°C)

4.3.3.1 Synchrotron X-ray diffractometry

We had earlier documented that an increase in headspace RH accelerated MHH dehydration. Therefore, synchrotron XRD studies were conducted at 40°C/55% RH, a condition favorable for rapid MHH dehydration. The details of the experimental setup are provided in the Methods section. For the HSA-mannitol-sucrose lyophile (Cycle 3), XRD diffractograms were collected for 10 hours at 5-minute intervals. Only representative patterns are overlaid in Figure 4.9. The relative peak intensities of the crystalline phases as a function of time are plotted in Figure 4.10. Initially (T0), the lyophile showed characteristic peaks of MHH and δ-mannitol.

On storage at 40°C/55% RH, at ~ 20 minutes, there was a sharp drop in the MHH peak intensity accompanied by appearance of the β-mannitol peak. This was followed by an abrupt increase, that was immediately followed by a decrease (dehydration) in MHH peak intensity (Figure 4.9 and Figure 4.10). The increase in MHH peak intensity suggests recrystallization of a fraction of the amorphous mannitol. Similar recrystallization behavior of MHH at ambient (or elevated) temperatures has been reported by Cao *et. al.* and Thakral *et. al.* [86, 125]. MHH dehydration was complete in ~ 80 minutes while β-mannitol peak intensities gradually increased up to ~ 150 minutes. Thus, there appeared to be a small lag time between MHH dehydration and complete anhydrous mannitol crystallization. The onset of sucrose crystallization was observed only after ~ 4 hours (255 minutes) and sucrose peak intensities gradually increased throughout the experiment (~ 600 minutes)

(Figure 4.10). While pronounced MHH dehydration occurred between 30 and 90 minutes of storage, there was an appreciable delay before the first evidence of sucrose crystallization at ~ 250 minutes.

The synchrotron experiment enabled us to map the phase transitions as a function of time at 40°C/55% RH (Figure 4.9). While the complete dehydration of MHH was quite rapid (< 100 min), the first evidence of sucrose crystallization was observed only at 250 min. In order to understand the kinetics of these reactions, it is necessary to know both the amount of water (total water content) and the state of the water in the lyophile. Therefore, the fresh lyophile was stored at 40° C/55% RH in an automated water sorption analyzer and the sample weight was continuously monitored. After transferring to the water sorption analyzer, the sample was initially equilibrated at 0% RH for 2 hours. During this time, there was negligible (< 0.2%) weight loss. When the RH was increased to 55% (40°C), there was a rapid weight gain of ~2.5% which occurred in ~ 15 minutes. Considering that the initial water content of the lyophile was ~ 2.3%, the total water content is now ~ 4.8%. The weight gain was immediately followed by a sharp weight loss of ~ 0.5% over the next 150 minutes and then a gradual two stage weight loss of 2% over the next 66 hours.

As we had pointed out earlier (section 4.3.1), in the lyophile, a major fraction of the water is associated with mannitol lattice (as hemihydrate). In the SXRD setup of 40°C/55% RH, the MHH dehydration was complete in ~ 80 minutes. We expected this dehydration process to be manifested as a weight loss in the water sorption analyzer. However, no such weight loss was observed. Therefore, following MHH dehydration, the released water is sorbed by the lyophile. The lyophile also takes up additional water from the environment,

manifested in the significant weight increase of 2.5%. If MHH → β-mannitol transition occurs through an amorphous intermediate (transient existence), this phase can sorb and retain water. However, a fraction of it crystallizes rapidly to β-mannitol, reflected in the abrupt weight loss of ~ 0.5%. Approximately in the same time frame (~ 160 minutes), the crystalline anhydrous mannitol (predominantly β-mannitol with a trace of δ) formation levels off in the SXRD. At this point, the amorphous components of the lyophile are sucrose (major component), mannitol and the protein. Assuming that only a fraction of the sucrose will be hydrogen bonded to the protein, while the rest will be "free" but will be substantially plasticized (discussed later). The plasticized sucrose started to crystallize in about 5 hours (SXRD; Figure 4.10) and this was gradual and continuous in the time scale of our experiment (10 hours). Unfortunately, because of the limited availability of beam time, the experiment had to be stopped at 10 hours. However, the automated water sorption instrument enabled us to monitor the reaction over a much longer time. Here the weight loss appeared to be complete in about 70 hours.

Thus, by exposing the lyophile to the same environmental condition (40°C/55% RH) in the SXRD and water sorption analyzer, we obtained a comprehensive picture of: (i) phase behavior, (ii) state of water, and (iii) the role of water mediating the series of observed transitions. The water vapor pressure in the atmosphere triggered both the MHH dehydration and sucrose plasticization. While the MHH dehydration was rapid, sucrose crystallization had a pronounced lag time.

However, some questions remain unanswered: (i) is the crystallization of sucrose complete? (ii) is all the mannitol existing in the crystalline state? While we do not have a

direct answer, the residual water content provides us a clue. After storage at 40°C/55% RH for 75 hours, the lyophile water content is ~ 2.3%. Such a high residual water content can only be explained by a fraction of the sucrose and mannitol being retained in the amorphous state along with some water bound to protein. In case of sucrose, we believe that the fraction hydrogen bonded to the protein effectively resists crystallization. Proteins as well as amorphous solute, in a concentration dependent manner, are known to inhibit mannitol crystallization [58, 130]. Therefore, it is reasonable to assume that a small but significant fraction of mannitol can be retained amorphous.

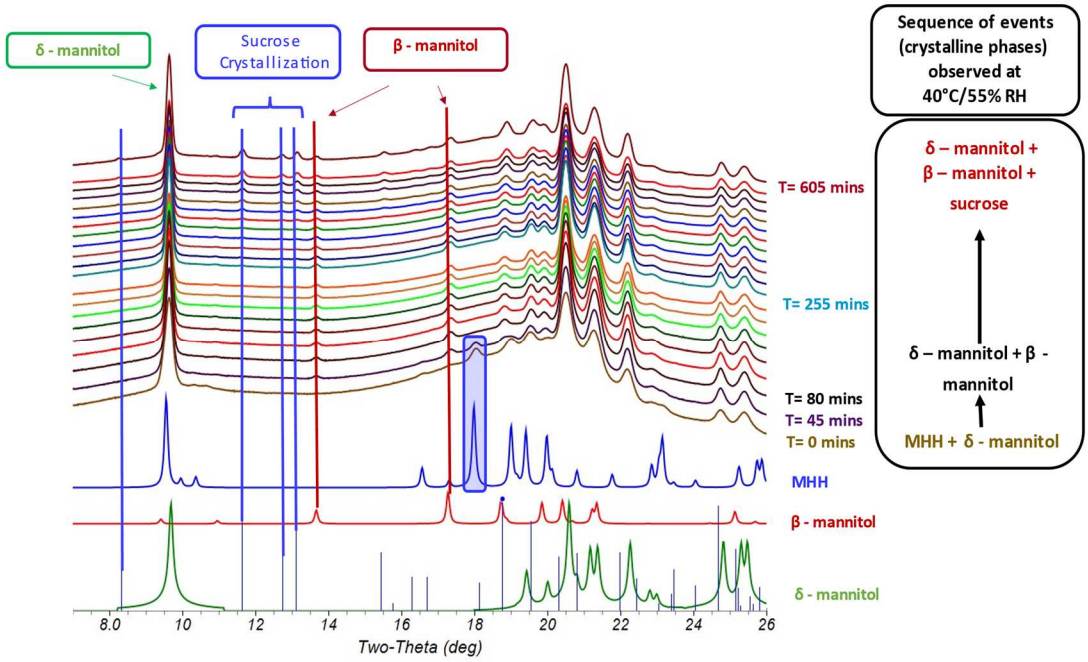

Figure 4.9 Overlay of synchrotron XRD patterns of HSA lyophile obtained using Cycle 3. The lyophile was held at 40°C/55% RH for 10 hours and XRD patterns were collected at 5 minute intervals. The reference patterns for sucrose are shown as dotted blue lines. The calculated patterns of β-, δ- mannitol and MHH are included for reference.

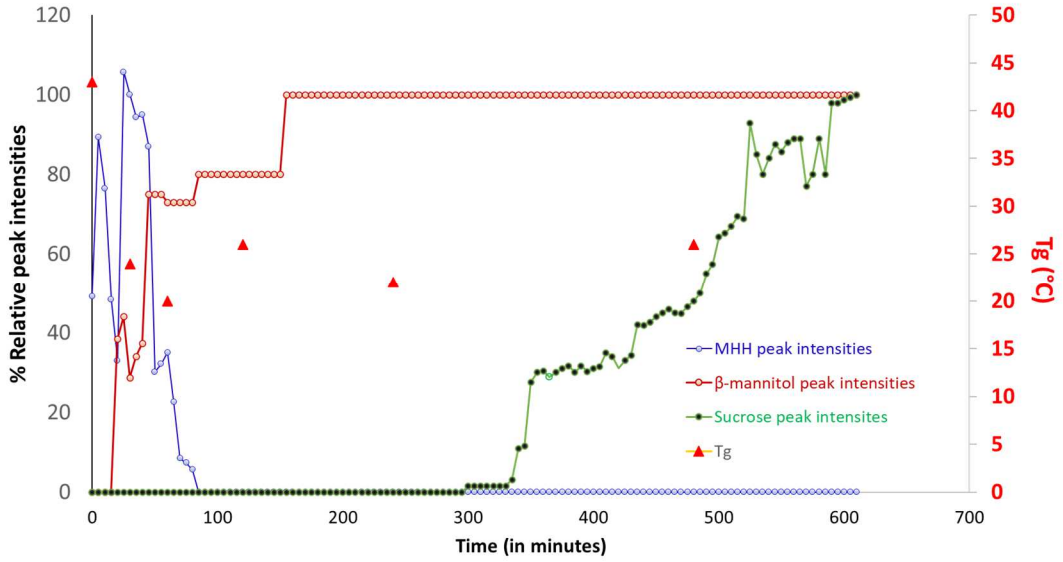

Figure 4.10 Relative intensities of 17.9° 2θ peak of MHH, 14.0° 2θ peak for β-mannitol and 11.6° 2θ peak for sucrose plotted as a function of function of time for lyophilized HSA (2 mg/mL) with mannitol:sucrose (4:1, 5% w/v) heated at 40°C and 55% RH for 10 hours. The data points are connected for visual aid to track the dehydration of MHH, crystallization of β-mannitol and sucrose.

In a separate experiment, the plasticizing effect of water on the lyophile was investigated using DSC (Figure 4.15). The T_g of the lyophile (Cycle 2), with a residual water content of 2.3%, was 45°C. Following storage at 40°C/55% RH, the T_g decreased rapidly and levelled off between 20 and 25°C (Figure 4.10). This decrease in T_g was brought about by the sorption of ~ 2.5% water (Figure 4.11). Thus, the total water lyophile water content at the onset of sucrose crystallization was ~ 4.8%.

The water sorption behavior of sucrose was comprehensively investigated by several groups and the results are summarized by Yu et al [120]. Amorphous sucrose has a strong propensity to sorb water enabling a plot of sucrose T_g as a function of water content (Figure 4.18). At a water content of 5%, the T_g was interpolated to be ~ 30°C. Sucrose was the predominant amorphous component in our lyophiles. The amorphous sucrose not only sorbed the water released by MHH but also sorbed additional water from the atmosphere,

reflected in the weight gain. The consequence of this pronounced plasticization was that the sucrose then existed in the supercooled state since the storage temperature (T = 40°C) was >> T_g (20 to 25°C). The first evidence of sucrose crystallization was observed at ~ 300 minutes (Figure 4.10). The crystallization progressed gradually.

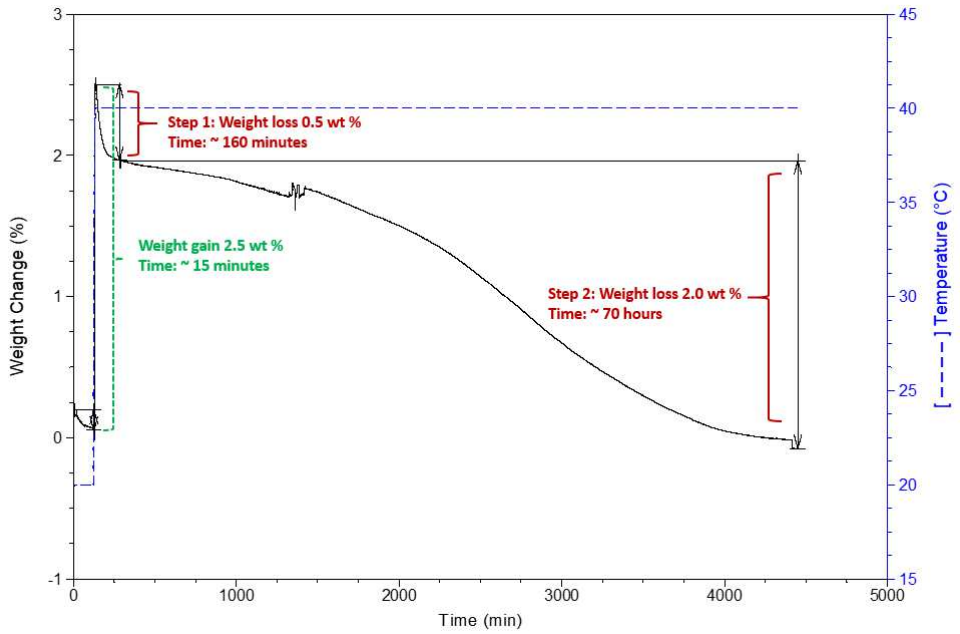

Figure 4.11 Moisture sorption-desorption behavior of mannitol-sucrose-HSA lyophile (from cycle 3). The lyophile was exposed to 20°C/0% RH for 120 minutes followed by 40°C/55%RH for 70 hours. The primary y-axis indicates the weight change (%) as a function of time indicated by a black curve. The secondary y-axis indicates the temperature as shown by the blue dotted line.

4.3.3.2 Influence of uncontrolled and controlled headspace RH

Our final objective was to determine the influence of headspace RH on the MHH dehydration → sucrose phase behavior → protein stability under: (i) controlled RH (33 and 55%) at RT, and (ii) uncontrolled RH (sealed vials) at 40°C.

At RT/33% RH, after 1 month of storage there was no evidence of MHH dehydration or sucrose crystallization reflecting their kinetic stability (Figure 4.12). Based on literature

reference, amorphous sucrose when stored under similar conditions, crystallized in < 3 days [112]. Thus, the matrix, and specifically the protein at such a low concentration, appears to significantly delay sucrose crystallization.

When the RH was increased to 55%, MHH dehydration was complete in < 24 hours accompanied by the crystallization of β-mannitol (Figure 4.19). Following a lag time of ~ 6 days, sucrose crystallization was observed. A progressive increase in the intensities of sucrose peaks were observed up to one month (Figure 4.19). Amorphous sucrose when stored under similar conditions, crystallized in about 2 hours [112, 131]. Thus, the pronounced crystallization inhibitory effect of the protein is again evident.

No protein aggregation was observed following storage for 1 month at RT/33% RH by SEC (Figure 4.12). These results were expected since MHH did not dehydrate, and sucrose was retained amorphous thus providing the necessary lyoprotection. In samples that were exposed to RT/55% RH, MHH dehydration as well as sucrose crystallization was observed in 7 days. Surprisingly, no HSA aggregation was observed by SEC (Figure 4.13). A 1:1 protein : sugar (weight ratio) has been found to be sufficient to prevent protein aggregation in freeze-dried formulations [132]. In our formulation, the protein to sugar ratio was 1:50. We postulate that although there was sucrose crystallization, it was incomplete. The amount of sucrose retained amorphous, and hydrogen bonded with the protein, was sufficient to provide lyoprotection. In a lyophilized sucrose and lactate dehydrogenase (LDH) formulation, it was shown that amorphous sucrose hydrogen-bonded with LDH. This interaction prevented protein aggregation as well as sucrose crystallization [133]. An increase in aggregates at day 30 in samples exposed to 55%RH (RT) was observed. At this point it

appears to be a consequence of higher sorbed water however, aggregation due to sucrose crystallization cannot be ruled out.

In the experiments discussed in Section 4.3.3.2, the headspace RH was controlled by storing the vials (without a stopper) in chambers at the desired water vapor pressure. However, in practice, after the secondary drying, the headspace is backfilled with nitrogen and the vials are sealed. At the end of secondary drying, vials lyophilized using Cycle 3 (HSA-sucrose-mannitol), were sealed under reduced pressure, and stored at 40°C for 3 months. The lyophiles were periodically subjected to XRD, KFT and SEC. There was no evidence of either MHH dehydration or sucrose crystallization. The lyophile water content as well as the HMWS remained unchanged. The water vapor pressure of the headspace was measured both in the fresh vials and following storage for 10 days using FMS. The initial water vapor pressure was ~ 1 torr (RH < 5% at 25°C) and following storage at 40°C, the water vapor pressure increased up to 3.5 torr (RH ~ 6% at 40°C) and was stabilized. These RH values will not favor MHH dehydration and explain the retention of MHH in the lyophiles during the storage period (3 months). Vials were also stored at 50°C and again no change in MHH peak intensities or in the lyophile water content were observed during the entire storage time (90 days).

The protein did not aggregate when stored at 40°C. In mannitol-sucrose lyophiles without the protein, we had observed complete MHH dehydration and sucrose crystallization after 20 days of storage at 40°C [125]. Addition of a protein appeared to significantly delay MHH dehydration in sealed vials at elevated temperatures. However, at 50°C, there was evidence of aggregation after 1 month of storage (data not shown). Since HSA degradation has been

reported at 64°C, aggregation after prolonged storage at 50°C is not surprising. It is important to note that there was no evidence of destabilization brought about by excipient phase behavior since MHH did not dehydrate and sucrose was retained amorphous at elevated temperatures.

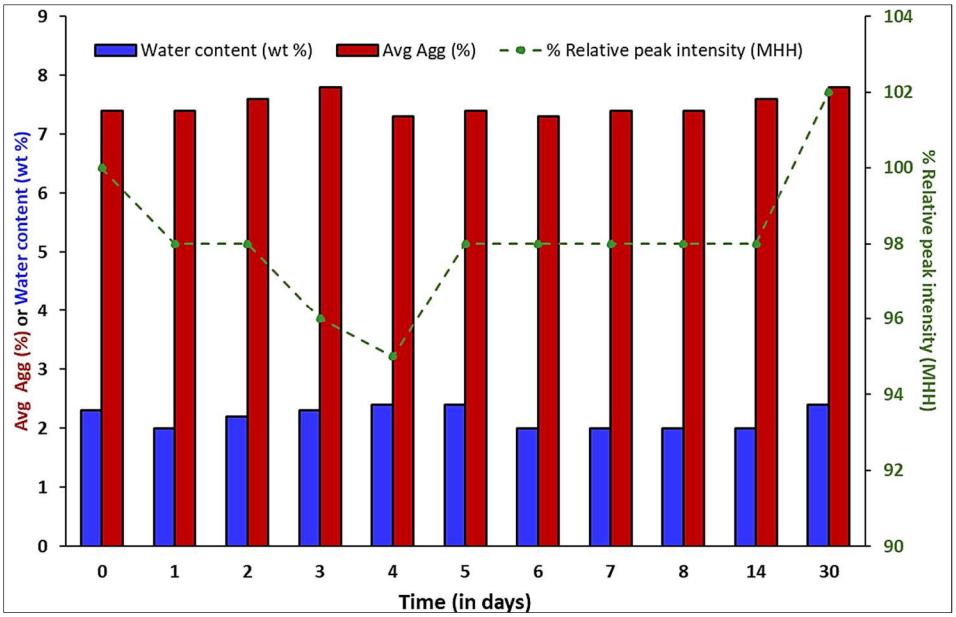

Figure 4.12 XRD, KFT and SEC of lyophilized HSA (2 mg/mL) with mannitol:sucrose (4:1, 5% w/v) exposed to 33% RH/RT. Left y-axis shows average aggregates (%) or water content (wt %) and right y-axis shows relative peak intensity* of MHH (XRD peak at 17.9 °2θ) plotted as a function of time. Individual vials from the same batch were pulled at different time points and stored at -20°C until analyzed.
***The initial intensity was considered 100%.**

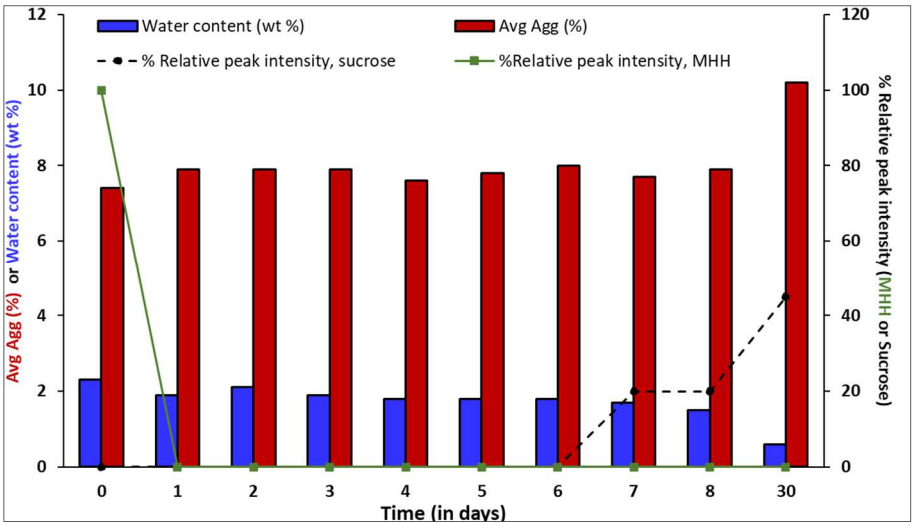

Figure 4.13 XRD, KFT and SEC of lyophilized HSA (2 mg/mL) with mannitol:sucrose (4:1, 5% w/v) exposed to 55% RH/RT. Left y-axis shows average aggregates (%) or water content (wt %) and right y-axis shows relative peak intensity* of MHH (XRD peak at 17.9 °2θ) or sucrose plotted as a function of time. Individual vials from the same batch were pulled at different time points and stored at -20°C until analyzed.**
***The initial intensity was considered 100%**. The peak intensity at the last data point was considered 45% (this was assumed to be the maximum crystallizing fraction).**

4.4 Significance

Ever since the existence of mannitol as a hemihydrate (MHH) has been identified in freeze-dried formulations, its dehydration and the potential instability of the released water has been a source of immense concern. The formation of mannitol hemihydrate in frozen solutions and its retention in the final lyophile has been of concern to the practitioners of freeze-drying. The apprehension stems from the potential of MHH to dehydrate during product storage.

Although we observed partial sucrose crystallization as a consequence of MHH dehydration, there was no detrimental effect on HSA aggregation. This suggests that if the fraction of the sugar responsible for protein stabilization (possibly by hydrogen bonding)

is retained amorphous, protein stability is maintained. Similar effect was observed in case of mAb, presence of MHH in the final lyophile did not impact mAb stability [102].

However, a robust formulation is characterized by the absence of phase transformations during product storage. If MHH is formed during freeze-drying, the ideal mitigation is to conduct secondary drying at elevated temperatures to facilitate MHH dehydration. However, this approach may not be practical under two circumstances: (i) when the protein is thermolabile, and (ii) when the protein delays MHH dehydration. If the final lyophile contains MHH, it will be prudent to identity conditions that will prevent MHH dehydration during the entire shelf-life of the product. For lyophiles stored at RT, headspace relative humidity (RH) ≤ 33% ensured MHH stability for the proteins investigated in this study. MHH stability in the final lyophile was also enabled by sealing lyophiles under reduced pressure.

Most of lyophilized products are stoppered either under vacuum or backfilled with nitrogen with minimum headspace humidity. The 55% RH used in our in-situ experiment was to accelerate the phase transformations that could be observed in mannitol-sucrose lyophilized formulations in cases where the headspace humidity can be higher. A high headspace RH (≥ 55% at RT) promoted rapid MHH dehydration. This can be brought about by: (a) initial dehydration of MHH, (b) high sorbed water content, or (c) moisture transfer from the stopper during storage.

Currently, the formation of MHH in lyophilized formulations is one of the factors limiting its use as a bulking agent in marketed formulations. In lyophiles that contain MHH,

comprehensive knowledge of the temperature and humidity conditions triggering its dehydration can help generate appropriate mitigation strategies.

4.5 Conclusions

Based on our results, MHH in a mannitol-sucrose-protein matrix can remain kinetically stable for an unusually long time during storage if the headspace relative humidity (RH) is ≤ 33% and the storage temperature is ≤ 50°C. However, if the RH is ≥ 55%, dehydration of MHH → release of water → plasticization of the sucrose followed by its crystallization was observed irrespective of the storage temperature (RT and 40°C). However, this did not result in protein destabilization. If appropriate storage precautions are in place, the presence of MHH in the final lyophile may not be as deleterious as had been previously considered. In addition, in the event of MHH dehydration followed by sucrose crystallization, "excess" sucrose is recommended to protect the protein from aggregation.

4.6 Supplementary information

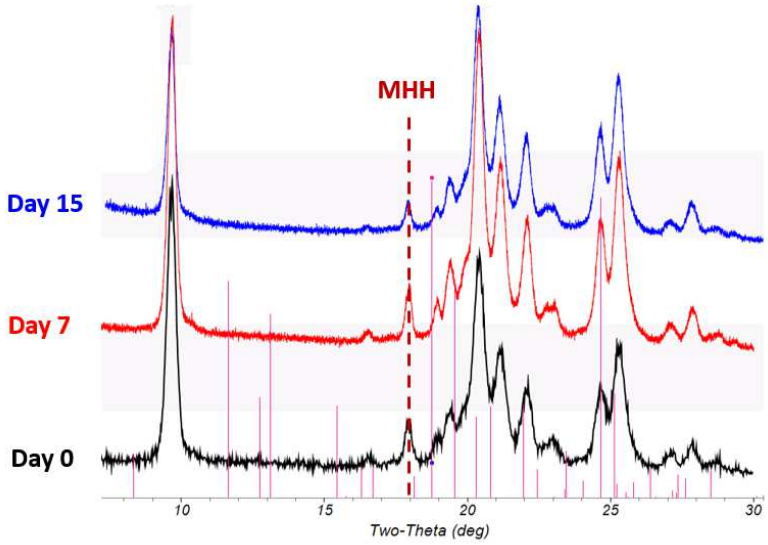

Figure 4.14 XRD overlay of lyophiles obtained by freeze-drying (cycle 2) solutions containing HSA (2 mg/mL) in mannitol: sucrose (4:1, 5% w/v). The sealed vials were stored at 40°C and XRD patterns were collected at day 7 and 15. MHH was retained for 15 days. The stick pattern for sucrose reference pattern is highlighted by the solid (pink) lines whereas the characteristic 17.9 2θ peak is highlighted by a dotted (red) line.

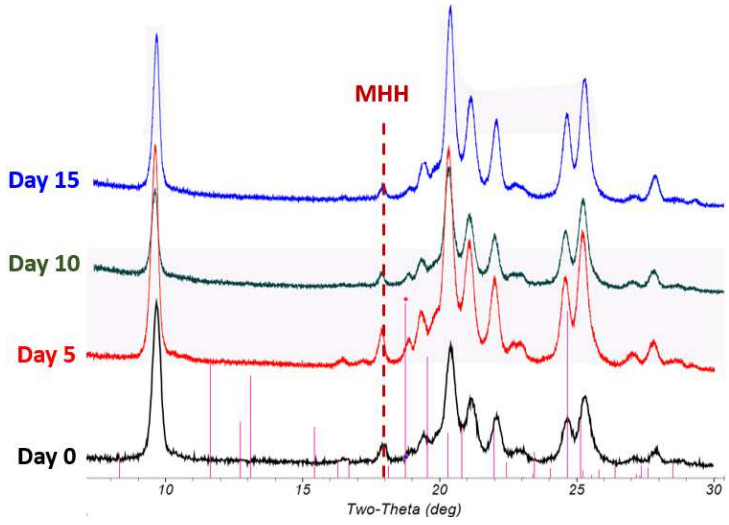

Figure 4.15 XRD overlay of lyophiles obtained by freeze-drying (cycle 3) solutions containing HSA (2 mg/mL) in mannitol: sucrose (4:1, 5% w/v). The sealed vials were stored at 40°C and XRD patterns were collected at day 5, 10 and 15. MHH was retained for 15 days. The stick pattern for sucrose reference pattern is highlighted by the solid (pink) lines whereas the characteristic 17.9 2θ peak is highlighted by a dotted (red) line.

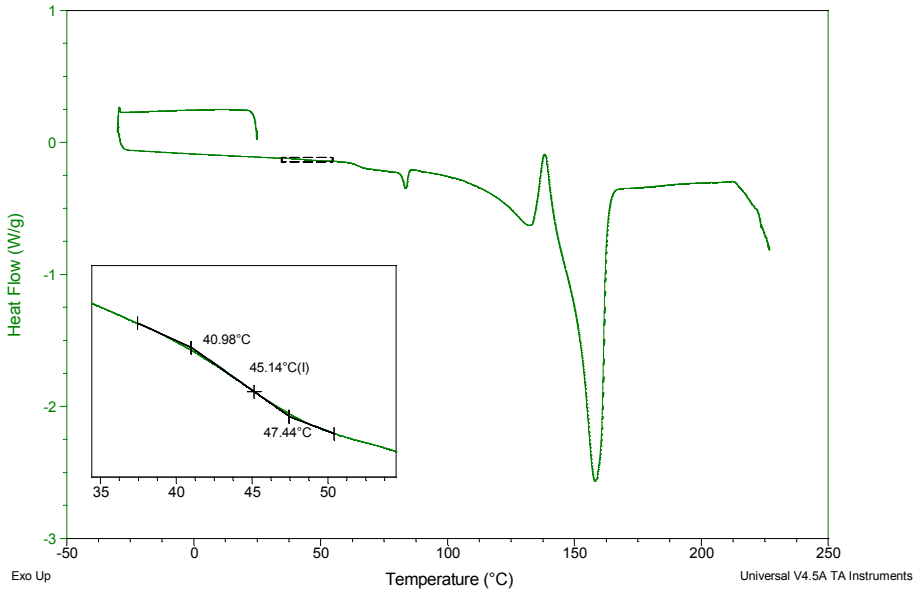

Figure 4.16 DSC of fresh (day 0) M:S 4:1 + 2 mg/mL HSA (Cycle 2) lyophile. Sample was cooled in a hermetically sealed pan from RT to -30°C and heated to 230°C at 10°C/min. The inset highlights the region with glass transition temperature.

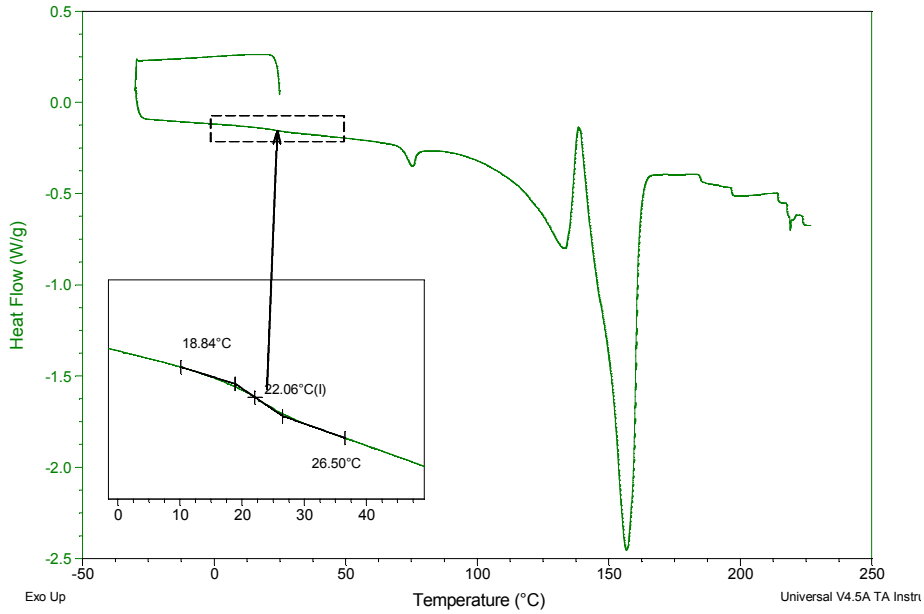

Figure 4.17 DSC of M:S 4:1 + 2 mg/mL HSA (Cycle 2) lyophile. The lyophile was exposed to 40°C/55%RH for 30 minutes. Sample was cooled in a hermetically sealed pan from RT to -30°C and heated to 230°C at 10°C/min. The inset highlights the region with glass transition temperature.

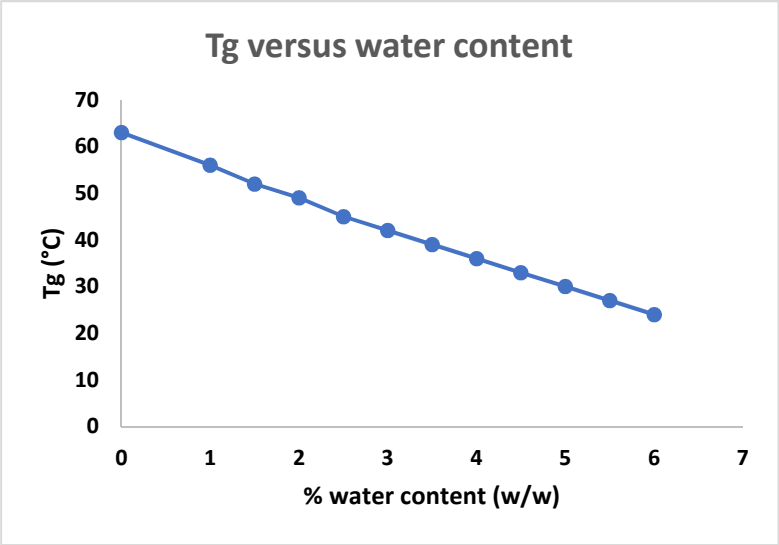

Figure 4.18 Glass transition as a function of water content for sucrose. These values were calculated from the equation $y = 62.859 – 746.96x + 1684.2x^2 – 1862.1x^3$ derived by Yu et al. [134]

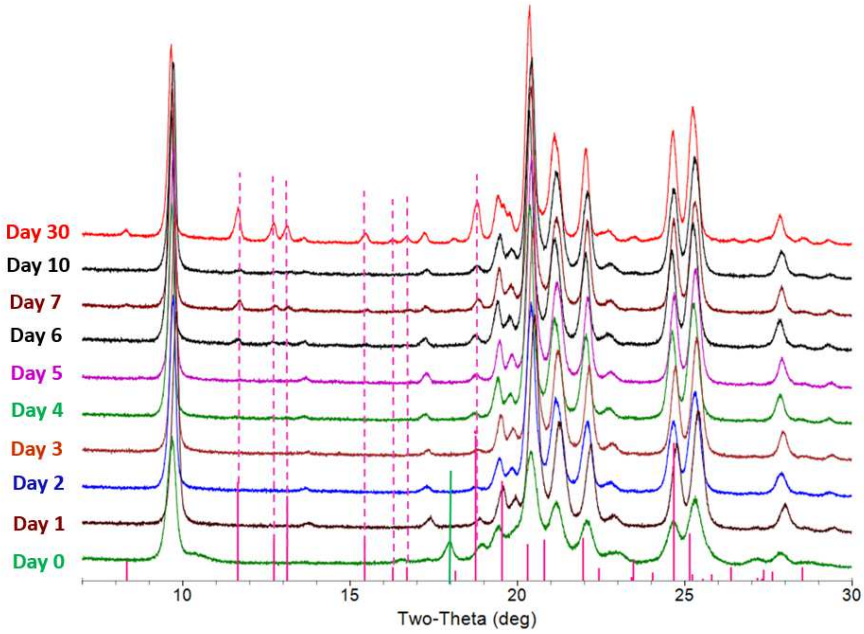

Figure 4.19 XRD overlay of lyophiles obtained by freeze-drying (cycle 3) solutions containing HSA (2 mg/mL) in mannitol: sucrose (4:1, 5% w/v). The sealed vials were stored at RT/55%RH°C and XRD patterns were collected at regular intervals for up to a month. MHH completely dehydrated in one day while sucrose crystallization was observed starting from day 6. The stick pattern for sucrose reference pattern is highlighted by the dotted (pink) lines whereas the characteristic 17.9 2θ peak is highlighted by a solid (green) line.

Chapter 5 Long-term frozen storage of proteins: use of mannitol to generate a homogenous freeze-concentrate

5.1 Introduction

Manufacturing of macromolecules is often divided into two steps – Drug Substance (DS) and Drug Product (DP) manufacturing [135]. The DS is often stored in the frozen state and thawed for DP manufacturing. Occasionally, intermediate solutions and drug product (DP) are also stored frozen [16]. The frozen state substantially enhances the shelf life of the DS by minimizing its mobility and hence slowing down reaction rates. It also reduces the risk of microbial growth and helps overcome transport-related stress (e.g. shaking, agitation etc.) [26, 135]. However, destabilization of macromolecules can occur during freezing and thawing and freeze-thaw related issues can be challenging to overcome. Successful frozen storage of DS as well as intermediates requires careful consideration of the biophysical principles dictating stability [26].

Protein formulations commonly contain several excipients including a buffer, a sugar or sugar-alcohol, and a surfactant to prevent protein degradation which can occur through various mechanisms. Freeze concentration or cold denaturation induced aggregation is of concern during freezing and frozen storage [21, 23]. Freezing is initiated by ice nucleation followed by ice crystal growth. Due to supercooling, ice nucleation is often observed substantially below the equilibrium freezing point [5]. Most of the water then separates into ice crystals. The solute may either crystallize or be retained as a freeze-concentrate. Ice formation is influenced by numerous factors including shelf temperature, freezing, and thawing rates, formulation composition and concentration, as well as container shape and

size. Once ice nucleates, crystallization and phase separation of the ice continues until a maximally freeze concentrated solution is achieved (assuming the solute is retained amorphous). During the freezing process, proteins are exposed to stresses including adsorption at the ice-water interface, pH changes due to freeze-concentration and phase separation causing unequal distribution of the stabilizer and protein [22, 136, 137]. The cooling rate and the type and concentration of excipients are important factors governing DS stability.

The role of stabilizers (also referred to as lyoprotectants) is to prevent protein denaturation including aggregation during processing and storage. Non-crystallizing excipients (stabilizers) are known to prevent protein denaturation by preferential exclusion and viscous glass formation [28]. The most important role of these stabilizers is to prevent the unfolding of the protein both during freezing and thawing. According to the preferential exclusion mechanism, the amorphous excipient is selectively excluded from the immediate vicinity of the protein surface thereby enabling its stabilization in the native state. A second mechanism is the decrease in protein mobility brought about by the increase in viscosity of the freeze-concentrate [138]. In order to exert their protective action, these stabilizers should remain amorphous.

When a solution containing a crystallizing solute is cooled, at the eutectic temperature, complete crystallization of the solute and ice should ideally occur. However, most of the solutes used in protein formulations do not crystallize readily when frozen. When a solute is retained amorphous, an important attribute of the frozen system is the glass transition temperature of the freeze-concentrate (Tg'). Stabilizers used in protein formulations

including sugars, surfactants, and amino acids contribute to formation of an amorphous matrix. Their utility comes from their ability to remain amorphous with the protein in the freeze concentrated phase. Ideally, storage of the frozen mass in the deeply glassy state, for example at approximately 50°C below the glass transition temperature (Tg' - 50), is assumed to inhibit mobility sufficiently to prevent mobility-induced protein degradation or excipient crystallization [139]. However, given the nature of supply chain logistics, it can be challenging to store the frozen bulk at very low temperatures. There are examples of several systems stored at -70ºC which can be practically difficult, expensive, and pose significant challenges with maintaining the cold chain. The freeze-concentrate composition dictates the Tg' and decreases with an increase in unfrozen water content. From a processing and storage perspective, we desire compositions with the highest possible Tg' to avoid the need for storage at very low temperatures.

Sugars such as trehalose and sucrose are used as stabilizers in protein solutions due to their ability to serve as lyoprotectants and resist crystallization. In lyophilized formulations, a combination of stabilizer and a bulking agent has been used as a successful strategy to prevent protein aggregation as well as provide necessary mechanical strength to the final cake [87]. Mannitol, a popular bulking agent, has been used due its high propensity to crystallize during freezing along with its high eutectic melting temperature which results in short drying cycles [83]. Sucrose-mannitol-water ternary solutions exhibit two Tg' (~ -48 and -34ºC) during freezing. The multiple Tg' values reflect heterogeneity in the freeze concentrate. The composition with a lower glass transition temperature has a higher amount of unfrozen water ("water rich" phase) while the composition with the higher glass

transition temperature is a "solute rich" phase). However, irrespective of composition and processing (annealing), sucrose is consistently retained in the amorphous state. Annealing is typically conducted to facilitate solute crystallization in frozen systems [140]. In ternary mannitol-sucrose-water systems, complete mannitol crystallization), and hence its phase separation, will result in a frozen matrix which will resemble sucrose-water binary system. Since mannitol has a strong propensity to crystallize, this can be achieved with the judicious selection of processing steps.

Trehalose-mannitol-water ternary solutions also exhibit two Tg' (~ -45 and -32ºC) reflecting heterogeneity in the freeze concentrate. Investigation of different weight ratios of mannitol to trehalose (R) revealed that when R=1, at annealing temperatures higher than Tg', mannitol crystallization led to trehalose crystallization, whereas at R = 3 only mannitol crystallized [141]. Crystallization of trehalose may compromise its lyoprotectant function. Connolly et al. investigated the impact of cooling rate, storage temperature and formulation composition on mAb aggregation in presence of trehalose during lyophilization. The trehalose crystallization in this case was ensured either by seeding or by controlled ice nucleation. The mAb showed highest aggregation after 12-months storage at a temperature of -20°C as opposed to no aggregation in samples stored at -40°C. The study highlights that if the storage temperature is below the Tg' of the frozen matrix, protein aggregation can be significantly prevented [137]. Therefore, it is necessary to identify trehalose to mannitol ratios which will lead to selective crystallization of only mannitol and not trehalose. It is also instructive to recognize that the protein, in a concentration dependent

manner, will inhibit the crystallization of both trehalose and mannitol. The process parameters for annealing may be designed to promote the crystallization of only mannitol.

In ternary mannitol-sugar-water systems, substantial if not complete mannitol phase separation (crystallization) can be accomplished if it is initiated early in the freezing process. Complete mannitol phase separation (crystallization) in a frozen matrix is a desirable attribute. Mannitol crystallization will also result in the crystallization of the associated unfrozen water. This has the potential to result in a homogenous freeze-concentrate with a single Tg'. We hypothesize that in frozen systems, mannitol crystallization *during* freezing can result in a homogeneous freeze concentrate (characterized by a single Tg'). Complete mannitol crystallization can be accomplished by (i) annealing the solution during cooling and (ii) using specific mannitol to sugar ratios. In other words, the goal of our work was to use a crystallizing excipient to promote ice crystallization and obtain a freeze-concentrate of consistent and constant composition. Baseline thermal characterization of mannitol-sucrose and mannitol-trehalose mixtures of different compositions will be performed using DSC. In order to identify the phases crystallizing from solution, *in situ* (during cooling as well as heating) low temperature X-ray diffractometric measurements (synchrotron source) will be performed. The overall goal is to achieve maximum mannitol and ice crystallization. This will be done by (i) cooling at slow rates, and (ii) isothermally holding the optimized mannitol-sugar compositions at desired subambient temperatures during cooling. In the context of this work, we refer to the isothermal hold during cooling step as 'annealing'. Human serum albumin buffered

with histidine was the model protein. A sugar (sucrose or trehalose) served as a stabilizer and mannitol enabled the formation of a homogenous freeze-concentrate.

5.2 Materials and Methods

5.2.1 Materials

Mannitol ($C_6H_{14}O_6$), sucrose ($C_{12}H_{22}O_{11}$), trehalose ($C_{12}H_{22}O_{11}$), L-histidine, histidine monohydrochloride and human serum albumin (HSA, ≥ 99.0% purified) were purchased from Sigma-Aldrich (St. Louis, MO, USA). Aqueous solutions of mannitol and either sucrose or trehalose were prepared in 1:1, 2:1 and 3:1 ratio with a total solute concentration of 5% w/v in 10 mM histidine buffer solutions.

5.2.2 Differential scanning calorimetry (DSC)

A differential scanning calorimeter (model Q2000 TA instruments, New Castle, DE, USA) equipped with a cooling system was used. The instrument was calibrated with tin and indium. Dry nitrogen at 50 mL/min was used as the purge gas. In the first set of studies, approximately 15 mg of solution was weighed in an aluminum pan, sealed hermetically, cooled to -40°C and held for 15 minutes and warmed to 10°C at 10, 5 and 0.5°C/min.

In another set of studies, about 20 mg of the aqueous solutions were weighed into an aluminum pan, sealed hermetically, and cooled from room temperature to -60°C at 1°C/min, held isothermally for 10 min, and heated at 1°C/min to room temperature, under a stream of nitrogen. Annealing/temperature cycling was performed to achieve maximum solute and ice crystallization. Samples were annealed at -20°C for 2 to 16 hours above Tg' of the system during warming. The solutions were cooled to -60°C and rewarmed, the Tg',

heat capacity associated with Tg' (Δ Cp) and the enthalpy of ice and solute melting endotherms in the final warming curve were recorded.

5.2.3 Synchrotron X-ray diffractometry (sXRD)

Phase transformations during freezing and warming were also characterized at the synchrotron X-ray beamline 17-BM-B (sector 17; Advanced Photon Source, Argonne National Laboratory, IL, USA). A monochromatic X-ray beam (λ=0.45452 Å, beam size 300 μm x 300 μm) and a two-dimensional (2D) area detector (XRD-1621, Perkin Elmer) were used. More details with respect to the experimental setup can be found in our earlier publication [142].

The aqueous solutions were placed in a custom-made copper sample holder with a Kapton® window, polyether ether ketone (PEEK) base and a thermocouple. A T-thermocouple (Omega) was used to record the real-time temperature using a temperature input device (NI USB-TC01, National Instruments, TX). Freezing and warming of 100 μL of sample placed in the V-shaped copper sample holder was carried out with the aid of Cryostream 700 plus (Oxford Cryosystems Ltd, Oxford, UK) adjusted 3 to 5 cm above the sample holder. The temperature difference between the cryostream and sample holder was determined by cooling an aqueous sodium chloride (23% w/w) solution and determining the sodium chloride - water eutectic temperature. Background signal was collected by exposing the sample holder without any solution. The 2D X-ray patterns collected were converted to 1D 2θ scans using GSAS-II software (Edgewall Software) [143]. The data were collected using synchrotron radiation (0.45Å). They were converted and plotted for Cu Kα radiation (1.54 Å), to enable direct comparison with the reference patterns. The crystalline

phases were identified, and the integrated peak intensities were determined using commercial software (JADE 2010, Material Data, Inc.).

5.2.4 Freeze-thaw

Freeze-thawing was carried out in a benchtop freeze-dryer (VirTis AdVantage, Gardiner, NY). Each formulation was filled (3 mL) in 10 mL glass vials (DWK Wheaton, IL). For unannealed samples, the vials were first cooled from 25°C to 5°C, held for 30 min, and further cooled to - 40°C and held for 30 minutes. The frozen samples were thawed back to 20°C with an isothermal hold step at 5°C for 30 minutes. Both cooling and thawing rates were 1°C/min. After thawing the vials swirled. The process of freeze-thawing was repeated 5 times. Similar protocol was used for annealed samples with an additional annealing (isothermal hold) step at -20°C for 2 hours.

5.3 Results and discussions

5.3.1 Mannitol-sucrose systems

Thermal characterization of different ratios of mannitol to sugar were performed using DSC. The solutions were cooled from RT to -40 ºC and then heated to RT at cooling and heating rates of either 10 or 5 ºC/min. However, only the final heating curves are shown (Figure 5.1 and Figure 5.3). At M:S ratios of 1:1, 1:2 and 1:4, there was no evidence of mannitol crystallization, both during cooling (not shown) and heating (Figure 5.1, panels A (10 °C/min) and C (5 °C/min)). At a M:S ratio of 2:1, an exotherm was observed during heating, attributable to mannitol crystallization (Figure 5.1 A and C). The DSC curve of this composition has been expanded in panels B and D. The system was characterized by two glass transition events, Tg" (lower temperature transition) at ~-32 ºC and Tg' at ~ -27

ºC and these seemed to be unaffected by the cooling rate. However, at the lower cooling rate of 5 ºC/min, there was an increase in the fraction of mannitol crystallizing from solution (enthalpy of exotherm at ~ 10 ºC; panels B and D).

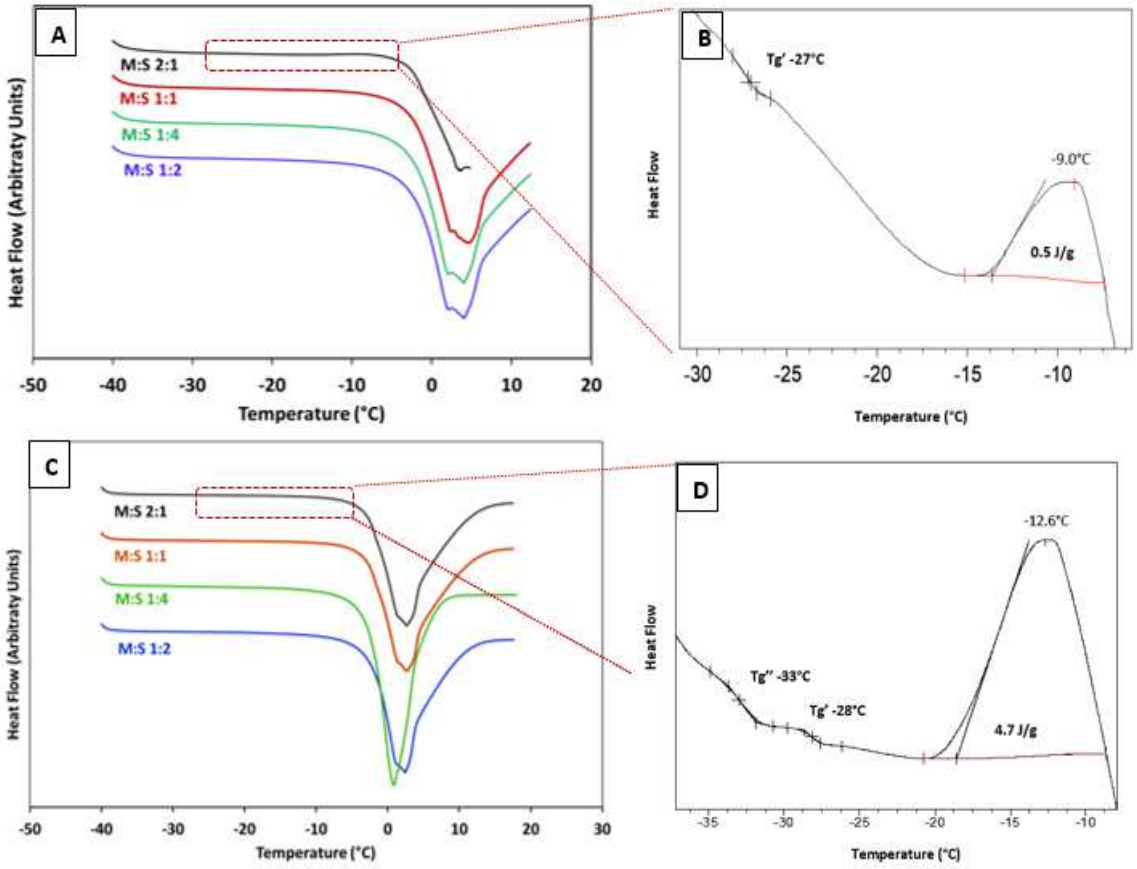

Figure 5.1 Overlaid DSC heating curves for four different mannitol-sucrose ratios (1:4, 1:2, 1:1 and 2:1) with a solute concentration of 5% w/v. Panel A. The solutions were initially cooled from room temperature to -40°C at 10°C/minute held for 5 minutes and heated to 15°C at 10°C/minute. Only the heating curves are shown. Panel B. Shows a magnified region with Tg' and crystallization exotherm for mannitol-sucrose 2:1 solution from panel A. Panel C. The solutions were initially cooled from room temperature to -40°C at 5°C/minute held for 5 minutes and heated to 15°C at 5°C/minute. Only the heating curves are shown. Panel D. Shows a magnified region with Tg' and crystallization exotherm for mannitol-sucrose 2:1 solution from panel C.

When the cooling rate was decreased to 0.5º C/min, there was evidence of mannitol crystallization during cooling (exotherm at ~-23 ºC; Figure 5.2A). The inset is an expanded view. When the solution was heated, again a crystallization exotherm was observed at ~ -

25 ºC. Thus, crystallization of mannitol was not complete during cooling. This amorphous fraction crystallized during heating, immediately above the Tg'

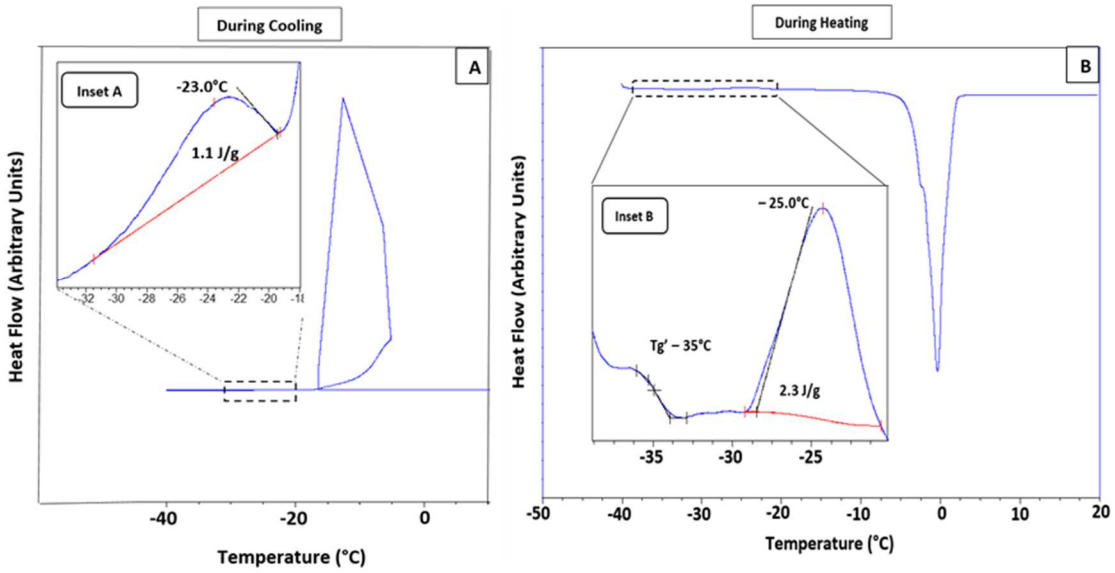

Figure 5.2 DSC heating curves for mannitol-sucrose 2:1 ratio with a solute concentration of 5% w/v. Panel A. DSC cooling curve from room temperature to -40°C. The cooling rate was 0.5°C/minute and sample was held at -40°C for 5 minutes. The cooling curve shows an initial exotherm for ice crystallization followed by an additional exotherm. The exotherm at -23°C was attributed to partial mannitol crystallization (inset A). Panel B. DSC heating curve from -40°C to 25°C. The heating rate was 0.5°C. A glass transition was observed at -35°C followed by a crystallization exotherm at -25.0°C (inset B).

5.3.2 Mannitol-trehalose systems

Qualitatively similar results were obtained in M:T systems with different ratios (Figure 5.3, panels A and C). Though this system also exhibited two glass transition events (Tg' and Tg"), the cooling rate influenced their values. However, this was not investigated further. The enthalpy of mannitol crystallization was much higher in presence of trehalose (Figure 5.3 B and D).

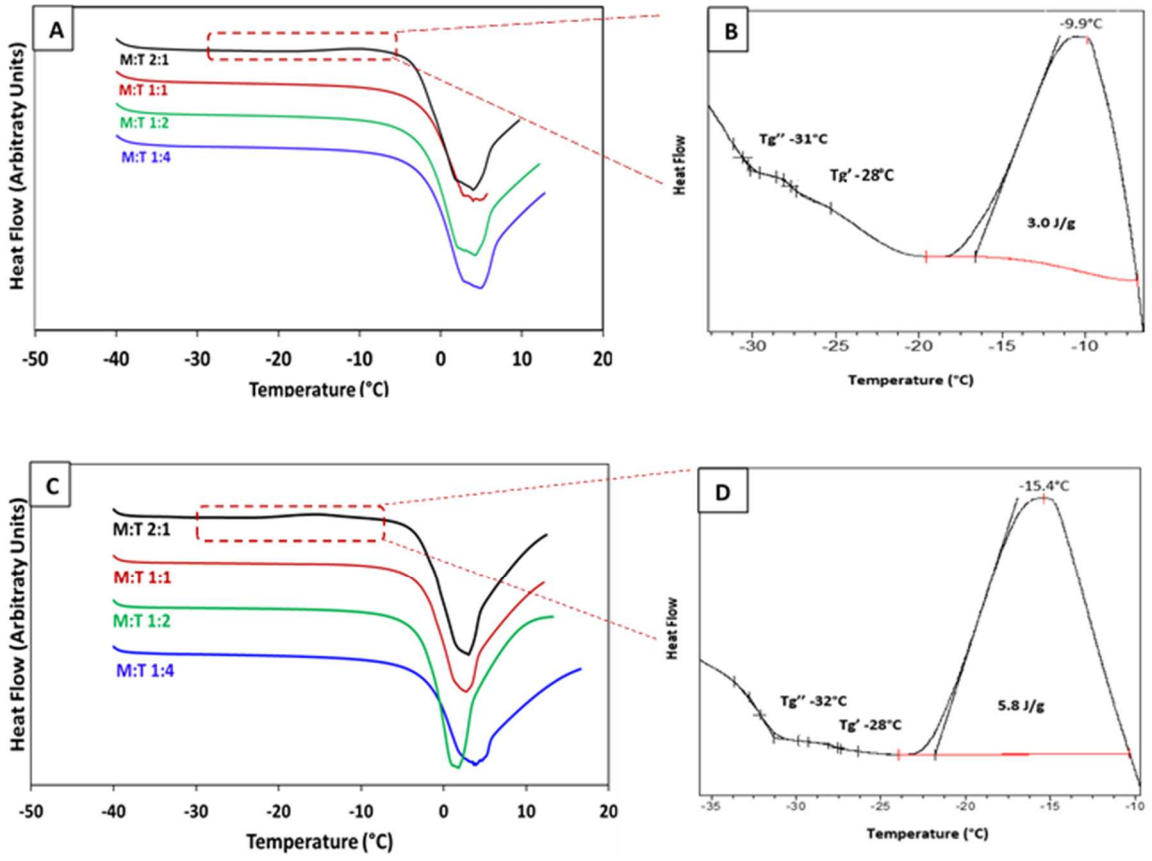

Figure 5.3 Overlaid DSC heating curves for four different mannitol-trehalose ratios (1:4, 1:2, 1:1 and 2:1) with a solute concentration of 5% w/v. Panel A. The solutions were initially cooled from room temperature to -40°C at 10°C/minute held for 5 minutes and heated to 15°C at 10°C/minute. Only the heating curves are shown. Panel B. Shows a magnified region with Tg' and crystallization exotherm for mannitol-trehalose 2:1 solution from panel A. Panel C. The solutions were initially cooled from room temperature to -40°C at 5°C/minute held for 5 minutes and heated to 15°C at 5°C/minute. Only the heating curves are shown. Panel D. Shows a magnified region with Tg' and crystallization exotherm for mannitol-trehalose 2:1 solution from panel C.

It is known that trehalose facilitates mannitol crystallization[130]. The influence of trehalose was further evident at a slower cooling rate of 0.5 ºC/min (data not shown). There was pronounced but incomplete crystallization of mannitol during cooling. However, the amorphous fraction crystallized during heating (Figure 5.4). Thus, the crystallization behavior of mannitol was similar in the presence of the two sugars, sucrose and trehalose.

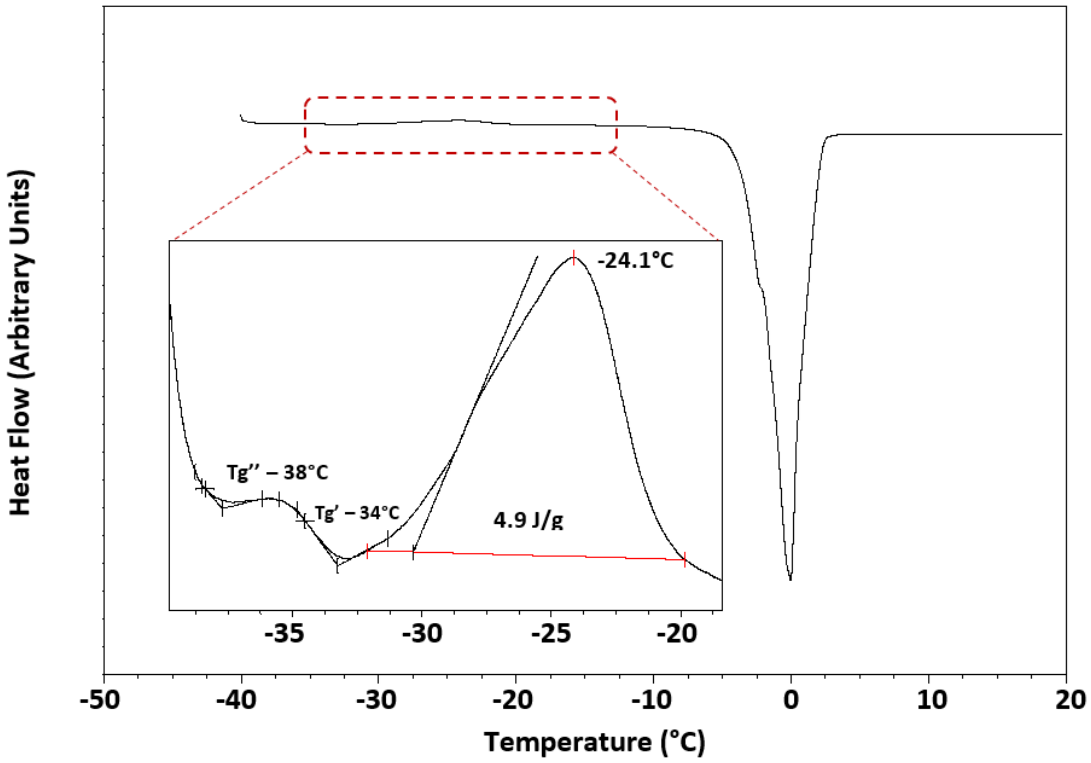

Figure 5.4 Mannitol-trehalose 2:1 composition. DSC heating curve from -40°C to 25°C at 0.5°C/min. The inset shows glass transition and crystallization exotherm from -40 to -20°C. The sample was cooled from room temperature to -40°C at 0.5°C/min (cooling curve not shown).

When the cooling rate was further decreased to 0.1 ºC/min, mannitol appeared to crystallize completely during cooling (Figure 5.12). An exotherm, attributable to mannitol crystallization, was not observed during heating and the system was characterized by a single glass transition event at ~ -32 ºC (Figure 5.5).

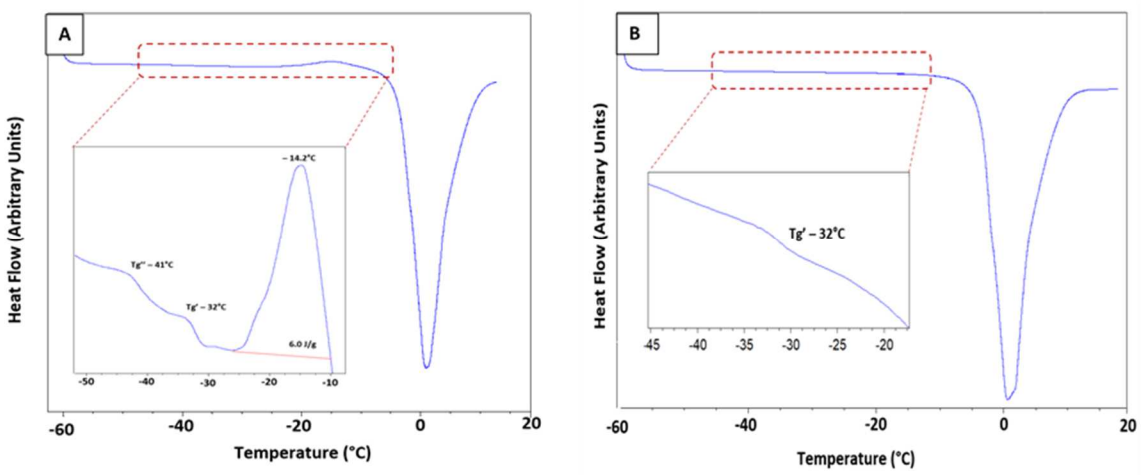

Figure 5.5 DSC heating curves for mannitol-trehalose 3:1 (A) sample was cooled to -20°C at 0.5°C/min held for 2 minutes and further cooled to -60°C at 5°C/min. The frozen sample was heated to 20°C at 5°C/min. Only the heating curve is shown in the figure. (B) sample was cooled to -20°C at 0.5°C/min held for 2 hours and further cooled to -60°C at 5°C/min. The frozen sample was heated to 20°C at 5°C/min. The heating curve in the figure shows the presence of only glass transition event.

To evaluate in greater detail the crystallization behavior of mannitol during cooling, the mannitol: trehalose ratio was increased (3:1). At a cooling rate of 0.1°C/min, ice crystallization occurred earlier (exotherm at ~ -5 °C) and was followed by a second crystallization exotherm at ~ -16 °C with an enthalpy of crystallization of ~9 J/g (Figure 5.13). Interestingly, when this sample was heated from -40 °C to 10 °C (at 0.1 °C/min), the Tg' as well as the mannitol crystallization exotherm were not seen (data not shown). This suggests that the crystallization exotherm post ice crystallization during cooling can be attributed to mannitol crystallization. The high enthalpy value (~9 J/g), coupled with the absence of crystallization exotherm during heating, suggests complete mannitol crystallization during cooling. The absence of glass transition during heating also supports this contention.

Synchrotron XRD experiments performed during cooling from room temperature to -45°C followed by heating the frozen solution back to room temperature at 1°C/min helped in further understanding of the mannitol-trehalose 3:1 (5% w/v) system. During cooling, ice peaks first appeared at ~ -9°C followed by appearance of mannitol hemihydrate peaks at ~ -18°C (Figure 5.6). Further cooling to - 45°C resulted in a slight increase in the hemihydrate and ice peak intensities. It was evident from the shape of the peaks that ice crystallization was substantially incomplete, indicating that a large fraction of the solute was in the freeze-concentrate along with unfrozen water. In addition, the heterogeneity of the freeze-concentrate was evident from the two glass transitions observed in the DSC. During heating, until ~ -23°C, the hemihydrate and ice peaks did not reveal any change in peak intensity. Further heating resulted in (i) increase in the hemihydrate as well as ice peak intensities, and (ii) transition of the hemihydrate to δ-form of mannitol prior to eutectic melting at ~ 0°C. A pronounced and sharp increase in mannitol peak intensities was observed around Tg'. Thus, the pronounced crystallization propensity of mannitol at T > Tg', observed earlier in the DSC (Figure 5.1 and Figure 5.3; panels B and D) was supported by the XRD results.

The propensity of an excipient to crystallize during thawing can have implications on protein stability. The effects would be exacerbated if a system undergoes multiple freeze-thaw cycling. Since proteins are stored frozen, often for prolonged time periods, freeze-thaw studies provide an avenue to understand the impact of long-term frozen storage. These results have some important practical implications. Desai et al showed in a glycine mAb formation, protein aggregation increased when the thawing rate was decreased [144]. They

attributed aggregation during thawing to the crystallization of glycine. The perturbations at the ice-liquid interface brought about by the crystallization of the unfrozen water associated with solute could be a major destabilizing factor. Thus, the existence of amorphous solute in the frozen state, which can then recrystallize during heating can be a source of protein instability. It is instructive to note that during slow thawing, it is not the solute crystallization per se, but the formation of these "new" ice interfaces (at T > Tg') that is the major destabilizing factor (Figure 5.7).

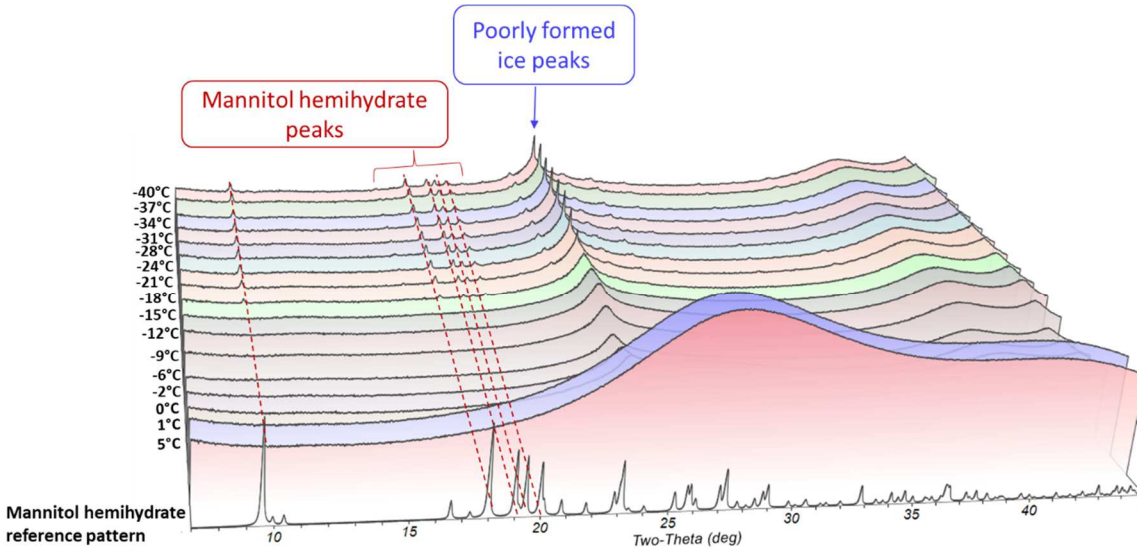

Figure 5.6 In situ synchrotron XRD patterns for mannitol-trehalose (3:1, 5% w/v) solution. Panel A shows overlays of XRD patterns during cooling from 5°C to -40°C; the solution was frozen from room temperature to -45°C at 1°C/min and held at -45°C for 10 minutes followed by heating the samples back to room temperature at 1°C/min. Mannitol hemihydrate reference pattern is shown at the bottom of the overlays.

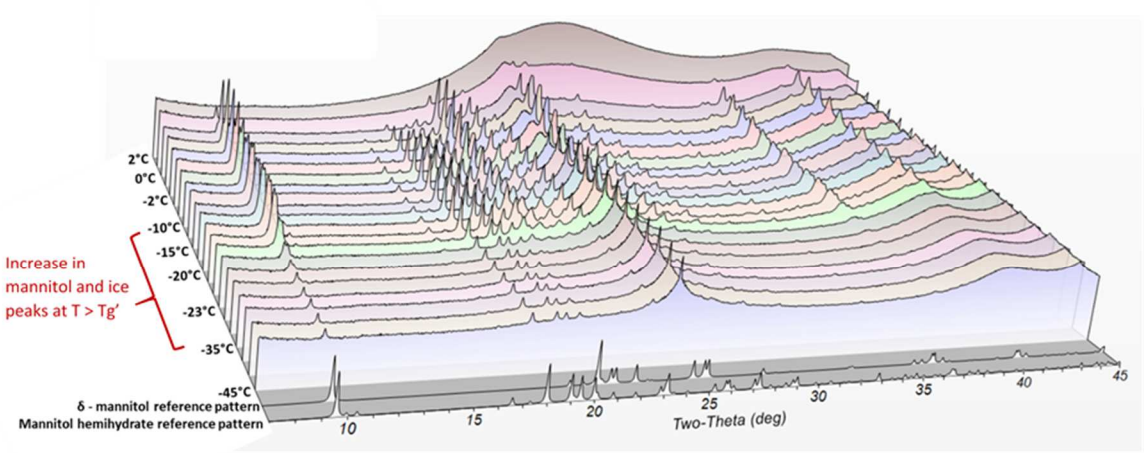

Figure 5.7 In situ synchrotron XRD patterns for mannitol-trehalose (3:1, 5% w/v) solution. Panel B shows overlays of XRD patterns during heating from -45°C to 2°C at 1°C/min; mannitol hemihydrate and δ-mannitol reference patterns are shown at the bottom of the overlays.

5.3.3 Mannitol-trehalose (3:1) systems – effect of isothermal hold

The next objective was to determine the effect of holding at -20 °C for different time periods on the phase behavior of excipient mixtures. Mannitol and trehalose individually are known to exhibit two characteristic glass transition temperatures. The glass transition temperatures of mannitol (5% w/w) were ~ -32 (Tg'') and ~ -25°C (Tg') and of trehalose were ~ -45°C (Tg'') and ~ -31°C (Tg') [145]. The Tg'" value of -31°C for the mannitol-trehalose (3:1) is close to the Tg'' values of mannitol (-32°C). However, the Tg' value (-32°C) of the mixture was closer to the Tg' of trehalose (Figure 5.8). The two glass transitions likely reflect the existence of two slightly different compositions in the freeze concentrate. The composition with the lower glass transition (Tg'') is expected to contain a higher amount of unfrozen water and this can be thought of as a "water-rich phase". The composition with the higher glass transition (Tg') is likely the maximally freeze-concentrated phase. The ΔCp value can an approximate measure of the "amount" of amorphous phase. The ΔCp values associated with Tg'' and Tg' were 0.19 and 0.09 J/g°C respectively (Table 5.1). Based on this, the composition characterized by Tg" would constitute the larger amorphous fraction.

Table 5.1 Mannitol-trehalose (3:1) – DSC data for isothermal hold (-20°C) experiments

Formulation	Annealing time at -20°C during cooling	Tg"		Tg'	Tc		ΔH (J/g) at Tm (Ice and mannitol-ice eutectic melting)
		Temperature (°C)	ΔCp (J/g°C)	Temper--ature (°C)	Temper--ature (°C)	ΔH (J/g)	
Mannitol:trehalose 3:1	No annealing	-41.5 ± 0.1	0.19 ± 0.0	-32 ± 0.1	-21	6.28 ± 0.2	323.0 ± 2.0
	2			-31 ± 0.2			336.7 ± 2.0
	4			-32 ± 0.0			339 ± 2.0
	8			-32 ± 0.0			336.1 ± 3.2
	16			-31 ± 0.0			333.0 ± 0.4

The next objective was to determine the effect of holding at -20 °C for different time periods on the phase behavior of excipient mixtures. In addition to the slow cooling rate, the effect of annealing during cooling, on the crystallization behavior of mannitol was investigated. The solutions were cooled to -20° C at 0.5 °C/min and held for up to 16 hours. They were then further cooled to -60°C and then heated back to RT. In the absence of isothermal hold, Tg" and Tg' were observed at ~ -41 and -32 ºC respectively (Figure 5.8A). When held for ≥ 2 hours at -20°C, the Tg" disappeared while the Tg' remained unaffected (Figure 5.8B). Thus, holding at -20 ºC even for only 2 hours seems to cause complete crystallization of the composition with the higher water content. There was also a pronounced reduction in ΔCp associated with Tg' suggesting substantial crystallization of this composition (Figure 5.8B). The holding time was progressively increased up to 16 hours. The Tg' remained unaffected confirming that this was the maximally freeze-concentrated system of constant composition (confirmed in the synchrotron XRD studies in the next section). There appeared to be a small decrease in the magnitude of ΔCp at the

longer annealing times. However, these results should be viewed with caution considering the low ΔCp values. Finally, the enthalpy of fusion (mannitol-ice eutectic + ice melting) also provided evidence of amorphous phase crystallization due to the isothermal hold at -20 ºC. Holding for 2 hours, caused an appreciable increase in the enthalpy value (Table 5.1). This could be a consequence of the crystallization of mannitol and the associated unfrozen water. Holding for a longer time did not have any noticeable effect on the observed enthalpy value. This result in not surprising in light of the small change in ΔCp (Tg') at holding times > 2 hours (Table 5.1). Annealing the samples at -37°C - a temperature above Tg'' (- 41°C) but below Tg' (-32°C) for 2 hours, resulted in disappearance of the Tg". On reheating, a single glass transition was observed at -34°C followed by an exotherm attributable to mannitol crystallization. Thus, when annealed at a temperature below Tg', mannitol was retained amorphous (Figure 5.14).

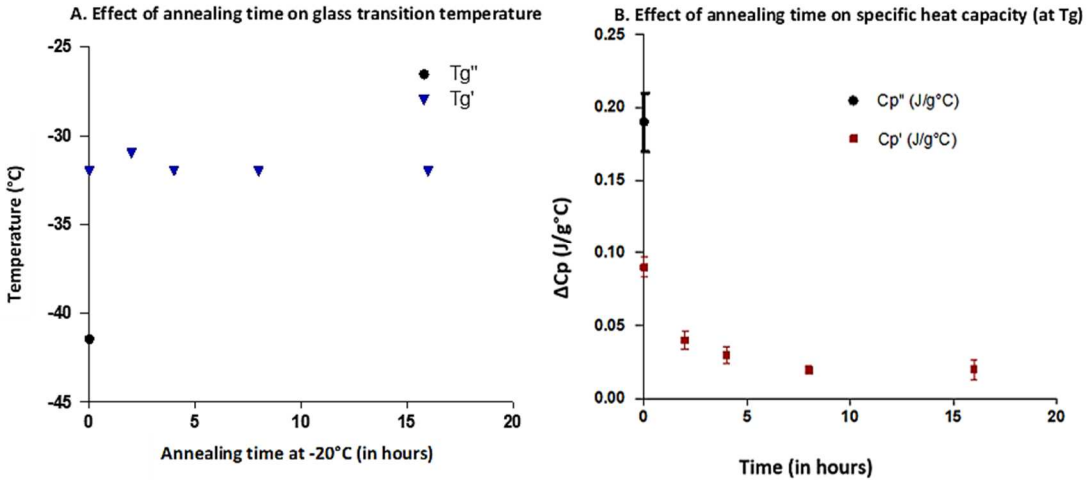

Figure 5.8 Graphical representation for mannitol:trehalose 3:1 (A) Change in glass transition temperature as a function of annealing time at -20°C (B) Change in heat capacity associated with glass transition temperature as a function of annealing time at -20°C.

The effect of annealing on the crystallization behavior of mannitol and ice could be discerned from synchrotron XRD experiments performed during cooling (Figure 5.9). Ice crystallization was the first event observed (~ -10°C) followed by the appearance of β-mannitol peaks at -12°C. During the isothermal hold at -12°C, there was a pronounced increase in the intensities of both mannitol and ice peaks. This was in line with the earlier report from Mehta *et al* that MHH formation was completely prevented when crystallization occurred between -10 and -15°C [84]. Once β-mannitol and ice peaks formed during annealing at -12°C, the peak intensities increased, both during annealing and further cooling until -15°C (Figure 5.10). On further cooling to -40°C, there was negligible change in the peak intensities.

On heating the frozen system from -45°C to -2°C, there was no increase in ice and mannitol peak intensities up to ~ - 5°C. There was then a progressive decrease in the peak intensities until they disappeared at ~ 1°C (Figure 5.10). Thus, the behavior of the annealed system during heating was very different from that of the unannealed solutions (compared Figure 5.7 and Figure 5.10).

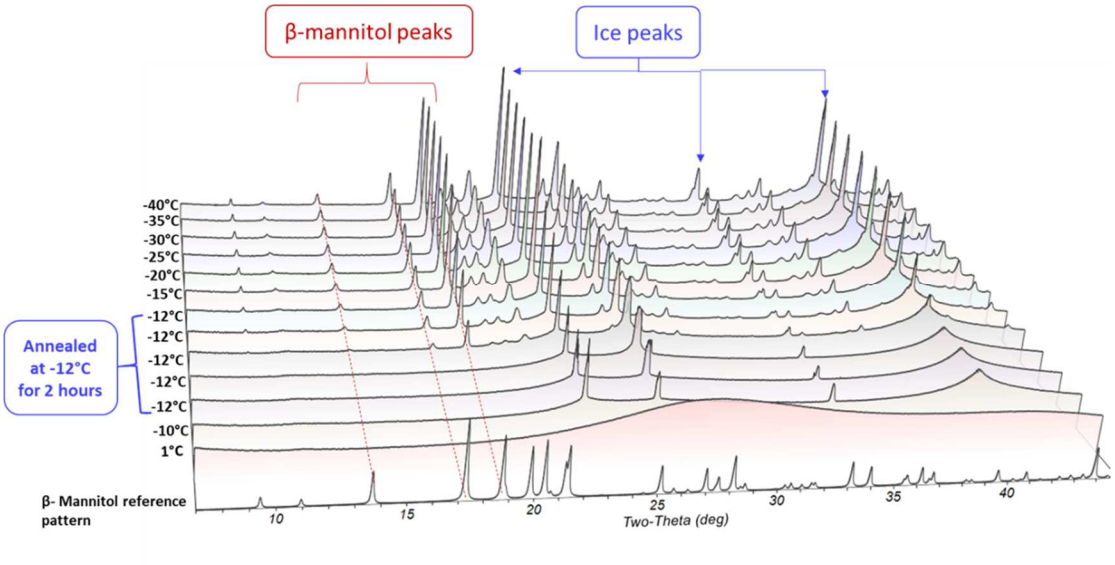

Figure 5.9 In situ synchrotron XRD patterns for mannitol-trehalose (3:1, 5% w/v) solution during cooling. Panel A shows overlays of XRD patterns during cooling from 5°C to -40°C; β-mannitol reference pattern is shown at the bottom of the overlays. The solution was frozen from room temperature to -12°C, held for 2 hours further cooled to -45°C at 1°C/min and held at -45°C for 10 minutes.

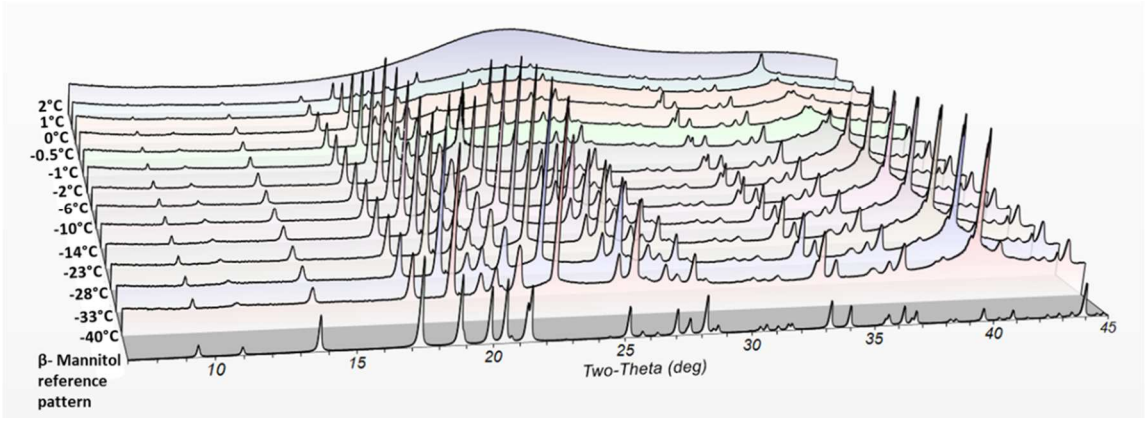

Figure 5.10 Insitu synchrotron XRD patterns for mannitol-trehalose (3:1, 5% w/v) solution during heating. Panel B shows overlays of XRD patterns during heating from -45°C to 2°C. The frozen solution was heated from -45°C back to room temperature at 1°C/min. β-mannitol reference patterns are shown at the bottom of the overlays.

The XRD results revealed that annealing during cooling enabled us to: (i) promote selective crystallization of the anhydrous form of mannitol, and (ii) maximize ice crystallization during cooling and thereby minimize the residual unfrozen water crystallization during heating (post Tg'). However, there is one potential challenge. It is well known that mannitol crystallization can promote trehalose crystallization [146]. The crystallization of trehalose would be highly undesirable since it could compromise its lyoprotectant function. To minimize the risk of trehalose crystallization, its concentration was low (1.25%). Moreover, despite the high sensitivity of the technique, there was no evidence of trehalose crystallization (Figure 5.7 and Figure 5.10). In frozen aqueous systems, trehalose crystallizes as a dihydrate with characteristic peaks at 8.8 and 12.6°2θ [147]. These peaks were absent in the frozen solutions (Figure 5.10). DSC provided additional evidence of the potential for trehalose to be retained in the amorphous state. Even when the annealing time was increased up to 24 hours, the Tg' was invariant (- 31°C) suggesting the retention of a freeze concentrate of constant composition.

Thus, with the judicious selection of the concentrations of trehalose and mannitol, while substantial crystallization of mannitol can be accomplished the trehalose is retained amorphous. Thus, the risk of trehalose-crystallization induced loss in cryoprotection would be minimized while causing substantial (if not complete) crystallization of mannitol in the desired anhydrous state.

Thus, annealing during cooling enabled us to: (i) promote the selective crystallization of the anhydrous form of mannitol, and (ii) obtain a single maximally freeze-concentrated phase of constant composition (Tg').

5.3.4 Mannitol-sucrose (3:1) systems – effect of isothermal hold

The behavior of these systems was substantially similar to that of mannitol-trehalose (3:1). While the DSC curves are not shown, the results are summarized in Table 5.2 The Tg" and the Tg' values were virtually identical for the unannealed mannitol-trehalose and mannitol-sucrose systems (Table 5.1 and Table 5.2). The one notable difference was the ΔCp at Tg" which was much less (0.08 J/g°C) for the sucrose containing systems. When this "population" was removed by annealing, presumably by crystallization of mannitol and the associated unfrozen water, the attendant increase in the enthalpy of fusion (overlapping of mannitol-ice eutectic and ice melting) was small (from 328 to 333 J/g; Table 5.2).

Table 5.2 Mannitol-sucrose (3:1) – DSC data for isothermal hold (-20°C) experiments

Formulation	Annealing time at -20°C during cooling	Tg"		Tg'	Tc		ΔH (J/g) at Tm (Ice and mannitol-ice eutectic melting)
		Temper--ature (°C)	ΔCp (J/g°C)	Temperature (°C)	Temperature (°C)	ΔH (J/g)	
Mannitol:sucrose 3:1	No annealing	-42 ± 0.5	0.1 ± 0.0	-33.0 ± 0.0	-15 ± 0.2	7.1 ± 0.3	328.1 ± 2.6
	2			-34.5 ± 0.7			332.5 ± 0.7
	8			-33.7 ± 1.1			334.5 ± 0.8
	16			-34.5 ± 0.7			332.8 ± 0.6

5.3.5 HSA aggregation: Effect of processing (annealed versus unannealed) and composition

Using HSA (1 mg/mL) as a model protein, in selected mannitol-sucrose and mannitol-trehalose buffered solutions, we evaluated the impact of processing on protein aggregation. Selected compositions were also subjected to DSC, at a cooling rate of 1°C/ min, with and without an isothermal hold step. HSA, at a concentration of 1 mg/mL, had no significant impact on mannitol phase behavior (data not shown). Buffered protein solutions in mannitol, sucrose, or trehalose alone and in mannitol-sugar (1:1 and 3:1) mixtures were subjected to multiple freezing and thawing cycles (5 F/T). The 5 freeze-thaw cycles were conducted at a ramp rate of 1°C/min. One set of samples were frozen with an annealing step at -20°C for 2 hours during cooling, while the other set did not include annealing. The protein stability before and after freezing and thawing was evaluated by SE-HPLC.

We will first look at the effect of freeze-thaw stress on unannealed HSA formulations that contained either mannitol, sucrose, or trehalose individually. All the formulations that were subjected to 5 F/T cycles showed an increase in high molecular weight species (HMWS) compared to their respective controls (Figure 5.11). This was not surprising since some protein aggregation is expected due to the freeze-thaw stress. The most pronounced increases in %HMWS (≥ 1.5.%) were observed in the freeze-thawed formulations containing mannitol or trehalose. In the former case, this is attributed to phase separation brought about by crystallization of mannitol, and the consequent lack of cryoprotection. It is important to note that there was pronounced mannitol crystallization during thawing (Figure 5.7) which explains aggregation in mannitol alone formulations. However, HSA

aggregation in the presence of trehalose, which remained amorphous during freezing, raises concern with respect to its stabilization potential.

There was a favorable effect of annealing in the presence of both mannitol and sucrose. In case of mannitol, there are two possible stabilization mechanisms. Substantial crystallization of mannitol during annealing, resulting in a homogenous freeze-concentrate may have facilitated protein stabilization. Secondly, there was no evidence of mannitol crystallization during thawing (Figure 5.10). As a result, there was no generation of "new" ice interfaces during thawing – hence reduced protein aggregation. While the effect of annealing was less pronounced in the presence of sucrose, the process resulted in a single Tg' again indicating a homogenous freeze-concentrate. While annealing also resulted in a single Tg' in the trehalose system, there was no reduction in % HMWS compared to the unannealed formulation.

Next, the effect of mannitol-sucrose combination (1:1) was compared with the individual solutes. The %HMWS after 5 freeze-thaw cycles was much lower than with either solute. Annealing had a pronounced stabilizing effect, again much more than the individual solutes. This composition appears to be better than all the other systems investigated. Similarly in the mannitol-trehalose combination (1:1) performed better than the individual solutes and annealing resulted in pronounced stabilization.

Increasing the mannitol concentration, either with sucrose or with trehalose (3:1) did not have an evident impact on HSA aggregation. The sucrose containing formulations continued to be superior. The 3:1 mannitol-sugar combinations were better than the two individual solutes when they were separately used. However, annealing did not appear to

have any additional stabilizing effect. However, this result is not surprising. Since mannitol is present at a much higher concentration than the sugar (3:1), it crystallized readily during cooling (Table 5.1). Thus, the annealing step is not expected to bring about additional mannitol crystallization and the consequent stabilization.

As we compare the two sugars, over a range of compositions as well as the effect of the annealing step, the superiority of sucrose is consistently evident. The underlying mechanism of cryoprotection was outside the scope of this work. Interestingly, the mannitol-sugar combination with annealing performed better or equivalent to the sugar alone formulations in terms of protein stabilization. Although limited to a single protein (HSA), the most pronounced stabilization effect following annealing was observed at a 1:1 ratio. This supports our hypothesis that inclusion of mannitol along with sugar and causing complete mannitol crystallization during freezing can generate a homogeneous matrix with the potential to improve protein stability.

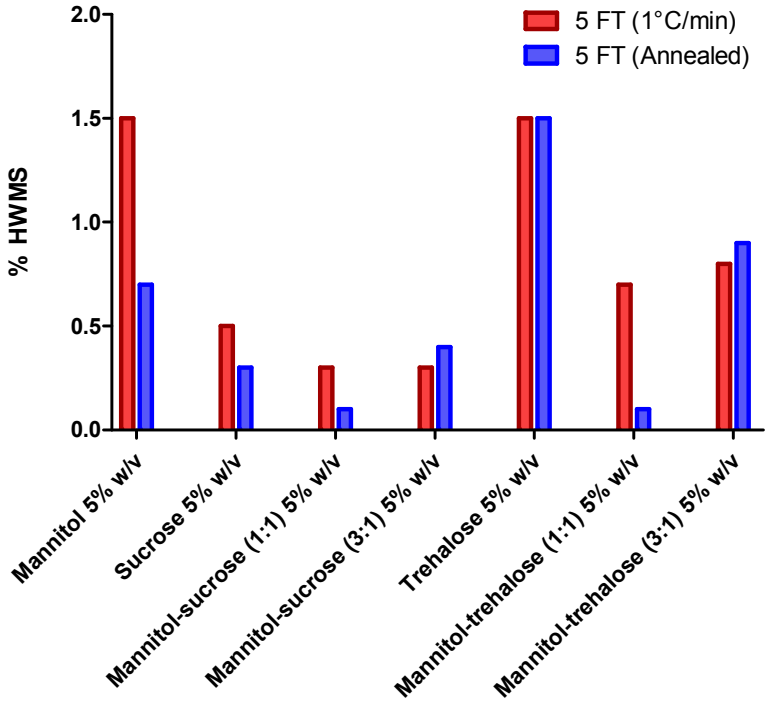

Figure 5.11 Size exclusion chromatography results for 1 mg/mL HSA with (i) 5% w/w Mannitol (ii) 5% w/w Sucrose (iii) 5% w/w mannitol-sucrose 1:1 (iv) 5% w/w mannitol-sucrose 3:1 (v) 5% w/w Trehalose (vi) 5% w/w mannitol-trehalose 1:1 and (vii) 5% w/w mannitol-sucrose 3:1. One set of formulations were cooled from room temperature to -45°C and held for 30 minutes at -45°C and reheated back to room temperature at 1°C/min, these formulations were labelled as 'unannealed'. Another set of samples were cooled to -20°C held for 2 hours and further cooled to -45°C and reheated back to room temperature at 1°C/min, these formulations were labelled as 'annealed'.

5.4 Conclusion

Freezing and thawing are important and critical unit operations in biotherapeutic manufacturing [23]. However, considering the limitations imposed in actual manufacturing setting, it can be challenging to implement controlled freezing and thawing rates [23, 148]. A lack of control in these steps, and specifically, fast freezing and slow thawing appeared to facilitate protein aggregation [144, 149]. Our goal was to minimize the detrimental kinetic effects of uncontrolled freeze-thaw cycling, using appropriate excipients and an annealing step. The addition of mannitol and facilitating its crystallization through annealing enabled

us to obtain a homogenous freeze-concentrate with a single glass transition (Tg'). Thus, annealing during cooling enabled us: (i) promote the selective crystallization of the anhydrous form of mannitol, and (ii) obtain a single maximally freeze-concentrated phase of constant composition (Tg').

Including an annealing step during freezing can be a practical approach to maximize excipient, as well as associated unfrozen water crystallization, early in the freezing process. This approach will minimize, if not eliminate, the need for precise control of the freezing and thawing rates. This protocol can also be applied for bulk drug substance storage, wherein the storage temperature < Tg'.

5.5 Supplementary information

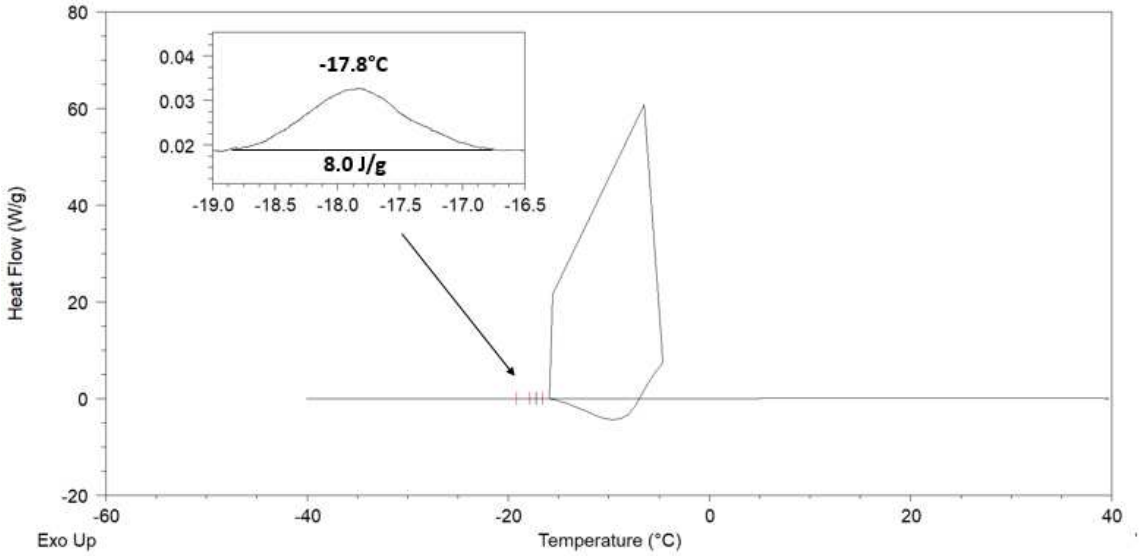

Figure 5.12 Mannitol-trehalose 2:1 composition. DSC cooling curve from 25°C to -40°C at 0.1°C/min shows ice crystallization exotherm at -4.5°C followed by mannitol crystallization exotherm at ~ -17°C. The inset highlights the exotherm that was observed during cooling.

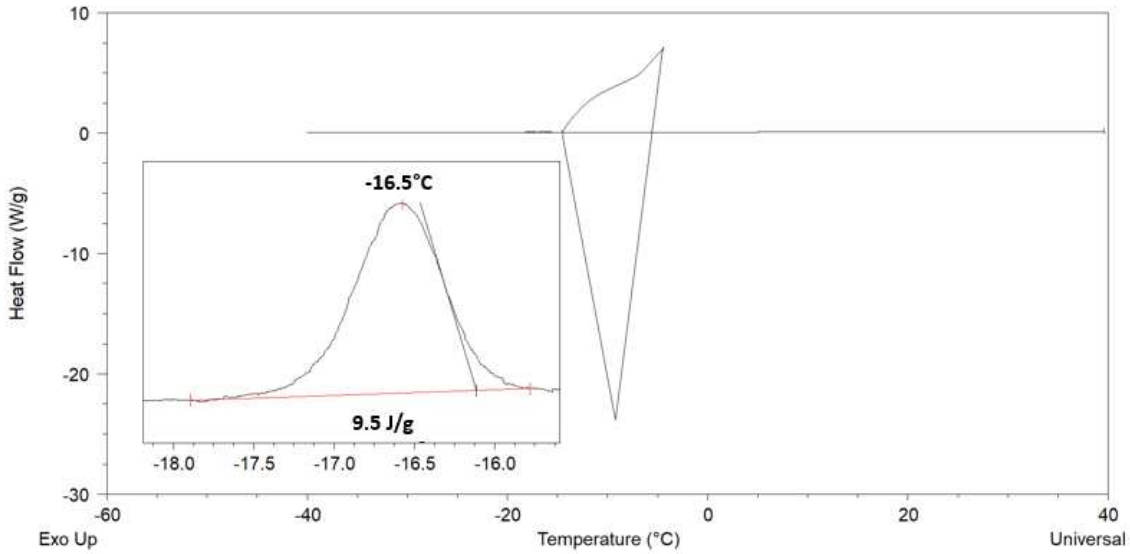

Figure 5.13 Mannitol-trehalose 3:1 composition. DSC cooling curve from 25°C to -40°C at 0.1°C/min shows ice crystallization exotherm at -4.5°C followed by mannitol crystallization exotherm at ~ -17°C. The inset highlights the exotherm that was observed during cooling.

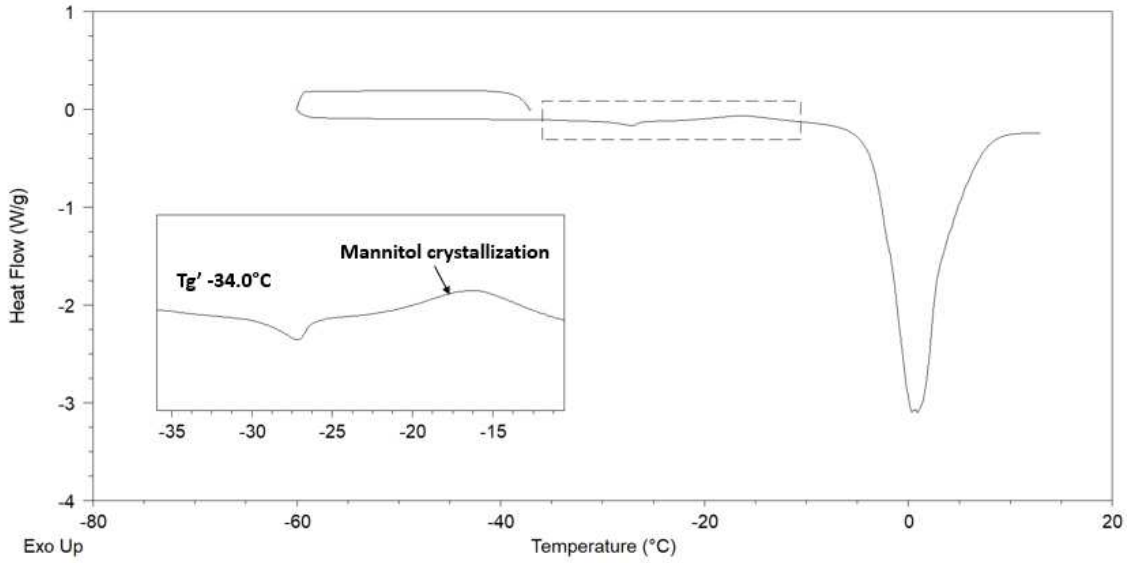

Figure 5.14 Mannitol-trehalose 3:1 composition. Sample was cooled to -60°C at 5°C/min and held for 5 minutes. The frozen solution was then heated to -37°C at 5°C and held for 2 hours. The annealed sample was cooled back to -60°C at 10°C/min and reheated to 15°C at 5°C/min. Only the final heating curve is shown.

Chapter 6 Summary

The overall goal of this thesis was to understand the role of excipient phase transitions in developing stable protein formulations. The formulation composition as well as processing parameters including but not limited to freeze-thawing, annealing, freeze-drying are inter-related and play a critical role in determining the fate of the drug product. The fundamental understanding of the mechanism of stabilization as well as protein characterization requires a multidisciplinary approach. The analytical techniques used for investigating excipient phase behavior were X-ray diffractometry (synchrotron as laboratory sources), differential scanning calorimetry (DSC), moisture analysis (moisture sorption analyzer, headspace moisture content and water content in the lyophile). Whereas for protein characterization during freezing, thawing and in the dried state using neutron scattering, dynamic light scattering, and size exclusion chromatography were utilized. The use of multiple complementary techniques enabled holistic understanding of the impact of processing conditions and accompanied phase behavior of solutes during freezing and freeze-drying, on protein stability. The summary of individual chapters is mentioned below.

Chapter 2

By combining SANS and DLS, comprehensive characterization of protein aggregation behavior was possible which could not have been accomplished with the individual techniques. The effect of crystallizing versus non-crystallizing buffer salt on lactate dehydrogenase (LDH) was evaluated. The initial LDH concentration was a key factor which resulted in reversible aggregation. In other words, LDH showed self-stabilization at

higher concentrations. Reversible LDH aggregation was observed at lower buffer concentration irrespective of phosphate or histidine buffer (scheme 6.1). These observations highlighted the importance of investigating the effects of buffer on protein stability in the frozen state to mechanistically understand protein aggregation behavior.

Based on our results, LDH at a high concentration (1000 µg/mL; buffer concentration 10 mM), had a pronounced self-stabilizing effect and did not aggregate after five freeze–thaw cycles. At lower LDH concentrations (10 and 100 µg/mL), only with the selection of an appropriate buffer, irreversible aggregation could be avoided. While SANS provided qualitative information with respect to protein conformation, the insights from DLS were quantitative with respect to the particle size of the aggregates. SANS is the only technique which can characterize the protein both in the frozen and thawed states.

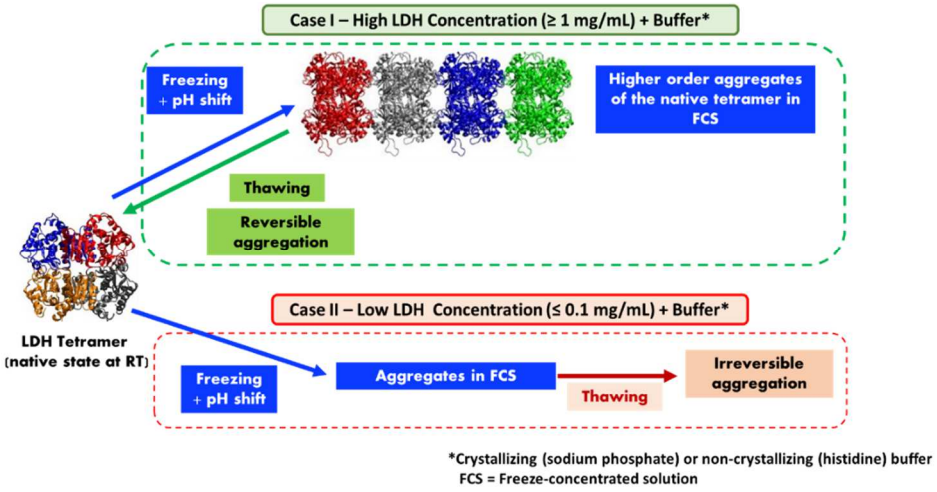

Figure 6.1 Schematic representation of LDH aggregation behavior in presence of crystallizing and non-crystallizing buffer salts during freeze-thawing

Chapter 3 and 4

Our first objective was to determine the influence of water vapor pressure on the kinetics of MHH dehydration and the implications on the physical stability of sucrose. Therefore, the lyophiles were exposed to a range of relative humidities (RH) and the kinetics of MHH dehydration and sucrose crystallization were monitored by X-ray diffractometry. A second set of vials (rubber stoppers fitted with humidity/temperature sensor) were stored at 40 °C, the headspace RH was continually recorded, and water content was determined by Karl Fischer titrimetry. The dehydration rate of MHH increased as a function of water vapor pressure, an anomalous behavior explained by the Smith–Topley effect. An increase in headspace RH and decrease in lyophile water content in sealed vials attributed to MHH dehydration, eventually triggered sucrose crystallization. There was also evidence of moisture transfer from the lyophile to the rubber stoppers. The conditions at which MHH dehydrates in mannitol-sucrose lyophiles were identified. However, does MHH dehydrate in presence of proteins resulting in moisture induced protein aggregation? This was the focus of chapter 4. Proteins in a concentration dependent manner are known to inhibit solute crystallization. In addition, there is a presumption in the freeze-drying community with respect to MHH formation in the lyophile and its consequences during storage. However, the lack of experimental evidence of the dehydration induced reactions on protein stability has not been well studied. Based on our results, MHH dehydration and sucrose crystallization were observed only in cases where the relative humidity was ≥ 55% RH. A relative humidity of ≤ 33% RH prevented MHH dehydration while retaining sucrose amorphous. No protein aggregation was observed irrespective of presence of MHH or its

dehydration. Equipped with this knowledge, appropriate mitigation strategies can be formulated to prevent MHH dehydration during storage. Although we used only albumins (HSA and BSA) in this study, we believe that the observations from this study will encourage formulation scientists to use mannitol in lyophilized protein formulation without the risk of its dehydration on storage.

Chapter 5

Freeze-thawing is one of the most common unit operations in manufacturing therapeutic proteins. Freezing is encountered routinely as a part of frozen storage for most protein drug substances. However, the freezing process (rate of cooling, storage temperature etc.) and the solution composition can impact protein stability. Sugars (sucrose or trehalose) are one of the most common excipients used as a stabilizer in such formulations. The potential for phase separation (heterogeneity), usually indicated by the presence of two glass transition temperatures in the cryo-concentrated state, can result in a lack of cryoprotection and destabilization of protein.

The addition of mannitol and facilitating its crystallization through annealing enabled us to obtain a homogenous freeze-concentrate with a single glass transition (Tg'). Thus, annealing during cooling at temperatures enabled us to promote the selective crystallization of the anhydrous form of mannitol and (ii) obtain a single maximally freeze-concentrated phase of constant composition (Tg'). Including an annealing step during freezing can be a practical approach to maximize excipient, as well as associated unfrozen water crystallization, early in the freezing process. This approach will minimize, if not eliminate,

the need for precise control of the freezing and thawing rates. This protocol can also be applied for bulk drug substance storage, wherein the storage temperature < Tg'.

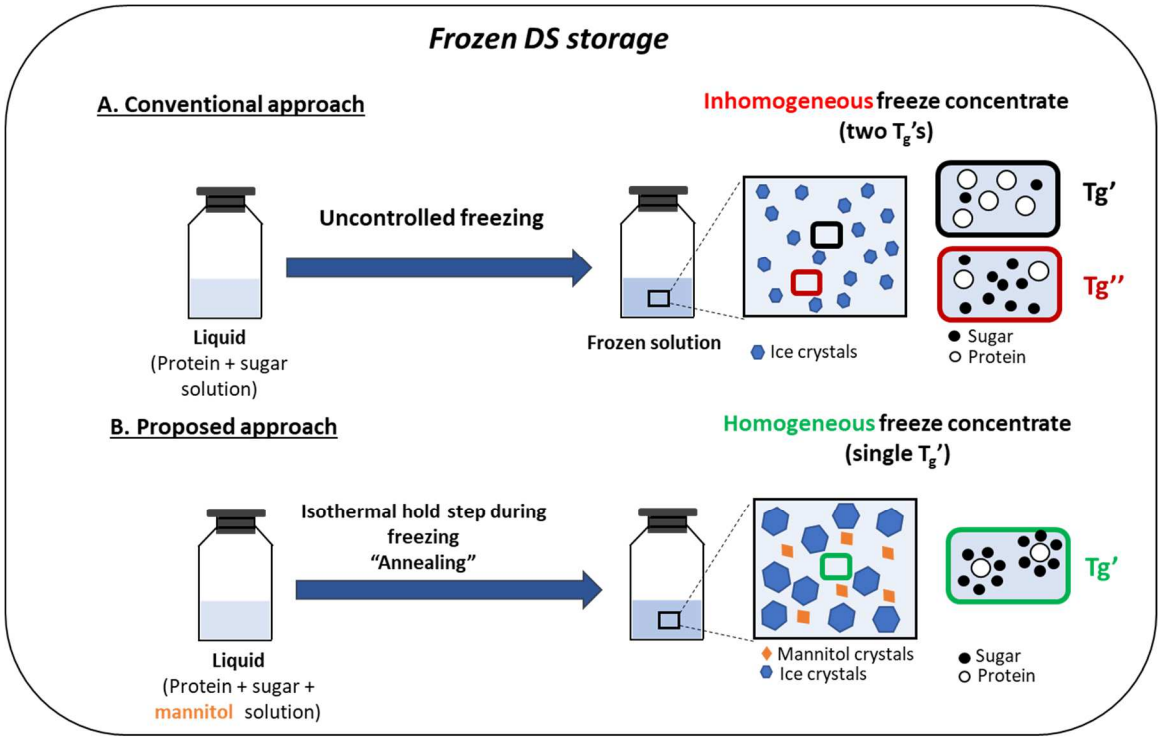

Figure 6.2 Schematic representation of the use of mannitol and an isothermal hold step to generate homogeneous freeze-concentrate represented by a single glass transition (Tg').

Chapter 7 Future work

With an improved understanding of the stability behavior of proteins in a multi-component DP, protein formulation development has evolved, from a predominantly trial-and-error process to a more systematic science-driven process. Nonetheless, several challenges still exist in the formulation development process. This thesis was designed to understand the role of excipient phase behavior on protein stability during various stages of processing including freezing, thawing, freeze-drying as well as post-processing during storage. Investigating the complex interplay of excipients, proteins, processing as well as packaging components can help understand the nuances of drug product development. A comprehensive characterization with a biophysical as well as material science perspective will help in optimizing the design space for developing and manufacturing robust protein formulations. As is evident from the discussion above, the stresses experienced by proteins during freezing, freeze-drying and mechanisms of excipient-induced protein stabilization are not completely understood. Multiple mechanisms have been proposed, but their validity seems to be specific to the protein and to the process conditions. A broad generalization may not be appropriate. However, recent efforts in the field of molecular dynamics and simulations look promising in identifying excipient ratios as well as in determining the effect of stresses during freezing on protein stability.

There is a growing interest in studying previously unidentified stresses experienced by protein during freezing, such as air bubbles formed on the ice crystallization front, local pressure, and mechanical stresses due to volume expansion during ice formation. It is postulated that a quasi-liquid layer (QLL), i.e., a thin film of liquid water formed on ice

crystals, plays an important role in protein stability. The physical microenvironment of a protein confined within this layer may be substantially different from that in the bulk. The freeze-induced destabilization might be attributed to preferred partitioning of proteins into the QLL and hence inability of stabilizer to provide cryoprotection. Further research in this area can provide mechanistic insights into properties and functional relevance of this layer and to help identify mitigation strategies to overcome freezing-associated stresses. Understanding the role of interfaces and using surfactants to prevent interface-induced protein instability will be of immense interest to advance the research further.

In Chapter 2, it was shown that during one freeze-thaw cycle, LDH aggregation in presence of sodium phosphate and histidine was reversible even in the absence of a stabilizer (sugar or surfactant). However, irrespective of the buffer used, following multiple freeze-thaw cycles, pronounced aggregation behavior was observed if the protein concentration was low. We postulated that in addition to pH shift, the ice interfaces and their surface area can also impact LDH conformation. It is well known that cooling rate has a direct impact on ice crystal surface area. A faster cooling rate results in a higher degree of supercooling and hence multiple small ice crystals with higher surface area whereas a slower cooling rate leads to larger ice crystals with a lower surface area. Thus, the surface area of ice and the magnitude of interfacial stress on the protein seem to be directly proportional to the cooling rate. In many freeze-thaw unit operations, the ramp rates can be uncontrolled. In case of freezing, for example, placing a 1 or 10 L bottle in -80°C freezer, the cooling rate that the formulation experiences can range from (10 to 0.1°C/min). Using SANS, complementary analytical techniques, and modeling approaches, the aggregation behavior of proteins due

to exposure to interfaces during freezing can be investigated further. Additionally, the use of surfactants, their concentration (polysorbates versus other surfactants) and mechanisms to prevent interfacial denaturation will help develop deeper insights in rational selection of surfactants for individual proteins.

In Chapters 3 and 4, we have identified the conditions under which MHH can be retained during storage. The work was done using bovine and human serum albumin as model proteins. However, it would be interesting to investigate if these observations can be extrapolated to other proteins as well. Further research with respect to varying the compositions as well as evaluating the stability of different proteins will be critical in understanding the kinetic stability of MHH. The presumed consequences of MHH on DP stability limits mannitol's widespread use as a bulking agent. Information on conditions of its formation and dehydration will provide guidance on use of appropriate process parameters as well as storage conditions. There have been attempts to generate mannitol-water phase diagram. However, this has been complicated by the formation of the unstable mannitol phases – MHH, as well as anhydrous forms. This behavior will be further complicated by addition of other solutes. Interestingly, the formation of MHH in known to be a sub-ambient phenomenon. MHH can only form from solutions during the freezing stage. Approaches such as stepwise cooling can enable the modulation of the physical form of mannitol crystallizing from solution. Controlled ice nucleation can enable the crystallization of anhydrous mannitol, i.e., prevent MHH formation. However, these approaches should be investigated on a case-by-case basis and will vary based on protein,

stabilizer concentration as well as processing parameters. More research will help in further understanding the interplay of various formulation and process parameters.

Finally, the storage of frozen drug substance is an important and commonly used approach for many therapeutic proteins. Although freeze-thaw has been successfully used in many cases, several articles report instability brought about by freezing and thawing stress. The effect of storage temperatures and time, freezing rates, excipient and protein concentrations needs further investigation for optimizing DS stability. Frozen DS, stored at higher storage temperatures (-20°C), possess adequate molecular mobility to induce changes in excipient phase behavior, eventually compromising stability. Stability testing for frozen DS should be carried out in real time at temperatures above and below Tg'. This will help establish excipient effect on protein stability. Heterogeneity (phase separation) is one of the proposed reason for protein instability in the cryoconcentrated state. The results from Chapter 4 provide an approach to reduce heterogeneity by (i) adding mannitol to the solution containing sucrose and protein and (ii) including an isothermal hold step to achieve a homogeneous matrix. The solutions, in this case, were evaluated on a small scale. It will be imperative to evaluate the system in containers with larger volume as well as varying protein concentrations. Furthermore, in freeze-dried formulations containing mannitol, annealing is generally performed post freezing. Based on our observations, heterogeneity in the system is initiated during freezing and an annealing step during freezing at temperatures > -20°C can have two advantages: Firstly, like frozen systems, it will help generate a homogeneous matrix, and secondly, the annealing step will selectively result in

the formation of anhydrous mannitol. In other words, MHH formation in the lyophile and its consequences during storage can be avoided.

Overall, characterization of excipient phase behavior combined with biophysical characterization of protein stability in multicomponent systems will help in developing mechanistic insights into protein stabilization against various processing and storage related stresses.

Bibliography

1. Tang, X. C.; Pikal, M. J., Design of freeze-drying processes for pharmaceuticals: practical advice. Pharm Res 2004, 21 (2), 191-200.
2. Muttenthaler, M.; King, G. F.; Adams, D. J.; Alewood, P. F., Trends in peptide drug discovery. Nat. Rev. Drug Discov 2021, 20 (4), 309-325.
3. Protein Therapeutics Market - Information by Type, Application, Protein Function, End User and Region - Forecast till 2027. (accessed January 15, 2022).
4. Bhatnagar, B. S.; Tchessalov, S.; Lewis, L. M.; Johnson, R., Freeze drying of biologics. In Encyclopedia of Pharmaceutical Science and Technology, Six Volume Set, CRC Press: 2013; pp 1673-1722.
5. Carpenter, J. F.; Pikal, M. J.; Chang, B. S.; Randolph, T. W., Rational design of stable lyophilized protein formulations: some practical advice. Pharm Res 1997, 14 (8), 969.
6. Costantino, H. R., Excipients for use in lyophilized pharmaceutical peptide, protein, and other bioproducts. Lyophilization of biopharmaceuticals 2004, 2, 139-228.
7. Nelson, D. L.; Lehninger, A. L.; Cox, M. M., Lehninger principles of biochemistry. Macmillan: 2008.
8. Chi, E. Y.; Krishnan, S.; Randolph, T. W.; Carpenter, J. F., Physical stability of proteins in aqueous solution: mechanism and driving forces in nonnative protein aggregation. Pharm Res 2003, 20 (9), 1325-1336.
9. Wang, W.; Roberts, C. J., Protein aggregation – Mechanisms, detection, and control. Int J Pharm 2018, 550 (1), 251-268.
10. Amin, S.; Barnett, G. V.; Pathak, J. A.; Roberts, C. J.; Sarangapani, P. S., Protein aggregation, particle formation, characterization & rheology. Curr Opin Colloid Interface Sci 2014, 19 (5), 438-449.
11. Wang, W.; Nema, S.; Teagarden, D., Protein aggregation--pathways and influencing factors. Int J Pharm 2010, 390 (2), 89-99.
12. Weiss IV, W. F.; Young, T. M.; Roberts, C. J., Principles, approaches, and challenges for predicting protein aggregation rates and shelf life. J Pharm Sci 2009, 98 (4), 1246-1277.
13. Hofmann, M.; Gieseler, H., Predictive screening tools used in high-concentration protein formulation development. J Pharm Sci 2018, 107 (3), 772-777.
14. Dill, K. A., Dominant forces in protein folding. Biochemistry 1990, 29 (31), 7133-7155.
15. Krishnan, S.; Chi, E. Y.; Webb, J. N.; Chang, B. S.; Shan, D.; Goldenberg, M.; Manning, M. C.; Randolph, T. W.; Carpenter, J. F., Aggregation of granulocyte

colony stimulating factor under physiological conditions: characterization and thermodynamic inhibition. Biochemistry 2002, 41 (20), 6422-6431.

16. Rathore, N.; Rajan, R. S., Current perspectives on stability of protein drug products during formulation, fill and finish operations. Biotechnology progress 2008, 24 (3), 504-514.
17. Kolhe, P.; Mehta, A.; Lary, A.; Chico, S.; Singh, S., Large Scale Freezing of Biologics (Part III). BioPharm International 2012, 25 (10), 40-48.
18. Thakral, S.; Sonje, J.; Munjal, B.; Suryanarayanan, R., Stabilizers and Their Interaction with Formulation Components in Frozen and Freeze-dried Protein Formulations. Adv. Drug Deliv. Rev. 2021.
19. Tsutomu, A.; Steven, J.; William, C.; John, F., Factors affecting short-term and long-term stabilities of proteins. Adv Drug Deliv Rev 2001, 46, 307-326.
20. Kasper, J. C.; Friess, W., The freezing step in lyophilization: physico-chemical fundamentals, freezing methods and consequences on process performance and quality attributes of biopharmaceuticals. Eur J Pharm Biopharm 2011, 78 (2), 248-263.
21. Arsiccio, A.; Pisano, R., The Ice-Water Interface and Protein Stability: A Review. J Pharm Sci 2020.
22. Bhatnagar, B. S.; Bogner, R. H.; Pikal, M. J., Protein stability during freezing: separation of stresses and mechanisms of protein stabilization. Pharm Dev Technol 2007, 12 (5), 505-523.
23. Authelin, J. R.; Rodrigues, M. A.; Tchessalov, S.; Singh, S. K.; McCoy, T.; Wang, S.; Shalaev, E., Freezing of Biologicals Revisited: Scale, Stability, Excipients, and Degradation Stresses. J Pharm Sci 2020, 109 (1), 44-61.
24. Assegehegn, G.; Brito-de la Fuente, E.; Franco, J. M.; Gallegos, C., The importance of understanding the freezing step and its impact on freeze-drying process performance. J Pharm Sci 2019, 108 (4), 1378-1395.
25. Fang, R.; Bogner, R. H.; Nail, S. L.; Pikal, M. J., Stability of Freeze-Dried Protein Formulations: Contributions of Ice Nucleation Temperature and Residence Time in the Freeze-Concentrate. J Pharm Sci 2020.
26. Singh, S.; Kolhe, P.; Wang, W.; Nema, S., Large Scale Freezing of Biologics, A Practitioner's Review, Part One: Fundamental Aspects. Bioprocess Int. 2009, 7, 32-44.
27. Lee, J., Timasheff s. N., The stabilization of proteins by sucrose. J. Biol. Chem 1981, 256 (14), 7193-7201.
28. Chang, L. L.; Pikal, M. J., Mechanisms of protein stabilization in the solid state. J Pharm Sci 2009, 98 (9), 2886-2908.

29. Arsiccio, A.; Pisano, R., Stability of Proteins in Carbohydrates and Other Additives during Freezing: The Human Growth Hormone as a Case Study. J Phys Chem B 2017, 121 (37), 8652-8660.

30. Dong, J.; Hubel, A.; Bischof, J. C.; Aksan, A., Freezing-induced phase separation and spatial microheterogeneity in protein solutions. J Phys Chem B 2009, 113 (30), 10081-10087.

31. Ohtake, S.; Kita, Y.; Arakawa, T., Interactions of formulation excipients with proteins in solution and in the dried state. Adv Drug Deliv Rev 2011, 63 (13), 1053-1073.

32. Horn, J.; Mahler, H. C.; Friess, W., Drying for Stabilization of Protein Formulations. Dry Technol Biotechnol Pharm Appl 2020, 91-119.

33. Piedmonte, D. M.; Hair, A.; Baker, P.; Brych, L.; Nagapudi, K.; Lin, H.; Cao, W.; Hershenson, S.; Ratnaswamy, G., Sorbitol crystallization-induced aggregation in frozen mAb formulations. J Pharm Sci 2015, 104 (2), 686-697.

34. Singh, S. K.; Kolhe, P.; Mehta, A. P.; Chico, S. C.; Lary, A. L.; Huang, M., Frozen state storage instability of a monoclonal antibody: aggregation as a consequence of trehalose crystallization and protein unfolding. Pharm Res 2011, 28 (4), 873-885.

35. Gómez, G.; Pikal, M. J.; Rodríguez-Hornedo, N., Effect of initial buffer composition on pH changes during far-from-equilibrium freezing of sodium phosphate buffer solutions. Pharm Res 2001, 18 (1), 90-97.

36. Gómez, G., Crystallization-relatedpH changes during freezing of sodium phosphate buffer solutions. 1996.

37. Pikal-Cleland, K. A.; Rodriguez-Hornedo, N.; Amidon, G. L.; Carpenter, J. F., Protein denaturation during freezing and thawing in phosphate buffer systems: monomeric and tetrameric beta-galactosidase. Arch Biochem Biophys 2000, 384 (2), 398-406.

38. Sundaramurthi, P.; Suryanarayanan, R., Thermophysical properties of carboxylic and amino acid buffers at subzero temperatures: relevance to frozen state stabilization. J Phys Chem B 2011, 115 (21), 7154-7164.

39. Thorat, A. A.; Munjal, B.; Geders, T. W.; Suryanarayanan, R., Freezing-induced protein aggregation - Role of pH shift and potential mitigation strategies. Journal of Controlled Release 2020, 323, 591-599.

40. Singh, S., Storage considerations as part of the formulation development program for biologics. American Pharmaceutical Review 2007, 10 (3), 26.

41. Sundaramurthi, P.; Shalaev, E.; Suryanarayanan, R., “pH Swing” In Frozen Solutions - Consequence of Sequential Crystallization of Buffer Components. J Phys Chem Lett 2010, 1 (1), 265-268.

42. Thorat, A. A.; Munjal, B.; Geders, T. W.; Suryanarayanan, R., Freezing-induced protein aggregation - Role of pH shift and potential mitigation strategies. J Control Release 2020.

43. Pikal□Cleland, K. A.; Carpenter, J. F., Lyophilization□induced protein denaturation in phosphate buffer systems: Monomeric and tetrameric β□galactosidase. J Pharm Sci 2001, 90 (9), 1255-1268.

44. Duran, T.; Minatovicz, B.; Bai, J.; Shin, D.; Mohammadiarani, H.; Chaudhuri, B., Molecular Dynamics Simulation to Uncover the Mechanisms of Protein Instability During Freezing. J Pharm Sci 2021, 110 (6), 2457-2471.

45. Minatovicz, B.; Sun, L.; Foran, C.; Chaudhuri, B.; Tang, C. X.; Shameem, M., Freeze-concentration of solutes during bulk freezing and its impact on protein stability. Journal of Drug Delivery Science and Technology 2020, 58, 101703.

46. Minatovicz, B.; Bogner, R.; Chaudhuri, B., Use of a Design of Experiments (DoE) Approach to Optimize Large-Scale Freeze-Thaw Process of Biologics. AAPS PharmSciTech 2021, 22 (4), 153.

47. Esfandiary, R.; Parupudi, A.; Casas-Finet, J.; Gadre, D.; Sathish, H., Mechanism of reversible self-association of a monoclonal antibody: role of electrostatic and hydrophobic interactions. Journal of pharmaceutical sciences 2015, 104 (2), 577-586.

48. Jacques, D. A.; Trewhella, J., Small□angle scattering for structural biology—Expanding the frontier while avoiding the pitfalls. Protein science 2010, 19 (4), 642-657.

49. Curtis, J. E.; Nanda, H.; Khodadadi, S.; Cicerone, M.; Lee, H. J.; McAuley, A.; Krueger, S., Small-angle neutron scattering study of protein crowding in liquid and solid phases: lysozyme in aqueous solution, frozen solution, and carbohydrate powders. J Phys Chem B 2012, 116 (32), 9653-67.

50. Khodadadi, S.; Clark, N. J.; McAuley, A.; Cristiglio, V.; Curtis, J. E.; Shalaev, E. Y.; Krueger, S., Influence of sorbitol on protein crowding in solution and freeze-concentrated phases. Soft Matter 2014, 10 (23), 4056-60.

51. Yearley, E. J.; Zarraga, I. E.; Shire, S. J.; Scherer, T. M.; Gokarn, Y.; Wagner, N. J.; Liu, Y., Small-angle neutron scattering characterization of monoclonal antibody conformations and interactions at high concentrations. Biophys J 2013, 105 (3), 720-31.

52. Chilson, O. P.; Kitto, G. B.; Kaplan, N. O., Factors affecting the reversible dissociation of dehydrogenases. Proceedings of the National Academy of Sciences of the United States of America 1965, 53 (5), 1006.

53. Vesell, E. S.; Yielding, K. L., Effects of pH, ionic strength, and metabolic intermediates on the rates of heat inactivation of lactate dehydrogenase isozymes. Proceedings of the National Academy of Sciences of the United States of America 1966, 56 (4), 1317.

54. Anchordoquy, T. J.; Carpenter, J. F., Polymers protect lactate dehydrogenase during freeze-drying by inhibiting dissociation in the frozen state. Archives of biochemistry and biophysics 1996, 332 (2), 231-238.

55. Bhatnagar, B. S.; Pikal, M. J.; Bogner, R. H., Study of the individual contributions of ice formation and freeze-concentration on isothermal stability of lactate dehydrogenase during freezing. J Pharm Sci 2008, 97 (2), 798-814.

56. Schwegman, J. J.; Carpenter, J. F.; Nail, S. L., Evidence of partial unfolding of proteins at the ice/freeze□concentrate interface by infrared microscopy. J Pharm Sci 2009, 98 (9), 3239-3246.

57. Fang, R.; Tanaka, K.; Mudhivarthi, V.; Bogner, R. H.; Pikal, M. J., Effect of controlled ice nucleation on stability of lactate dehydrogenase during freeze-drying. J Phram Sci 2018, 107 (3), 824-830.

58. Liao, X.; Krishnamurthy, R.; Suryanarayanan, R., Influence of the active pharmaceutical ingredient concentration on the physical state of mannitol—implications in freeze-drying. Pharm Res 2005, 22 (11), 1978-1985.

59. Gómez, G. Crystallization-related pH changes during freezing of sodium phosphate buffer solutions. University of Michigan, 1995.

60. Coquelle, N.; Fioravanti, E.; Weik, M.; Vellieux, F.; Madern, D., Activity, stability and structural studies of lactate dehydrogenases adapted to extreme thermal environments. J. Mol. Biol 2007, 374 (2), 547-562.

61. Malterer, M.; Glass, S.; Newman, J., Scalable molecular dynamics with NAMD. J. Comput. Chem 2005, 26 (16), 1781-1802.

62. Best Robert, B.; Xiao, Z.; Jihyun, S.; Lopes Pedro, E.; Jeetain, M.; Michael, F.; MacKerell Alexander, D., Optimization of the Additive CHARMM All-Atom Protein Force Field Targeting Improved Sampling of the Backbone ϕ, ψ and Side-Chain χ1 and χ2 Dihedral Angles. J. Chem. Theory Comput. 2012, 8 (9), 3257-3273.

63. Curtis, J. E.; Raghunandan, S.; Nanda, H.; Krueger, S., SASSIE: A program to study intrinsically disordered biological molecules and macromolecular ensembles using experimental scattering restraints. Comput. Phys. Commun 2012, 183 (2), 382-389.

64. Humphrey, W.; Dalke, A.; Schulten, K., J. lVlolec. Graphics 1996, 14, 33-38.

65. Fujisawa, T.; Kato, M.; Inoko, Y., Structural characterization of lactate dehydrogenase dissociation under high pressure studied by synchrotron high-pressure small-angle X-ray scattering. Biochemistry 1999, 38 (20), 6411-6418.

66. Watson, M. C.; Curtis, J. E., Rapid and accurate calculation of small-angle scattering profiles using the golden ratio. J. Appl. Crystallogr. 2013, 46 (4), 1171-1177.

67. Sarachan, K. L.; Curtis, J. E.; Krueger, S., Small-angle scattering contrast calculator for protein and nucleic acid complexes in solution. Journal of Applied Crystallography 2013, 46 (6), 1889-1893.

68. Al-Hussein, A.; Gieseler, H., Investigation of histidine stabilizing effects on LDH during freeze-drying. J Pharm Sci 2013, 102 (3), 813-826.

69. Kolhe, P.; Amend, E.; K. Singh, S., Impact of freezing on pH of buffered solutions and consequences for monoclonal antibody aggregation. Biotechnology progress 2010, 26 (3), 727-733.

70. Nick Pace, C.; Alston, R. W.; Shaw, K. L., Charge–charge interactions influence the denatured state ensemble and contribute to protein stability. Protein science 2000, 9 (7), 1395-1398.

71. Yadav, S.; Laue, T. M.; Kalonia, D. S.; Singh, S. N.; Shire, S. J., The influence of charge distribution on self-association and viscosity behavior of monoclonal antibody solutions. Mol Pharm 2012, 9 (4), 791-802.

72. Varshney, D. B.; Kumar, S.; Shalaev, E. Y.; Kang, S.-W.; Gatlin, L. A.; Suryanarayanan, R., Solute crystallization in frozen systems–use of synchrotron radiation to improve sensitivity. Pharm Res 2006, 23 (10), 2368-2374.

73. Lovell, S. J.; Winzor, D. J., Effects of phosphate on the dissociation and enzymic stability of rabbit muscle lactate dehydrogenase. Biochemistry 1974, 13 (17), 3527-3531.

74. Anchordoquy, T. J.; Izutsu, K.-I.; Randolph, T. W.; Carpenter, J. F., Maintenance of quaternary structure in the frozen state stabilizes lactate dehydrogenase during freeze–drying. Archives of Biochemistry and Biophysics 2001, 390 (1), 35-41.

75. Rudolph, R.; Jaenicke, R., Kinetics of reassociation and reactivation of pig□muscle lactic dehydrogenase after acid dissociation. Eur J Pharm Biochem 1976, 63 (2), 409-417.

76. Baheti, A.; Kumar, L.; Bansal, A. K., Excipients used in lyophilization of small molecules. J. Excipients Food Chem. 2016, 1 (1), 1135.

77. Nail, S. L.; Jiang, S.; Chongprasert, S.; Knopp, S. A., Fundamentals of freeze-drying. Pharm Biotechnol 2002, 14, 281-360.

78. Kulkarni, S. S.; Suryanarayanan, R.; Rinella Jr, J. V.; Bogner, R. H., Mechanisms by which crystalline mannitol improves the reconstitution time of high concentration lyophilized protein formulations. Eur J Pharm Biopharm 2018, 131, 70-81.

79. Izutsu, K.-i.; Kojima, S., Excipient crystallinity and its protein-structure-stabilizing effect during freeze-drying. J. Pharm. Pharmacol. 2002, 54 (8), 1033-1039.

80. Izutsu, K.-i.; Yosohika, S.; Terao, T., Effect of mannitol crystallinity on the stabilization of enzymes during freeze-drying. Chem. Pharm. Bull. 1994, 42 (1), 5-8.

81. Sonje, J.; Thakral, S.; Suryanarayanan, R., t-Butanol Enables Dual Functionality of Mannitol: A Cryoprotectant in Frozen Systems and Bulking Agent in Freeze-Dried Formulations. Mol Pharm 2020.

82. Burger, A.; Henck, J.-O.; Hetz, S.; Rollinger, J. M.; Weissnicht, A. A.; Stöttner, H., Energy/Temperature Diagram and Compression Behavior of the Polymorphs of d-Mannitol. J Pharm Sci 2000, 89 (4), 457-468.

83. Kim, A. I.; Akers, M. J.; Nail, S. L., The physical state of mannitol after freeze-drying: effects of mannitol concentration, freezing rate, and a noncrystallizing cosolute. J Pharm Sci 1998, 87 (8), 931-935.

84. Mehta, M.; Bhardwaj, S. P.; Suryanarayanan, R., Controlling the physical form of mannitol in freeze-dried systems. Eur J Pharm Biopharm 2013, 85 (2), 207-213.

85. Srinivasan, J. M.; Wegiel, L. A.; Hardwick, L. M.; Nail, S. L., The Influence of Mannitol Hemihydrate on the Secondary Drying Dynamics of a Protein Formulation: A Case Study. J Pharm Sci 2017, 106 (12), 3583-3590.

86. Cao, W.; Mao, C.; Chen, W.; Lin, H.; Krishnan, S.; Cauchon, N., Differentiation and quantitative determination of surface and hydrate water in lyophilized mannitol using NIR spectroscopy. J Pharm Sci 2006, 95 (9), 2077-2086.

87. Johnson, R. E.; Kirchhoff, C. F.; Gaud, H. T., Mannitol-sucrose mixtures--versatile formulations for protein lyophilization. J Pharm Sci 2002, 91 (4), 914-22.

88. Yu, L.; Milton, N.; Groleau, E. G.; Mishra, D. S.; Vansickle, R. E., Existence of a mannitol hydrate during freeze□drying and practical implications. J Pharm Sci 1999, 88 (2), 196-198.

89. Sundaramurthi, P.; Burcusa, M. R.; Suryanarayanan, R., Physical characterization of pentamidine isethionate during freeze-drying—relevance to development of stable lyophilized product. J Pharm Sci 2012, 101 (5), 1732-1743.

90. Cavatur, R.; Vemuri Murti, N.; Pyne, A.; Chrzan, Z.; Toledo-Velasquez, D.; Suryanarayanan, R., Crystallization Behavior of Mannitol in Frozen Aqueous Solutions. Pharm Res 2002, 19 (6), 894-900.

91. Dierks, T. M.; Korter, T. M., Origins of the relative stabilities of anhydrous and hydrated D-mannitol crystals. J. Phys. Chem 2016, 120 (33), 6629-6636.

92. Thakral, S.; Koranne, S.; Suryanarayanan, R., Intra-Vial Heterogeneity in Physical Form of Mannitol in Colyophilized Binary Systems. Pharm Res 2018, 35 (11), 214.

93. Hawe, A.; Frieß, W., Impact of freezing procedure and annealing on the physico-chemical properties and the formation of mannitol hydrate in mannitol–sucrose–NaCl formulations. Eur. J. Pharm. Biopharm. 2006, 64 (3), 316-325.

94. Lueckel, B.; Bodmer, D.; Helk, B.; Leuenberger, H., Formulations of sugars with amino acids or mannitol–influence of concentration ratio on the properties of the freeze-concentrate and the lyophilizate. Pharm. Dev. Technol 1998, 3 (3), 325-336.

95. Larsen, H. M. L.; Trnka, H.; Grohganz, H., Formation of mannitol hemihydrate in freeze-dried protein formulations—A design of experiment approach. Int J Pharm 2014, 460 (1), 45-52.

96. Dixon, D.; Tchessalov, S.; Barry, A.; Warne, N., The impact of protein concentration on mannitol and sodium chloride crystallinity and polymorphism upon lyophilization. J Pharm Sci 2009, 98 (9), 3419-29.

97. Liao, X.; Krishnamurthy, R.; Suryanarayanan, R., Influence of processing conditions on the physical state of mannitol—implications in freeze-drying. Pharm Res 2007, 24 (2), 370-376.

98. Cao, W.; Xie, Y.; Krishnan, S.; Lin, H.; Ricci, M., Influence of process conditions on the crystallization and transition of metastable mannitol forms in protein formulations during lyophilization. Pharm Res 2013, 30 (1), 131-139.

99. Al-Hussein, A.; Gieseler, H., The effect of mannitol crystallization in mannitol–sucrose systems on LDH stability during freeze-drying. J Pharm Sci 2012, 101 (7), 2534-2544.

100. Snell, J. R.; Kumar, N. K.; Suryanarayanan, R.; Randolph, T. W., Nanobubbles in Reconstituted Lyophilized Formulations: Interaction With Proteins and Mechanism of Formation. J Pharm Sci 2020, 109 (1), 284-292.

101. Nunes, C.; Suryanarayanan, R.; Botez, C. E.; Stephens, P. W., Characterization and crystal structure of D-mannitol hemihydrate. J Pharm Sci 2004, 93 (11), 2800-9.

102. Anko, M.; Bjelošević, M.; Planinšek, O.; Trstenjak, U.; Logar, M.; Grabnar, P. A.; Brus, B., The formation and effect of mannitol hemihydrate on the stability of monoclonal antibody in the lyophilized state. International journal of pharmaceutics 2019, 564, 106-116.

103. Digital Humidity Sensor SHT7x (RH/T).

104. Templeton, A. C.; Placek, J.; Xu, H.; Mahajan, R.; Hunke, W. A.; Reed, R. A., Determination of the moisture content of bromobutyl rubber stoppers as a function of processing: implications for the stability of lyophilized products. PDA. J. Pharm. Sci. Technol. 2003, 57 (2), 75-87.

105. L'vov, B. V., Thermal decomposition of solids and melts: new thermochemical approach to the mechanism, kinetics and methodology. Springer Science & Business Media: 2007; Vol. 7.

106. Wheeler, R.; Frost, G., A comparative study of the dehydration kinetics of several hydrated salts. Can. J. Chem. 1955, 33 (3), 546-561.

107. Galwey, A. K., Theory of solid-state thermal decomposition reactions: scientific stagnation or chemical catastrophe? An alternative approach appraised and advocated. J. Therm. Anal. Calorim. 2012, 109 (3), 1625-1635.

108. Kaushal, A. M.; Vangala, V. R.; Suryanarayanan, R., Unusual effect of water vapor pressure on dehydration of dibasic calcium phosphate dihydrate. J. Pharm. Sci 2011, 100 (4), 1456-1466.

109. Griesser, U.; Burger, A., The effect of water vapor pressure on desolvation kinetics of caffeine 4/5-hydrate. Int J Pharm 1995, 120 (1), 83-93.

110. Galwey, A. K.; Brown, M. E., Thermal decomposition of ionic solids: chemical properties and reactivities of ionic crystalline phases. Elsevier: 1999.

111. Costantino, H. R.; Griebenow, K.; Langer, R.; Klibanov, A. M., On the pH memory of lyophilized compounds containing protein functional groups. Biotechnology and bioengineering 1997, 53 (3), 345-348.

112. Makower, B.; Dye, W., Sugar crystallization, equilibrium moisture content and crystallization of amorphous sucrose and glucose. J Agric Food Chem 1956, 4 (1), 72-77.

113. Salameh, A. K.; Mauer, L. J.; Taylor, L. S., Deliquescence lowering in food ingredient mixtures. J. Food Sci. 2006, 71 (1), E10-E16.

114. Carstensen, J. T.; Van Scoik, K., Amorphous-to-crystalline transformation of sucrose. Pharm Res 1990, 7 (12), 1278-1281.

115. Patel, S. M.; Nail, S. L.; Pikal, M. J.; Geidobler, R.; Winter, G.; Hawe, A.; Davagnino, J.; Gupta, S. R., Lyophilized drug product cake appearance: what is acceptable? J. Pharm. Sci 2017, 106 (7), 1706-1721.

116. Saleki-Gerhardt, A.; Zografi, G., Non-isothermal and isothermal crystallization of sucrose from the amorphous state. Pharm Res 1994, 11 (8), 1166-1173.

117. Palmer, K.; Dye, W. B.; Black, D., Sugar crystallization, X-ray diffractometer and microscopic investigation of crystallization of amorphous sucrose. J. Agric. Food Chem 1956, 4 (1), 77-81.

118. Leinen, K.; Labuza, T., Crystallization inhibition of an amorphous sucrose system using raffinose. J. Zhejiang Univ. Sci. B 2006, 7 (2), 85-89.

119. Labuza, T. P.; Labuza, P. S., Influence of temperature and relative humidity on the physical states of cotton candy. J. Food Process. Preserv. 2004, 28 (4), 274-287.

120. Yu, X.; Kappes, S.; Bello□Perez, L. A.; Schmidt, S., Investigating the moisture sorption behavior of amorphous sucrose using a dynamic humidity generating instrument. J. Food Sci. 2008, 73 (1), E25-E35.

121. te Booy, M. P.; de Ruiter, R. A.; de Meere, A. L., Evaluation of the physical stability of freeze-dried sucrose-containing formulations by differential scanning calorimetry. Pharm. Res. 1992, 9 (1), 109-114.

122. Cook, I. A.; Ward, K. R., Applications of headspace moisture analysis for investigating the water dynamics within a sealed vial containing freeze-dried material. PDA J. Pharm. Sci. Technol. 2011, 65 (1), 2-11.

123. Singh, S. K., Sucrose and trehalose in therapeutic protein formulations. In Challenges in Protein Product Development, Springer: 2018; pp 63-95.

124. Deluca, P.; Lachman, L., Lyophilization of pharmaceuticals I. Effect of certain physical□chemical properties. J Pharm Sci 1965, 54 (4), 617-624.

125. Thakral, S.; Sonje, J.; Suryanarayanan, R., Anomalous behavior of mannitol hemihydrate: Implications on sucrose crystallization in colyophilized systems. Int J Pharm 2020, 119629.

126. Meyer, J. D.; Nayar, R.; Manning, M. C., Impact of bulking agents on the stability of a lyophilized monoclonal antibody. Eur J Pharm Sci 2009, 38 (1), 29-38.

127. Koranne, S.; Govindarajan, R.; Suryanarayanan, R., Investigation of Spatial Heterogeneity of Salt Disproportionation in Tablets by Synchrotron X-ray Diffractometry. Mol Pharm 2017, 14 (4), 1133-1144.

128. Jordan, G. M.; Yoshioka, S.; Terao, T., The aggregation of bovine serum albumin in solution and in the solid state. J Pharm Pharmacol 1994, 46 (3), 182-185.

129. Roos, Y.; Karel, M., Plasticizing effect of water on thermal behavior and crystallization of amorphous food models. J Food Sci 1991, 56 (1), 38-43.

130. Sundaramurthi, P.; Suryanarayanan, R., Influence of crystallizing and non-crystallizing cosolutes on trehalose crystallization during freeze-drying. Pharm Res 2010, 27 (11), 2384-2393.

131. Langrish, T.; Wang, S., Crystallization rates for amorphous sucrose and lactose powders from spray drying: A comparison. Drying Technol 2009, 27 (4), 606-614.

132. Wang, B.; Tchessalov, S.; Warne, N. W.; Pikal, M. J., Impact of sucrose level on storage stability of proteins in freeze-dried solids: I. Correlation of protein–sugar interaction with native structure preservation. J Pharm Sci 2009, 98 (9), 3131-3144.

133. Suzuki, T.; Imamura, K.; Fujimoto, H.; Okazaki, M., Role of sucrose-LDH hydrogen bond for thermal stabilizing effect of sucrose on freeze-dried LDH. Drying technol 1999, 17 (7-8), 1429-1439.

134. Yu, X.; Kappes, S.; Bello□Perez, L. A.; Schmidt, S., Investigating the moisture sorption behavior of amorphous sucrose using a dynamic humidity generating instrument. J Food Sci 2008, 73 (1), E25-E35.

135. Kolhe, P.; Badkar, A., Protein and solute distribution in drug substance containers during frozen storage and post□thawing: A tool to understand and define freezing–thawing parameters in biotechnology process development. Biotechnology progress 2011, 27 (2), 494-504.

136. Piedmonte, D. M.; Summers, C.; McAuley, A.; Karamujic, L.; Ratnaswamy, G., Sorbitol crystallization can lead to protein aggregation in frozen protein formulations. Pharm Res 2007, 24 (1), 136-46.

137. Connolly, B. D.; Le, L.; Patapoff, T. W.; Cromwell, M. E. M.; Moore, J. M. R.; Lam, P., Protein Aggregation in Frozen Trehalose Formulations: Effects of

Composition, Cooling Rate, and Storage Temperature. J Pharm Sci 2015, 104 (12), 4170-4184.

138. Wang, W., Protein aggregation and its inhibition in biopharmaceutics. Int J Pharm 2005, 289 (1-2), 1-30.

139. Hancock, B. C.; Zografi, G., Characteristics and significance of the amorphous state in pharmaceutical systems. Journal of pharmaceutical sciences 1997, 86 (1), 1-12.

140. Searles, J. A.; Carpenter, J. F.; Randolph, T. W., Annealing to optimize the primary drying rate, reduce freezing□induced drying rate heterogeneity, and determine Tg′ in pharmaceutical lyophilization. Journal of pharmaceutical sciences 2001, 90 (7), 872-887.

141. Jena, S.; Horn, J.; Suryanarayanan, R.; Friess, W.; Aksan, A., Effects of excipient interactions on the state of the freeze-concentrate and protein stability. Pharm Res 2017, 34 (2), 462-478.

142. Bhatnagar, B. S.; Sonje, J.; Shalaev, E.; Martin, S. W.; Teagarden, D. L.; Suryanarayanan, R., A refined phase diagram of the tert-butanol–water system and implications on lyophilization process optimization of pharmaceuticals. Phys Chem Chem Phys 2020.

143. Toby, B. H.; Von Dreele, R. B., GSAS-II: the genesis of a modern open-source all purpose crystallography software package. J. Appl. Crystallogr 2013, 46 (2), 544-549.

144. Desai, K. G., W. Aaron Pruett, Peter J. Martin, James D. Colandene, and Douglas P. Nesta, Impact of manufacturing-scale freeze-thaw conditions on a mAb solution. BioPharm Int 2017, 30 no. 2, 30-36.

145. Pyne, A.; Surana, R.; Suryanarayanan, R., Crystallization of mannitol below Tg′ during freeze-drying in binary and ternary aqueous systems. Pharm Res 2002, 19 (6), 901-908.

146. Sundaramurthi, P.; Suryanarayanan, R., Trehalose crystallization during freeze-drying: implications on lyoprotection. J Phys Chem Lett 2010, 1 (2), 510-514.

147. Sundaramurthi, P.; Patapoff, T. W.; Suryanarayanan, R., Crystallization of trehalose in frozen solutions and its phase behavior during drying. Pharm Res 2010, 27 (11), 2374-2383.

148. Kolhe, P.; Goswami, S., Bulk Protein Solution: Freeze–Thaw Process, Storage and Shipping Considerations. In Challenges in Protein Product Development, Springer: 2018; pp 313-336.

149. Jain, K.; Salamat-Miller, N.; Taylor, K., Freeze–thaw characterization process to minimize aggregation and enable drug product manufacturing of protein based therapeutics. Scientific Reports 2021, 11 (1), 1-9.